Fluoride, Alkalinity and Hardness Removal from Contaminated Water by Electrolysis in relation to Sri Lankan Context

2022 March

Amarasooriya Arachchige Gayan Darshana Amarasooriya

Doctoral Dissertation

Fluoride, Alkalinity and Hardness Removal from Contaminated Water by Electrolysis in relation to Sri Lankan Context

Supervisor's Name: Professor Tomonori Kawakami

Graduate School of

Toyama Prefectural University

Student's Name: Amarasooriya Arachchige Gayan Darshana Amarasooriya

Student No: 1777001

TABLE OF CONTENTS

Abstract

Three types of electrolysis (ELC) systems were proposed to remove F^- as well as coexisting F^-, Ca^{2+}, Mg^{2+}, CO_3^{2-}, and HCO_3^- from the groundwater to meet the standard drinking water quality guidelines in relation to Sri Lankan context. The first ELC system was designed to remove co-existing F^-, Ca^{2+}, Mg^{2+} and CO_3^{2-}, and HCO_3^- ions with 50% of water recovery. The second one was designed to reduce the reject water quantity and to enhance the CO_3^{2-}, and HCO_3^- removal efficiency which suppressed the F^- and Mg^{2+} removal. The last system was designed to remove F^- for the water which contain lower Mg^{2+} concentration by using Fe sacrificial electrode coupled with ELC reactor with 67% water recovery.

A Platinum (Pt) and stainless steel (SS) electrodes for an anode and a cathode respectively, were used for all three ELC systems. Additionally, for the first stage of the third ELC system, Fe and SS electrodes were used. The effects of charge loading, initial ion concentration, the ion removal mechanism and the system performances in real conditions, as well as operational costs, were studied for all three systems. Furthermore, a mathematical model was proposed for the first two ELC system to model the output water quality as well as ion removal mechanisms.

According to the findings, increasing the charge loading and the initial Mg^{2+} increased the removal amount of F^- in all of the systems. Increasing the initial concentrations of Ca^{2+} and Mg^{2+} increased the removal of Ca^{2+}, Mg^{2+}, and (HCO_3^-+ CO_3^{2-}) in the first two continuous flow ELC systems. It was found that F^- ions were mainly removed by co-precipitation with $Mg(OH)_2$ and slight adsorption to $MgCO_3$, $CaCO_3$ and $Mg(OH)_2$ mixture in first two ELC systems. Also, Coulomb transfer removed F^- in first ELC system which was operated with 50% water rejection.

The second ELC system shows a 100% water recovery and higher removal of (HCO_3^-+ CO_3^{2-}) ions. Therefore, Mg^{2+} and F^- removal increment was observed. Moreover, second ELC system can be operated with lower charge loading to meet

significant F^- removal. The community-level treatment system established in Sri Lanka for both first and second ELC systems confirmed the effective removal of F^- and Ca^{2+}in the cathode and (HCO_3^-+ CO_3^{2-}) in the anode and delivered a quality water under Sri Lankan guideline.

Experimental results of the third ELC system revealed that incorporating Fe with low concentration of Mg^{2+} significantly increased the removal of F^-. The F^- was removed mainly by co-precipitation with $Mg(OH)_2$ +$Fe(OH)_3$ mixture. Also, Coulomb force transfer helped to remove F^- by transferring to the anode. The optimum operating cost for the proposed three systems was calculated as 2.02, 1.70 and 0.56 US$/$m^3$ respectively.

GENERAL INTRODUCTION

With the rapid growth of the world population and industries, water demand for drinking purposes, as well as industrial requirements, is rapidly increasing. On the other hand, global warming, increase consumption of water, natural water contaminants and water contaminated by industrial discharges deteriorate the water quantity, water quality, as well as many consumable water sources. However, the usability of groundwater for domestic and industrial purposes depends directly upon the water quality. Due to contamination, communities and industries struggle or abandon the easily accessible water sources and seek decent quality water sources or technologies to remove the contaminants from drinking water and wastewater.

Nowadays, industry-induced and naturally occurring Fluoride (F^-), has become the primary contaminant in groundwater and surface water (Bhatnagar et al., 2011; Mukherjee and Halder, 2018). Even though F^- is essential to humans for preventing dental and skeletal caries, excess intake is detrimental to human health (Browne et al., 2005, Iano et al., 2014, Mandinic et al., 2010, Tiwari et al., 2017, Ayoob and Gupta, 2006). Moreover, excessive F^- exposure can damage human body systems through gastrointestinal or respiratory track accumulation (Spencer and Lewln, 1970). It was reported that there was an excessive level of F^- in the groundwater in more than 20 countries worldwide, causing fluorosis to humans (Meenakshi and Maheshwari, 2006). As per estimates, 200–260 million people in various nations are at risk of fluorosis (Amini et al., 2008; Ayoob and Gupta, 2006). This situation has become a major global issue, and the World Health Organization (WHO) has recommended a maximum F^- concentration of 1.5 mg/L for drinking water (WHO, 2017).

However, the main source of drinking water in many countries, such as Africa, China, the Middle East, Sri Lanka, and India, is groundwater rich in F^-, where endemic fluorosis is commonly found (Ayoob and Gupta, 2006; Chung et al., 1997; Dissanayake, 2005; Herath et al., 2017; Mameri et al., 1998; Paranagama et al., 2018;

Perera et al., 2018). Due to the water scarcity in those regions, the removal of excessive F^- is essential for humans to consume.

Sri Lanka is currently struggling to acquire qualified water not only without F^- but also without hardness and alkalinity for their populations. A vast number of water sources in the northern, north-central and some areas of central, Uva provinces (in arid and semi-arid zones) are contaminated with naturally occurring F^-, hardness and alkalinity. About 10% of the population who are living in those areas consume those groundwater rich in F^- and are reported to suffer from not only dental and skeletal fluorosis but also chronic kidney disease of unknown etiology (CKDu). Moreover, there are many people who already dead by CKDu. Wide-ranging previous studies have reported that the dental and skeleton fluorosis in Sri Lanka were caused by a high concentration of F^- (Dissanayake, 2005; Kawakami et al., 2014). Moreover, F^- is supposed to be one of the most suspicious elements causing CKDu in Sri Lanka since a higher concentration of F^- was found in the groundwater in the CKDu prevalent areas (Herath et al., 2017; Paranagama et al., 2018). Furthermore, the causes of CKDu were reported to be multifactorial and were related to the excessive level of alkalinity, and hardness which co-existed with F^-(Chandrajith et al., 2011a; Lanka et al., 2014).

According to many studies, not only in Sri Lanka but also in many regions of the world either Ca^{2+}, Mg^{2+}, $HCO_3^-$and CO_3^{2-} (hardness and alkalinity-causing agents), or a mixture of Ca^{2+}, Mg^{2+}, $HCO_3^-$and CO_3^{2-} were found to coexist with F^- (Karimi et al., 2018; Ketata et al., 2011; Kim and Jeong, 2005; Luo et al., 2018; Rafique et al., 2009; Rango et al., 2012; Salifu et al., 2012; Singaraja et al., 2014; Su et al., 2013; Thapa et al., 2018; Wickramarathna et al., 2017). Hardness does not have a direct adverse effect on human health; however, it is troublesome for industries as well as households, causing scaling on equipment, pipelines, and storage tanks. Hardness in drinking water is important for aesthetic acceptability such as palatability, odor, appearance, and color. (Zhi and Zhang, 2016). Degrees of hardness is categorized as soft, moderately hard, hard, and very hard according to the following range of

equivalent $CaCO_3$ concentrations converted from Ca^{2+} and Mg^{2+} concentrations ($CaCO_3$< 60 mg/L: soft; 60 mg/L ≤ $CaCO_3$ <120 mg/L: moderately hard; 120 mg/L ≤ $CaCO_3$ <180 mg/L: hard; and 180 mg/L ≤ $CaCO_3$: extremely hard). Therefore, in real conditions, the removal of F^- only, would not be sufficient to meet the standards for drinking water quality or the sustainable use of groundwater for household or for industrial purposes. Hence, our prime objective is to introduce novel treatment technologies that are capable of removing co-existing F^-, Ca^{2+}, Mg^{2+}, $HCO_3^-$and CO_3^{2-} from the groundwater.

By far, F^- is one of the most frequently studied contaminants in the world (Fu et al., 2013). Therefore many technologies have evolved and been used in past decades for F^- removal; such as adsorption, chemical coagulation, membrane separation, reverse osmosis (RO), nanofiltration (NF), ultrafiltration (UF), and electrochemical methods (Bhatnagar et al., 2011; Jadhav et al., 2015; Mohapatra et al., 2009; Pulkka et al., 2014; Shen and Schafer, 2014). However, among those methods, electrochemical methods have been proven as an effective way to remove F^- (De Francesco and Costamagna, 2004; Martínez-Huitle et al., 2006; Pulkka et al., 2014). Common electrochemical methods used in F^- removal are categorized as electrochemical precipitation (ECP), electrochemical reduction, electrochemical oxidation, indirect electro-oxidation with strong oxidants, photo-assisted electrochemical methods and electrodialysis (ELD) (Brillas and Martínez-Huitle, 2015). Among these categories, ECP has a long history as a water and wastewater treatment technology widely employed to remove F^- as well as hardness, and heavy metals (Nidheesh and Singh, 2017; Sandoval et al., 2014; Zuo et al., 2008).

The most common technologies reported to remove coexisting F^-, Ca^{2+}, Mg^{2+}, HCO_3^-, and CO_3^{2-} are RO, NF, ion exchange (IE), chemical treatment (CT), and the ECP and ELD (Gabrielli et al., 2006; Gascó and Méndez, 2005; Janson et al., 2018; Kuokkanen et al., 2013; Shen and Schafer, 2014; Zhi and Zhang, 2016). With the exception of RO, NF, and ELD, the main disadvantage of CT and ECP is that they commonly introduce ions by an exchange to the water during the treatment process.

IE cost is high and needs to regeneration IE resins when saturated. However, ECP attracts much attention as a process for removing coexisting Ca^{2+}, Mg^{2+}, HCO_3^-, and CO_3^{2-} ions since it can be performed with or without introducing chemicals to the source water (Gabrielli et al., 2006; Zeppenfeld, 2011; Zeppenfeld, 1998; Zhi and Zhang, 2016). So far, none of the ECP studies has investigated the removal of co-existing F^-, Ca^{2+}, Mg^{2+}, HCO_3^-, and CO_3^{2-} ions without chemical addition. Therefore, developing an ECP method without any chemical addition, that removes coexisting F^-, Ca^{2+}, Mg^{2+}, HCO_3^-, and CO_3^{2-} ions, will be of interest to the scientific community.

Chemical adding, ECP method, "electrocoagulation (EC)" has been identified as an emerging technology for de-fluoridation as well as Ca^{2+}, Mg^{2+}, HCO_3^-, and CO_3^{2-} removals because of its environmental compatibility and significant process efficiency (Mollah et al., 2001; Zhi and Zhang, 2016). Additionally, the environmental sector has shown a growing interest in the treatment of different types of water and wastewater by EC (Kuokkanen et al., 2013). However, commonly used aluminum and iron electrodes in EC limit its applicability in water and wastewater treatment due to the presence of a high concentration of residual electrode material in treated water as well as the generation of high quantities of sludge. Nevertheless, it's worth developing EC technology further for F^-, alkalinity, and hardness removal by overcoming the major drawback of electrode dissociation.

Usually, EC is performed in a common cell reactor and uses the OH^- formed by water electrolysis around the cathode to coagulate the metal ion. Most commonly, sacrificial electrodes corrode to release metal ion (active coagulant) precursors (usually aluminum or iron cations) to form a metal hydroxide coagulant near the cathode. Over time anode passivation and sludge deposition on the electrodes inhibits the ELC and EC process. Also, high amounts of iron and aluminum ions are dissolved in the effluent (Brillas et al., 2003; Nidheesh and Singh, 2017). On the other hand, EC is still struggling to emerge as a conventional water treatment technology due to the lack of a systematic approach to EC reactor design/operation and the issue of electrode reliability, particularly the passivation of the electrodes over time (Holt et al., 2005;

Mollah et al., 2001).

Electrolysis (ELC) has been identified as a well-established technology for Cl_2(g) and H_2(g) production. Nevertheless, ELC functionality can be used to overcome the above-described disadvantages in the EC. Principally, in the ELC system, stainless steel (SS) and platinum (Pt) were employed for the electrodes of cathode and anode, respectively to prevent the introduction of ions. Furthermore, ELC cell's diaphragm allowed maintaining a low pH level in the anode and a high pH level in the cathode. These pH levels are very much useful to start the reactions required for the removal of co-existing F^- , Mg^{2+}, Ca^{2+}, $HCO_3^-$and CO_3^{2-}. Nevertheless, several studies presented that Ca^{2+}, $HCO_3^-$and CO_3^{2-} could be effectively removed by ELC methods (Hasson et al., 2010; Zeppenfeld, 1998). Accordingly, our prime objective was to remove F^- and co-existed Mg^{2+}, Ca^{2+}, $HCO_3^-$and CO_3^{2-} by ELC.

In this study, three types of ELC methods were studied to remove co-existing F^-, Mg^{2+}, Ca^{2+}, $HCO_3^-$and CO_3^{2-} from simulated and real groundwater. For the design of ELC systems, each system performance for different level of initail ion concentrations and those syetms drawbacks were considerd. Accordingly, the first ELC system was designed to remove co-existing F^-, Ca^{2+}, Mg^{2+} and CO_3^{2-}, and HCO_3^- ions with 50% of water recovery. The second one was designed to reduce the reject water quantity and to enhance the CO_3^{2-}, and HCO_3^- removal efficiency which suppressed the F^- and Mg^{2+} removal. The last system was designed to remove F^- for the water which contain lower Mg^{2+} concentration by using Fe sacrificial electrode coupled with ELC reactor with 67% water recovery.

For all three systems, the performance under different initial ion concentrations, operational parameters such as charge loading, cost, water rejection were studied. Furthermore, for the first two ELC systems, a mathematical model to estimate the ion removal was established and validated with simulated and real groundwater. The model was used to propose ion removal, removal mechanism as well as to approximate the operational conditions required to meet the water quality

guidelines. For the first two continuous, ELC systems, Platinum (Pt) and Stainless steel(SS) electrodes were used in the anode and the cathode respectively. For the third ELC system's first stage operation, sacrificial iron-anode, and SS-cathode were used. In its second stage, Pt- anode and SS- cathode were used. For the first two continuous flow ELC systems, Mg^{2+}, Ca^{2+}, HCO_3^- and CO_3^{2-} available in the groundwater were used as F^- removing agents and the third ELC system utilized dissociated Fe and naturally available Mg^{2+} for F^- removal. The three proposed ELC systems were operated in a laboratory with simulated groundwater. According to the results obtained in the laboratory, two types of community-scale treatment systems were operated in Sri Lanka to confirm the performance of the system.

CHAPTER 1

Removal of Coexisting F^-, Ca^{2+} and Mg^{2+} from Groundwater by Electrolysis System and its Mathematical Modeling.

1. Introduction

Electrolysis (ELC) cell configuration allows maintaining adequate pH levels in the anode and cathode as well as the transference of cations and anions through a diaphragm without any specific ion selectivity similar to the electrodialysis (ELD). Generally, in batch-type ELC cell operation, the anode pH level decreases, and the cathode pH level increases with time. This function can be utilized to remove F^-, alkalinity and hardness. Moreover, ELC F^- ion removal was reported only once in a scientific journal (Kawakami et al., 2018).

Accordingly, the main objective of this section was to explore the removal of coexisting F^-, Ca^{2+}, Mg^{2+}, $HCO_3^-$and CO_3^{2-} from groundwater. Furthermore, the removal mechanism was elucidated by establishing a mathematical model. Subsequently, the system performance against charge loading, various initial concentrations of F^-, Ca^{2+}, Mg^{2+}, $HCO_3^-$and CO_3^{2-} were studied to establish the operational guidelines. Furthermore, the proposed systems' performance and stability were confirmed by operating the system in Sri Lanka, where fluorosis and other related diseases were endemic (Herath et al., 2017; Paranagama et al., 2018; Perera et al., 2018)

2. Materials and methods

2.1 Experimental setup of the ELC cell

A tank made of acrylic resin with dimensions of 20 cm × 10.2 cm × 5 cm (length × height × width, respectively) was used as an ELC reactor for the laboratory experiments. The tank was separated into two cells by employing a 2 mm thick (effective area: 20 cm × 10.2 cm) ceramic diaphragm (F-C1, Nikkato corp., Japan). The diaphragm helped separate the anode and the cathode solutions, preventing the mixing of sludge formed in the cathode, and to facilitate the ion exchange between the cells (Fig.1.1). To lengthen the water flow in each cell, individual cells were further divided into two equal slots with an acrylic plate, keeping open 10 mm from the bottom.

The effective volume of the cathode and anode cells was 490 mL. U-shaped platinum (Pt) (effective length = 30 cm, φ = 0.40 mm) and stainless steel (SS) (effective length = 30 cm, φ = 1.00 mm) wires were used as electrodes for the anode and the cathode, respectively. The inter-electrode distance was kept at 3.3 cm. The assembly was connected to a constant current power supply for all experiments and the voltages were recorded after the system stabilization. The raw water inflow rates were kept at 10 mL/min for both the anode and the cathode in all experiments and the outflow rates were measured after stabilization of the system. For the community-scale treatment system, two parallelly connected reactors made out of a material similar to that of the laboratory experimental ELC reactor were utilized. The effective total volume of the anode and the cathode was 12 L (28 cm × 40 cm × 5.357 cm × 2). U shaped Pt wires (30 cm × 2) and SS mesh (2cm×2cm) with a size of 24 cm × 36 cm ×2 were used as anode and cathode electrodes, respectively. The inter-electrode distance was kept at 0.9 cm.

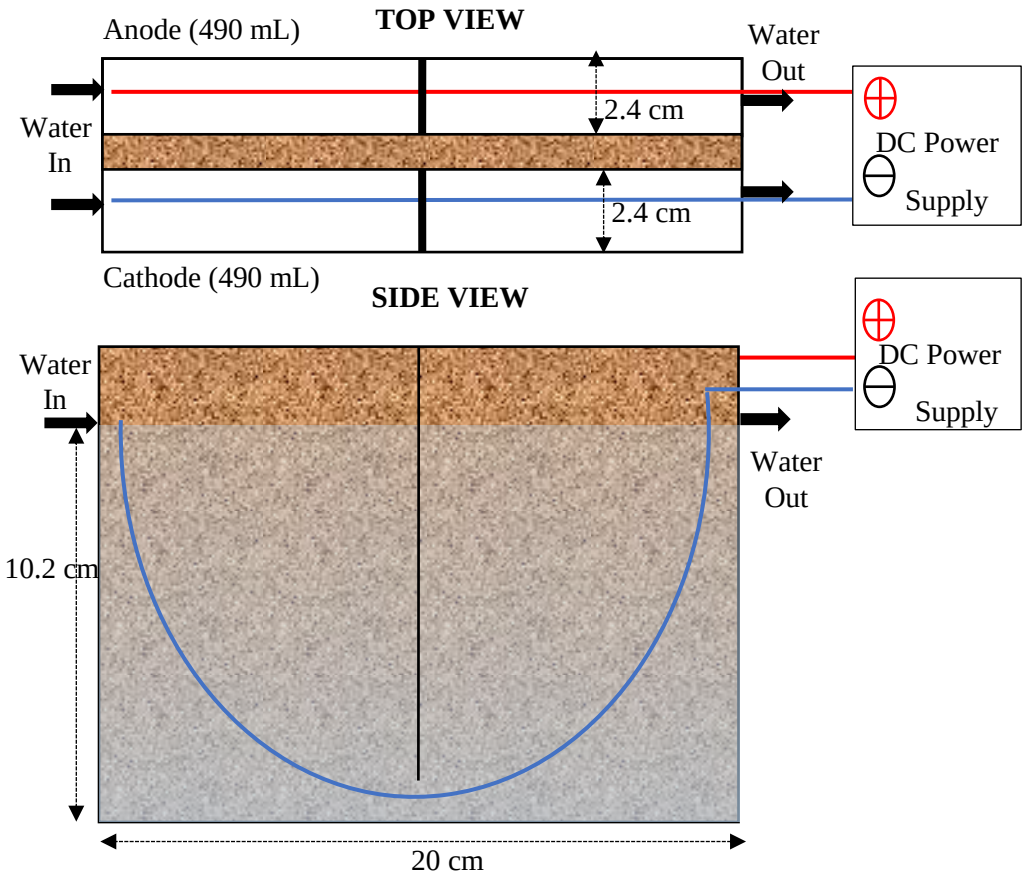

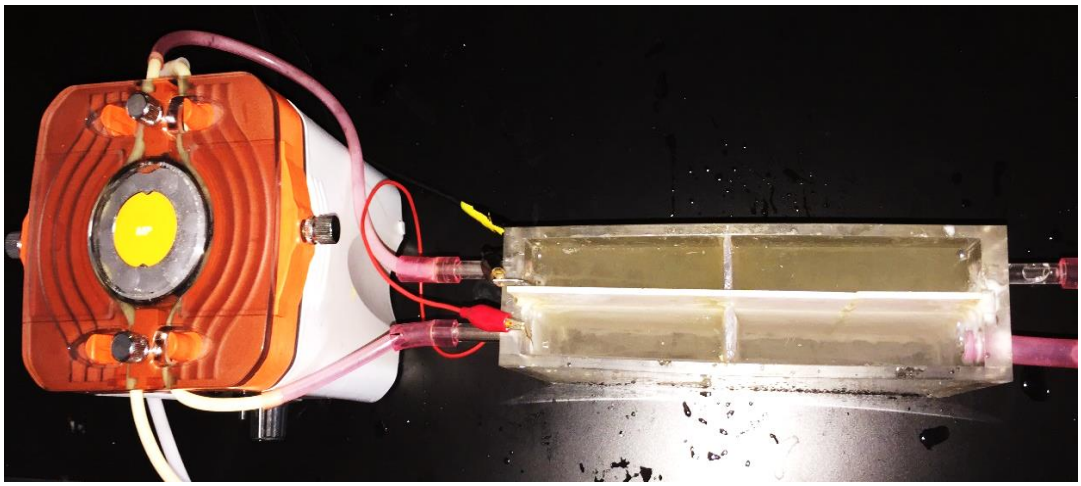

Fig. 1. 1: Electrolysis Cell Configuration

2.2 Unit treatment steps and operational description

The electrolysis setup employed for the laboratory and the field experiments is shown in Fig.1.2. To adjust the pH of the cathode water, an adequate amount of the anode water was mixed (Treated water) and the rest of the anode water was discarded (rejected water). If the system was used for alkalinity and hardness removal purposes, the rejected water should be minimized by utilizing the anode water to neutralize the pH, as well as to remove the (HCO_3^-+ CO_3^{2-}).

As electrolysis progressed, H^+ was formed in the anode cell (Eq. 1.1) while OH^- was formed in the cathode cell. (Eq. 1.3). H^+ formed in the anode cell could effectively remove $HCO_3^-$and CO_3^{2-} as carbon dioxide (Eq. 1.2). Also, Mg^{2+} and Ca^{2+} were removed in the cathode cell by reacting with CO_3^{2-} and OH^- (Eqs. 1.4–1.8). OH^- formed in the cathode cell started precipitation/co-precipitation of F^- with $Mg(OH)_2$ (Eq. 1.2). Furthermore, F^- could be removed as MgF_2, CaF_2 and by adsorption to the

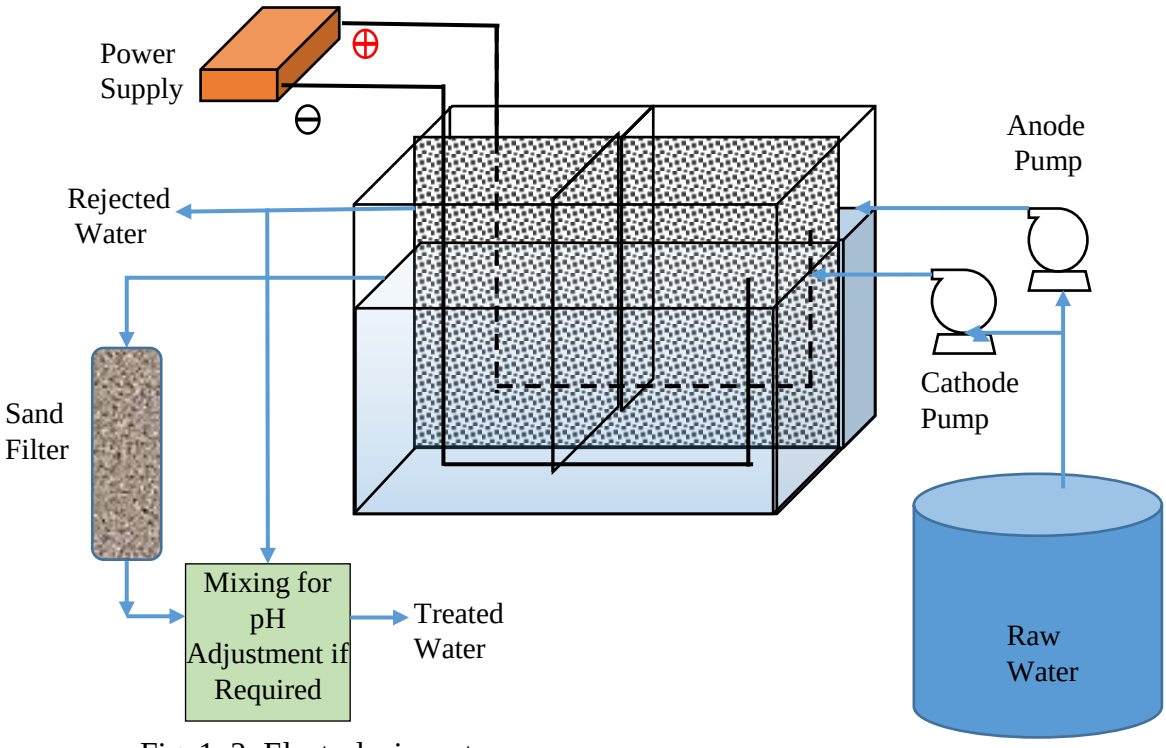

Fig. 1. 2: Electrolysis system

$CaCO_3$ and $MgCO_3$ (Eqs. 1.10–1.12). Additionally, Coulomb force could be an advantage for either ion concentrating or diluting in the cathode or the anode.

For the laboratory experiments, a series of F^-, Mg^{2+}, Ca^{2+}, and (HCO_3^-+ CO_3^{2-}) spiked tap water (hereafter initial concentrations will be denoted as F^-_0, Mg^{2+}_0, Ca^{2+}_0, and (HCO_3^-+ CO_3^{2-}) $_0$) was used as synthetic groundwater. For the laboratory ELC experiments, a constant current power supply was used. For the community scale treatment system, a constant voltage power supply was used. Based on the applied current and water flow rates in the reactor applied Charge loadings (Coulomb per liter=C/L) were calculated. The initial ion concentrations, flow rates and the applied charge loading for different experiments are summarized in Table 1. 1.

To study the effect of charge loading on ion's removal, conditions and initial concentrations listed in the "Charge loading" row of Table 1.1 were utilized. The conditions and initial concentrations listed in Table1.1 "Isotherm_1, Isotherm_2 and Isotehrm_3" were used to prepare the Mg^{2+} and Ca^{2+} forming precipitates, Mg^{2+} forming precipitates and Ca^{2+} forming precipitate in the presence of (HCO_3^-+ CO_3^{2-}) respectively. Collected precipitates were filtered dried and used for the F^- adsorption isotherm experiments discussed in section 3.2. The conditions and initial concentrations listed in the rows of "Anode flow rate, F^-_0, Mg^{2+}_0, Ca^{2+}_0, (HCO_3^-+ CO_3^{2-}) $_0$ and system stability" were used for the experiments discussed in the 3.5, 3.6, 3.7, 3.8, 3.9 and 3.10, sections respectively. Field conditions used in the community scale treatment system were listed in the "Average" row of Table 1.1.

Table 1. 1**:** Operational conditions, initial ion concentrations maintained at the laboratory and the field experiments and related water quality guidelines

Laboratory conditions										
Versus ion Removal / Experiment	**C/L**	**Current (A)**	**Initial Concentrations**				**Inflow rate (mL/min)**		**Outflow rate (mL/min)**	
			F^-(mg/L)	**Mg^{2+} (mg/L)**	**Ca^{2+}(mg/L)**	**HCO_3^-+ CO_3^{2-} (mmol/L)**	**Anode**	**Cathode**	**Anode**	**Cathode**
Charge loading	0-1500	0-0.25	10	100	100	10	10	10	10	10
Isotherm_1	1500	0.25	0	100	100	10	10	10	10	10
Isotherm_2	1500	0.25	0	100	0	0	10	10	10	10
Isotherm_3	1500	0.25	0	0	100	10	10	10	10	10
Anode flow rate	1500	0.25	10	100	100	10	2.5-20	10	2.5-20	10
F^-_0	1500	0.25	5-20	100	100	10	10	10	10	10
Mg^{2+}_0	1500	0.25	10	0-125	100	10	10	10	4-10	14-10
Ca^{2+}_0	1500	0.25	10	100	0-125	10	10	10	8-10	12-10
$(HCO_3^-+ CO_3^{2-})_0$	1500	0.25	10	100	100	0-12.5	10	10	10	10
System stability	1500	0.25	10	45	200	10	10	10	10	10
Field conditions used in the community scale treatment system										
	C/L	**Current (A)**	**F^-(mg/L)**	**Mg^{2+}(mg/L)**	**Ca^{2+}(mg/L)**	**HCO_3^-+ CO_3^{2-} (mmol/L)**	**Anode**	**Cathode**	**Anode**	**Cathode**
Average	1324	5.74	2.71	130.8	54.7	13.75	260	260	260	260
Guideline values										
			F^-(mg/L)	**Mg^{2+}(mg/L)**	**Ca^{2+}(mg/L)**	**HCO_3^-+ CO_3^{2-} (mmol/L)**				
Sri Lankan Guideline			1.0	30	240	8.0				
WHO Guideline			1.5	50	75	6.1				

The Anode reactions:

$$H_2O(l) \rightarrow \frac{1}{2}O_2(g) + 2H^+ + 2e^- \qquad (1.1)$$

$$HCO_3^-(aq) + H^+ \xleftrightarrow{K1=4.448\times10^{-7}} H_2CO_3(aq) \rightarrow CO_2(g)\uparrow + H_2O(l) \qquad (1.2)$$

The Cathode reactions:

$$2H_2O(l)+2e^- \rightarrow 2OH^- + H_2(g) \quad (1.3)$$

$$HCO_3{}^- + OH^- \xleftrightarrow{K2=4.690 \text{ x } 10^{-11}} CO_3{}^{2-} + H_2O(l) \quad (1.4)$$

$$CO_3{}^{2-} + Ca^{2+} \xleftrightarrow{Ksp=3.3 \times 10^{-9}} CaCO_3\,(s) \downarrow \quad (1.5)$$

$$CO_3{}^{2-} + Mg^{2+} \xleftrightarrow{Ksp=1.6 \times 10^{-8}} MgCO_3\,(s) \downarrow \quad (1.6)$$

$$Mg^{2+} + 2OH^- \xleftrightarrow{Ksp=\ 5.61 \times 10^{-12}} Mg(OH)_2(s) \quad (1.7)$$

$$Ca^{2+} + 2OH^- \xleftrightarrow{Ksp=5.02 \times 10^{-6}} Ca(OH)_2(s) \downarrow \quad (1.8)$$

Plausible F^- removal mechanisms

$$xMg^{2+} + 2zOH^- + yF^- \rightarrow Mg_x(OH)_{2z-y}F_y(s) \downarrow$$
$$+yOH^- \quad (co\ precipitation) \quad (1.9)$$

$$Mg^{2+} + 2F^- \xleftrightarrow{ksp=5.16 \times 10^{-11}} Mg(F)_2(s) \downarrow \quad (1.10)$$

$$Ca^{2+} + 2F^- \xleftrightarrow{ksp=3.45 \times 10^{-11}} Ca(F)_2(s) \downarrow \quad (1.11)$$

$$(Ca.Mg)(CO_3)_2(s) + 2xF^-$$
$$\Longleftrightarrow (Ca.Mg)(CO_3)_{2-x}F_{2x} \downarrow + xCO_3{}^{2-}(adsorption) \quad (1.12)$$

2.3 Sample collection, storage, and quality control

A groundwater source located in Sri Lanka's Medawachchiya area (8°32'02.8"N 80°29'57.6"E) of the Anuradhapura District (Fig. 1.3) was selected for the field study. Samples were collected after three hours of system stabilizing time from the anode and the cathode outlets. The system stabilization point was determined by measuring the pH levels in the cathode and the anode outlets at frequent time intervals. Within 2.5 hours pH levels were stabilized in the anode and the cathode. Accordingly, by the addition of one additional hour, a three-hour time frame was considered as the system's stabilizing time.

Water samples from the field and the laboratory were filtered into 50 mL polyethylene bottles on location using a membrane filter with a pore size of 0.45 µm to eradicate bacteriological activities affecting the water quality and to remove non-dissolved particles. Collected samples from the field and laboratory were analyzed in Japan within 45 days of their collection.

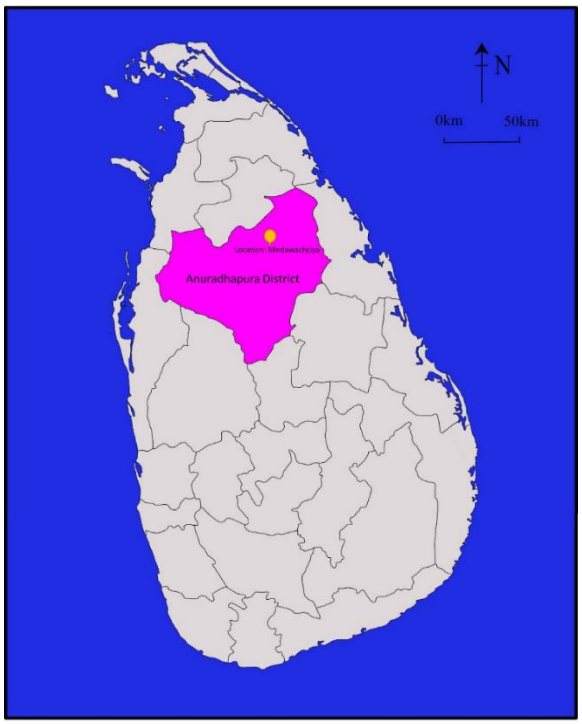

Fig. 1. 3: Field study location in Anuradapura District, Sri Lanka

2.4 Chemicals, instruments, and calculations

All chemicals used in the experiments were analytical grade and were purchased from Wako Chemicals, Japan. Platinum electrodes were purchased from the Nilaco Corporation, Japan, and stainless-steel electrodes were obtained from the local market in Japan. Anions were analyzed using an ion chromatograph (Thermo Dionex ICS-2000; separation column: IonPac AS18; eluent: KOH 23–40 mmol/L gradient; suppressor ASRS 300 4mm; Thermo Scientific, USA). Cations were analyzed using an ion chromatograph (Thermo Dionex ICS-1500; separation column:

IonPac CS12; eluent: Methanesulfonic acid (MSA) 30 mmol/L isocratic; suppressor CSRS 500 4mm; Thermo Scientific, USA). By analyzing the calibration standard solution after every 20 samples, the stability of the ion chromatographic detector was monitored for quality control. If the overall concentration variability of the examined calibration standard solution was not below 5%, a re-analysis was performed.

The pH was measured by the glass electrode method (Orion Star A324; Thermo Scientific, USA). X-ray diffraction (XRD) analysis of the precipitates was performed with a RIGAKU MiniFlex (Japan) machine equipped with CuK-Alpha radiation (configuration: 2theta/min 30KV, 15mA (450W)). Voltage logging for current and charge loading calculations applied in a community-scale treatment system was performed with a data logger (ONSET, HOBO).

For the isotherm experiments, precipitate prepared under the conditions listed in Table 1.1 was used. After three hours of the stabilization period, 20 L of the cathode water was collected and the supernatant was discarded to thicken the formed precipitate. After that, the precipitate was filtered with a 0.45 μm membrane filter. The filtrate was dried in an oven for three hours under 70 ^{0}C. 0.025, 0.050, 0.10, 0.20 and 0.36 g of the samples were added to the 50 mL of pH (10.2) adjusted 10 mg/L F^- solution. Samples were shaken with an electrical shaker with a 180 reciprocation for 0.77 hours equal to the ELC reactor resident time. After 0.77 hours, the supernatant was filtered with a 0.45 μm membrane filter and analyzed for F^- concentration.

Due to the diprotic nature of carbonic acid (H_2CO_3) in the solution, both $HCO_3^-$and CO_3^{2-} ions are available, and their concentrations change with the solution's pH. Therefore, the sum of the carbonate ($HCO_3^-$and CO_3^{2-}) concentrations (hereafter (HCO_3^-+ CO_3^{2-})) as mmol/L account for the alkalinity. The charge of water samples' (HCO_3^-+ CO_3^{2-}) was calculated by accounting for the system's ion charge balances. Trace ion concentrations were neglected, and the calculation focused on major ions in Eq. 1.13. For calculating individual $HCO_3^-$and CO_3^{2-} concentrations as mmol/L, the carbonates' charge balance equation (Eq. 1.14) and carbonates' equilibria

(Eq. 1.15) were employed.

(T_C)= Total charge of $HCO_3^-$and CO_3^{2-} = (sum of cation charge – the sum of anion charge except for $HCO_3^-$and CO_3^{2-})

$$\{2[CO_3^{2-}] + [HCO_3^-]\}(eq/L) = \{[H^+] + [Na^+] + [NH_4^+] + [K^+] + 2[Mg^{2+}] + 2[Ca^{2+}]\} - \{[OH^-] + [F^-] + [Cl^-] + 2[SO_4^{2-}] + [NO_3^-]\}(eq/L) \quad (1.13)$$

The charge balance for $HCO_3^-$and CO_3^{2-} can be written as

$$T_C = 2[CO_3^{2-}] + [HCO_3^-] \quad (1.14)$$

$HCO_3^- \leftrightarrow CO_3^{2-}$ equilibria:

$$HCO_3^- \Longleftrightarrow CO_3^{2-} + H^+ \quad (1.15)$$

The K_2 value of 4.69 × 10^{-11} was taken from Plummer and Busenberg's study (Busenberg, 1982). The K value depends on the temperature as well as ion complexes formed between the carbonic ions and molecules (Ex. $CaCO_3$, $MgCO_3$, etc.). Furthermore, ions in the solution obstruct the dissolved carbonic molecules and ions to take part in the thermodynamic equilibrium reactions. Therefore, in the thermodynamic equation (Eq. 1.16), the concentrations have to be replaced by their activities, which are smaller than the concentrations. For the calculation of thermodynamic equilibrium constant (K_2') in Eq.1.17, an iterative method was utilized. At a specific pH value, using K_2 (4.69 × 10^{-11}) as K_2' and assuming activity coefficients of H^+, $HCO_3^-$and CO_3^{2-} were equal to one, $HCO_3^-$and CO_3^{2-} concentrations were calculated as a first step of the iteration (Eq. 1.19 and 1.20). By utilizing, those $HCO_3^-$and CO_3^{2-} concentrations to calculate new ionic strength and new activities of H^+, $HCO_3^-$and CO_3^{2-}, K_2' was recalculated with Eq. 1.17. Then by using that K_2', $HCO_3^-$and CO_3^{2-} concentrations were calculated again and used to calculated new K_2'. This process was repeated until the difference between the input

K_2' and newly calculated K_2' become minimal.

$$K_2' = \frac{\gamma_{(CO_3^{2-})}[CO_3^{2-}] \times \gamma_{(H^+)}[H^+]}{\gamma_{(HCO_3^-)}[HCO_3^-]} \quad (1.16)$$

$$K_2 = \frac{[CO_3^{2-}] \times [H^+]}{[HCO_3^-]} = \frac{\gamma_{(HCO_3^-)}}{\gamma_{(CO_3^{2-})}\gamma_{(H^+)}} K_2' \quad (1.17)$$

Where: γ represents the activity coefficients and it can be calculated with the Debye–Hückel equation defined for the solutions having ionic strength <0.1 at temperature 25 ^{0}C (Eq. 1.18).

$$-log(\gamma_x) = \frac{(0.51 \times Z_x^2 \times \sqrt{\mu})}{1 + (3.3 \times \alpha_x \times \sqrt{\mu})} \quad (1.18)$$

Where:

$Z_x = Charge\ of\ the\ ion$

α_x =Effective diameter of the hydrated ion in nanometers (Table 1. 2)(Morse and Mackenzie, 1990)

$\mu = Ionic\ strength\ of\ the\ solution = \frac{1}{2}\Sigma([x] \times Z_x^2)$

$[x] = Concentration\ of\ the\ ion\ (mol/L)$

Table 1. 2: Effective diameter of the ions(Morse and Mackenzie, 1990)

Ion	**F^-**	**Cl^-**	**Na^+**	**Mg^{2+}**	**Ca^{2+}**	**CO_3^{2-}**	**HCO_3^-**	**OH^-**	**H^+**
Charge (Z_x)	-1	-1	1	2	2	-2	-1	-1	1
Effective diameter (nm)	0.35	0.3	0.45	0.8	0.6	0.45	0.45	0.35	0.9

Combining Eq. 1.14 and Eq. 1.17:

$$[HCO_3^-] = \frac{T_C}{1 + \left(\frac{2K_2}{[H^+]}\right)} = \frac{T_C}{1 + \left(\frac{2\frac{\gamma_{(HCO_3^-)}}{\gamma_{(CO_3^{2-})}\gamma_{(H^+)}}K_2'}{[H^+]}\right)} (mol/L) \quad (1.19)$$

By rearranging Eq. 1.17

$$[CO_3^{2-}] = \frac{K_2[HCO_3^-]}{[H^+]} = \frac{\frac{\gamma_{(HCO_3^-)}}{\gamma_{(CO_3^{2-})}\gamma_{(H^+)}}K_2'\,[HCO_3^-]}{[H^+]} (mol/L) \quad (1.20)$$

For the determination of ion activity product (IAP), thermodynamic equilibrium reactions were employed (Eq. 1.21 and 1.22). For different ionic strengths, thermodynamic $Ksp\,'$ value is calculated with Eq 1.23. Respective ion activities were calculated by using Eq. 1.18.

$$A(s) \Longleftrightarrow bB(aq) + dD(aq) \tag{1.21}$$

$$IAP(A) = [\gamma_B B(aq)]^b [\gamma_D D(aq)]^d \tag{1.22}$$

Where:

A= Solid species formed

B, D= Ion concentration (mol/L)

b, d= B, D aqueous species stoichiometric number

Thermodynamic solubility constant A species in its saturation level can be expressed as $IAP(A)$= $Ksp\,'(A)$

$$Ksp\,'(A) = [\gamma_B B(aq)]^b [\gamma_D D(aq)]^d$$

$$= \gamma_B^b \gamma_D^d [B(aq)]^b\ [D(aq)]^d = \gamma_B^b \gamma_D^d Ksp(A) \tag{1.23}$$

Where:

Ksp (A)= Theoretical solubility constant of A

In the ELC reactors, when Cl^- is present, Cl_2 (g) is produced in the anode by consuming electrons. Therefore, electrons involved in the ELC of water should be calculated by reducing the removed Cl^- (mol/L) (from both anode and cathode) from introduced electrons (mol/L). Accordingly, the amount of OH^- and H^+ introduced can be calculated with equation 1.24.

$$OH^-/H^+\ introduced\ \left(\frac{mol}{L}\right)$$

$$= \frac{Charge\ Loading\left(\frac{C}{L}\right)}{Faraday\ constant(96485)(C/mol)}$$

$$- Total\ Cl\ removed\ from\ both\ anode\ and\ cathode\ \left(\frac{mol}{L}\right) \tag{1.24}$$

3 Results and discussion

3.1 Effect of charge loading on ion-removal efficiencies and plausible ion-removal pathways

After three hours of stabilization time, the water outflow rates from the anode and from the cathode were measured. It was found that the flow through the diaphragm was negligible. Electrolysis time or charge loading (A/(L/s)=C/L) is the key parameter that affects ion removal efficiencies. According to the conditions shown in Table 1. 1, electrolysis experiments were performed with artificial groundwater. Fig. 1.4 illustrates the variations of F^-, Cl^-, Na^+, Mg^{2+}, Ca^{2+}, and (HCO_3^-+ CO_3^{2-}) removal percentages for the cathode (Fig. 1.4a), the anode (Fig. 1.4 b), and particular pH variations in the anode and in the cathode (Fig. 1.4 c) over the charge loading. The calculated K_2' values are shown in Table 1. 3. and were used to calculate (HCO_3^-+ CO_3^{2-}) concentrations in the anode and the cathode.

According to Figure 1.4, increasing charge loading resulted in higher removals of F^-, Mg^{2+}, Ca^{2+}, as precipitates (Eq. 1.3-1.12) with increased OH^- productions. However, charge loading higher than 1250 C/L showed a slight influence on the F^-, Mg^{2+}, Ca^{2+}, Cl^- and (HCO_3^-+ CO_3^{2-}) removals. The highest F^-, Mg^{2+}, Ca^{2+}, Cl^- and (HCO_3^-+ CO_3^{2-}) removals of 65, 96, 44, 36 and 36%, respectively, were achieved at 1500C/L. Hence, 1500 C/L was used for further experiments. The removal of HCO_3^-+ CO_3^{2-} in the cathode could have resulted from the formation of $CaCO_3$ and $MgCO_3$.

Moreover, the positive removal of Cl^- and negative removal of Na^+ can be observed in the cathode. The positive and negative removal of the $Cl^-$and Na^+ ions in the cathode was obviously due to Coulomb force transfer to the anode and transfer from the anode. However, the difference between Cl^- removal in the cathode and the anode was increased from 1 to 7 % for 250 to 1500 C/L, respectively. With ion chromatographic analysis, the presence of the OCl^- ion was confirmed; thus, Cl^- was removed as Cl_2 (g) in the anode, which caused a 1–7 % difference in Cl^- in the anode-

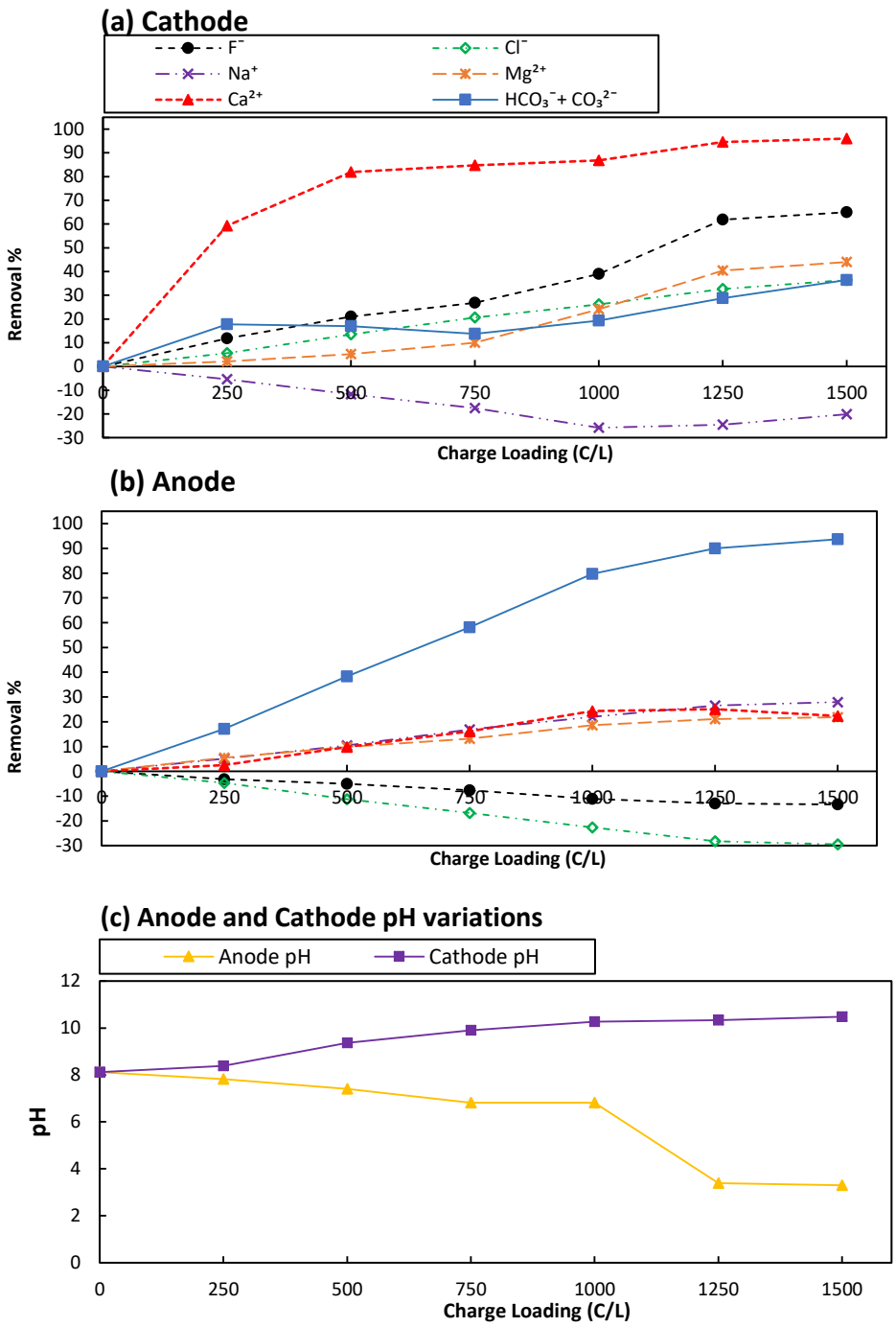

Fig. 1. 4: Influence of the charge loading in the electrolytes on the ion removal percentage and the pH. (a) Cathode, (b) Anode, (c) pH variation; F^-_0 = 10 mg/L, Ca^{2+}_0 = 100 mg/L, Mg^{2+}_0 = 100 mg/L, and $(HCO_3^- + CO_3^{2-})_0$ = 10 mmol/L.

Table 1. 3: Iteratively calculated K_2' (mol/L) and respective ionic strength of the solution

	Charge loading (C/L)	**K_2'**	**The ionic strength of the solution**
Raw Water	0	1.37×10^{-11}	0.61
Anode	250	1.40×10^{-11}	0.058
	500	1.45×10^{-11}	0.054
	750	1.50×10^{-11}	0.051
	1000	1.56×10^{-11}	0.048
	1250	1.47×10^{-11}	0.047
	1500	1.56×10^{-11}	0.048
Cathode	250	1.48×10^{-11}	0.052
	500	1.53×10^{-11}	0.050
	750	1.53×10^{-11}	0.051
	1000	1.57×10^{-11}	0.051
	1250	1.67×10^{-11}	0.045
	1500	1.70×10^{-11}	0.044

-and the cathode for 250 to 1500 C/L, respectively. Na^+ transferred from the anode to cathode as a result of the Coulomb force was equal to the increment of Na^+ in the cathode. Therefore, Na^+ was not removed by the system in any form.

The amount of precipitation of each species depends on the solubility product (Ksp) of each compound. Accordingly, thermodynamic K'sp values and the ion activity products (IAP) of $Mg(OH)_2$, $Ca(OH)_2$, $CaCO_3$, $MgCO_3$, CaF_2, and MgF_2 were calculated with the equation 1.22 and 1.23, and the results for the cathode solution are shown in Table 1. 4. When the IAP value is higher than the K'sp, precipitation is taken place. The IAP value of $Ca(OH)_2$ was lower than K'sp-$Ca(OH)_2$ for 0-1500 C/L, indicating that $Ca(OH)_2$ formation was not plausible in the ELC system. $CaCO_3$ formation was plausible in 250-1500 C/L range since the IAP of $CaCO_3$ was higher than K'sp-$CaCO_3$. The IAP value of $Mg(OH)_2$ increased with increasing charge loading thus precipitation of $Mg(OH)_2$ increased with increasing charge loading. $MgCO_3$ was found very much closer to the equilibrium (Ksp-$MgCO_3$=IAP-$MgCO_3$) for 500-1500 C/L. Even though MgF_2 and CaF_2 IAP values showed oversaturated or very much closer to the equilibrium conditions, XRD analysis of precipitate (Fig.1.5) revealed that MgF_2 and CaF_2 were not present. On the other hand, lower removal of F^- with respect to higher removal of Ca^{2+} and Mg^{2+} confirmed that MgF_2 and CaF_2

could not be formed in the system. However, the cause of such a deviation from the calculation could be F^- transfer due to the Coulomb force. Therefore, even in equilibrium conditions, Ca^{2+}, Mg^{2+} ions could still be precipitated as $Mg(OH)_2$, $CaCO_3$, and $MgCO_3$.

Furthermore, the XRD analysis performed for the precipitates collected from the cathode for 1500, 1250 and 1000 C/L showed the presence of $CaCO_3$, $MgCO_3$, and $Mg(OH)_2$ (Fig. 1.5).The predominant mineral phase of $CaCO_3$ found was calcite; nevertheless, aragonite mineral phase existed significantly. In comparison, XRD peak intensities of $CaCO_3$ and $MgCO_3$ increased with the increasing charge loading; thus, crystallinity seems to be increased. The intensity of $Mg(OH)_2$ peaks increased with the increasing charge loading and it is evident that the increased formation $Mg(OH)_2$ was caused by increased OH^- generation. Obviously, lower removal of Ca^{2+} at lower charge loading caused by lower formation CO_3^{2-} ion due to the lower production of OH^- (Fig. 1.4b).

Table 1. 4: saturation status and calculated equilibrium concentrations

Theoretical Saturation Indices (Ksp)						
	$CaCO_3$ $(mol/L)^2$	**$Ca(OH)_2$ $(mol/L)^3$**	**CaF_2 $(mol/L)^3$**	**$MgCO_3$ $(mol/L)^2$**	**$Mg(OH)_2$ $(mol/L)^3$**	**MgF_2 $(mol/L)^3$**
	3.31×10^{-9}	5.02×10^{-6}	3.45×10^{-11}	6.82×10^{-6}	1.82×10^{-11}	5.16×10^{-11}
Thermodynamic Saturation Indices (Ksp)						
C/L	**$CaCO_3$ $(mol/L)^2$**	**$Ca(OH)_2$ $(mol/L)^3$**	**CaF_2 $(mol/L)^3$**	**$MgCO_3$ $(mol/L)^2$**	**$Mg(OH)_2$ $(mol/L)^3$**	**MgF_2 $(mol/L)^3$**
250	4.43×10^{-10}	8.65×10^{-7}	5.94×10^{-12}	8.45×10^{-7}	2.90×10^{-12}	8.22×10^{-12}
500	4.63×10^{-10}	8.99×10^{-7}	6.18×10^{-12}	8.84×10^{-7}	3.02×10^{-12}	8.56×10^{-12}
750	4.54×10^{-10}	8.84×10^{-7}	6.07×10^{-12}	8.67×10^{-7}	2.97×10^{-12}	8.41×10^{-12}
1000	4.56×10^{-10}	8.86×10^{-7}	6.09×10^{-12}	8.70×10^{-7}	2.98×10^{-12}	8.44×10^{-12}
1250	5.06×10^{-10}	9.70×10^{-7}	6.66×10^{-12}	9.67×10^{-7}	3.27×10^{-12}	9.26×10^{-12}
1500	5.17×10^{-10}	9.89×10^{-7}	6.80×10^{-12}	9.91×10^{-7}	3.33×10^{-12}	9.45×10^{-12}
Ion Activity Product (IAP)						
C/L	**$CaCO_3$ $(mol/L)^2$**	**$Ca(OH)_2$ $(mol/L)^3$**	**CaF_2 $(mol/L)^3$**	**$MgCO_3$ $(mol/L)^2$**	**$Mg(OH)_2$ $(mol/L)^3$**	**MgF_2 $(mol/L)^3$**
250	4.14×10^{-9}	1.06×10^{-15}	3.79×10^{-11}	1.47×10^{-8}	3.79×10^{-15}	1.35×10^{-10}
500	1.81×10^{-8}	4.27×10^{-14}	1.40×10^{-11}	1.41×10^{-7}	3.32×10^{-13}	1.09×10^{-11}
750	4.99×10^{-8}	4.26×10^{-13}	9.99×10^{-12}	4.37×10^{-7}	3.73×10^{-12}	8.74×10^{-11}
1000	8.42×10^{-8}	2.03×10^{-12}	6.01×10^{-12}	7.19×10^{-7}	1.73×10^{-11}	5.13×10^{-11}
1250	3.97×10^{-8}	1.21×10^{-12}	1.06×10^{-12}	6.44×10^{-7}	1.97×10^{-11}	1.72×10^{-11}
1500	3.38×10^{-8}	1.78×10^{-12}	6.70×10^{-13}	7.29×10^{-7}	3.84×10^{-11}	1.45×10^{-11}

Concluded from the results, 1500 C/L charge loading was only good enough to remove the Ca^{2+} from the cathode to meet the WHO and Sri Lankan water quality guidelines for the drinking water. Conversely, at 500C/L, HCO_3^-+CO_3^{2-} removal in the anode comply with both WHO and Sri Lankan water quality guidelines. If the initial concentrations of F^-, Mg^{2+} and HCO_3^-+CO_3^{2-}, were lower than the experimental concentrations used in this section, there is a higher probability of meeting the drinking water quality guidelines for F^-, Mg^{2+} as well as HCO_3^-+CO_3^{2-} in the cathode. However, in prior to applying the proposed ELC system in real conditions, output water quality from the cathode should be estimated. Nevertheless, a clear picture of the ion removal mechanism and ion removal efficiencies cannot be established from the discussed results. Accordingly, mathematical model development (section 3.3) and ELC experiment for different initial concentrations as described in sections 3.5 - 3.9 were performed.

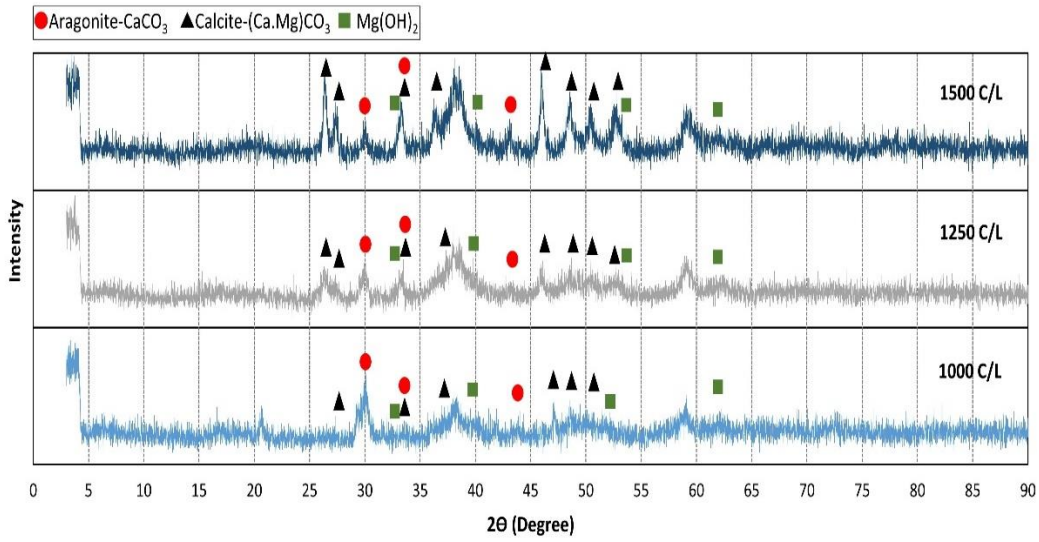

Fig. 1.5: XRD patterns of precipitates collected from various C/Ls

3.2 Fluoride removal pathways

With the results of section 3.1, F^- removal mechanisms in the cathode can be recognized in two ways. The first mechanism was F^- transferring to the anode by Coulomb's force, which can be seen as the negative removal of F^- in the anode (Fig. 1.4b). The second mechanism of F^- removal is precipitation, which could occur in

different ways. The absence of MgF_2 and CaF_2 peaks in XRD revealed that fluoride could only be removed by either adsorption or co-precipitation with the predominantly formed $CaCO_3$, $MgCO_3$, and $Mg(OH)_2$. Turner (2005) reported that $CaCO_3$ has a high affinity for removing F^- ion by surface adsorption dependent on the $CaCO_3$ surface area. Furthermore, Masindi (2015) investigation suggested that cryptocrystalline $MgCO_3$ could effectively remove F^- by adsorption(Masindi et al., 2015; Turner et al., 2005).

Since our experimental conditions in the ELC with high pH were different from those studies, the possibility of adsorptive F^- removal at high pH was verified with an adsorptive experiment. To perform the adsorptive removals of F^- by Ca^{2+} and Mg^{2+} forming precipitates in ELC, precipitates were generated under the experiment conditions listed in Table 1. 1 as Isotherm_1. The adsorption isotherm for ELC prepared precipitate was presented in Fig. 1.6, and the Freundlich isotherm was found to be the best fit. In Fig. 1.6, C is F^- concentration in the solution expressed in a unit of mg/L. Q is the adsorption capacity (mg/g) at a specific concentration of F^-. According to the Freundlich isotherm, the F^- adsorption capacity was 0.60 mg/g at the F^- concentration of 3.52 mg/L. Obviously, Ca^{2+} and Mg^{2+} were removed from the cathode cell occurred by precipitation as $CaCO_3$, $MgCO_3$, and $Mg(OH)_2$. If we assume, at 1500 C/L charge loading Ca^{2+} and Mg^{2+} were removed either as $CaCO_3$ +$MgCO_3$ or $CaCO_3$+ $Mg(OH)_2$, and F^- was removed only by adsorption, F^- adsorption can be calculated as 8.15 and 9.42 mg/g respectively. Those calculated adsorption capacities were much higher than the Freundlich isotherm, given the F^- adsorption capacity of 0.60 mg/g. Therefore, the fraction of F^- adsorbed by a mixture of $CaCO_3$, $MgCO_3$, and $Mg(OH)_2$ was not significant. Accordingly, the co- precipitative F^- removal mechanism should be taken into account for the ELC.

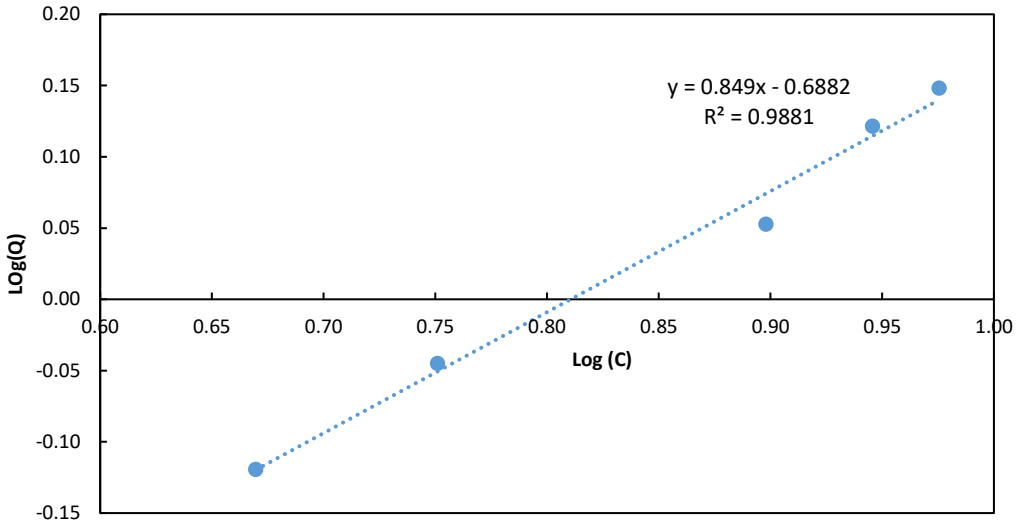

Fig. 1.6: Freundlich adsorption isotherm for the precipitate collected from ELC without F^-

Kawakami proposed that F^- co-precipitation occurred by $Mg(OH)_2$ (Kawakami et al., 2018). Besides, previous studies of the de-fluoridation of water using nano-magnesium oxide suggested that F^- exchange between $Mg(OH)_2$'s OH^- and F^- could take place due to the similar radius of F^- and OH^- (Devi et al., 2012; Oladoja et al., 2016), and the co-precipitation mechanism for F^- removal by $Mg(OH)_2$ was proposed by Devi et al (2012) (Devi et al., 2012).

To verify the F^- removal by the adsorption by ELC prepared $Mg(OH)_2$, an isotherm experiment was performed for the precipitate generated in the absence of F^-, HCO_3^-+CO_3^{2-} and Ca^{2+} under the experiment conditions listed in Table 1. 1, Isotherm_2. The isotherm experiment showed insignificant adsorption of F^-. This adsorption was negligible compared to the actually removing F^- by the ELC system discussed in section 3.1. Furthermore, for the precipitate prepared in the absence of F^-, and Mg^{2+} under the experiment conditions listed in Table 1. 1, Isotherm_3, confirmed that $CaCO_3$ could not remove the F^- by adsorption. Therefore, the only mechanism of F^- removal was co-precipitation with $Mg(OH)_2$. Accordingly, F^-

removal mainly took place by co-precipitation with $Mg(OH)_2$ other than the slight adsorption to the $CaCO_3$ +$MgCO_3$ and $Mg(OH)_2$ mixture, and by Coulomb transfer to the anode. A mathematical model to describe the molar relationship between Mg^{2+} and F^- precipitated in section 3.3 was discussed.

3.3 Mathematical model of the ELC system for ion removal in the cathode

3.3.1 Mg^{2+}, Ca^{2+}, H_2CO_3+HCO_3^-+CO_3^{2-} ion removal model development and validation

As described in sections 3.1 and 3.2, the establishment of a mathematical model was required to propose the ion removal mechanism as well as to estimate the ion removals based on the initial ion concentrations. The model output results can be used to design the system as well as the operational conditions required to meet the desired water quality guideline. Therefore, a mathematical model was derived as described below.

Carbonate equilibrium reactions and dissociation constants

In the presence of gaseous CO_2, dissolved CO_2 exchanges with CO_2 gas (Eq. 1.25) and converted to $H_2CO_3(aq)$ ion (Eq. 1.26).

$$CO_2(g) \Longleftrightarrow CO_2(aq) \qquad (1.25)$$

$$CO_2(aq) + H_2O \Longleftrightarrow H_2CO_3(aq) \qquad (1.26)$$

However, the concentration of $CO_2(aq)$ far exceeds that of dissolved $H_2CO_3(aq)$ thus, the concentration of dissolved $CO_2(aq)$ can be denoted as $H_2CO_3{}^*(aq) = [(H_2CO_3(aq) + CO_2(aq)]$.

The equilibrium condition between the phase is expressed by the molar solubility K_H (Eq. 1.27) (henry's law).

$$\frac{\gamma_{H_2CO_3{}^*}[H_2CO_3{}^*]}{[P_{Co2}]} = K_H \qquad (1.27)$$

$$\frac{[H_2CO_3{}^*]}{[P_{Co2}]} = K_H/\gamma_{H_2CO_3{}^*} \qquad (1.28)$$

Where:

P_{Co2} = atmospheric partial pressure of $CO_2(g)$

K_H =solubility (mol/L)

$\gamma_{H_2CO_3{}^*}$=Activity of the $H_2CO_3{}^*$ in the solution

In the presence of hydroxyl ion, $H_2CO_3{}^*$ is converted to $HCO_3{}^-(aq)$(Eq. 1.29) and $HCO_3{}^-(aq)$ is converted to $CO_3{}^{2-}(aq)$ as shown in Eq. 1.30

$$H_2CO_3{}^*(aq) + OH^- \Longleftrightarrow HCO_3{}^-(aq) + H_2O\ (l) \qquad (1.29)$$

$$HCO_3{}^-(aq) + OH^-(aq) \Longleftrightarrow CO_3{}^{2-}(aq) + H_2O(l) \qquad (1.30)$$

Thus, the dissociation constants of $H_2CO_3{}^*(aq)$and $HCO_3{}^-(aq)$ can be written as Eq. 1.31and Eq. 1.32, respectively.

$$\frac{\gamma_{HCO_3^-}[HCO_3^-]}{\gamma_{H_2CO_3{}^*}[H_2CO_3{}^*]\gamma_{OH^-}[OH^-]} = K_1' = 10^{-6.38}\ /K_w$$

$$\frac{[HCO_3^-]}{[H_2CO_3{}^*][OH^-]} = (K_1'.\gamma_{OH^-}.\gamma_{H_2CO_3{}^*})\ /\gamma_{HCO_3^-} = K_1 \qquad (1.31)$$

and

$$\frac{\gamma_{CO_3^{2-}}[CO_3^{2-}]}{\gamma_{HCO_3^-}[HCO_3^-]\gamma_{OH^-}[OH^-]} = K_2' = 4.68 \times 10^3 \text{ (Plummer and Busenberg, 1982)}$$

$$\frac{[CO_3^{2-}]}{[HCO_3^-][OH^-]} = (K_2'\ .\gamma_{OH^-}.\gamma_{HCO_3^-}\ )/\gamma_{CO_3^{2-}} = K_2 \qquad (1.32)$$

Where:

$K_w' = \gamma_{OH^-}[OH^-].\gamma_{H^+}[H^+] = 10^{-14}$

$[OH^-].[H^+] = K_w'/(\gamma_{H^+}.\gamma_{OH^-}) = K_w$

And

$\gamma_{OH^-}, \gamma_{H^+}, \gamma_{HCO_3^-}$ and $\gamma_{CO_3^{2-}}$ were activity coefficients of OH^-, H^+, HCO_3^- and CO_3^{2-}, respectively.

Formation of $CaCO_3$

$CaCO_3$ formation was expressed in Eq. 1.33 and its solubility product constant can be expressed as Eq. 1.34. Ksp'_{CaCO3}, Ksp'_{MgCO3} and $Ksp'_{Mg(OH)_2}$ were taken from the Michałowska and Asuero, 2012 study.

$$Ca^{2+}(aq) + {CO_3}^{2-}(aq) \Longleftrightarrow CaCO_3(s) \qquad (1.33)$$

$$\gamma_{Ca^{2+}}[Ca^{2+}]\gamma_{CO_3^{2-}}[CO_3^{2-}] = Ksp'_{CaCO3} = 10^{-8.48}$$

$$[Ca^{2+}][CO_3^{2-}] = Ksp'_{CaCO3} \ /(\gamma_{Ca^{2+}}.\gamma_{CO_3^{2-}}) = Ksp_{CaCO3} \qquad (1.34)$$

Formation of $MgCO_3$

$MgCO_3$ formation was expressed in Eq. 1.35 and its solubility product constant can be expressed as Eq. 1.36

$$Mg^{2+}(aq) + {CO_3}^{2-}(aq) \Longleftrightarrow MgCO_3(s) \qquad (1.35)$$

$$\gamma_{Mg^{2+}}[Mg^{2+}]\gamma_{CO_3^{2-}}[CO_3^{2-}] = Ksp'_{MgCO3} = 10^{-7.46}$$

$$[Mg^{2+}][CO_3^{2-}] = Ksp'_{MgCO3} \ /(\gamma_{Mg^{2+}}.\gamma_{CO_3^{2-}}) = Ksp_{MgCO3} \qquad (1.36)$$

Formation of $Mg(OH)_2$

$Mg(OH)_2$ formation was expressed in Eq. 1.37 and its solubility product constant can be expressed as Eq. 1.38

$$Mg^{2+}(aq) + OH^-(aq) \Longleftrightarrow Mg(OH)_2(s) \qquad (1.37)$$

$$\gamma_{Mg^{2+}}[Mg^{2+}](\gamma_{OH^-}[OH^-])^2 = Ksp'_{Mg(OH)_2} = 10^{-10.74}$$

$$[Mg^{2+}][OH^-]^2 = Ksp'_{Mg(OH)_2} \ /(\gamma_{Mg^{2+}}.(\gamma_{OH^-})^2) = Ksp_{Mg(OH)_2} \quad (1.38)$$

Where: $\gamma_{Mg^{2+}}, \gamma_{Ca^{2+}}$ are the activity coefficients of Mg^{2+}, Ca^{2+}

For activity coefficient calculations, Extended Debye–Hückel equation (Eq.1.18) was employed.

Mg^{2+}Mass balance

The mass balance equation for Mg^{2+} in the cathode can be written as Eq. 1.39

$$(Mg^{2+})_0 = (Mg^{2+}) + (Mg(OH)_2)_{ppt} + (MgCO_3)_{ppt}$$

$$(Mg^{2+}) = (Mg^{2+})_0 - (Mg(OH)_2)_{ppt} - (MgCO_3)_{ppt} \qquad (1.39)$$

Where:

$(Mg^{2+})_0$ is the amount of initial Mg^{2+}

(Mg^{2+}) is the concentration of Mg^{2+} in the cathode after the ELC treatment

$(Mg(OH)_2)_{ppt}$ is the amount of Mg^{2+} precipitated as $Mg(OH)_2$ in the cathode

$(MgCO_3)_{ppt}$ is the amount of Mg^{2+} precipitated as $MgCO_3$ in the cathode

Ca^{2+}Mass balance

The mass balance equation for Ca^{2+} can be written as Eq. 1.40

$$(Ca^{2+})_0 = (Ca^{2+}) + (Ca(OH)_2)_{ppt} + (CaCO_3)_{ppt} \qquad (1.40)$$

Since $Ca(OH)_{2ppt}$ was not detected in the XRD analysis, Eq. 1.40 can be rearranged as Eq. 1.41

$$(Ca^{2+}) = (Ca^{2+})_0 - (CaCO_3)_{ppt} \qquad (1.41)$$

Where:

$(Ca^{2+})_0$ is the amount of initial Ca^{2+}

$(CaCO_3)_{ppt}$ is the amount of Ca^{2+} precipitated as $CaCO_3$ in the cathode

Carbon Mass balance

For the closed system, the mass balance of the C ion expressed as Eq 1.42

$$(H_2CO_3^*)_0 + (CO_3^{2-})_0 + (HCO_3^-)_0 = (H_2CO_3^*) + (CO_3^{2-}) + (HCO_3^-) + (MgCO_3)_{ppt} + (CaCO_3)_{ppt} \qquad (1.42)$$

OH^- Mass balance

The mass balance of the OH^- ion can be expressed as Eq. 1.43

$$(OH^-)_0 = OH^- + HCO_3^- \; converted \; to \; CO_3^{2^-} + H_2CO_3^* \; converted \; to \; HCO_3^- + 2.Mg(OH)_{2ppt} + 2.Ca(OH)_{2ppt} \quad (1.43)$$

Where:

(OH^-) is an equilibrium concentration of OH^-(mol/L)

$(H_2CO_3^*)_0, (CO_3^{2^-})_0, (HCO_3^-)_0$, are initial ion amounts

$(OH^-)_0$ is introduced OH^- amount.

since $Ca(OH)_{2ppt}$ was not detected in the XRD analysis, Eq 1.43 can be rearranged as Eq. 1.44

$$(OH^-)_0 = OH^- + (HCO_3^-)_0 - (HCO_3^-) + (H_2CO_3^*)_0 - (H_2CO_3^*) + 2.(Mg(OH)_{2ppt}) \quad (1.44)$$

By combining Eq. 1.39 and Eq. 1.41 Eq. 1.45 is obtained

$$\left(MgCO_3\right)_{ppt} + \left(CaCO_3\right)_{ppt} = (Mg^{2+})_0 + (Ca^{2+})_0 - \left(Mg^{2+}\right) - \left(Ca^{2+}\right) - (Mg(OH)_2)_{ppt} \quad (1.45)$$

Subtracting Eq. 1.42 from Eq. 1.45 Eq. 1.46 is obtained

$$(Mg(OH)_2)_{ppt} = (Mg^{2+})_0 + (Ca^{2+})_0 - (H_2CO_3^*)_0 - (HCO_3^-)_0 - (CO_3^{2^-})_0 + (H_2CO_3^*) + (HCO_3^-) + (CO_3^{2^-}) - (Mg^{2+}) - (Ca^{2+}) \quad (1.46)$$

By using OH^- mass balance of Eq.1.43 and Eq1.46, Eq. 1.47 is obtained

$$(Mg(OH)_2)_{ppt} = (Mg^{2+})_0 + (Ca^{2+})_0 - (H_2CO_3^*)_0 - (HCO_3^-)_0 - (CO_3^{2^-})_0 + (H_2CO_3^*) + (HCO_3^-) + (CO_3^{2^-}) - (Mg^{2+}) - (Ca^{2+}) \quad (1.47)$$

Subtracting Eq. 1.43 from Eq. 1.47 Eq. 1.48 is obtained

$$0 = 2(Mg^{2+})_0 + 2(Ca^{2+})_0 - (OH^-)_0 - (H_2CO_3^*)_0 - (HCO_3^-)_0 - 2(CO_3^{2-})_0 + OH^- + (H_2CO_3^*) + (HCO_3^-) + 2(CO_3^{2-}) - 2(Mg^{2+}) - 2(Ca^{2+}) \quad (1.48)$$

Substituting $(Mg^{2+}), (Ca^{2+}), (H_2CO_3^*)$ *and* (HCO_3^-) from Eq.1.34, 1.38,1.31 and 1.32 to Eq. 1.48 we can obtain Eq. 1.49

$$0 = 2(Mg^{2+})_0 + 2(Ca^{2+})_0 - (OH^-)_0 - (H_2CO_3^*)_0 - (HCO_3^-)_0 - 2\,(CO_3^{2-})_0 + (OH^-) + \frac{CO_3^{2-}}{K_1K_2(OH^-)^2} + \frac{CO_3^{2-}}{K_2(OH^-)} + 2(CO_3^{2-}) - \frac{2.Ksp_{Mg(OH)_2}}{(OH^-)^2} - \frac{2.Ksp_{CaCO3}}{CO_3^{2-}} \quad (1.49)$$

Assuming $(MgCO_3)_{ppt}$ is negligible, and rearranging Eq. 1.42, by substituting, $(Ca^{2+})(H_2CO_3^*)$ *and* (HCO_3^-) from Eq.1.38, Eq. 1.31 and Eq. 1.32 Eq. 1.50 is obtained.

$$0 = (Ca^{2+})_0 - (H_2CO_3^*)_0 - (HCO_3^-)_0 - (CO_3^{2-})_0 + \frac{CO_3^{2-}}{K_1K_2(OH^-)^2} + \frac{CO_3^{2-}}{K_2(OH^-)} + (CO_3^{2-}) - \frac{Ksp_{CaCO3}}{CO_3^{2-}} \quad (1.50)$$

Eq. 1.49 and Eq.1.50 have two unknowns CO_3^{2-} and OH^-, therefore it can be solved for both CO_3^{2-} and OH^- concentrations iteratively. By using calculated OH^- and solubility product Eq. 1.38, the equilibrium concentration of (Mg^{2+}) can be calculated.

For the validation of the model, the data obtained from the chemical precipitation experiment were used. The initial concentrations used for F^-_0, Mg^{2+}_0, Ca^{2+}_0 and $(H_2CO_3^*+HCO_3^-+CO_3^{2-})_0$ were 10mg/L, 100mg/L, 100mg/L and 10mmol/L, respectively. Experiments were performed in a glass beaker and Nitrogen gas was continuously bubbled to ensure no dissociation of the atmospheric CO_2 gas. While F^-,

Mg^{2+} $Ca^{2+}$and (H_2CO_3*+HCO_3^-+CO_3^{2-}) spiked distilled water was stirring, 0.5 N NaOH was added with the micropipette. After the 5 minutes of stabilizing time pH level was recorded and 20 mL of the sample was collected into the airtight plastic bottle. The same procedure was repeated and the samples were kept for 24 hours to settle the precipitate. After 24 hours, samples were filtered with a 0.45 µm membrane filter and analyzed with the ion chromatograph.

Calculated and measured Mg^{2+} concentrations in the addition of OH^- are shown in Fig. 1.7. According to Fig. 1.7, the measured Mg^{2+} concentration deviated significantly from the model calculated Mg^{2+} concentration for OH^- concentration of less than 0.0063 mol/L. The model was derived based on the Ksp of $Mg(OH)_2$ by assuming the solution was saturated from the beginning (OH_0^-=0mol/L). However, in the experiment $Mg(OH)_2$ was under-saturated at lower charge loadings. Under-saturation occurred due to the rapid reaction of OH^- with HCO_3^- to form CO_3^{2-} and to be precipitated with Ca^{2+} as $CaCO_3$ and $MgCO_3$. Therefore, model calculations for the Mg^{2+} concentration only valid in the region where $Mg(OH)_2$ starts its saturation. According to Fig. 1.7, for the OH^-_0 concentration less than 0.005 mmol/L, the model calculated Mg^{2+} concentration was similar to the measured Mg^{2+} concentration. Therefore, it can be concluded that the model can be used only for the OH^-_0 concentration of less than 0.005mmol/L.

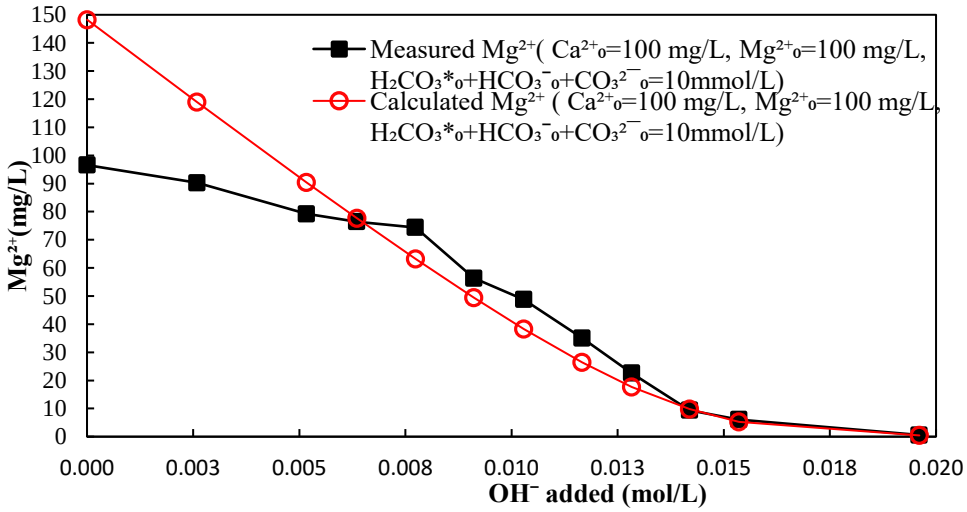

Fig. 1. 7: Measured and calculated Mg^{2+} concentration in the solution

Furthermore, XRD analysis results of the chemical precipitation discussed in section 3.1 revealed that the removal of Mg^{2+} was occurred by the formation of $MgCO_3$ in the $0<OH_0^-=6.3$ mmol/L. Therefore, the slight deviation between measured and model-calculated Mg^{2+} concentration observed caused by the assumption of "$MgCO_3$ formation was negligible". However, without the assumption "$MgCO_3$ formation was negligible", a model derivation was impossible. Accordingly, the F^- removal model utilized the Mg^{2+} concentrations only for OH^-_0 higher than 0.005 mol/L

Furthermore, measured and calculated Ca^{2+} and $H_2CO_3^*+HCO_3^-+CO_3^{2-}$ concentrations were shown in Fig. 1.8a and b. Calculated Ca^{2+} concentrations were approximately similar to the measured Ca^{2+} concentrations for the added $OH_0^->0.005$ mol/L. This is caused due to the model assumption of $Mg(OH)_2$ saturation, even in the OH^- concentrations lower than the saturation level of $Mg(OH)_2$. Furthermore, XRD data shows the formation of $MgCO_3$ and we have neglected its formation in the model calculation due to quantity of $MgCO_3$ formed at higher pH levels were negligible compared to $Mg(OH)_2$ formation. Therefore, calculated and measured $H_2CO_3^*+HCO_3^-+CO_3^{2-}$ were slightly different (Fig. 1.8b). However, the model

provides equitable approximations for the Mg^{2+} and Ca^{2+} concentrations while providing reasonable approximation for the $H_2CO_3^*+HCO_3^-+CO_3^{2-}$.

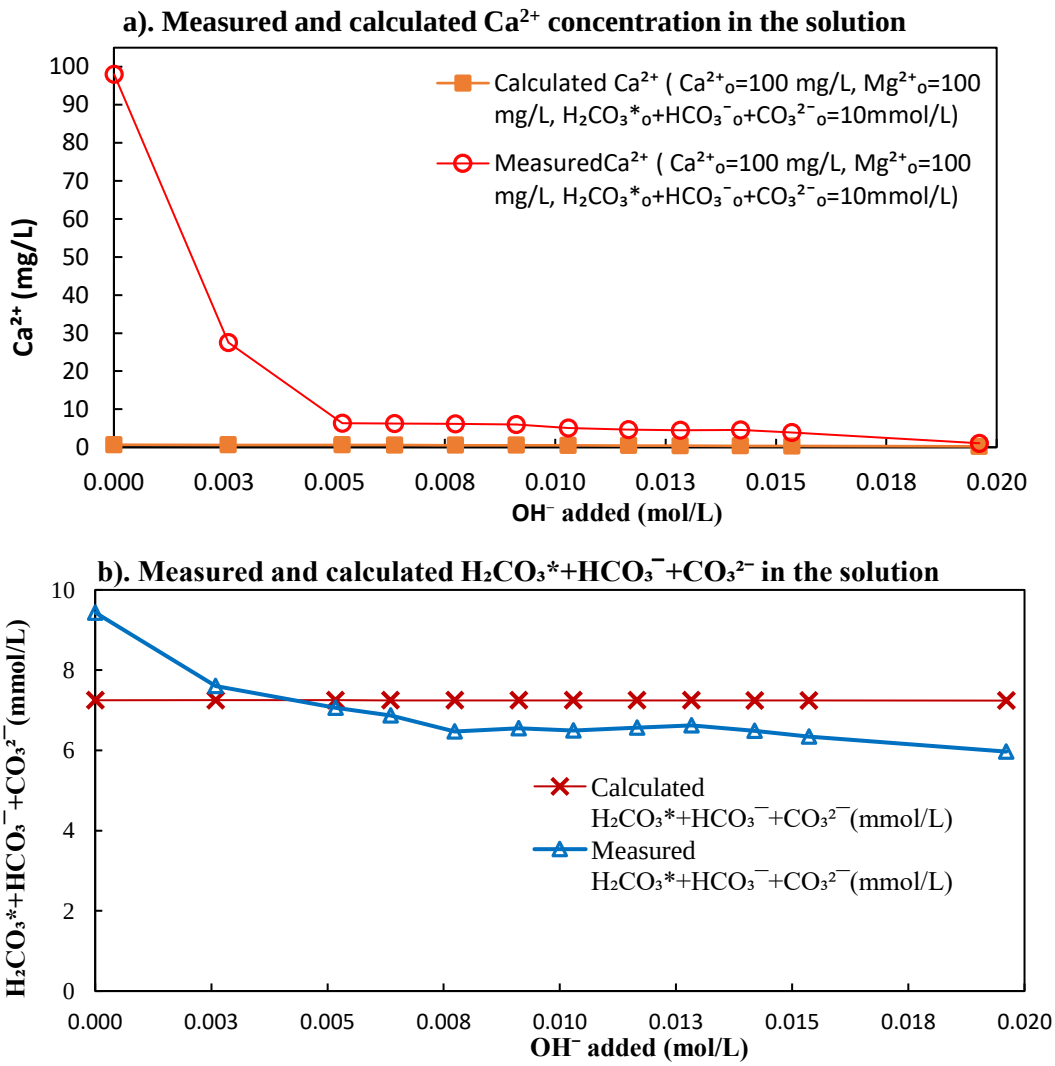

Fig. 1. 8: Measured and calculated Mg^{2+} concentration in the solution

3.3.2. Development and validation of the F^- removal model

To elucidate the F^- removal model, it is important to understand the behavior of F^- removal in the solution. The recent study from Imai and Kawakami, 2019 proposed a model for F^- co-precipitation by $Mg(OH)_2$. As per section 3.2, F- removal occurred via the same co-precipitation mechanism, the proposed model may be applicable to this study. As Imai and Kawakami, 2019 proposed, the change of F^- concentration (-d(F)) is considered proportional to the reduction amount of Mg^{2+}(-d(Mg)) (Eq.1.51). Moreover, the change of F^- concentration is also proportional to the F^- concentration at that time given by the fitted curve function (f(F)). Accordingly, the change of F^- concentration was expressed as Eq.1.51. However, Imai and Kawakami, 2019 did not investigate F^- removal in the presence of Ca^{2+} and HCO_3^- $+CO_3^{2-}$ which may change the proportionality constant K. Therefore, the same procedure described by them was adopted and experiments were repeated in the presence of Ca^{2+} and HCO_3^-+CO_3^{2-} along with Mg^{2+} and F^-.

Figure 1.9 shows the measured Mg^{2+} and F^- concentrations and respective fitted curve functions in the solution of chemical precipitation study. According to Figure 1.9, F^- concentration decreased with increasing OH^-_0, an F^- concentration increment was observed after OH^-_0> 0.0128 mol/L and Mg^{2+}<22 mg/L) (Fig. 1.9). At the earlier stage of the ELC reaction in the cathode

(with low OH^-_0), most of the OH^- were consumed for CO_3^{2-} as well as $Mg(OH)_2$ formation. Therefore, the availability of the free OH^- ions were low. Due to the higher concentration of F^-_0 in the earlier stage, F^- replaces OH^- ion in the precipitate easily. However, with increasing OH^-_0, Mg^{2+} removal reached its maximum and freely available OH^- increased. This causes increased competition between free OH^- and co-precipitated F^- and OH^- starts replacing the co-precipitated F^-, and eventually F^- concentration in the solution increased. Furthermore, the trends of Mg^{2+} and F^- removals were similar to the Imai and Kawakami, 2019 study. Accordingly, for the F^- removal model development, 0.005 mol/L<OH^-< 0.0153 mol/L range was selected.

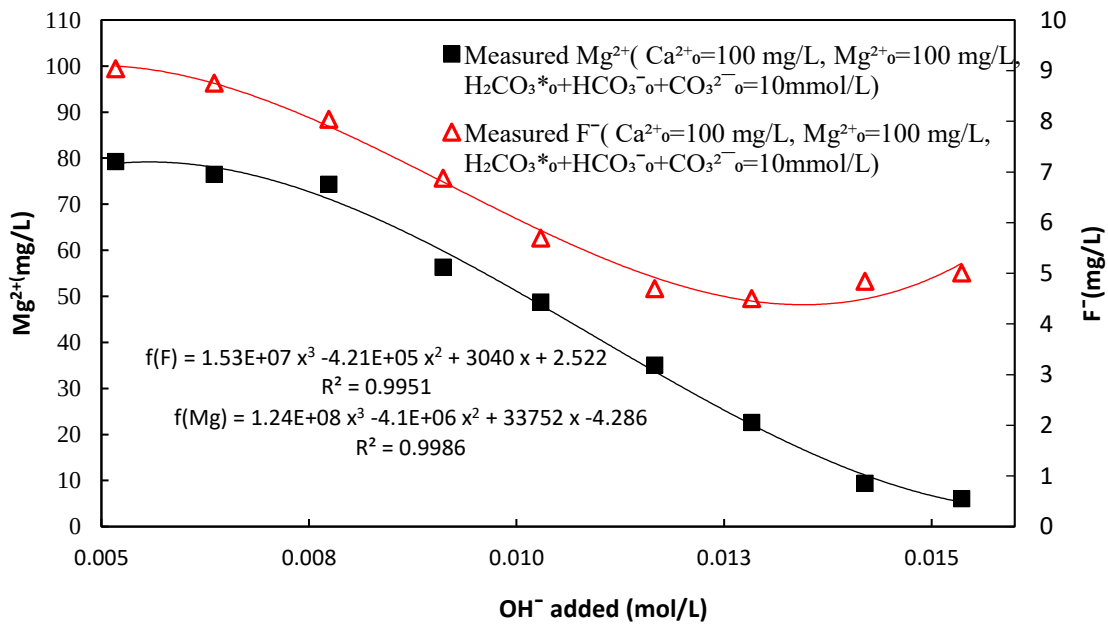

Fig. 1.9: Measured Mg^{2+} and F^- concentration in the solution

$$-d(F) = K(-d(Mg))(F) \qquad (1.51)$$

$$K = \frac{1}{(F)} \cdot \frac{d(F)}{d(Mg)} \qquad (1.52)$$

Where K is proportionality constant and F is F^- concentration at that time

$d(F)/d(Mg)$ can be calculated with differentiated curve functions ($df(F)/dOH$, $df(Mg)/dOH$) estimated from the measured values (Fig. 1.9). Then the K value can be calculated from Eq. 1.52. Fig. 1.10 shows the changes in K value when 0.0005 mol/L of OH^- was added to the system consecutively. A valley and peak of the K value were observed in the OH range of 0.005-0.0060 mol/L could be because of the cubic curve which was selected. Moreover, the K value decreased sharply from the point the OH^- concentration exceeds 0.0145 mol/L where the F^- was no longer decreases with increasing OH^-.

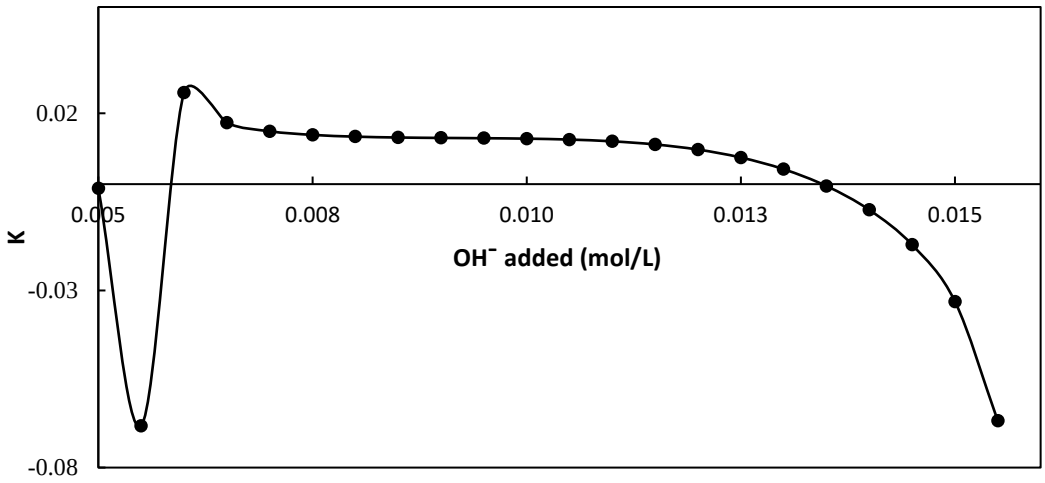

Fig. 1. 10: Calculated K values with increasing initial OH^- concentration in the solution

According to Fig. 1.9 and Fig. 1.10, the K value constant only when $Mg(OH)_2$ precipitates and free OH^- concentration is reached. The K values were averaged in the OH^- concentration range 0.065-0.0145 mmol/L and was estimated as (8.47×10^{-3}). Respective F^- concentrations were calculated by substituting the estimated K value and calculated Mg^{2+} concentration (using the Mg^{2+} estimation model) to the equation Eq. 1.53 (obtained by integrating Eq. 1.52). Calculated and measured F^- concentrations were shown in Fig. 1.11. According to Fig. 1.11 calculated F^- concentration well matched with the measured F^- concentration in the range of 0.005mol/L<OH^-< 0.0153 mol/L.

$$F = F_0 e^{K(Mg^{2+}{}_{calculated} - Mg_0^{2+})} \qquad (1.53)$$

In order to identify the behavior of the K for different initial F^- concentrations and to derive a function describing the relation between K and F^-, chemical precipitation experiments were performed. Initial F^- concentrations of 2, 3 and 5 mg/L, was used for the experiments while keeping $Mg^{2+}{}_0$, $Ca^{2+}{}_0$ 100 mg/L, $(H_2CO_3{*}+HCO_3^- +CO_3^{2-})_0$=10 mmol/L constant. Fitted curve functions are shown in Fig. 1.12 a, b, c and d for initial F- concentration 7, 5, 3 and 2 mg/L, respectively. According to Fig. 1.13, no F^- removal increment was noticed for the Mg^{2+}< 25 mg/L. K value variations over increasing OH^- concentration for initial F^- 10, 5, 3 and 2 mg/L are shown in Fig. 1.13. According to Fig. 1.13, the variation of the K value was not noticed for the OH^- concentration of less than 0.014 mol/L. By averaging the K values in the range of OH^- <0.014 mol/L, F^- concentrations were calculated with the calculated Mg^{2+} concentrations (Fig. 1.14). Comparison between measured and calculated F^- concentrations are shown in Fig. 1.14. Calculated F^- concentrations were in good agreement with the measured F^- concentrations. Fig. 1.15 shows the relationship between the K value and the initial F^- concentrations. The higher initial F^- concentration gave smaller K value, and the lower initial F^- concentration gave higher the K value.

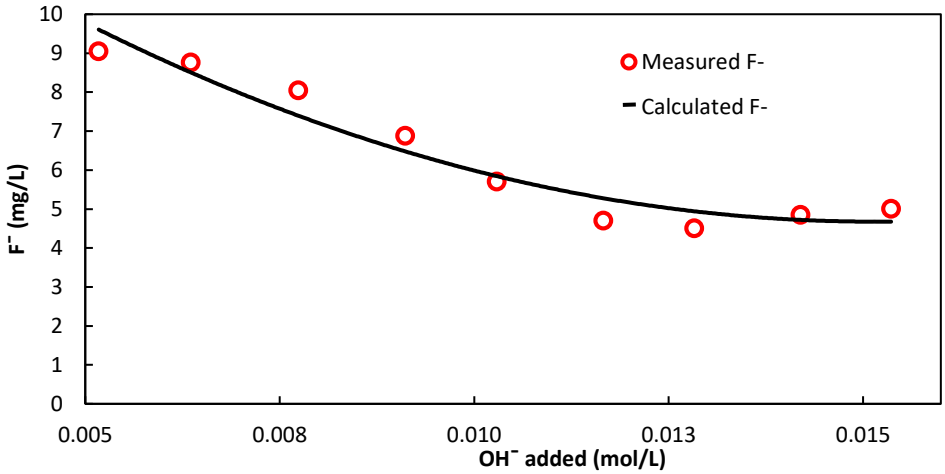

Fig. 1. 11: Calculated and measured F^- concentrations

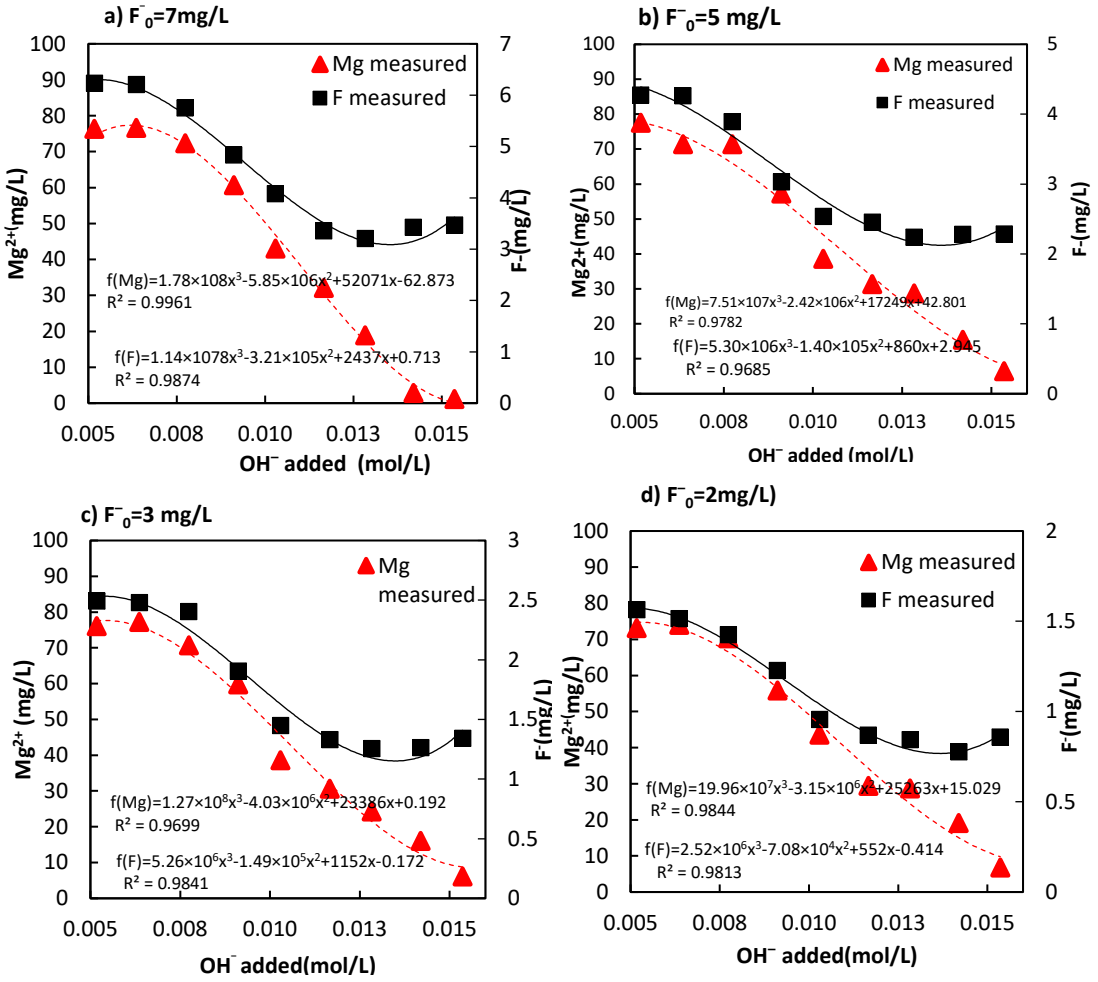

Fig. 1. 12: Fitted curve functions for different F^- concentrations

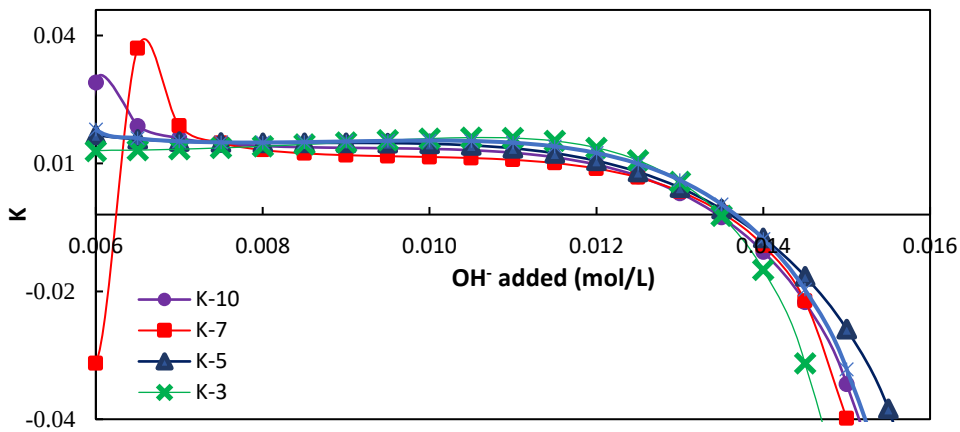

Fig. 1.13: Calculated K values with increasing initial OH^- concentration for different F^- concentrations

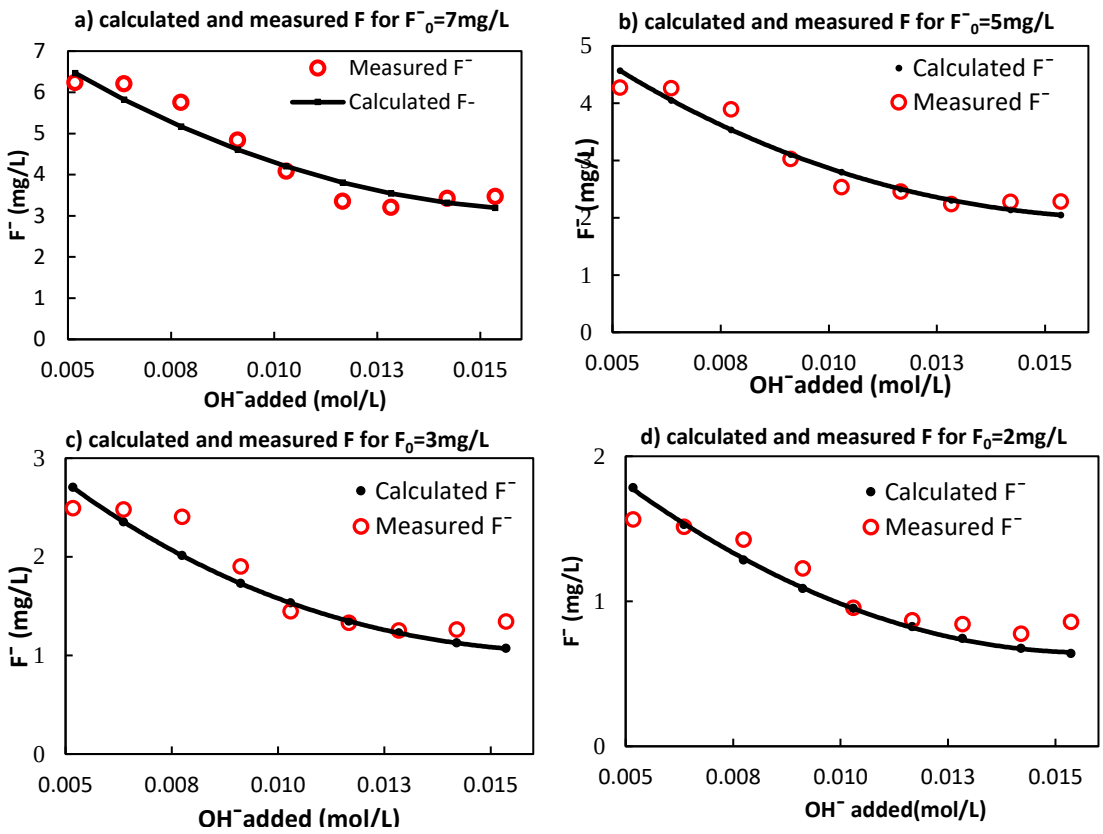

Fig. 1. 14: Calculated and measured F^- concentrations for different initial F^- concentrations

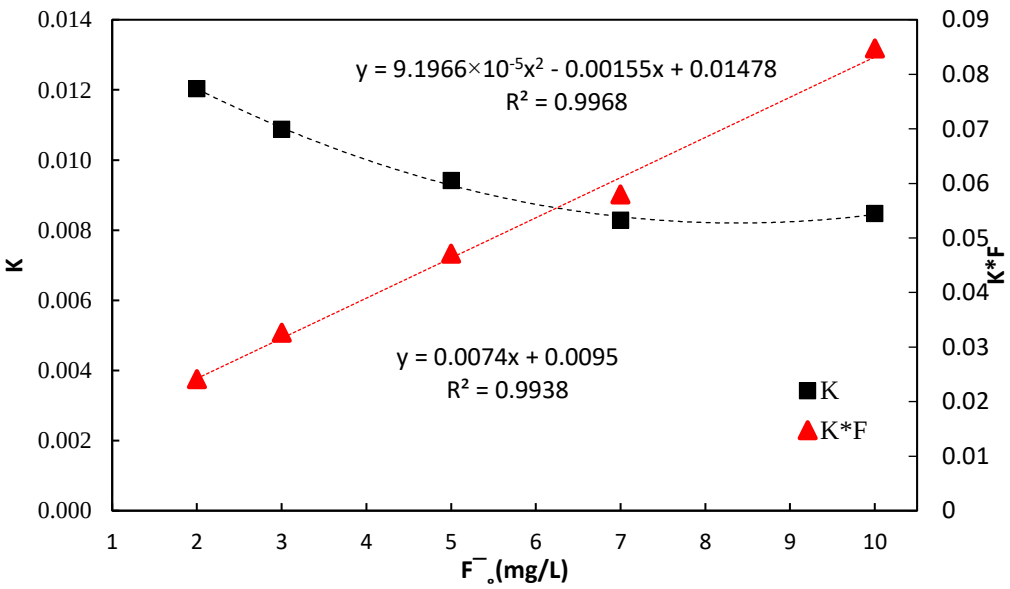

Fig. 1. 15: Relation of initial F^- concentration and K, K*F values

Accordingly, the proposed models in section 3.3.1 and 3.3.2 can be used to approximate the Mg^{2+}, Ca^{2+}, H_2CO_3*+HCO_3^-+CO_3^{2-} and F^- removals. For the estimation, only initial concentrations of the F^-, Mg^{2+}, Ca^{2+} and H_2CO_3*+HCO_3^- +CO_3^{2-} (hereafter F^-_0, Mg^{2+}_0, $Ca^{2+}{}_0$ and (H_2CO_3*+HCO_3^-+CO_3^{2-})$_0$) and added OH^- concentration were required. Since the model can regenerate the experimental results; the proposed mechanism of ion removal in ELC was similar to the prosed mechanism for developing the model. Additionally, the model calculated values can be used to determine whether water can be treated or non-treated to meet the drinking water quality guidelines.

3.4 Application of the model to the ELC treatment system.

In the continuous flow ELC system, OH^- in the cathode is mainly consumed by HCO_3^- to form CO_3^{2-} and by the formation of $Mg(OH)_2$. In the anode, H^+ is consumed by HCO_3^- and CO_3^{2-} to form CO_2(g). However, introduced OH^- (OH^-_0) and H^+ (H^+_0) by electrolysis theoretically (Eq. 1.24) may not be equal to the consumed OH^- and H^+ which were calculated with the experimental OH^- and H^+ concentrations (Hereafter OH^-_e and H^+_e) due to the neutralization. Comparison of (OH^-_0), (H^+_0), and OH^-_e, H^+_e is shown in Table 1.5. To calculate the OH^-_0 and H^+_0 from the experimental results, the mass balances equation of OH^-_e (Eq. 1.54) and H^+_e (Eq. 1.57) was employed by assuming dissociation of atmospheric CO_2 negligible. Furthermore, since the absence of $Ca(OH)_2$ was verified previously by the XRD analysis, $Ca(OH)_2$ can be neglected in the OH^-_e mass balance calculation (Eq. 1.54). Table 1. 5 describes the difference between theoretically calculated OH^-_0, H^+_0 (Left side (LS) of Eq. 1.24 with actually consumed OH^-_e and H^+_e (Right side (RS) of Eq.1.54 and 1.57 respectively).

$$[OH^-]_e = OH^- + [CO_3^{2-}]_{formed} + 2Mg(OH)_{2ppt} \quad (mol) \qquad (1.54)$$

Where:

$$[CO_3^{2-}]_{formed} + 2[CO_3^{2-}]_0 = [CO_3^{2-}]_{anode} + [CO_3^{2-}]_{cathode} + [CO_3^{2-}]_{precipitated} \quad (mol)$$

$$[CO_3^{2-}]_{formed} = [CO_3^{2-}]_{anode} + [CO_3^{2-}]_{cathode} + [Ca^{2+}]_{precipitated} - 2[CO_3^{2-}]_0 \ (mol) \qquad (1.54)$$

In Eq. 1.55, HCO_3^- transferred to the cathode was neglected, as at high pH, HCO_3^- ion existed in lower concentrations in the cathode.

$$Mg(OH)_{2ppt} = 2Mg_0^{2+} - Mg_{anode}^{2+} - Mg_{cathode}^{2+} \qquad (1.55)$$

$$H_e^+ = H^+ + Carbon\ removed\ in\ the\ anode\ as\ CO_2 - Ca^{2+}\ precipitated\ in\ the\ cathode \qquad (1.56)$$

Where:

$$Carbon\ removed\ in\ the\ anode\ as\ CO_2 = C\ removed\ in\ both\ the\ andoe\ and\ cathode - Ca^{2+}\ precipitated\ in\ the\ cathode$$

$$Carbon\ removed\ in\ the\ anode\ as\ CO_2 + [CO_3^{2-}]_{precipitated} = [HCO_3^- + CO_3^{2-}]_{removed\ from\ anode\ and\ cathode}$$

According to Table 1. 5, OH_e^- and H_e^+ were less than the introduced (theoretically calculated) OH_0^- and H_0^+ concentrations by the ELC. However, the molar concentrations of consumed OH_e^- and H_e^+ were equal. Therefore, the difference observed between calculated OH^-_0, H^+_0 with OH_e^-, H_e^+ should be obviously attributed those consumed to produce H_2O in the order to fulfill the total system mass balance. Accordingly, correction to the initial OH^-_0 should be made prior to the model simulation.

Ion transfer by the Coulomb force and initial molar concentration change the ion concentrations in the cathode and the anode. Therefore, in the perspective of model input ion concentration, initial ion concentrations should be recalculated considering those effects. The mathematical model was developed without

considering Coulomb ion transfer, initial ion concentrations should be corrected prior to the input to the model. Accordingly, mathematical relationships between coulomb forces and ion's charge can be described with Eq.1.58. The stable voltages of 51.5, 114.3, 183.3,259.0, 333.7 and 336.0 were observed respectively when applying 250, 500,750,1000, and 1500 C/L to the system. Since the maximum voltage of the power supply was reached, 1500 C/L was not achieved at the final ELC stage. Therefore, by adding 2mL of NaCl solution conductivity was increased and 1500 C/L was achieved by lowering the voltage. Accordingly, 51.5, 114.3, 183.3, 259.0, 333.7 and 336.0 V were used for Eq. 1.57 calculations.

Fig. 1.16 shows the relationships between the applied voltage and transferred ion concentrations. Since the amount of ion transferred were linear to the voltage, the assumption that Coulomb force is proportional to the ion transferred was correct. Related best fitted linear curve functions were shown in the same Fig. 1.17. It was noticed that HCO_3^- transfer occurred from anode to cathode for the charge loading< 750 C/L.

Table 1. 5: Variation of introduced OH^-_0, H^+_0 and consumed OH^-, H^+ for anode and cathode reactions

Charge Loading (C/L)	**OH^-_0(mol/L)**	**H^+_0 (mol/L)**	**OH^-_e(mol/L)**	**H^+_e (mol/L)**
250	0.0019	0.0019	0.0017	0.0025
500	0.0043	0.0043	0.0034	0.0045
750	0.0067	0.0067	0.0055	0.0067
1000	0.0093	0.0093	0.0082	0.0098
1250	0.0118	0.0118	0.0102	0.0114
1500	0.0145	0.0145	0.0110	0.0117

$$F_c = \mathrm{qE} \tag{1.57}$$

Where:

F_c is Coulomb's force (N)

$E\ (V/m) = \Delta\mathrm{v}(\text{ voltage})/\mathrm{d}\ (\ distance\ between\ electrodes = 3.5 \times 10^{-2}\ m)$

$\mathrm{q}(Coulomb) = \text{Valence of the ion } \times \text{charge of electrons}(1.6 \times 10^{-19}\ \mathrm{C})$

By accounting for the best-fitted linear equations shown in Fig. 1.16, ions transferred to the cathode or transferred from the cathode can be calculated. By using initial concentrations (F^-_0, Mg^{2+}_0, Ca^{2+}_0, $HCO_3^{2-}{}_0$ and $CO_3^{2-}{}_0$) and fitted curve functions, model input ion concentrations were recalculated for the mathematical model (section 3.3). According to the results, the amount of ion transferred to either cathode or anode depended not only on the Force but also on molar concentration. Measured and model calculated final Mg^{2+} and F^- concentrations are shown in Fig. 1.17a and b, respectively. According to Fig. 1.17a and b, the proposed model well described the removal of Mg^{2+} and F^- by the ELC system for charge loading>500 C/L. For the charge loading < 500 C/L model values were higher than that of measured. The model assumption of saturation of $Mg(OH)_2$ for every C/L applied to cause this phenomenon.

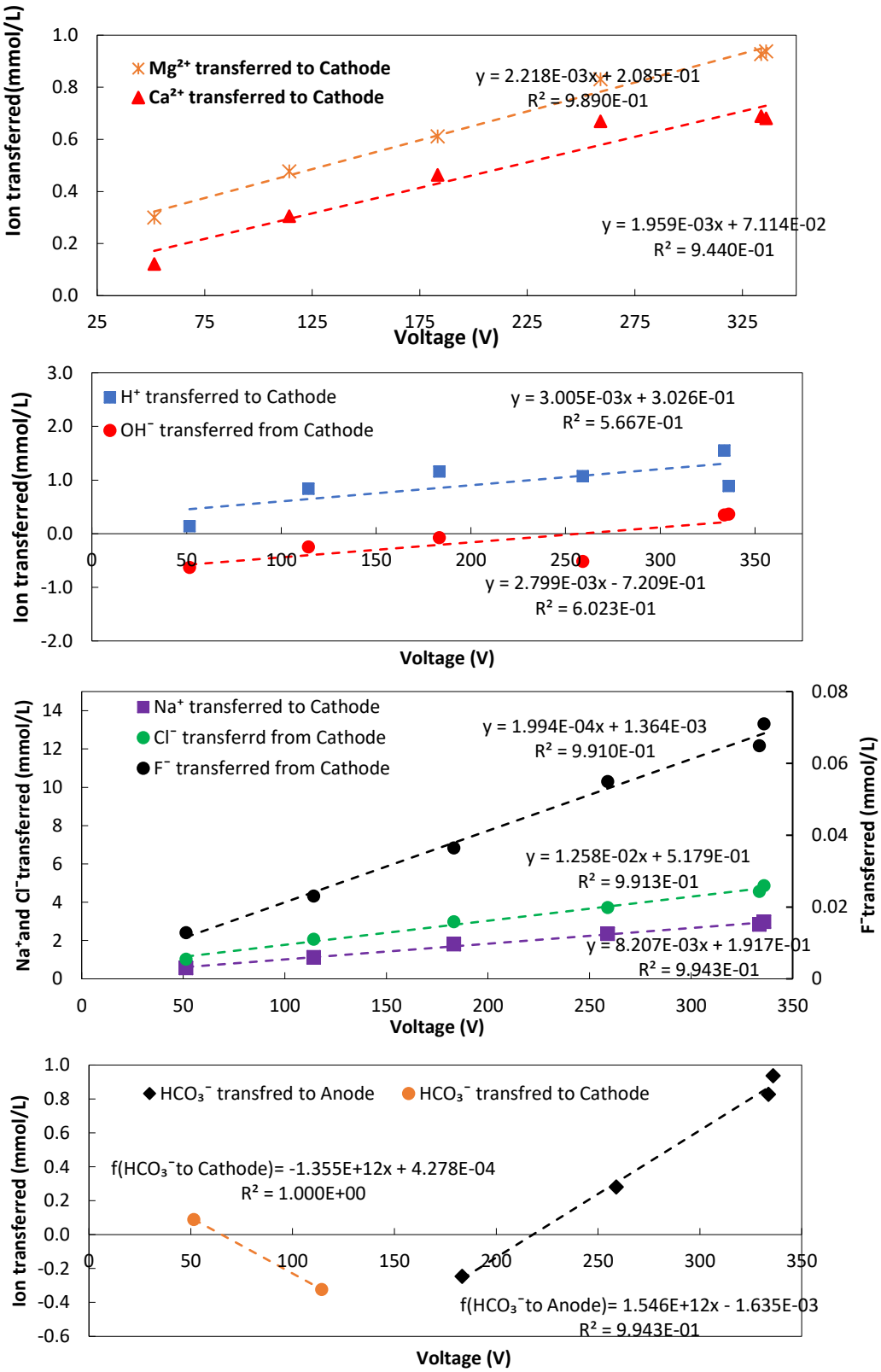

Fig. 1. 16: Coulomb force versus ion transferred

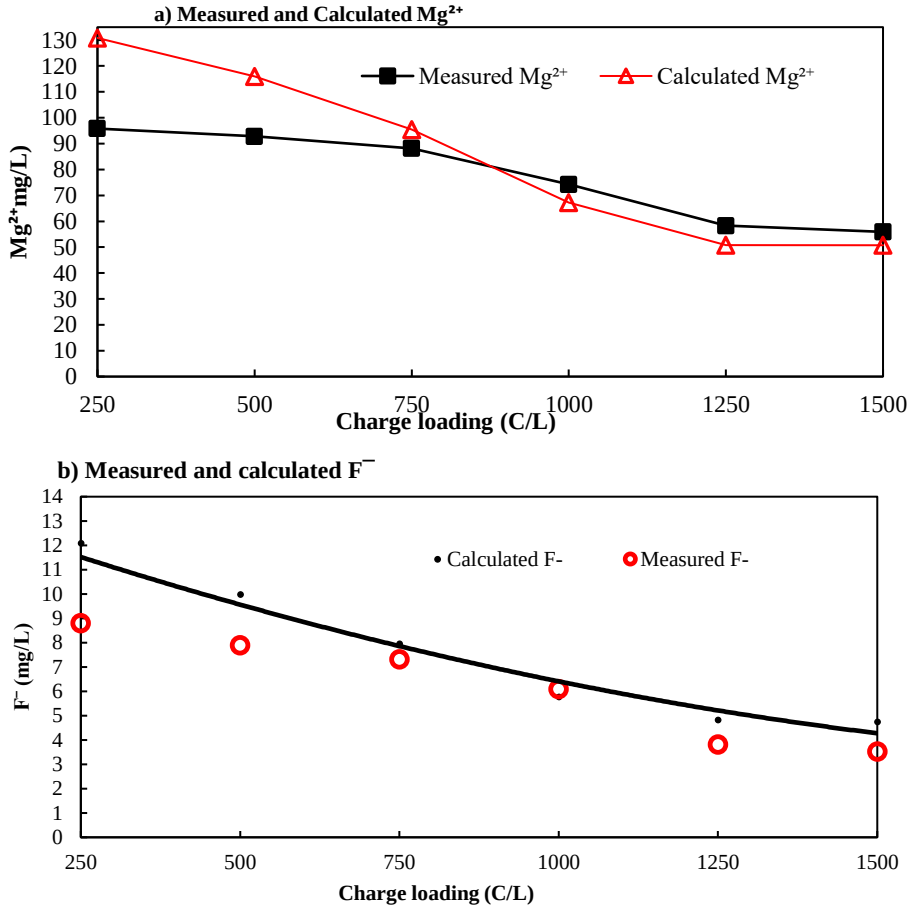

Fig. 1. 17: Measured and model-calculated Mg^{2+} and F^{-} concentrations over the increasing charge loading

3.5 Effect of the anode flow rate on ion removal

To minimize the rejected water quantity and to find the best ion removal, the anode outflow rate was varied while the cathode outflow rate was kept constant. The experimental conditions are outlined in Table 1. 1. Removal percentages in the cathode, those in the anode, and pH variations in the anode and in the cathode are shown in Figs 1.18a, 1.18b and 1.18c respectively.

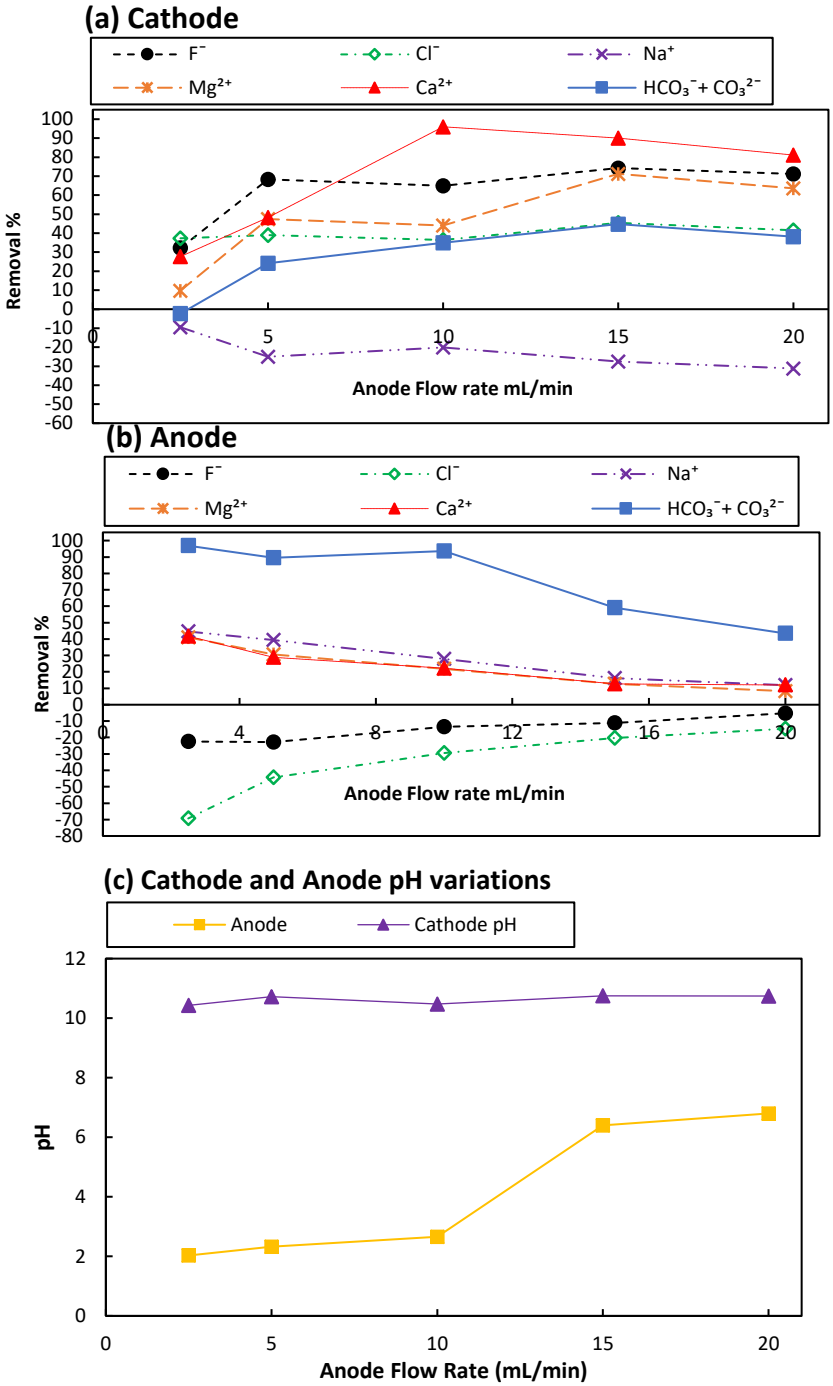

Fig. 1. 18: Influence of the anode flow rate in the electrolytes on the ion removal and pH. (a) Cathode, (b) Anode, (c) pH variation; Cathode flow rate 10 mL/min, F^-_0 = 10 mg/L, Ca^{2+}_0 = 100 mg/L, Mg^{2+}_0 = 100 mg/L, and $(HCO_3^- + CO_3^{2-})_0$ = 10000 µmol/L, 1500 C/L.

According to Fig. 1.18a, removal of Ca^{2+}, $Mg^{2+,}$ and HCO_3^-+CO_3^{2-} reached its maximum in 10, 15 and 15 mL/min of the anode flow rates, respectively. Fluoride removal reached its maximum at the anode flow rate of 15 mL/min. However, with the anode flow rate of 5-20 mL/min range, F^- removal increased marginally. According to Fig. 1.18a, the removal of (HCO_3^-+ CO_3^{2-}) in the cathode slightly increased when the anode flow rate increased. Moreover, the anode pH level increased with increasing anode flow rate due to the reduction of the H^+ concentration by dilution (Fig. 1.18c). Accordingly, it can be concluded that the anode flow rate around 10 mL/min was better for the F^-, Mg^{2+}, and Ca^{2+} removal in the cathode while removing (HCO_3^-+ CO_3^{2-}) in the anode effectively. Therefore, the anode flow rate of 10 mL/min was selected for the further experiments.

3.6 Effect of initial F^- concentration (F^-_0) on ion removal

ELC experiment was carried out under the conditions listed in Table 1.1. After three hours of the operation for stabilization, the anode and the cathode outflow rates were measured. No flow through the diaphragm was observed. Fig. 1.19a, b, and c describe ion removal in the cathode, in the anode, and the pH change in the anode and the cathode, respectively. According to Fig. 1.19a, it was observed that the rate of de-fluoridation decreased slightly from 66 to 58% as the F^-_0 concentration increased. According to Fig. 1.19, an insignificant change of Ca^{2+}, Mg^{2+}, and (HCO_3^-+ CO_3^{2-}) removal was observed with increased F^-_0 in the cathode. Taking the flat F^- removal trend and the proportionality constant "K" into consideration, there is strong evidence that F^- removal for F^-_0<5mg/L will not be reduced by more than 66%. Hence, in the presence of maximum F^-_0 =4.3 mg/L, a desirable drinking concentration of F^- 1.5mg/L recommended by WHO can be achieved. To meet the Sri Lankan standard of 1 mg/L, a maximum concentration of F^-_0 in raw water should be less than 2.9 mg/L. Na^+ and Cl^- ion removals in both the anode and the cathode did not show significant changes with the increasing F^-_0 concentration. The pH levels in both the anode and the cathode did not change significantly for increasing F^-_0 (Fig. 1.19c).

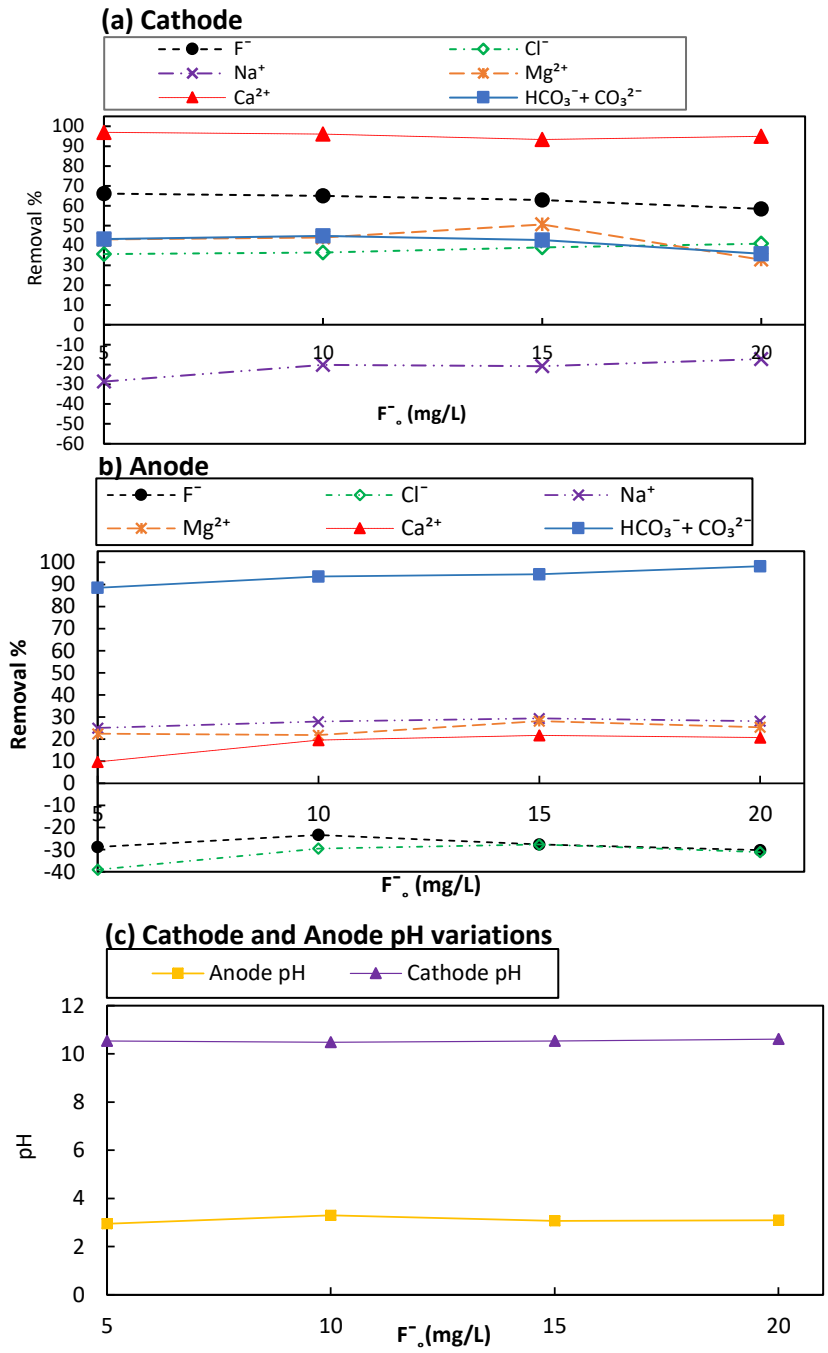

Fig. 1. 19**:** Influence of the initial F^- concentration in the electrolytes on the ion removal percentage and pH. (a) Cathode, (b) Anode, (c) pH variation; F^-_0 = 5-20 mg/L, Ca^{2+}_0 = 100 mg/L, Mg^{2+}_0 = 100 mg/L, and $(HCO_3^- + CO_3^{2-})_0$ = 10000 µmol/L, 1500 C/L.

The mathematical model simulation was performed in order to validate the F^- removal mechanism applicability to the ELC continuous flow reactor. Due to the Coulomb force, F^-, Mg^{2+}, Ca^{2+}, HCO_3^- and CO_3^{2-} ions were transferred to either anode or cathode. Therefore, concentration changes due to the Coulomb force have to be considered in model calculations. Due to the transfer of ions, initial ions concentrations (F^-_0, Mg^{2+}_0, Ca^{2+}_0, $HCO_3^-{}_0$ and $CO_3^{2-}{}_0$), in the anode and the cathode changed from those of raw water. Since such initial ion concentration changes due to Coulomb force were not included in the mathematical model, the model input initial ion concentrations should be calculated based on the F^-_0, Mg^{2+}_0, Ca^{2+}_0, $HCO_3^-{}_0$ and $CO_3^{2-}{}_0$ and transferred ion concentrations. As described in section 3.4, using fitted curve functions, ion transferred from the anode to cathode and cathode to anode can be calculated. Those calculated values can be used to calculate model input initial ion concentrations. As per the observations from Fig. 1.19, F^-, Mg^{2+}, Ca^{2+}, HCO_3^- and CO_3^{2-} ions were transferred to either anode or cathode. However, except for F^-, other ion transfers were not significantly increased over the increasing F^-_0. Accordingly, the fitted curve functions are shown in Fig. 1.20 and F^-_0, Mg^{2+}_0, Ca^{2+}_0, $HCO_3^-{}_0$ and $CO_3^{2-}{}_0$ were used for model input ion concentration calculation.

Measured and model calculated F^- and Mg^{2+} concentrations vs F^-_0 are shown in Fig. 1.21. According to Fig. 1.21, both modeled F^- concentrations and measured F^- concentrations values were found similar. Therefore, according to the F^- removal model, the change of F^- concentration $(-d(F))$ is proportional to the reduction amount of $Mg^{2+}(-d(Mg))$. Moreover, the change of F^- concentration is also proportional to the F^- concentration at that time. Since, the model input initial Mg^{2+} concentration (calculated with Mg^{2+}_0 and fitted curve function (Fig 1.20)) was not changed, $(-d(F))$ was proportional only to the F^- concentration at that time (section 3.2.3).

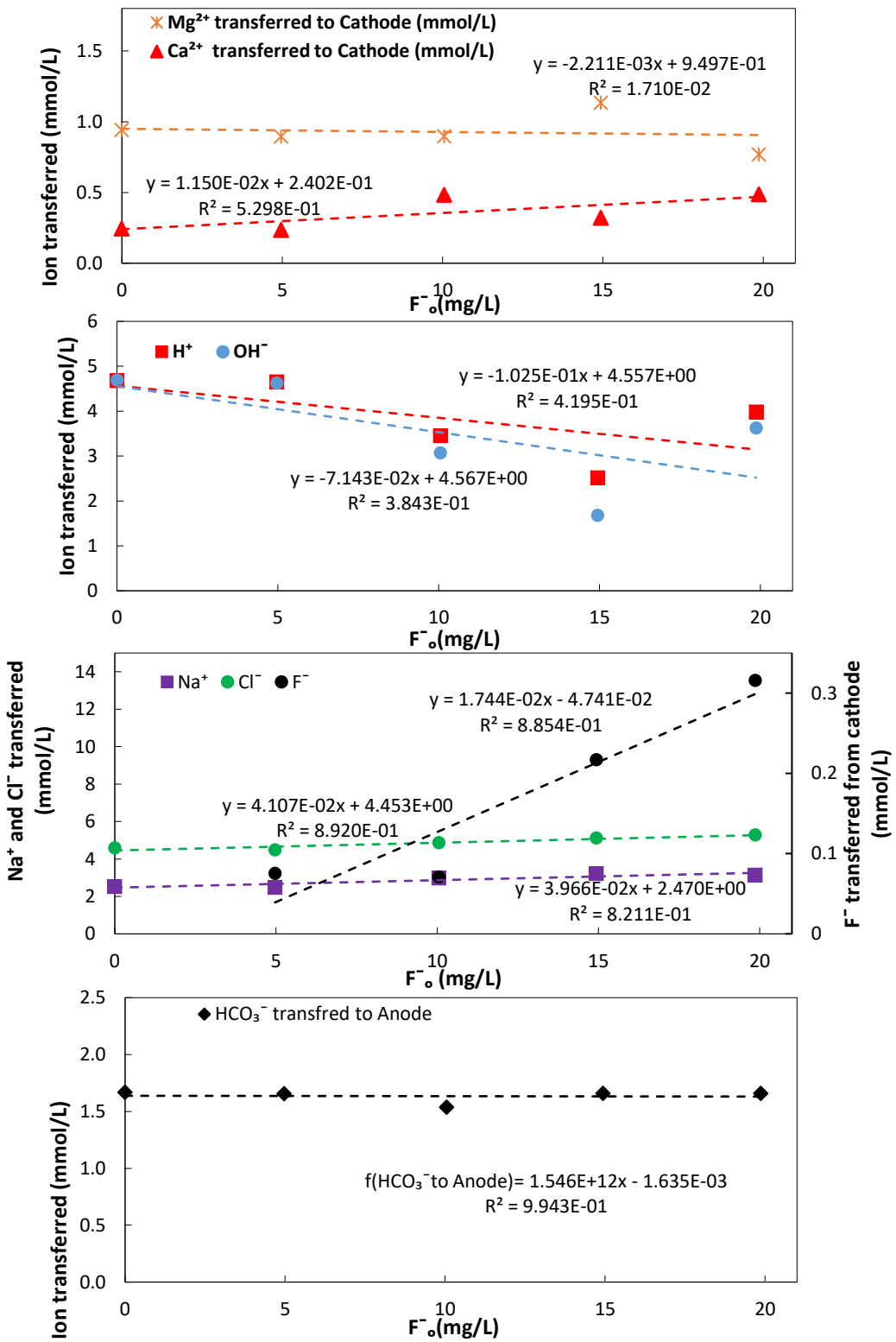

Fig. 1. 20: F^-_0 versus ion transferred in 1500 C/L charge loading

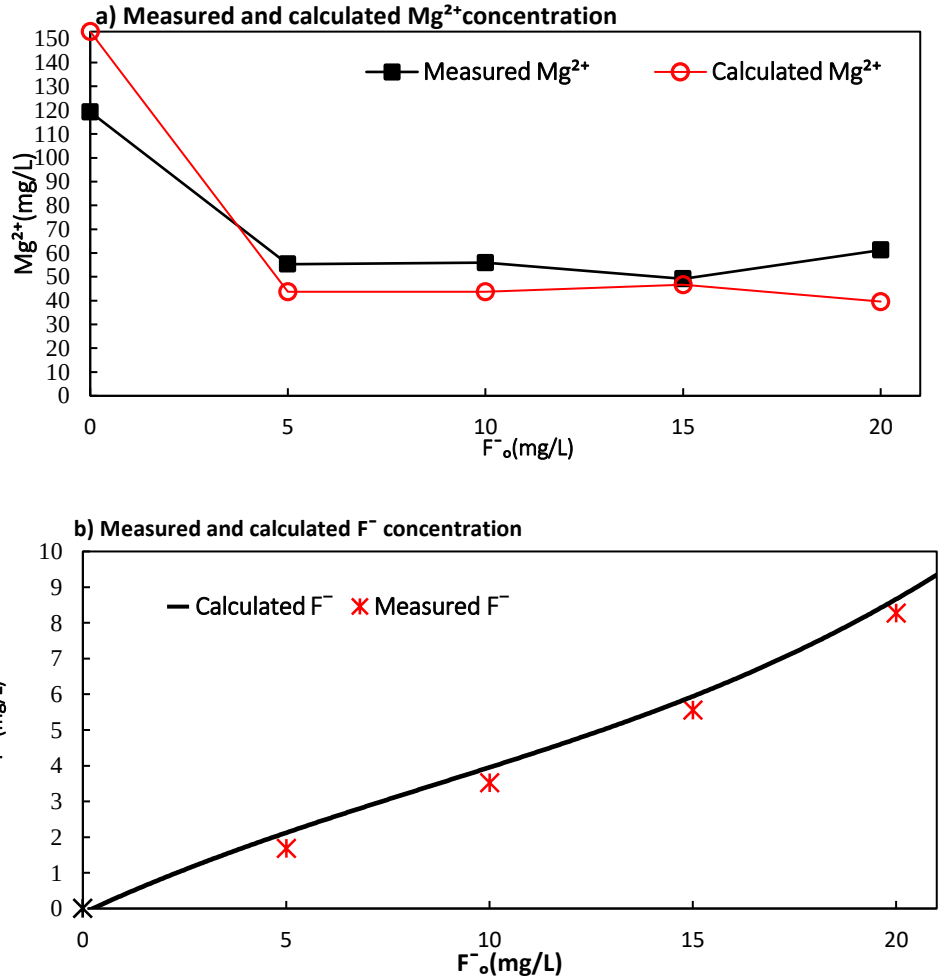

Fig. 1. 21: Measured and calculated final Mg^{2+} and F^- concentrations over the increasing F^-_0

3.7 Effect of the initial Mg^{2+} concentration (Mg^{2+}_0) on ion removal and related pH

This section describes the effect of the Mg^{2+}_0 (0 to 125 mg/L) on the ion removal. The experimental conditions are as described in Table 1. 1. After three hours of system stabilization, flow through the diaphragm was observed as 4.20, 3.66, 3.16, 1.99, 0, and 0 mL/min, respectively, for Mg^{2+}_0 concentrations of 0, 25, 50, 75, 100, and 125 mg/L. Accordingly, ion removal percentages were calculated by accounting for the inflow and outflow weight of the elements.

Calculated removal percentages in the cathode, anode and related pH are illustrated in Fig. 1.22a, Fig. 1.22b, and Fig. 1.22 c, respectively. According to Fig. 1.22a (cathode), for the initial Mg^{2+} >50 mg/L, the removal of F^- increased sharply and became steady when the $Mg^{2+}{}_0$ was in the 75–125 mg/L range. Even with the absence of Mg^{2+}, F^- was removed by both precipitations (10%) and transfer by the Coulomb force (11%) to the anode (Fig. 1.22b). For $Mg^{2+}{}_0$ =0 mg/L, the thermodynamic Ksps of CaF_2 and $CaCO_3$ can be corrected with Eq. 1.23 as 6.80×10^{-12} $(mol/L)^3$ and 5.25×10^{-12} $(mol/L)^2$, respectively. Measured concentrations of 5.53 mg/L F^- and CO_3^{2-} 3.25 mmol/L, Ca^{2+} can be used with corrected Ksps to calculate Ca^{2+} concentrations. Ca^{2+} concentrations were calculated to be 3.2 mg/L and 6.46×10^{-5} mg/L for Ksp CaF_2 and $CaCO_3$, respectively. Comparatively, the measured Ca^{2+} (0.35 mg/L) concentration was much closer to the Ca^{2+} calculated with Ksp of CaF_2. Therefore, F^- removal without Mg^{2+} occurred could be due to precipitation as CaF_2. Furthermore, the isotherm experiment performed for the precipitates collected under the condition (Table 1. 1, Isotherm_3) verified that F^- was not adsorbed by $CaCO_3$, thus CaF_2 formation should have occurred.

According to Fig. 1.22a, $HCO_3^- + CO_3^{2-}$ removal was not significant for $Mg^{2+}{}_0$ < 50 mg/L in the cathode. Transfer of HCO_3^- ions from the anode was caused for that slight $HCO_3^- + CO_3^{2-}$ removal in the anode. Ca^{2+} removal in the cathode was observed at its maximum of 97%. Since anode Ca^{2+} removal also exhibited a positive removal percentage, the formation of $CaCO_3$ in the cathode was obvious. However, lower ($HCO_3^- + CO_3^{2-}$) removal in the cathode for a lower level of $Mg^{2+}{}_0$ restricted the system performance for the drinking water treatment process. For an increased $Mg^{2+}{}_0$ concentration, the removal rate of ($HCO_3^- + CO_3^{2-}$) from the anode showed more than 80% (Fig. 1.19b). The ($HCO_3^- + CO_3^{2-}$) in the anode and those transferred from the cathode were removed by the reaction with H^+ to produce CO_2 (g) in the anode.

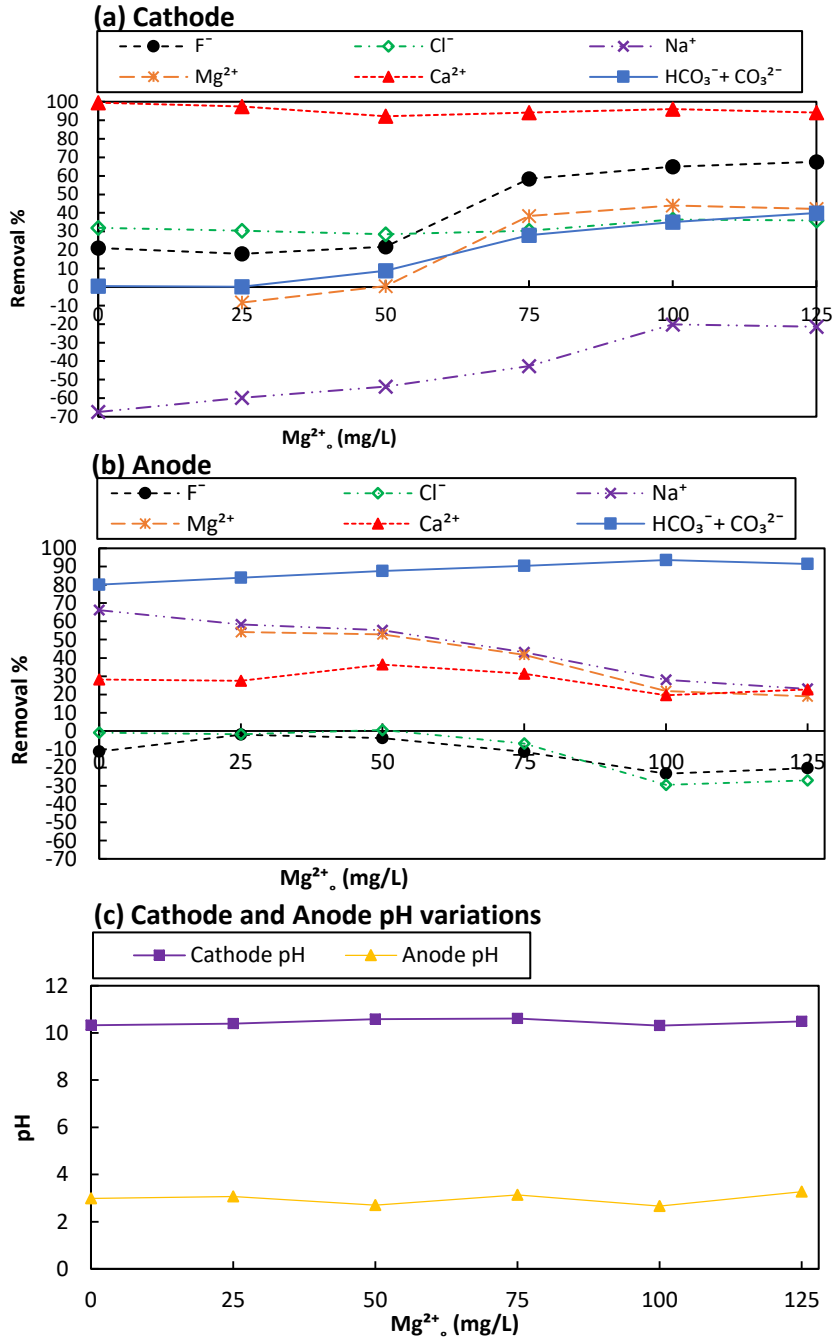

Fig. 1. 22**:** Influence of the initial Mg^{2+} concentration in the electrolytes on the ion removal percentage and pH. (a) Cathode, (b) Anode, (c) pH variation; F^{-}_{0} = 10 mg/L, Ca^{2+}_{0} = 100 mg/L, Mg^{2+}_{0} = 0–125 mg/L, and ($HCO_3^{-}$and CO_3^{2-})$_0$ = 10000 µmol/L, 1500 C/L

At the system equilibrium stages (after reaching Anode and cathode pH to a constant level), a significant change in the applied voltages was not observed. Accordingly, as the model input concentrations, concentration calculated by accounting transferred ion concentrations as described in section 3.4 was used. However, according to Fig. 1.23, except Ca^{2+} and H^+ other ion transfers varied with $Mg^{2+}{}_0$. Therefore, fitted curve functions for F^-, $Mg^{2+,}$ and HCO_3^-, described in section 3.4 should be modified accordingly. According to Fig. 1.24a, the model calculated and measured Mg^{2+} concentrations were found similar. Therefore, the assumption that "$MgCO_3$ formation is negligible" was suitable for reproducing the system performance in the ELC system. For the lower $Mg^{2+}{}_0$ concentrations model calculated Mg^{2+}concentration was much closer to the experimental results. This was occurred due to the $Mg(OH)_2$ saturation starts at a lower $Mg^{2+}{}_0$ concentration in solution rather than at a high $Mg^{2+}{}_0$ concentration in the solution. The model calculated and measured F^- concentrations were found similar in Figure 1.24b for the $Mg^{2+}{}_0$> 50 mg/L. The larger deviation of the model calculated and measured F^- concentrations for $Mg^{2+}{}_0$<50 mg/L was due to that the fraction of F^- transferred to the anode by the Coulomb force was higher than the fraction of F^- co-precipitated with $Mg(OH)_2$. Furthermore, with the lower $Mg^{2+}{}_0$, formation of $Mg(OH)_2$ was found lower (Section 3.4).

The positive and negative removal of the Na^+ ion in the anode and the cathode respectively, as shown in Fig. 1.22 confirmed that Na^+ was transferred to the anode by the Coulomb force. Moreover, Cl^- ion removal in the cathode was caused (Fig. 1.22) by transfer to the anode. Even though the Coulomb force did not change with increasing $Mg^{2+}{}_0$, F^- removal negatively increased in the anode. The transfer of F^- from cathode to anode and co-precipitation in the cathode were not enough to remove an adequate level of F^- for drinking purposes for $Mg^{2+}{}_0$ and $F^-{}_0$ concentrations lower than 75 mg/L and higher than 4.29 mg/L (section 3.4 finding) respectively. Furthermore, the system cannot be utilized for water having $Mg^{2+}{}_0$<75, mg/L, and $F^-{}_0$ >4.29 mg/L for either wastewater or industrial water fluoridation for drinking purposes. According to Fig. 1.22b, and Fig. 1.23 significant amount of Mg^{2+} -

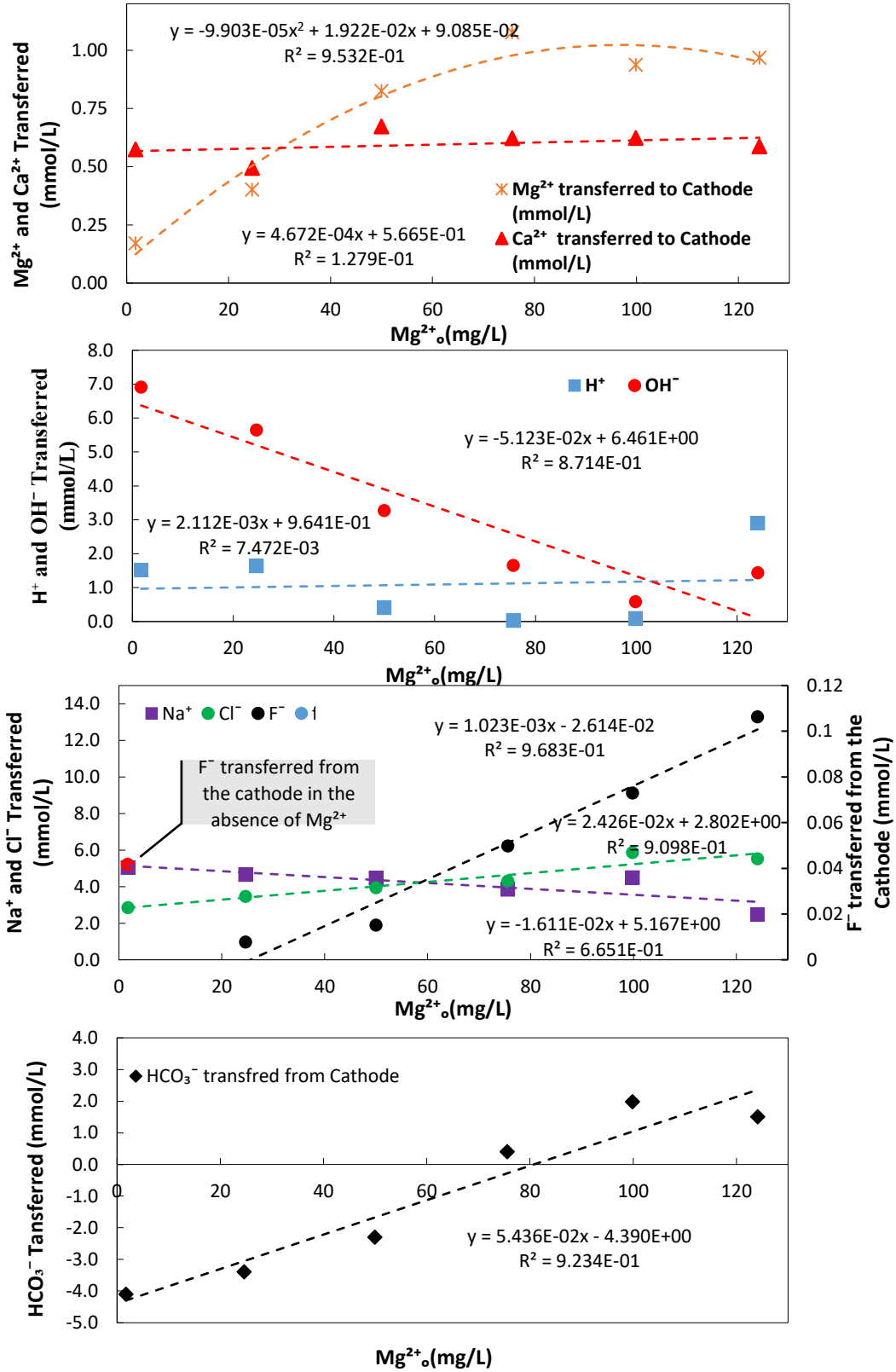

Fig. 1. 23: $Mg^{2+}{}_0$ versus ion transferred in 1500 C/L charge loading

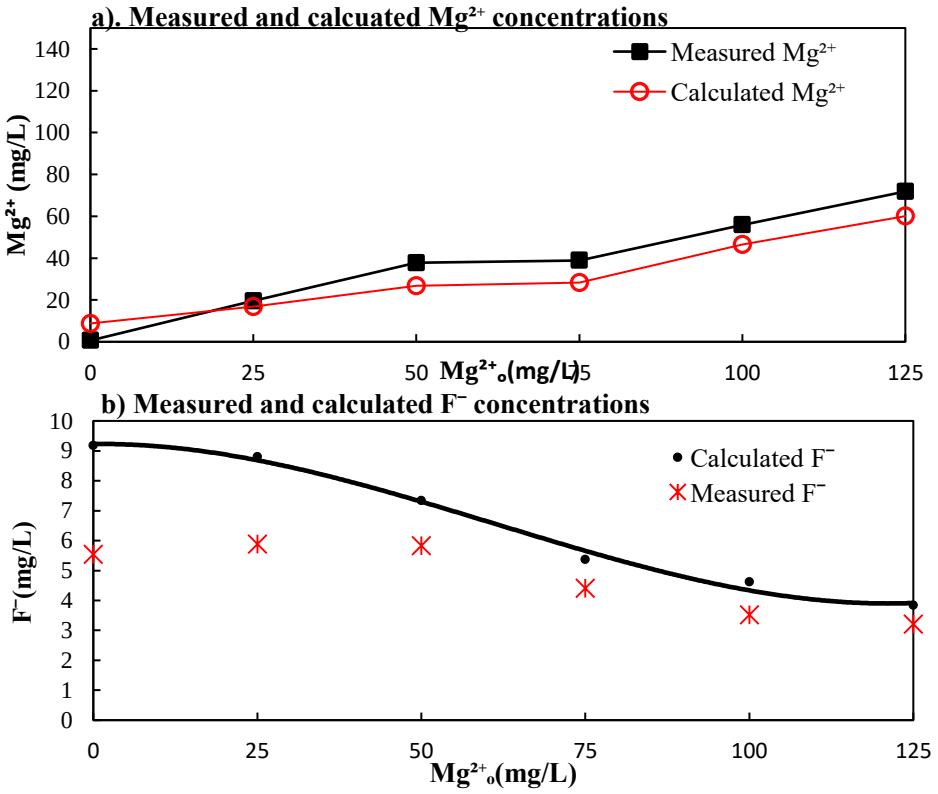

Fig. 1. 24: Measured and calculated Mg^{2+} and F^- concentrations over the increasing $Mg^{2+}{}_{o}$

was removed from the anode by transfer to the cathode by both Coulomb force and the concentration gradient created in the cathode due to the higher removal rate of Mg^{2+}.

3.8 Effect of initial Ca^{2+} concentration ($Ca^{2+}{}_0$) on ion removal and related pH

This section describes the effect of the $Ca^{2+}{}_0$ concentration on ion removal under the conditions described in Table 1. 1. After three hours of the system stabilization, the anode and the cathode water out-flow rates were measured. It was found that 2.40, 1.99, 0.51, 0.24, 0, and 0 mL/min flowed through the diaphragm from the anode to the cathode for the initial Ca^{2+} concentrations of 0, 25, 50, 75, 100, and 125 mg/L, respectively. Accordingly, the removal percentage of ions was calculated by accounting for the inflow weight and the outflow weight of the elements for a better comparison. The calculated removal percentages against increasing initial Ca^{2+}

concentrations are illustrated in Fig. 1.25a and b for the cathode and the anode, respectively. Fig. 1.25c shows the pH levels in the anode and the cathode for different Ca^{2+}_0 concentrations.

According to Fig. 1.25a, the removal of F^- and Mg^{2+} increased marginally for concentrations of Ca^{2+}_0<50 mg/L. Then the removal of F^- and Mg^{2+} were maximized after Ca^{2+}_0>50 mg/L. Accordingly, the addition of Ca^{2+}_0 (0-50 mg/L) contributed to increased F^- removal up to 24% (39 to 63%) in the cathode. Furthermore, by accounting for the findings discussed in section 3.6 and in this section, it can be concluded that, for the Ca^{2+}_0 >50mg/L and F^-_0 <4.29 mg/L, adequate F^- removal for drinking purpose was attainable in the cathode.

According to Fig. 1.25b, more than 91% of (HCO_3^-+ CO_3^{2-}) in the anode was removed with increasing Ca^{2+}_0. And, the removal of (HCO_3^-+ CO_3^{2-}) in the cathode increased from 2.4 to 46 % (Fig. 1.25). The equivalent positive and negative removal of the Na^+ ion in the anode and the cathode, respectively, confirmed that Na^+ was transferred to the anode by Coulomb force and was not affected by the concentration of Ca^{2+}_0. Cl^- ion removal in the cathode by transfer to the anode by Coulomb force increased slightly with increasing Ca^{2+} concentration, while negatively increasing in the anode. Cl^- removal in the cathode resulted from transfer to the anode by Coulomb force and the concentration gradient created in the anode due to the removal of Cl^- as Cl_2 (g). By using the Fig. 1.26 fitted curve function for Cl^- transferred to the anode and final concentration of Cl^- in the anode Cl^- removed as Cl_2 can be estimated.

Similar voltages applied (to obtain charge loading of 1500 C/L) for different Ca^{2+}_0 ensured that constant Coulomb force was induced to the ions. Due to the Coulomb force, F^-, Mg^{2+}, Ca^{2+}, HCO_3^- and CO_3^{2-} ions were transferred to either anode or cathode. Therefore, concentration changes due to the Coulomb force have to be considered in model calculations. However, except HCO_3^- and H^+ the amount of ions transferred was varied with Ca^{2+}_0 according to Fig. 1.26. Due to the transfer of ions, initial ions concentrations (F^-_0, Mg^{2+}_0, Ca^{2+}_0, $HCO_3^{2-}{}_0$ and $CO_3^{2-}{}_0$), in the anode and cathode were changed than that of raw water. Since such initial ion concentration-

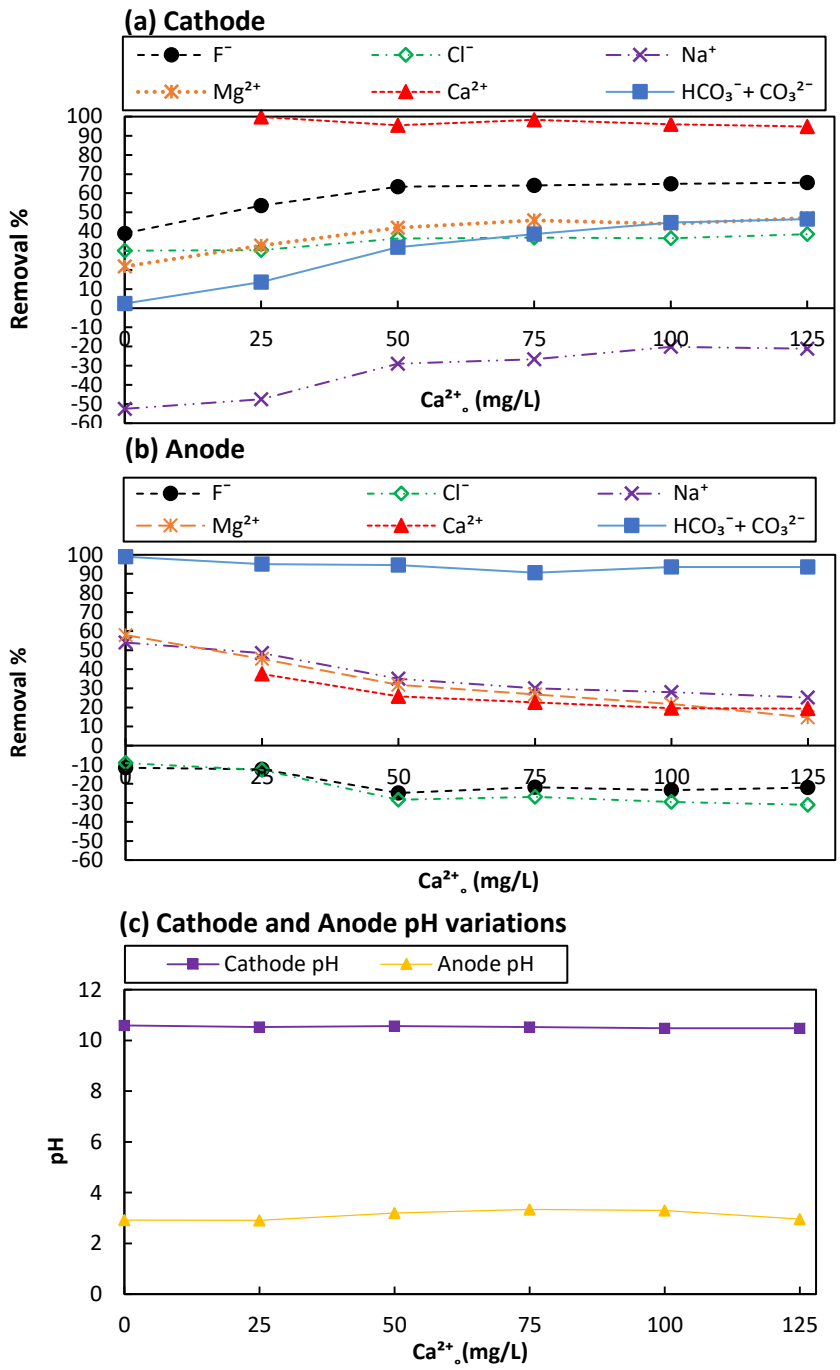

Fig. 1.25: Influence of the Ca^{2+}_{0} in the electrolytes on the ion removal percentage and pH. (a) Cathode, (b) Anode, (c) pH variation; F^{-}_{0} = 10 mg/L, Ca^{2+}_{0} = 0–125 mg/L, Mg^{2+}_{0} = 100 mg/L, and $(HCO_3^{-} + CO_3^{2-})_0$ = 10000 µmol/L, 1500 C/L

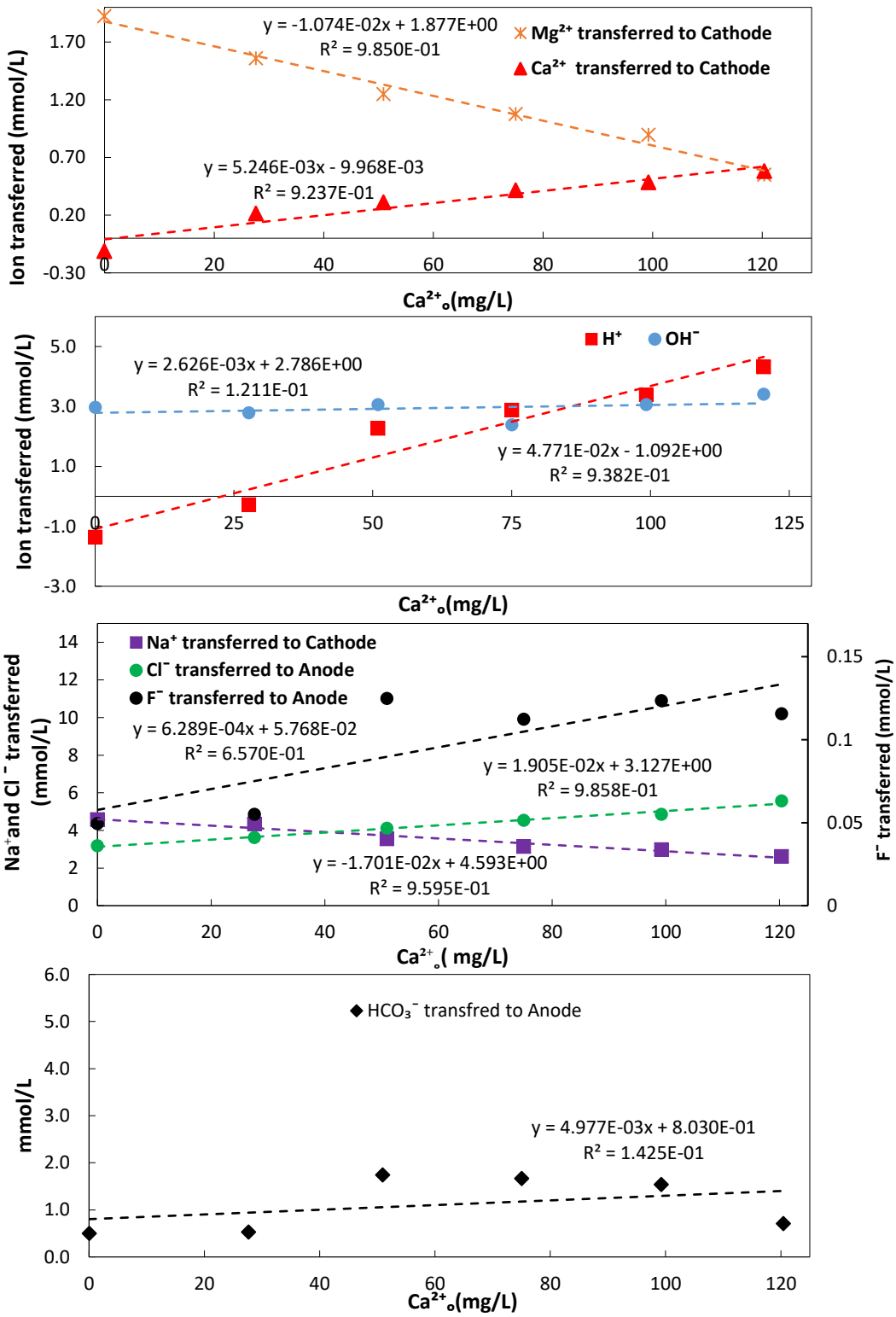

Fig. 1. 26: Ca^{2+}_0 versus ion transferred in 1500 C/L charge loading

-changes due to Coulomb force were not included in the mathematical model, the model input initial ion concentrations should be calculated based on the F^{-}_{0}, Mg^{2+}_{0}, Ca^{2+}_{0}, $HCO_3^{2-}{}_0$ and $CO_3^{2-}{}_0$ and transferred ion concentration.

As described in section 3.4, using fitted curve functions (Fig. 1.25), iron transferred from the anode to cathode and cathode to anode can be calculated. Those calculated values can be used to calculate model input initial ion concentrations. The calculated Mg^{2+}, F^{-} concentrations by the model and measured Mg^{2+}, F^{-} were shown in Fig.1.27. The calculated and measured Mg^{2+} and F^{-} concentrations were found similar

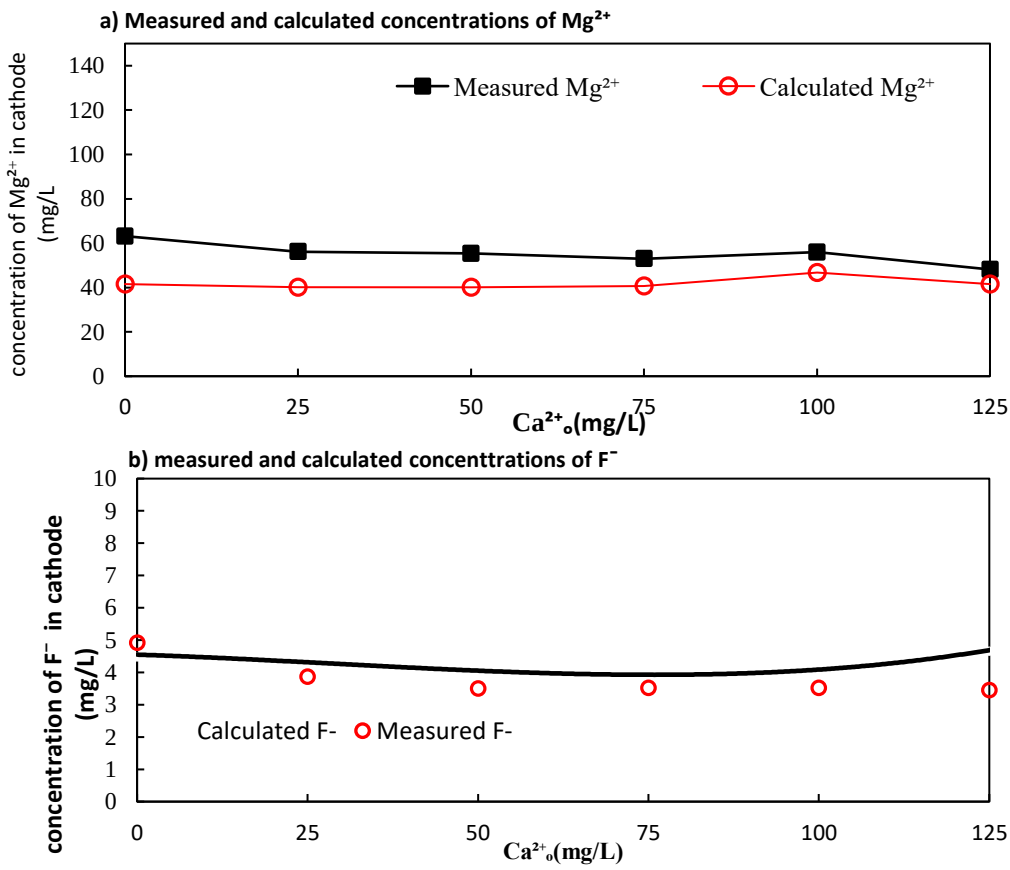

Fig. 1. 27: Ca^{2+}_{0} versus measured and calculated Mg^{2+} and F^{-} concentrations in cathode

3.9 Effect of the initial $HCO_3^- + CO_3^{2-}$ concentration $(HCO_3^- + CO_3^{2-})_0$ on ion removal and related pH

To understand the ion removal rates of F^- and other ions at different initial concentrations of $HCO_3^- + CO_3^{2-}$, experiments were performed under the conditions listed in Table 1.1. The water flow through a diaphragm from the anode to the cathode was found negligible. The calculated removal percentages of ions in the cathode, the anode, and pH values are shown in Fig. 1.28a, b, and c, respectively. In the absence of $HCO_3^-$and CO_3^{2-}, the removal of F^- and Mg^{2+} increased up to 70% in the cathode (Fig. 1.28a). Only 1% of F^- was transferred from the cathode to the anode by Coulomb force due to the high co-precipitation rate of F^- with $Mg(OH)_2$. Transfer of the Mg^{2+} (19%) from the anode to the cathode further verified that phenomenon.

Equal positive and negative removal percentages of Ca^{2+} in the anode and the cathode respectively confirmed that the Ca^{2+} removal by as precipitation, in the form of $Ca(OH)_2$ or CaF_2, in the absence of $(HCO_3^- + CO_3^{2-})_0$. Therefore, the only mechanism that removed F^- was co-precipitation with $Mg(OH)_2$. Compared to section 3.8 data, in the absence of Ca^{2+} and the presence of $(HCO_3^- + CO_3^{2-})$, 39% of F^- and 23% of Mg^{2+} removal were noticed. According to Fig. 1.28, the presence of Ca^{2+} and the absence of $(HCO_3^- + CO_3^{2-})_0$ showed 74% of F^- and 70% of Mg^{2+} removal. Therefore, Mg^{2+} removal is hardly affected by Ca^{2+} but significantly by $(HCO_3^- + CO_3^{2-})_0$. Therefore, it can be concluded the presence of $(HCO_3^- + CO_3^{2-})_0$ inhibits F^- removal, as well as Mg^{2+}removal, by decreasing the formation of $Mg(OH)_2$ and by increasing the formation of $Mg(CO)_3$. From section 3.2, we identified that $Mg(OH)_2$ was the main F^- removing agent. Following the removal percentages of F^- (assuming the same 74% removal observed for 10 mg/L F^-_0), F^-_0 which can be treatable to meet WHO guidelines for drinking water is 5-6 mg/L. However, it only valid when $(HCO_3^- + CO_3^{2-})_0$ concentration is lower than 5.0 mmol/L. The higher removal rate of $(HCO_3^- + CO_3^{2-})$ in the anode of more than 90% for $(HCO_3^- + CO_3^{2-})_0$ = 0-12.5 mmol/L showed that the proposed ELC system would be applicable for both industrial and drinking water $(HCO_3^- + CO_3^{2-})$ removal at a lower charge loading

range (750-1000 C/L) in which water meets required pH level.

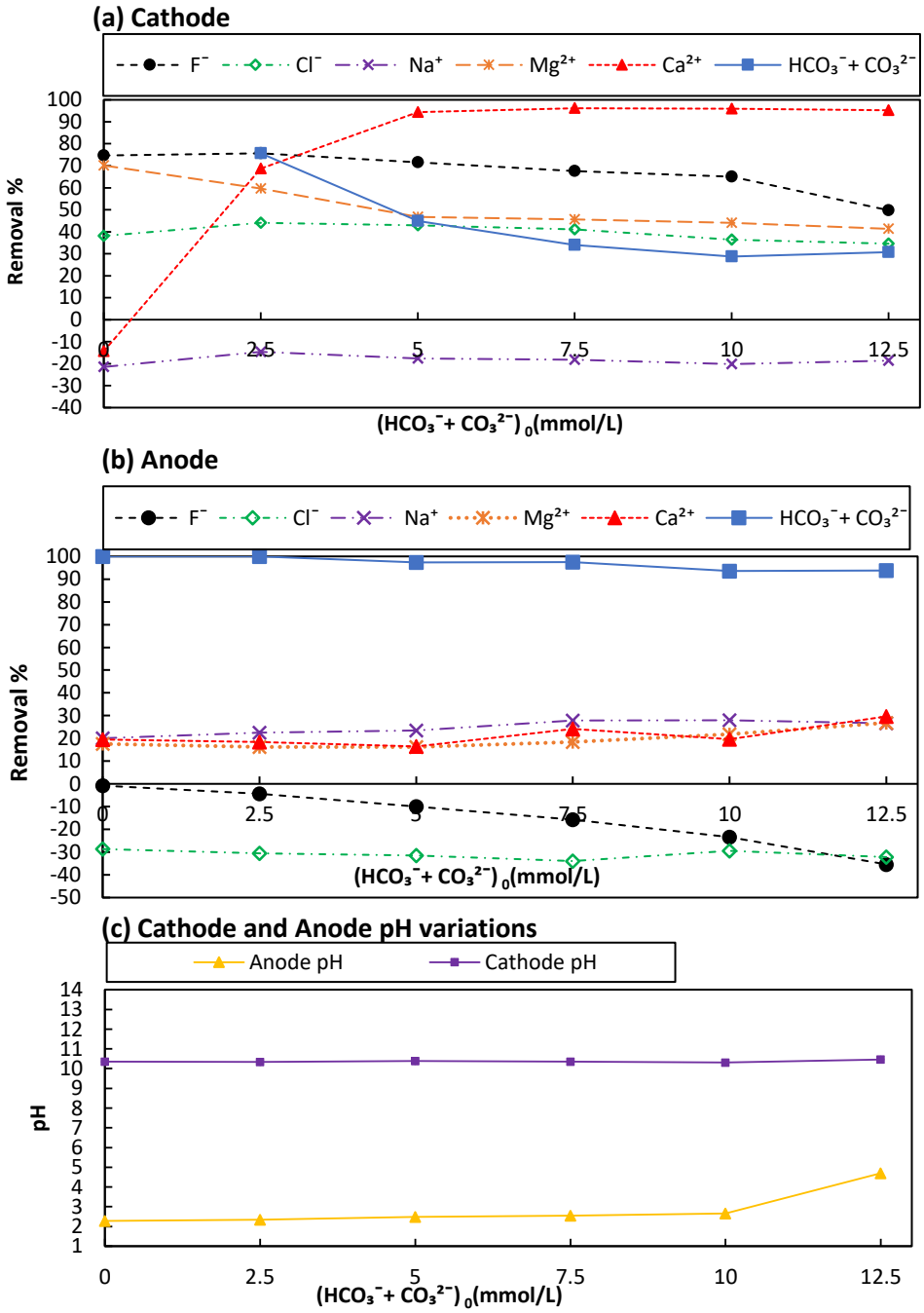

Fig. 1. 28: Effect of the initial HCO_3^-+ CO_3^{2-}concentration on the ion removal percentage and pH. (a) Cathode, (b) Anode, (c) pH variation; F^-_0= 10 mg/L, Ca^{2+}_0=100 mg/L, Mg^{2+}_0= 100 mg/L, and $(CO_3^{2-}+HCO_3^-)_0$=0-12500 µmol/L, 1500 C/L.

The transfer of Na^+ from the anode to the cathode was observed. Cl^- removal in the cathode occurred due to the transferring to the anode by Coulomb force and the concentration gradient. Therefore, Cl^- ions were creating a concentration gradient because it was removed as $Cl_2(g)$ in the anode. The increment of $(HCO_3^- + CO_3^{2-})_0$ slightly affects the Na^+ and Cl^- ion removal in both the anode and the cathode. According to Fig. 1.28c, a slight increase in pH in the anode was observed for $HCO_3^- + CO_3^{2-}$ <10.0 mmol/L. Thereafter, the pH increased sharply. Since the increasing concentration of $(HCO_3^- + CO_3^{2-})_0$ consumed high H^+, pH increase can be observed in the anode. To derive the best fit curve functions to correct initial concentration for mathematical model simulation, ion removal versus $(CO_3^{2-}+HCO_3^-)_0$ was plotted as shown in Fig. 1.29.

According to Fig. 1.29. F^- and HCO_3^- transferred to the cathode were increased with increasing $(CO_3^{2-}+HCO_3^-)_0$. The transfer of Ca^{2+} and Mg^{2+} to the cathode remained unchanged over increasing $(CO_3^{2-}+HCO_3^-)_0$. However, due to the transfer of ions, initial ions concentrations (F^-_0, Mg^{2+}_0, Ca^{2+}_0, $HCO_3^-{}_0$ and $CO_3^{2-}{}_0$), in the anode and cathode were changed than that of raw water. Therefore, concentration changes occurred by the Coulomb force have to be considered in model calculations. Accordingly, for the determination of the concentrations of Ca^{2+} and Mg^{2+}, curve functions defined in section 3.3 were used. For the F^- and HCO_3^- concentrations calculations Fig. 1.29 fitted curve functions were used. Calculated concentrations of Ca^{2+}, Mg^{2+}, F^- and HCO_3^- were used to simulate the model and obtained results were shown in Fig. 1.30. According to the model, the calculated Mg^{2+} concentration coincided with the measured concentration for the lower $(CO_3^{2-}+HCO_3^-)_0$. This occurred due to the saturation of $Mg(OH)_2$. Since OH^- availability is higher in a lower concentration of $(CO_3^{2-}+HCO_3^-)_0$ $Mg(OH)_2$ production was increased. If high $(CO_3^{2-}+HCO_3^-)_0$ present OH^- reacts mostly with HCO_3^- to form CO_3^{2-} other than to form $Mg(OH)_2$.

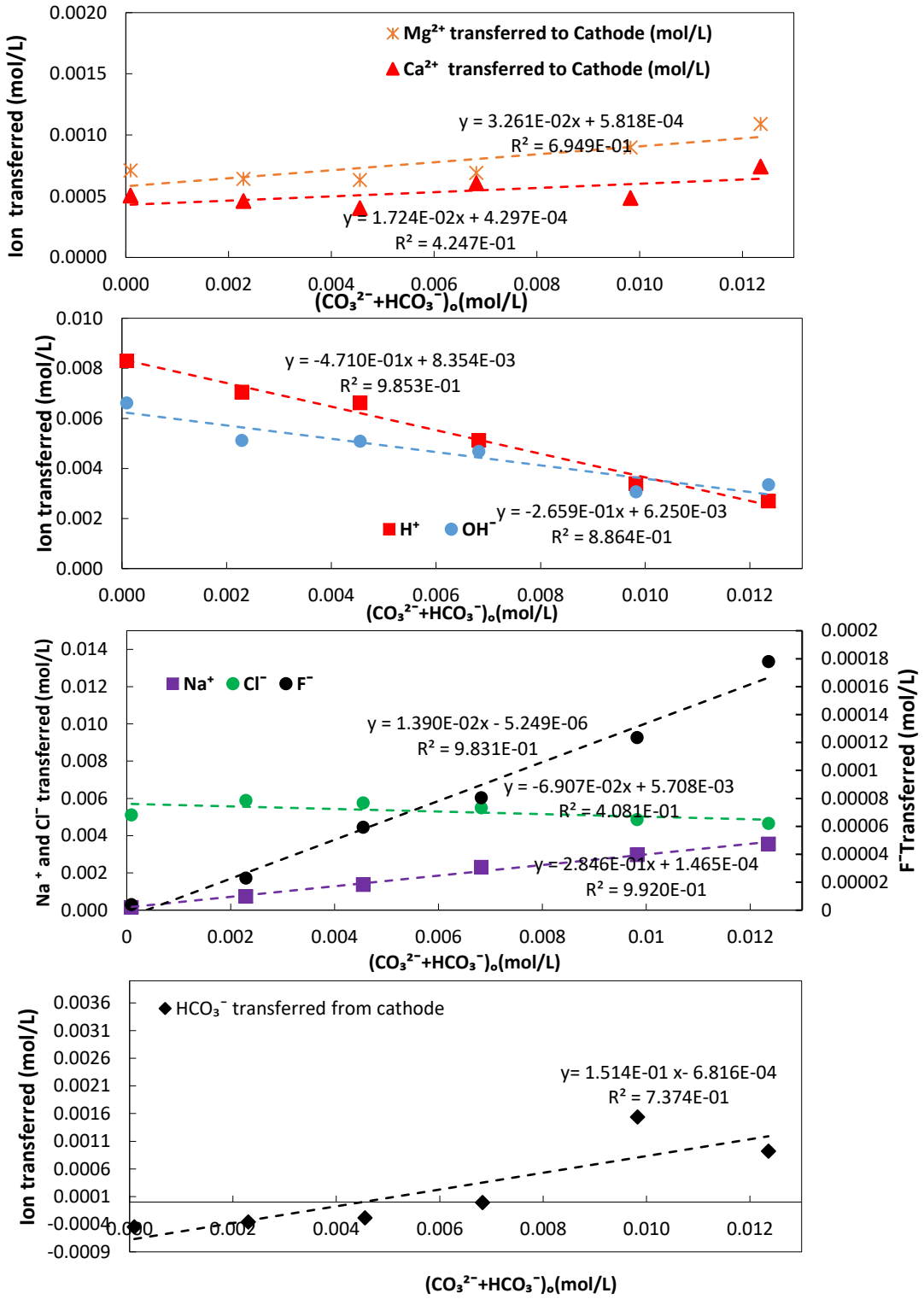

Fig. 1.29: $(CO_3^{2-}+HCO_3^-)_0$ versus ion transferred in 1500 C/L charge loading

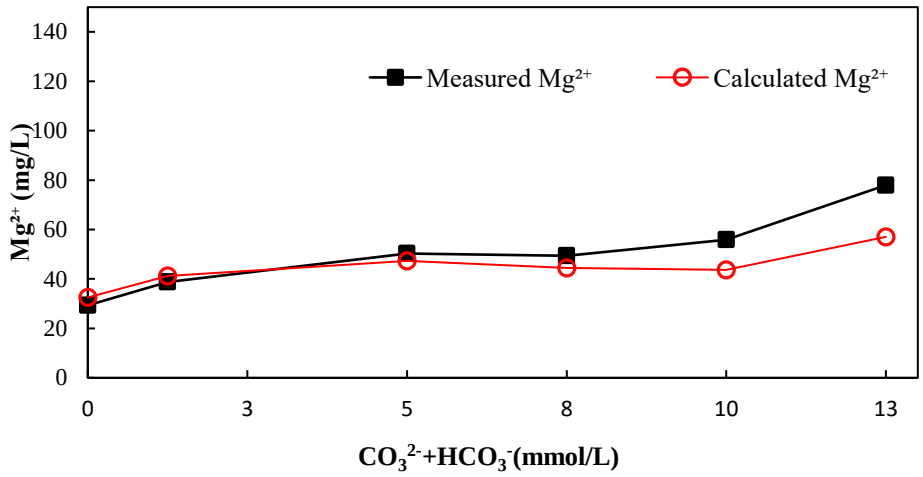

Fig. 1. 30: Measured and model-calculated final Mg^{2+} over the increasing $(CO_3^{2-}+HCO_3^-)_0$

Even though the Mg^{2+} concentrations calculated from the proposed model have coincided with measured Mg^{2+} concentrations (for $(CO_3^{2-}+HCO_3^-)_0$ <10 mmol/L), F^- concentrations calculated by F^- determination model was significantly deviated except for the $(CO_3^{2-}+HCO_3^-)_0$=10 mmol/L. Since F^- removal model was established at $(CO_3^{2-}+HCO_3^-)_0$=10 mmol/L, calculated and measured F- concentrations were obviously coincided (Fig. 1.30). Based on the model proposed by Imai and Kawakami, 2019, calculated F^- concentrations coincided with lower $(CO_3^{2-}+HCO_3^-)_0$<5mmol/L. Since that model was established for $(CO_3^{2-}+HCO_3^-)_0$ = 0 mmol/L, it seems that F^- co-precipitation was affected by $CO_3^{2-}+HCO_3^-$. Therefore, for different $(CO_3^{2-}+HCO_3^-)_0$, K values of the F removal model should be estimated.

According to Fig. 1.31, it is clear that Imai and Kawakami, 2019 proposed model is suitable for lower concentrations of the K values. But the revised model of Imai and Kawakami, 2019 is suitable to calculate F^- concentration in the presence of higher level of $(CO_3^{2-}+HCO_3)_0$. Therefore, without additional experiments, F^- removal model K values (for different $(CO_3^{2-}+HCO_3)_0$ can be estimated with the best-fitted curve function for the measured F^- concentrations. The best-fit curve function from Fig 1.30 for measured F^- concentrations, can be rearranged as Eq. 1.59 by substituting

to Eq 1.53. However, this formula only valid for the charge loading of 1500 C/L.

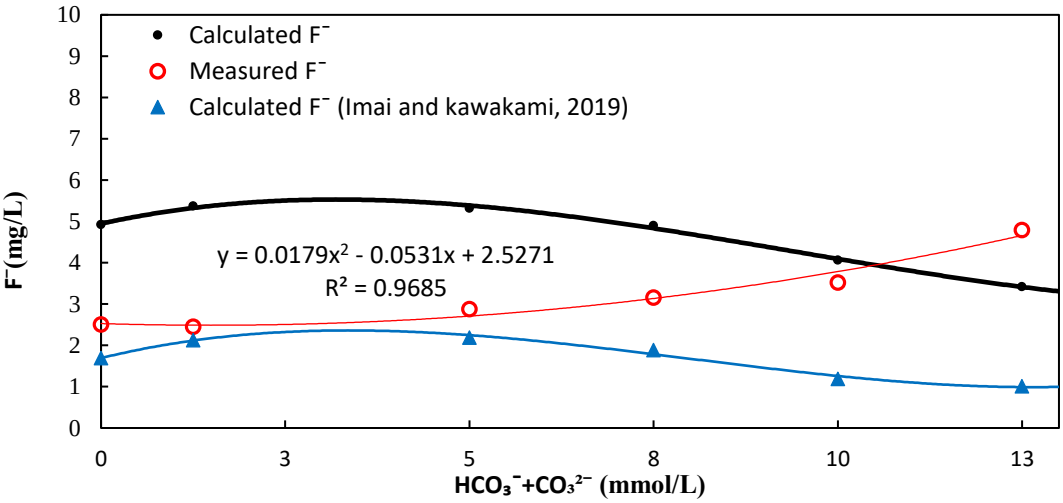

Fig. 1. 31: Measured and model-calculated final F^- over the increasing $(CO_3^{2-}+HCO_3^-)_0$

$$K = \frac{\ln\left[\frac{(0.0179\,(HCO_3^- + CO_3^{2-})_0^{\,2} - 0.0531(HCO_3^- + CO_3^{2-})_0 + 2.5271}{F_0^-}\right]}{(Mg^{2+}{}_{calculated} - Mg_0^{2+})} \quad (1.59)$$

Accordingly, K value for different initial $(CO_3^{2-}+HCO_3^-)$ and calculated equilibrium concentrations of Mg^{2+} were calculated from the Eq 1.53 was illustrated as Figure 1.32 and it can be used for fluoride concentration estimation.

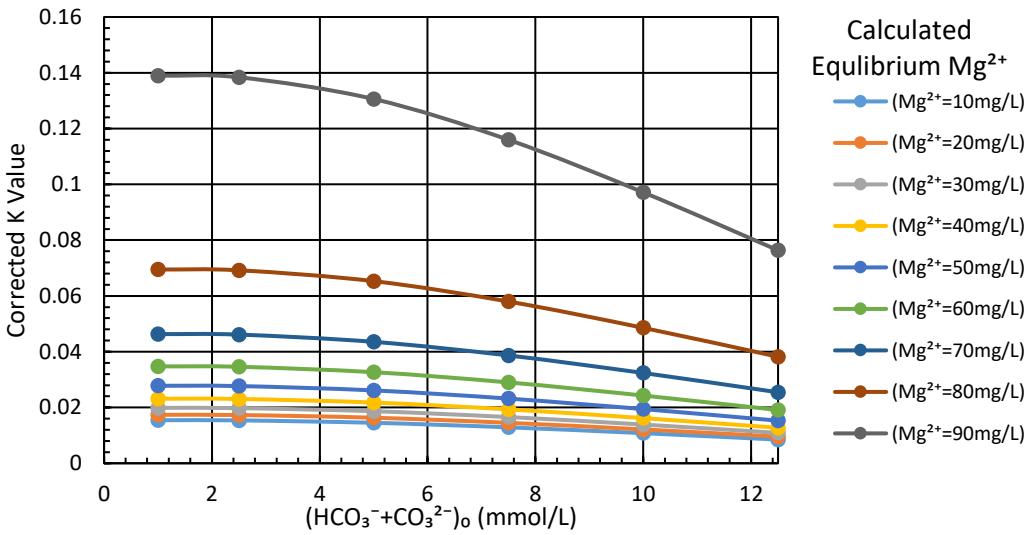

Fig. 1. 32: Calculated K values for different levels of $(CO_3^{2-}+HCO_3^-)_0$; Charge loading 1500C/L, $(Mg^{2+})_0$ =100mg/L, (F_0=10mg/L)

From section 3.3-3.8 data, Mg^{2+} concentration can be estimated with the proposed mathematical model for both chemical precipitation and continuous flow ELC systems. Moreover, from sections 3.3, 3.4 and 3.8 it is clear that removal of F^- can be estimated with calculated Mg^{2+} concentration and the proposed F removal model adopted by Imai and Kawakami, 2019 study.

3.10 Determination of the system stability

The stability of the proposed system is crucial in its operation for the development of a community-scale system. An experiment was performed with the conditions described in Table 1.1 to evaluate system stability. The initial F^- concentration was selected so that its limit exceeded the Sri Lankan water quality guideline. Moreover, low $Mg^{2+}{}_0$ and higher $Ca^{2+}{}_0$ concentrations were maintained in the reactions since low $Mg^{2+}{}_0$ reduce the F^- removal (section 3.7) and increasing $Ca^{2+}{}_0$ increase the $HCO_3^- + CO_3^{2-}$ removal (section 3.8). A charge loading of 1500 C/L and the inflow rate of 10 mL/min for both the anode and the cathode were applied. Figure 1.33 shows ion removal percentage and pH change versus time of operation. According to Fig. 1.33a, b, and c, it is clear that ion removal percentages and pH were stabilized after 2.5 hours of the operation.

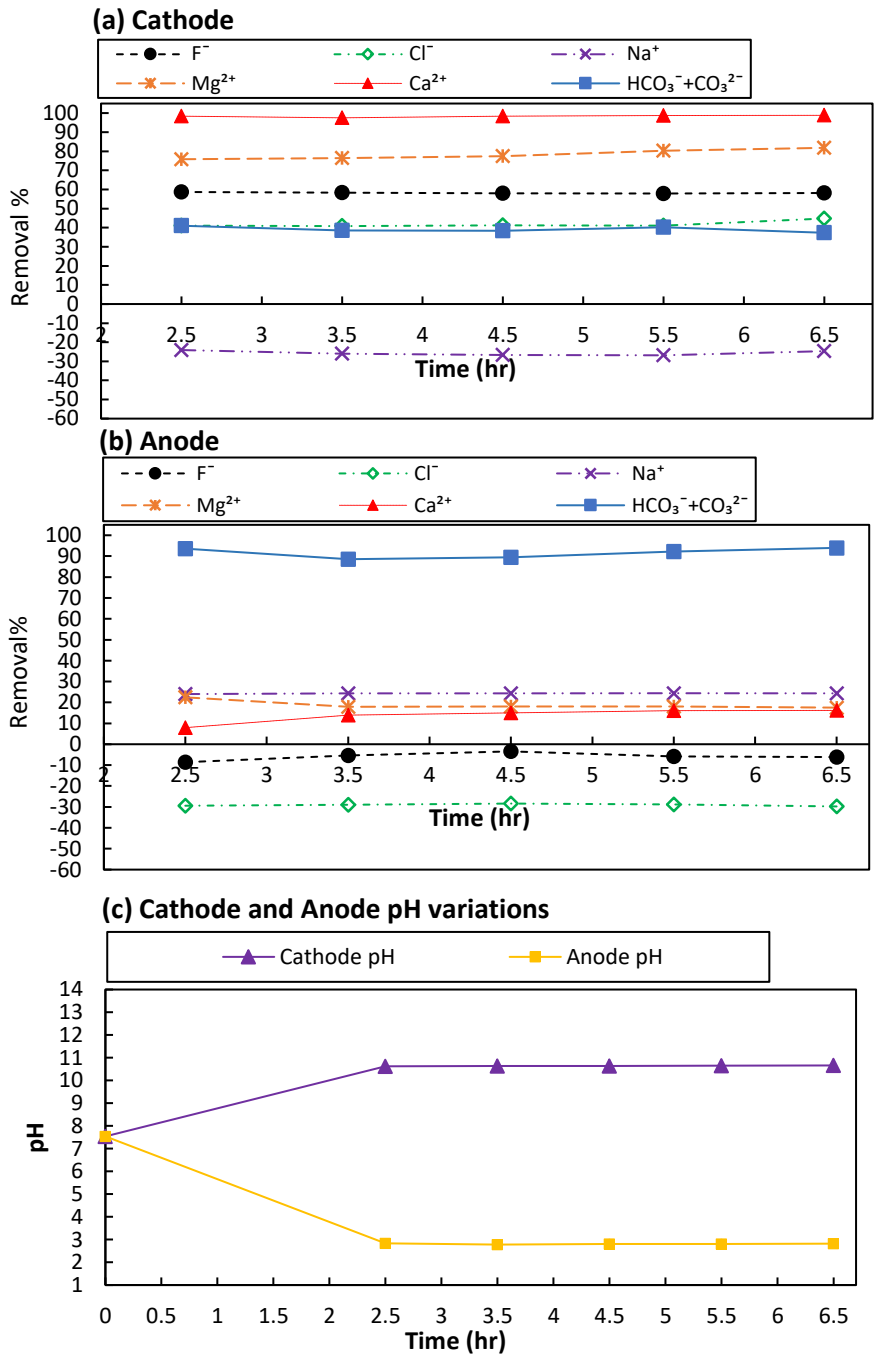

Fig. 1. 33: Ion removal percentage and pH versus time of operation, (a) Cathode, (b) Anode, (c) pH variation; F^{-}_{0} = 10 mg/L, Ca^{2+}_{0} = 200 mg/L, Mg^{2+}_{0} = 45 mg/L, and (HCO_3^{-}+ CO_3^{2-})$_0$ = 10000 µmol/L, C/L=1500

3.11 Community-scale treatment system performance under the real conditions

Groundwater in the northern part of Sri Lanka was found to be highly contaminated with F^-, Mg^{2+}, and Ca^{2+}, and with HCO_3^- and CO_3^{2-} (Kawakami et al., 2014; Weragoda and Kawakami, 2016). Dental and skeletal fluorosis, as well as chronic kidney disease, are common and F^- is mostly suspected as being involved (Chandrajith et al., 2011b; Herath et al., 2017). Therefore, the proposed ELC system was implemented in Sri Lanka as a community-scale treatment system for 5-6 families where there was an urgent need for qualified groundwater for drinking purposes. Accordingly, a groundwater source located in the Medawachchiya area of the Anuradhapura District (location: 8°32'02.8"N 80°29'57.6"E) of Sri Lanka was selected. The treatment system was established with a production capacity of 374 L/Day. The process was similar to the laboratory experiment but utilizing series-connected two reactors. The rejected water quantity was 50% (374 L/Day). During the operation, negligible flow through the diaphragm was observed.

The water quality of the well water (WW), ion removals in the anode and the cathode are shown in Table 1. 6. According to Table 1. 6, the concentration of F^- in the well water exceeded the Sri Lankan maximum guideline of 1 mg/L, as well as the WHO guideline of 1.5 mg/L (SLSI, 2013; WHO, 2017). The concentrations of other ions were also found to be extremely high and did not fluctuate significantly during the operating period. Fig. 1.34 shows the charge loading calculated at the sampling time during 30 days of continuous operation. The charge loading was found to fluctuated 1152-1474 C/L. The ion removal efficiencies for the cathode, the anode, and the related pH are shown in Fig. 1.35a, b, and c, respectively. According to Fig. 1.35a, after being treated with the ELC system, the F^- concentration in the cathode was reduced dramatically and was stable during the one month of operation. The average concentration of F^- was found to be 1.25 mg/L (Table 1. 6) which was under the WHO guideline. However, F^- and Mg^{2+} removal tended to decrease with time. This phenomenon could be an effect of the clay diaphragm clogging due to the

formation of $Mg(OH)_2$ in its pores.

Table 1. 6**:** Well water (WW) quality

Date	**mg/L**						**mmol/L**	
	F^-	**Cl^-**	**SO_4^{2-}**	**Na^+**	**Mg^{2+}**	**Ca^{2+}**	**HCO_3^-+ CO_3^{2-}**	**pH**
2019/2/13	2.70	248	59	201	128	53	13.3	8.32
2019/2/16	2.70	249	60	203	131	55	13.8	8.26
2019/2/20	2.69	244	59	200	128	54	13.6	8.28
2019/2/23	2.69	249	60	202	129	53	13.6	8.23
2019/2/27	2.70	255	61	207	132	56	13.9	8.14
2019/3/02	2.72	258	61	208	132	56	13.9	8.09
2019/3/06	2.72	260	61	209	133	55	13.9	8.05
2019/3/09	2.70	257	60	208	132	55	13.9	8.09
2019/3/13	2.75	255	58	207	131	54	13.8	7.97
Avg.	2.71	253	60	205	131	54	13.8	7.97
Avg. Anode	3.45	360	88	125	82	34	1.9	6.45
Avg. cathode	1.25	173	44	243	95	0.1	11.3	9.36
WHO guideline for drinking water	**1.50**	**250**	**400**	**200**	**50**	**75**	**6.1**	**8.5**

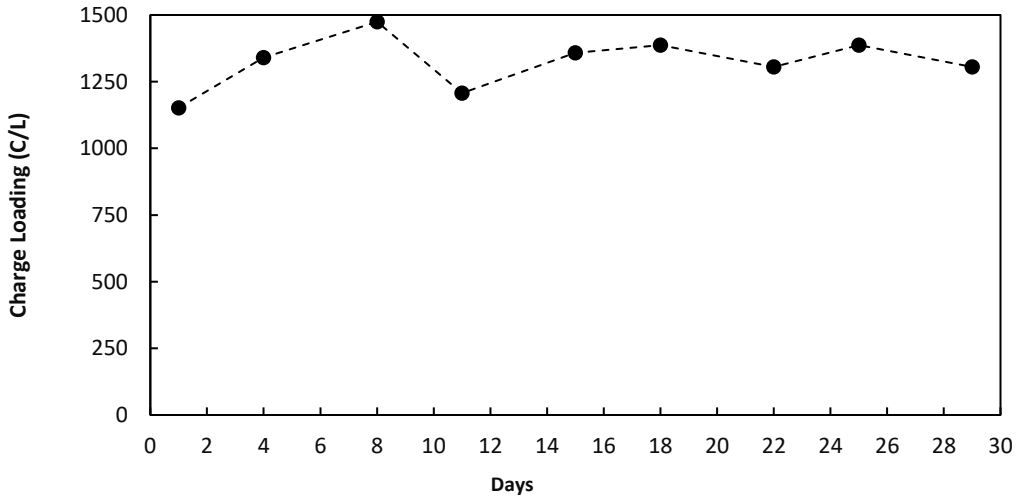

Fig. 1. 34: Charge loading changes in the community scale treatment plant

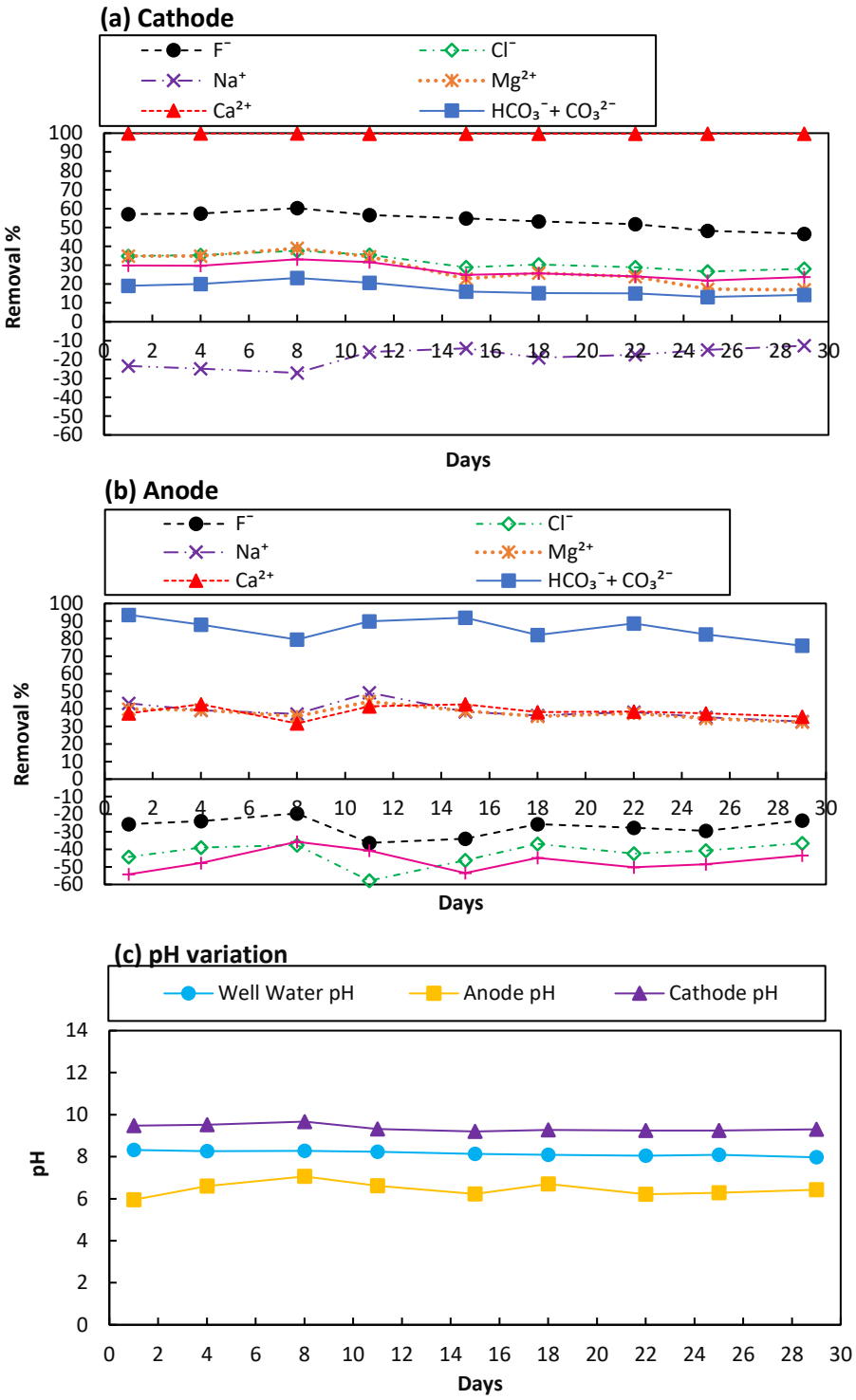

Fig. 1. 35: Ion removal percentage and pH variation of the community-scale treatment plant (a) Cathode, (b) Anode, (c) pH variation

The average concentration of Mg^{2+} in the cathode was 81.7 mg/L (average removal 27.9 %) which did not meet the WHO guideline of 50 mg/L. This lower removal could be a result of the high $HCO_3^- + CO_3^{2-}$ concentration in the WW, as described in section 3.9. The removal of Ca^{2+} in the cathode was significantly high (>99%), but the removal of $HCO3^- + CO3^{2-}$ did not meet the WHO guideline of 6.1 mol/L (Fig. 1.35a). As expected, in the anode (Fig. 1.35b and Table 1. 6) $HCO3^- + CO3^{2-}$ removal was high enough to meet the drinking water quality standard of both WHO and Sri Lanka. In the cathode, only F^-, and Ca^{2+} was removed sufficiently to meet the WHO guidelines for drinking water. However, applying higher charge loadings than the experiment to the system could increase the Mg^{2+}, F^-, and $HCO_3^- + CO_3^{2-}$ removal in both the anode and the cathode to meet WHO and Sri Lankan drinking water quality guidelines.

For the community scale treatment system, a constant 90 (V) voltage power supply was used. The distance between electrodes was kept at approximately 0.9cm (the width of the diaphragm). The calculated Coulomb force of the laboratory-scale system operated at 1500C/L was much similar to the community scale system. Therefore, fitted curve functions defined in sections 3.6 to 3.9 can be used to correct the initial concentrations. Atmospheric CO_2 dissociation was neglected in the calculations. Fig. 1.36 shows the measured and calculated Mg^{2+} and F^- concentrations. From the results, it's clear that the proposed model could estimate both Mg^{2+} and F^- when initial concentrations of Mg^{2+}, Ca^{2+}, $HCO_3^- + CO_3^{2-}$, the applied charge loading and the voltage were known.

Moreover, generated waste of Mg.Ca (CO_3) and $Mg(OH)_2$ precipitate can be used as long term fertilizer for the coconut cultivation areas where currently dolomite is widely used as fertilizer in Sri Lanka.

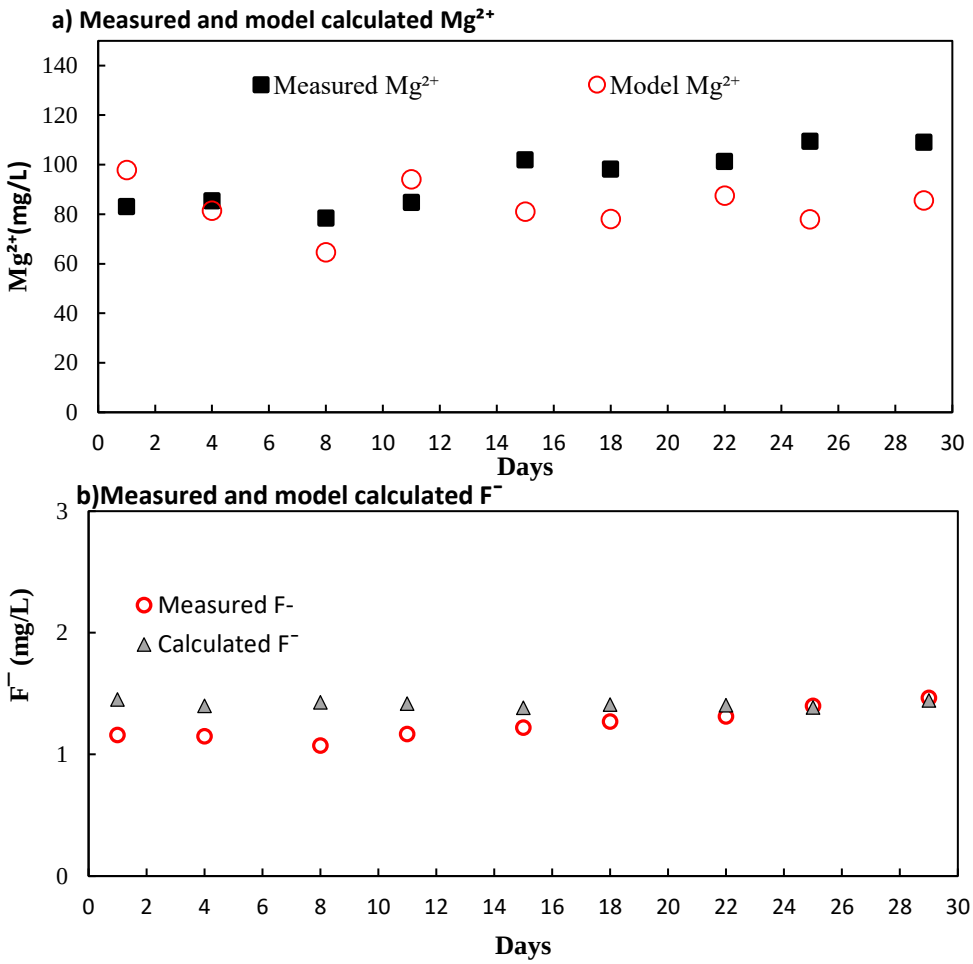

Fig. 1. 36: Measured and model-calculated Mg^{2+} and F^- during the community scale system operational time

3.12 Countermeasure to decrease Mg^{2+} and F^- concentration by using model

To increase the Mg^{2+} removal, HCO_3^-+CO_3^{2-} concentration should be decreased (either by increasing charge loading or pretreatment method) and it can be verified with the model simulated results shown in Fig. 1.37. To increase F^- removal, Mg^{2+} concentration should be increased and HCO_3^-+CO_3^{2-} concentration should be decreased. Model data showed in Fig. 1.38 can be used to estimate the F^- removal.

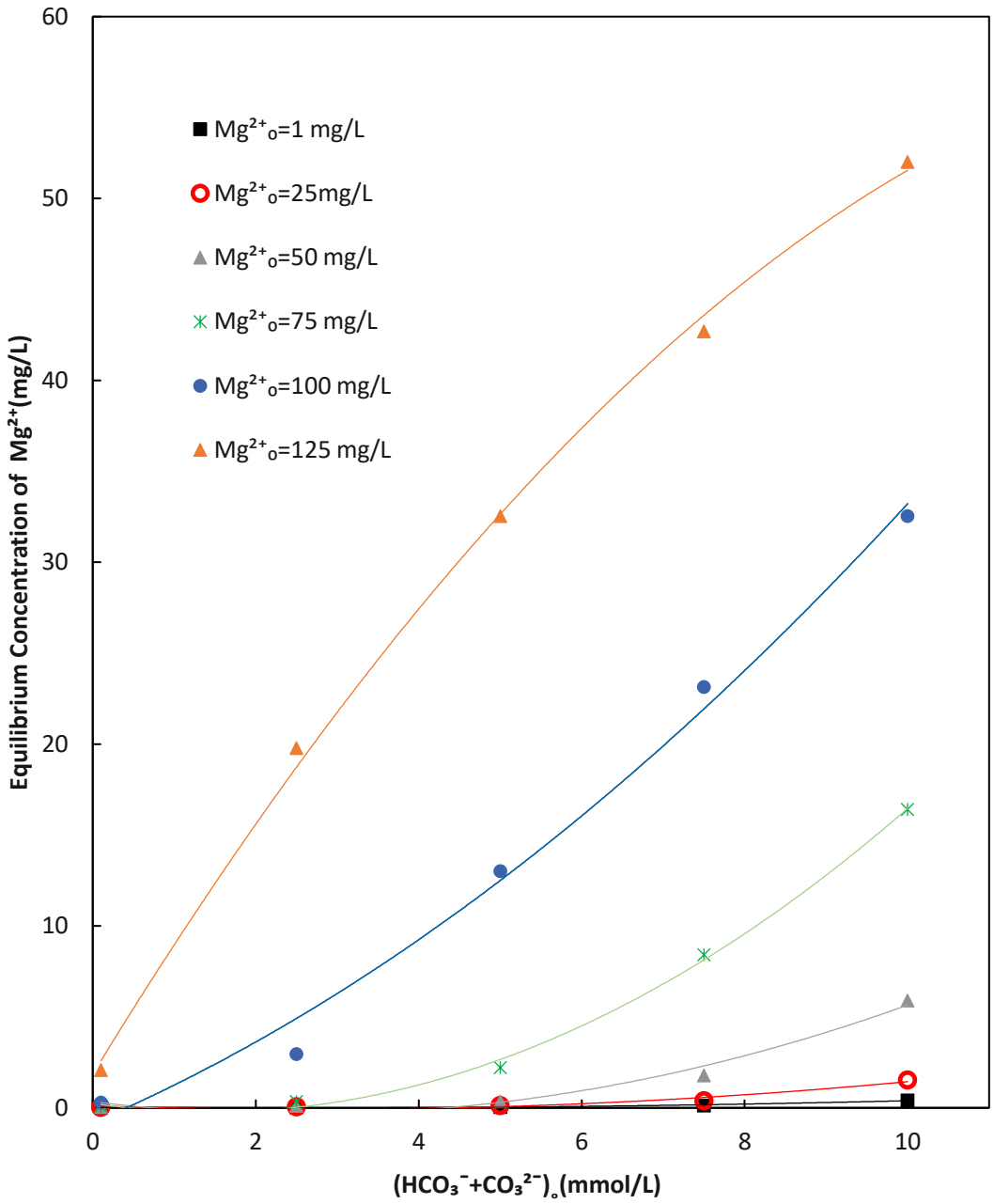

Fig. 1. 37: Model calculated equilibrium concentration of Mg^{2+} for different concentrations of initial Mg^{2+}, HCO_3^-+CO_3^{2-} at 1500 C/L charge loading

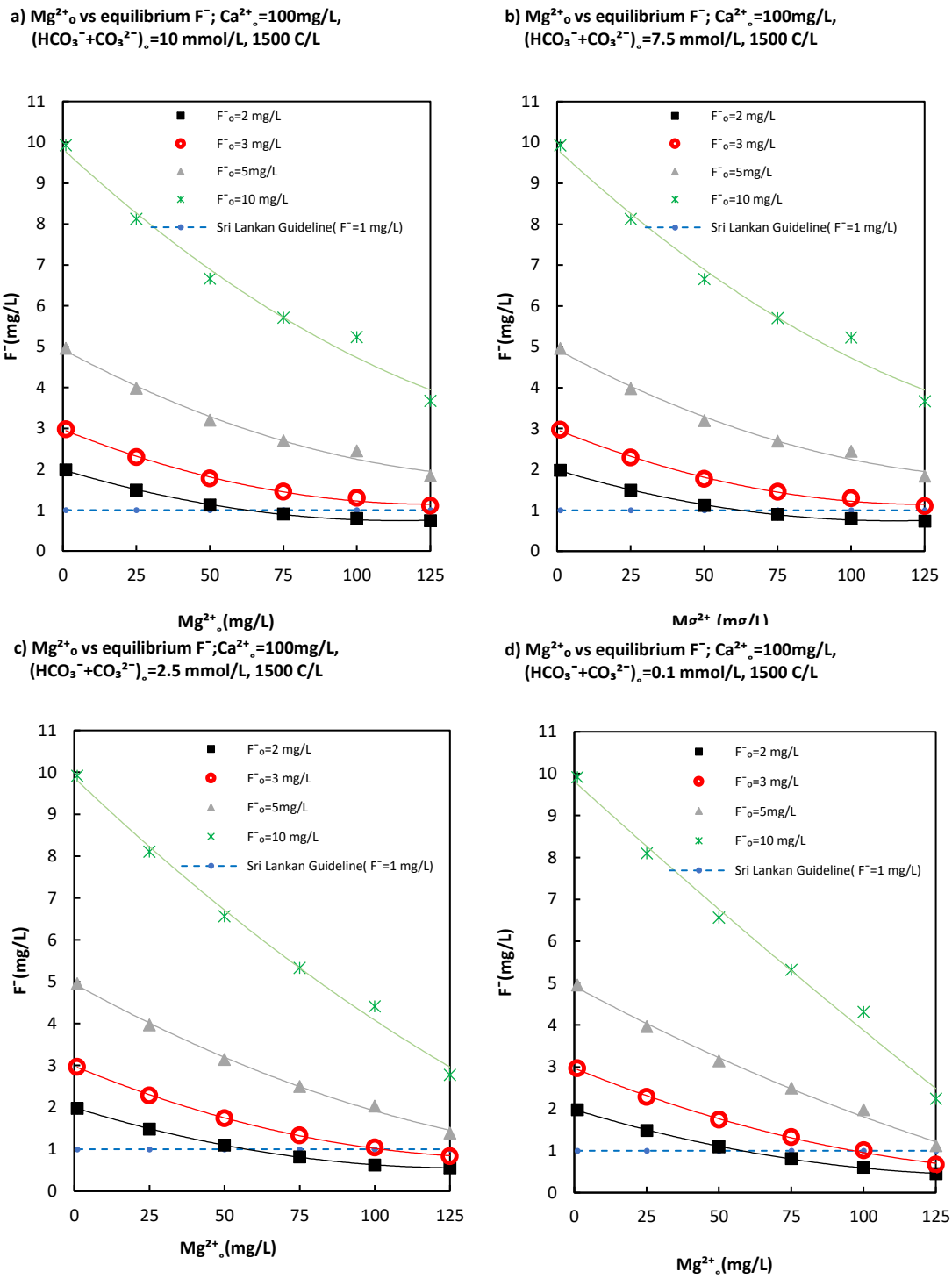

Fig. 1. 38: Model calculated equilibrium concentration of F^- for different concentrations of initial Mg^{2+}, $HCO_3^-+CO_3^{2-}$ and F^- at 1500 C/L charge loading

3.13 Estimation of operational costs

The proposed system's power consumption mainly depends on the cost of power consumption. Based on the commercial diaphragm used in the laboratory experiment and the terra-cotta clay diaphragm used in the community-scale treatment plant, operational costs were calculated (Eq.1.60). The minimum and maximum voltage values for the commercial diaphragm employed in the laboratory experiment were 13.2–22.5 V for 0.1 A at 1500 C/L. The average current used for the community level treatment plant that employed a terra cotta diaphragm was 5.738 A at a constant 90 V for 374 L/day production capacity in the cathode. The market price of electricity (0.061 US$/kWh) in Sri Lanka for the year 2019 was used for the calculations (CEB, 2019). Accordingly, it was found that the operational costs for treatment using a commercial diaphragm or terra cotta clay diaphragm were 0.23–0.14 or 2.02 US$/m^3, respectively, with 50% water rejection. Unit production cost for the treatment plant was 2872 US$.

$$Power\ Cost\left(\frac{US\$}{m^3}\right) = \frac{Average\ Voltage(V) \times Current(I) \times Time\ (h)}{Volume\ treated\ (m^3) \times 10^3} \times Energy\ Price\left(\frac{US\$}{kWh}\right) \tag{1.60}$$

4 Conclusions

The main objective of the study was to propose an ELC method for removing coexisting F^-, Ca^{2+}, Mg^{2+}, $HCO_3^-$and CO_3^{2-} from groundwater without adding any chemicals and to meet the drinking water quality guidelines. System performance against charge loading and various initial concentrations of F^-, Ca^{2+}, Mg^{2+}, $HCO_3^-$and CO_3^{2-} were also studied to set the operational guidelines to elucidate the removal mechanism and to establish the mathematical model. The performance of the proposed system was tested with real groundwater to evaluate the system's performance and drawbacks and to validate the mathematical model.

Findings revealed that the proposed system was capable of removing coexisting F^-, Ca^{2+}, Mg^{2+}, $HCO_3^-$and CO_3^{2-} without adding any chemicals as well as 50% water recovery. Primarily, F^-, Ca^{2+}, and Mg^{2+} ions were significantly removed in the cathode, while $HCO_3^-$and CO_3^{2-} removal was significant in the anode. $Ca^{2+}$and Mg^{2+} were removed by precipitation as $CaCO_3$ and $Mg(OH)_2$ respectively. $F^-$was removed by co-precipitation with $Mg(OH)_2$ while $HCO_3^-$and CO_3^{2-} was removed as CO_2 in the anode. moreover, Coulomb transfer removed F^- as well. Accordingly, a proposed mathematical model was validated by the experimental results and calculated removals for the laboratory and the community-scale systems were in line with the measured values.

Applied charge loading and changes in the initial concentrations of F^-, Mg^{2+}, Ca^{2+}, and HCO_3^-+ CO_3^{2-} contributed for ion removal efficiencies by coulomb transfer and precipitation. A range of initial ion concentrations as, F^-_0=4.29-6 mg/L, Mg^{2+}_0=75-125 mg/L, Ca^{2+}_0 >50 mg/L and $(HCO_3^-+ CO_3^{2-})_0$<10 mmol/L in place of 1500 C/L should be in raw water to meet drinkable level F^- concentration. A maximum level of, F^-_0=20, Ca^{2+}_0=125, Mg^{2+}_0=100 mg/L showed a maximum removal of 50, 95>,40% respectively in the cathode and removal of higher than 93%> for $(HCO_3^-+ CO_3^{2-})_0$=12.5 mmol/L in the anode.

Proposed system performance was acceptable to treat the Sri Lankan groundwater where high F^-, Mg^{2+}, Ca^{2+}, and HCO_3^-+ CO_3^{2-} present and the model countermeasure calculations shall be incorporated to determine whether the system is capable of delivering water quality guideline

References

Amini, M., Mueller, K., Abbaspour, K. C., Rosenberg, T., Afyuni, M., Møller, K. N., Sarr, M., and Johnson, C. (2008) Statistical Modeling of Global Geogenic Fluoride Contamination in Groundwaters. *Environmental Science and Technology*, 42(10), 3662–3668.

Ayoob, S. and Gupta, A. K. (2006) Fluoride in drinking water: A review on the status and stress effects, *Critical Reviews in Environmental Science and Technology*,36 (6), 433-487.

Bhatnagar, A., Kumar, E., and Sillanpää, M. (2011) Fluoride removal from water by adsorption-A review. *Chemical Engineering Journal*, 171(3), 811–840.

Brillas, E., Cabolt, P.L., Casado, J., 2003. Chemical degradation methods for wastes and pollutants:*environmental and industrial applications*. Marcel Dekker, New York.

Brillas, E., Martínez-huitle, C.A., 2015. Decontamination of wastewaters containing synthetic organic dyes by electrochemical methods. An updated review. *Applied Catal. B, Environ*. 166–167, 603–643.

Browne, D., Whelton, H., O'Mullane, D., 2005. Fluoride metabolism and fluorosis. *J. Dent.* 33,177-186

Ceylon Electricity Board, (2019), Tariff Plan, CEB, last accessed 2019.11.21: *https://www.ceb.lk/commercial-tariff/en*

Chandrajith, R., Nanayakkara, S., Itai, K., Aturaliya, T. N. C., Dissanayake, C. B., Abeysekera, T., Harada, K., Watanabe, T., and Koizumi, A. (2011) chronic kidney diseases of uncertain etiology (CKDue) in Sri Lanka: geographic distribution and environmental implications. *Environmental Geochemistry and Health*, 33(3), 267–278.

Chung, Y., Shin, D., Park, S., Lim, Y., Choi, Y., Cho, S., Yang, J., Hwang, M., Park, Y., Lee, H., (1997). Risk assessment and management of drinking water pollutants in Korea, *Water Science and Technology*. 309–323.

De Francesco, M., Costamagna, P., (2004). On the design of electrochemical reactors for the treatment of polluted water, *Journal of Cleaner Production*. pp. 159–163.

Devi, R. R., Umlong, I. M., Raul, P. K., Das, B., Banerjee, S., and Singh, L. (2012) Defluoridation of water using nano-magnesium oxide. *Journal of Experimental Nanoscience*, 1(13), 512–524.

Dissanayake, C.B., (2005). Water quality in the dry zone of Sri Lanka -some interesting health aspects. *J. Natn.Sci.Foundation Sri Lanka* 33, 161–168.

Fawell, J., Bailey, K., Chilton, J., Dahi, E., Fewtrell, L., and Magara, Y. (2006) Fluoride in Drinking-water, WHO, IWA publishing.

Fu, H., Wang, M., Ho, Y., (2013). Mapping of drinking water research: A bibliometric analysis of research output during 1992 – 2011. *Sci. Total Environ*. 443, 757–765.

Gabrielli, C., Maurin, G., Francy-Chausson, H., Thery, P., Tran, T. T. M., and Tlili, M. (2006) Electrochemical water softening: principle and application. *Desalination*, 201(1–3), 150–163.

Gascó, G. and Méndez, A. (2005) Sorption of Ca^{2+}, Mg^{2+}, Na+ and K+ by clay minerals. *Desalination*, 182(1–3), 333–338.

Herath, H. M. A. S., Kubota, K., Kawakami, T., Nagasawa, S., Motoyama, A., Weragoda, S. K., Chaminda, G. G. T., and Yatigammana, S. K. (2017) Potential risk of drinking water to human health in Sri Lanka. *Environmental Forensics*, 18(3), 241–250.

Holt, P.K., Barton, G.W., Mitchell, C.A., (2005). The future for electrocoagulation as a localized water treatment technology. *Chemosphere*.59-3,355-367

Iano, F.G., Ferreira, M.C., Quaggio, G.B., Fernandes, M.S., Oliveira, R.C., Ximenes, V.F., Buzalaf, M.A.R., (2014). Effects of chronic fluoride intake on the antioxidant systems of the liver and kidney in rats. *J. Fluor. Chem*. 168, 212–217.

Imai, Y., Kawakami, T., (2019) Fluoride removal from hot spring waste water by an electrolysis method and its mechanism., Global Environment Engineering Research, *J stage*, 27(5), 403-410

Jadhav, S. V., Bringas, E., Yadav, G.D., Rathod, V.K., Ortiz, I., Marathe, K. V., 2015. Arsenic and fluoride contaminated groundwaters: A review of current technologies for contaminants removal. *J. Environ. Manage*.162, 306-325

Janson, A., Minier-Matar, J., Al-Shamari, E., Hussain, A., Sharma, R., Adham, S., and Rowley, D. (2018) Evaluation of new ion exchange resins for hardness removal from boiler feedwater. *Emergent Materials*, 1(1–2), 77–87.

Karimi, A., Radfard, M., Abbasi, M., Naghizadeh, A., Biglari, H., Alvani, V., and Mahdavi, M. (2018) Fluoride concentration data in groundwater resources of Gonabad, Iran. *Data in Brief*, 21, 105–110.

Kawakami, T., Motoyama, A., Nagasawa, S., Weragoda, S., and Chaminda, T. (2014) Groundwater Quality Atlas of Sri Lanka, Kandy, Sanduni Offset Printers.

Kawakami, T., Nishino, M., Imai, Y., Miyazaki, H., and Amarasooriya, A. A. G. D. (2018) De-fluoridation of drinking water by co-precipitation with magnesium hydroxide in electrolysis. *Cogent Engineering*, 5(1), 1–13.

Ketata, M., Hamzaoui, F., Gueddari, M., Bouhlila, R., and Ribeiro, L. (2011) Hydrochemical and statistical study of groundwaters in Gabes-south deep aquifer (south-eastern Tunisia). *Physics and Chemistry of the Earth*, 36(5–6), 187–196.

Kim, K. and Jeong, G. Y. (2005) Factors influencing natural occurrence of fluoride-rich groundwaters: A case study in the southeastern part of the Korean Peninsula. *Chemosphere*, 58(10), 1399–1408.

Kuokkanen, V., Kuokkanen, T., Rämö, J., and Lassi, U. (2013) Recent Applications of Electrocoagulation in Treatment of Water and Wastewater—A Review. *Green and Sustainable Chemistry*, 03(02), 89–121.

Lin, Y. P. and Singer, P. C. (2009) Effect of Mg^{2+} on the kinetics of calcite crystal growth. *Journal of Crystal Growth*, 312(1).

Luo, W., Gao, X., and Zhang, X. (2018) Geochemical processes controlling the groundwater chemistry and fluoride contamination in the yuncheng basin, China—an area with complex hydrogeochemical conditions. *PLoS ONE*, 13(7), 1–25.

Mameri, N., Yeddou, A.R., Lounici, H., Belhocine, D., Grib, H., Bariou, B., (1998). Defluoridation of septentrional Sahara water of north Africa by electrocoagulation process using bipolar aluminium electrodes. *Water Res.* 32, 1604–1612.

Mandinic, Z., Curcic, M., Antonijevic, B., Carevic, M., Mandic, J., Djukic-Cosic, D., Lekic, C.P., (2010). Fluoride in drinking water and dental fluorosis. *Sci. Total Environ*. 408, 3507–3512.

Martínez-Huitle, C. a, Ferro, S., Martı, C.A., (2006). Electrochemical oxidation of organic pollutants for the wastewater treatment: direct and indirect processes. *Chem. Soc. Rev.* 35, 1324–40.

Masindi, V., Gitari, W. M., and Ngulube, T. (2015) Kinetics and equilibrium studies for removal of fluoride from underground water using cryptocrystalline magnesite. *Journal of Water Reuse and Desalination*, 5(3), 282–292.

Meenakshi and Maheshwari, R. C. (2006) Fluoride in drinking water and its removal. *Journal of Hazardous Materials*, 137, 456–463.

Michałowski, T., Asuero, A.G., (2012). Thermodynamic Modelling of Dolomite Behavior in Aqueous Media, *J Thermodyn*, 1-12

Mohapatra, M., Anand, S., Mishra, B.K.K., Giles, D.E., Singh, P., (2009). Review of fluoride removal from drinking water. *J. Environ. Manage*. 91, 67–77.

Mollah, M. Y., Schennach, R., Parga, J. R., and Cocke, D. L. (2001) Electrocoagulation (EC)--Science and Applications. *Journal of Hazardous Materials*, 84(1), 29–41.

Mukherjee, S. and Halder, G. (2018) A review on the sorptive elimination of fluoride from contaminated wastewater. *Journal of Environmental Chemical Engineering*. 6(1), 1257-1270.

Nidheesh, P. V. and Singh, T. S. A. (2017) Arsenic removal by electrocoagulation process: Recent trends and removal mechanism. *Chemosphere*, 181, 418–432.

Oladoja, N. A., Hu, S., Drewes, J. E., and Helmreich, B. (2016) Insight into the defluoridation efficiency of nano magnesium oxide in groundwater system contaminated with hexavalent chromium and fluoride. *Separation and Purification Technology*, 162(February), 195–202.

Paranagama, D. G. A., Bhuiyan, M. A., and Jayasuriya, N. (2018) Factors associated with chronic kidney disease of unknown aetiology (CKDu) in North Central Province of Sri Lanka: a comparative analysis of drinking water samples. *Applied Water Science*, 8(6), 151.

Perera, T., Ranasinghe, S., Alles, N., and Waduge, R. (2018) Effect of fluoride on major organs with the different time of exposure in rats. *Environmental Health and Preventive Medicine*, 23(1).

Plummer, L. N. and Busenberg, E. (1982) The solubilities of calcite, aragonite and vaterite in CO2-H2O solutions between 0 and 90°C, and an evaluation of the aqueous

model for the system CaCO3-CO2-H2O. *Geochimica et Cosmochimica Acta*, 46(6), 1011–1040.

Pulkka, S., Martikainen, M., Bhatnagar, A., Sillanpää, M., (2014). Electrochemical methods for the removal of anionic contaminants from water - A review. *Sep. Purif. Technol.*132, 252-271.

Rafique, T., Naseem, S., Usmani, T. H., Bashir, E., Khan, F. A., and Bhanger, M. I. (2009) Geochemical factors controlling the occurrence of high fluoride groundwater in the Nagar Parkar area, Sindh, *Pakistan. Journal of Hazardous Materials*, 171(1–3), 424–430.

Rango, T., Kravchenko, J., Atlaw, B., McCornick, P. G., Jeuland, M., Merola, B., and Vengosh, A. (2012) Groundwater quality and its health impact: An assessment of dental fluorosis in rural inhabitants of the Main Ethiopian Rift. *Environment International*, 43(1), 37–47.

Salifu, A., Petrusevski, B., Ghebremichael, K., Buamah, R., and Amy, G. (2012) Multivariate statistical analysis for fluoride occurrence in groundwater in the Northern region of Ghana. *Journal of Contaminant Hydrology*, 140–141, 34–44.

Sandoval, M.A., Fuentes, R., Nava, J.L., Rodríguez, I., (2014). Fluoride removal from drinking water by electrocoagulation in a continuous filter press reactor coupled to a flocculator and clarifier. *Sep. Purif. Technol*. 134, 163–170.

Shen, J. and Schafer, A. (2014) Removal of fluoride and uranium by nanofiltration and reverse osmosis: A review. *Chemosphere*, 117(1), 679–691.

Singaraja, C., Chidambaram, S., Anandhan, P., Prasanna, M. V., Thivya, C., Thilagavathi, R., and Sarathidasan, J. (2014) Geochemical evaluation of fluoride contamination of groundwater in the Thoothukudi District of Tamilnadu, India. *Applied Water Science*, 4(3), 241–250.

SLSI (2013) “Sri Lanka Standards for potable water-(SLS 614)” in Drinking water standards. *Sri Lankan Standards Institute*.

Spencer, H., Lewln, I., 1970. Fluoride Metabolism in Man. *Am. J. Med*. 49, 807-813.

Su, C., Wang, Y., Xie, X., and Li, J. (2013) Aqueous geochemistry of high-fluoride groundwater in Datong Basin, Northern China. *Journal of Geochemical Exploration*, 135, 79–92.

Thapa, R., Gupta, S., Gupta, A., Reddy, D. V., and Kaur, H. (2018) Geochemical and geostatistical appraisal of fluoride contamination: An insight into the Quaternary aquifer. *Science of the Total Environment*, 640–641, 406–418.

Turner, B. D., Binning, P., and Stipp, S. L. S. (2005) Fluoride removal by calcite: Evidence for fluorite precipitation and surface adsorption. *Environmental Science and Technology*, 39(24), 9561–9568.

Weragoda, S. K. and Kawakami, T. (2016) “Evaluation of groundwater quality in 14 districts in Sri Lanka: A collaboration research between Sri Lanka and Japan” in *Trends in Asian Water Environmental Science and Technology*., 151–155.

WHO (2017) Guidelines for drinking-water quality: fourth edition incorporating the first addendum, *World Health Organization*.

Wickramarathna, S., Balasooriya, S., Diyabalanage, S., and Chandrajith, R. (2017) Tracing environmental aetiological factors of chronic kidney diseases in the dry zone of Sri Lanka—A hydrogeochemical and isotope approach. *Journal of Trace Elements in Medicine and Biology*, 44(June), 298–306.

Zeppenfeld, K. (2011) Electrochemical removal of calcium and magnesium ions from aqueous solutions. *Desalination*. 277(1-3), 99-105.

Zeppenfeld, K. (1998) Electrolysis as a method for partial decarbonisation. *GWF Wasser-Abwasser*, 139(2).86-91.

Zhi, S. and Zhang, K. (2016) Hardness removal by a novel electrochemical method. *Desalination*, 381, 8–14.

Zuo, Q., Chen, X., Li, W., Chen, G., (2008). Combined electrocoagulation and electroflotation for removal of fluoride from drinking water. *J. Hazard. Mater*. 159, 452–457.

CHAPTER 2

Removal of Fluoride, Alkalinity and Hardness Species (Ca^{2+}, Mg^{2+}) from Drinking Groundwater by Electrolysis

1. Introduction

In Chapter 1, we investigated the ELC method as a real scale implementation to remove F^-, co-existing Mg^{2+}, Ca^{2+}, and HCO_3^-+ CO_3^{2-} and its mathematical model. However, significant drawbacks found in Chapter 1 were the system's preferences for removing F^-, Mg^{2+}, HCO_3^-+ CO_3^{2-}, its water rejection, F^- removal decrement with higher HCO_3^-+ CO_3^{2-} and complexity of initial ion concentration correction for the model input. Moreover, for water-scarce areas, which also have higher concentrations of Mg^{2+} and HCO_3^-+ CO_3^{2-}, the proposed system would not be appropriate. Accordingly, in this Chapter, continuous flow electrolysis (ELC) system was re-designed to increase HCO_3^-+ CO_3^{2-} removal which will increase the Mg^{2+} and F^- removal without any water rejection. Furthermore, the proposed system was designed so that Coulomb force transfer least affected the initial ions concentration corrections thus simplifying the model calculations. Using synthetic groundwater containing Mg^{2+}, Ca^{2+}, and HCO_3^-+ CO_3^{2-} ions, the removal of F^-, Mg^{2+}, Ca^{2+}, and HCO_3^-+ CO_3^{2-} were studied by laboratory experiments. The community-scale system was also operated with natural groundwater.

Furthermore, mechanisms of ion removal, mathematical model implementation, and process optimization were studied for different concentrations of contaminants levels. Laboratory-prepared synthetic groundwater treatment efficiencies were compared with a community-scale ELC water treatment facility operated in Sri Lanka to validate experimental and model results.

2. Materials and methods

2.1 Chemicals, instruments, and calculations

Chemicals and analytical instruments used in this study for the analysis of Anions, Cations, X-ray diffraction (XRD), and pH were the same as those described in Chapter 1, section 2.2. Platinum electrodes were purchased from the Nilaco Corporation, Japan, and stainless-steel electrodes were obtained from the local market in Japan. Carbon concentrations in solid samples were analyzed with CHN CORDER MT-5 (Yanaco, Japan). Voltage logging was performed with (ONSET, HOBO) data loggers in the field experiment. Due to the diprotic nature of carbonic acid (H_2CO_3) in the solution, both CO_3^{2-} and HCO_3^-ions are present and their concentrations would change with the solution pH. Therefore, the sum of the carbonates ($HCO_3^-$and CO_3^{2-}) concentrations (hereafter $HCO_3^- + CO_3^{2-}$) as mmol/L was accounted for regarding the alkalinity. Accordingly, equations derived in Chapter 1 section 2.4 (Eq. 1.13-1.20) were employed for calculating individual concentrations of $HCO_3^-$and CO_3^{2-}.

2.2 Sample collection, storage, and quality control

A groundwater source located in Sri Lanka, in the Medawachchiya area (8°32'02.8"N 80°29'57.6"E) of the Anuradhapura District was selected to perform the field study. Water samples from the field and the laboratory were filtered into the 50 mL polyethylene bottles on location by using a membrane filter with a 0.45 µm pore size to eradicate bacteriological activities affecting the water quality and to remove the non-dissolved particles. The proposed system was kept for 24 hours to stabilize before sample collection. The collected water samples from the field were transported to Japan and analyzed within 45 days of their collection. Laboratory samples were analyzed within one week of their collection.

To analyze the precipitate's chemical composition, a known amount of (2-5 L) treated water from the cathode outlet was collected and kept a few hours until it had settled. After the precipitate had settled, supernatant water, as well as settled gelatinous liquid, were filtered with 0.45 µm membrane filter and dry (60^0C) weighted. For chemical composition analysis, 1g of dried sample was dissolved in 30% conc. Nitric acid, then filtered and analyzed with an Ion Chromatograph. By analyzing the calibration standard solution after every 20 samples, the stability of the Ion Chromatograph was monitored for quality control. Overall concentration variability of the examined calibration standard solution was obtained below the 5 % or otherwise, reanalysis was performed.

2.3 Experimental setup of ELC cell

An acrylic material tank, having dimensions of 20 cm × 10.5 cm × 5 cm (length × height × width), was used as an ELC reactor for the laboratory experiments. The tank was separated into two cells with a 4 mm thick (20 cm × 10.5 cm) permeable clay diaphragm. The diaphragm helped to separate the anode and the cathode solutions, preventing the mixing of sludge formed in the cathode, and facilitating the exchange of ions between the cells.

To lengthen the water flow in each cell, individual cells were further divided into two equal slots with an acrylic plate, keeping open 10 mm from the bottom. Effective volumes of the cathode and the anode cells were 525 mL and 420 mL, respectively. The asymmetric design was undertaken to acquire more space in the cathode to decrease volume error occurring due to the sludge settlements in longer continuous operational periods.

U-shaped platinum (Pt) (effective length = 30 cm, φ = 0.40 mm) and stainless steel (SS) (effective length = 30 cm, φ = 1.00 mm) wires were used as electrodes for the anodes and the cathodes, respectively. The inter-electrode distance was kept at 3.3 cm. The assembly was connected to a constant current power supply for all experiments; the ELC cell configuration is shown in Fig.2.1.

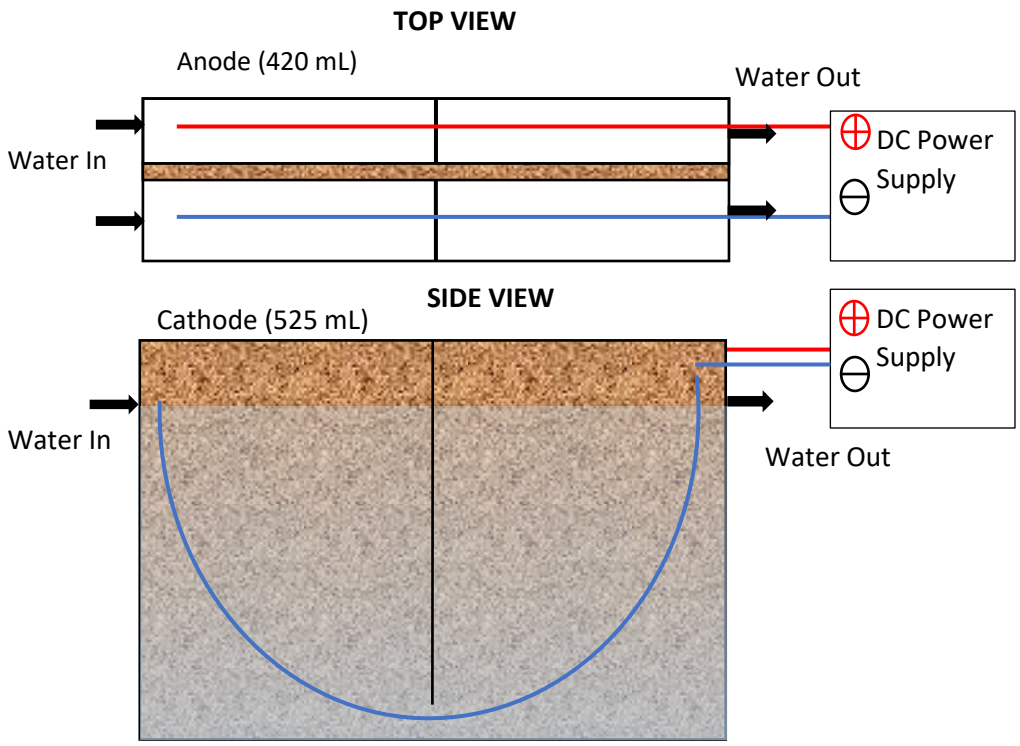

Fig. 2. 1: Electrolysis cell configuration

2.4 Unit treatment steps and operational conditions

The presence of high concentrations of HCO_3^-+ CO_3^{2-} significantly decreases the F^- and Mg^{2+} removal as concluded in Chapter 1. Accordingly, HCO_3^-+ CO_3^{2-} removal becomes extremely important to acquire high removal of F^- and to meet the guideline for drinking water quality. As such, ELC experimental setup was re-designed, and the experimental setup used in the laboratory is shown in Fig.2.2. It describes an ELC system comprised of an HCO_3^-+ CO_3^{2-} removal configuration in which an aerator was utilized. This system circulates the anode bath water with a lower pH to remove HCO_3^-+ CO_3^{2-} and both the anode and the aerator as carbon dioxide (CO_2) (Chapter1, Eq.1.2).

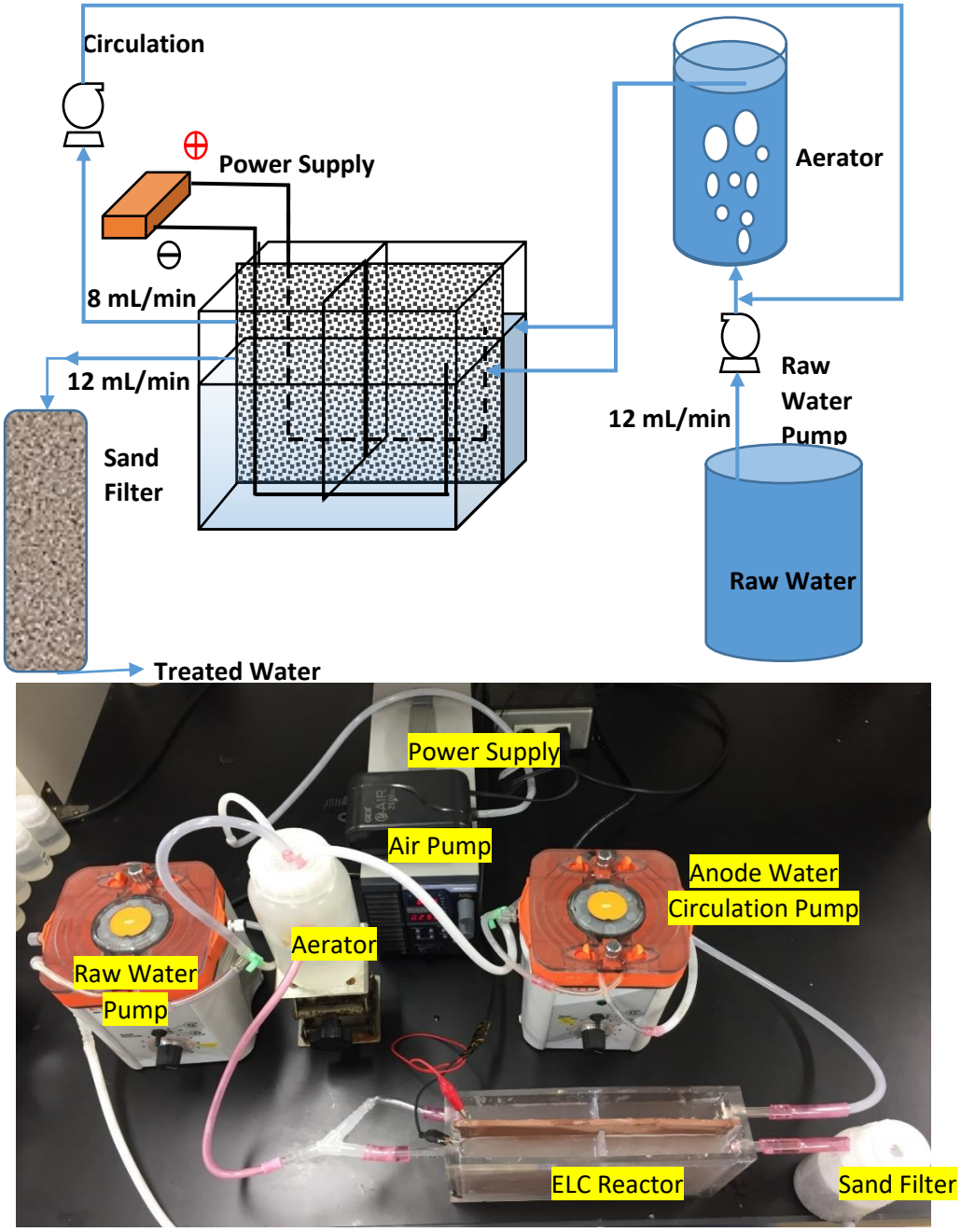

Fig. 2. 2: Schematic diagram and laboratory-scale image of the electrolysis system

Note that the HCO_3^-+ CO_3^{2-} removed from the system are the sum of the HCO_3^-+ CO_3^{2-} removed in the anode (H^+ ions reacting with HCO_3^-+ CO_3^{2-} to form CO_2(g)), HCO_3^-+ CO_3^{2-} removed in the aerator as CO_2(g) (by reacting with residual H^+ ions from the anode), and HCO_3^-+ CO_3^{2-} precipitated as $CaCO_3$ and $MgCO_3$ in the cathode. Moreover, the dilution of raw water HCO_3^-+ CO_3^{2-} took place at the aerator by mixing with a lesser or nil amount of HCO_3^-+ CO_3^{2-} solution circulating through the anode.

As electrolysis progressed, OH^- generated in the cathode cell (causing high pH) (Chapter 1, Eq. 1.3), while H^+ generated in the anode cell caused a low pH environment (Chapter 1, Eq. 1.1). The majority of ions could be removed in the cathode cell (Chapter 1, Eqs.1.4-1.12). The higher pH environment in the cathode could start precipitating/co-precipitating the Mg^{2+}, F^-, Ca^{2+}, and HCO_3^-+ CO_3^{2-}. Principally, Mg^{2+} forming coagulant $Mg(OH)_2$, could be involved in removing F^- (Chapter 1, Eq. 1.9). As a final treatment step, a rough sand filter was used to remove the precipitates.

In the electrochemical process of removing F^-, Mg^{2+}, Ca^{2+}, and HCO_3^-+ CO_3^{2-}, key parameters that affect the ions removal efficiencies include the current applied and charge loading. Therefore, electrolysis time or charge loading (A /(Ls^{-1}) =C/L) is an important parameter that affects the process performance. Moreover, charge loading is an appropriate parameter for maintaining performance when scaling to different treatment volumes. Hence, charge loading is the most important operational variable for ELC treatment efficiency.

For the community scale treatment system, aeration was performed in the anode bath to reduce the system complexity and the number of pumps. This system modification help to minimize the power consumption and cost of construction. As a power source, a constant voltage power supply (max 10A) was used. By measuring the voltage across the resistor using data loggers (ONSET, HOBO), the amperage was calculated. Two reactors made of a Perspex acrylic material similar to the laboratory

experimental ELC reactor were connected in series and utilized at the treatment plant. The effective total volume of the anode and cathode was 12 L (28cm×40cm×5.357cm×2). Pt wires (30 cm × 2) and SS mesh (2 cm × 2 cm) were used as anode and cathode electrodes, respectively.

As reviewed by Bhattacharya and Samal, 2018 and reported by Kawakami et. al., 2014, the maximum F^- concentrations in groundwater in India, Japan, Nigeria, Brazil, China, and Sri Lanka were less than 10 mg/L. Nevertheless, in Pakistan and Indonesia maximum concentration exceeded 14 mg/L (Farooqui et. Al., 2007; Heikens et al., 2005). Accordingly, this study was performed with a maximum F^- concentration of 10 mg/L. The charge loading applied and respective current densities used (A/m^2=Current/ (cross-sectional area of the electrolyte, between the anode and cathode)) were 250, 500, 750, 1000, 1250, 1500 C/L and 2.38, 4.76, 7.14, 9.52, 11.9, 14.29 A/m^2, respectively.

For the experiments, a series of F^-, Mg^{2+}, Ca^{2+}, and HCO_3^-+ CO_3^{2-} spiked tap water (hereafter initial concentrations will be denoted as F^-_0, Mg^{2+}_0, Ca^{2+}_0, and HCO_3^-+ $CO_3^{2-}{}_0$) was used as synthetic groundwater. Synthetic groundwater was continuously pumped to the ELC reactor. The system flow rates were kept constant, 12 mL/min in the cathode (retention time 0.73 hr) and 8 mL/min in the anode (retention time 0.88 hr). A constant current was applied to the immersed SS and Pt electrodes throughout the experiments. The initial ion concentration flow rates and the applied charge loading for different experiments are summarized in Table 2.1.

Table 2.1: Operational conditions and initial concentrations maintained at the laboratory and field experiments and related water quality guidelines.

Laboratory conditions								
Versus ion Removal / Experiment	**Charge Loading (C/L)**	**Current (A)**	**Initial Concentrations**				**Cathode inflow and outflow rate (mL/min)**	**Anode circulate rate (mL/min)**
			F^-(mg/L)	**Mg^{2+}(mg/L)**	**Ca^{2+}(mg/L)**	**HCO_3^-+ CO_3^{2-} (mmol/L)**		
Charge loading	0-1500	0-0.30	10.00	100	100	10	12	8
Mg^{2+}_0	750	0.15	10.00	0-100	100	10	12	8
Ca^{2+}_0	750	0.15	10.00	100	0-100	10	12	8
$(HCO_3^- + CO_3^{2-})_0$	750	0.15	10.00	100	100	0-10	12	8
Field conditions								
	Charge Loading (C/L)	**Current (A)**	**F^-(mg/L)**	**Mg^{2+}(mg/L)**	**Ca^{2+}(mg/L)**	**HCO_3^-+ CO_3^{2-} (mmol/L)**	**Cathode flow rate (mL/min)**	**Anode flow rate (mL/min)**
Average	1315	5.7	2.42	105.6	50.4	12.5	260	260

Guideline values				
	F^-(mg/L)	**Mg^{2+}(mg/L)**	**Ca^{2+}(mg/L)**	**HCO_3^-+ CO_3^{2-} (mmol/L)**
Sri Lankan Guideline	1.00	30	240	8.0
WHO Guideline	1.50	50	75	6.1

3. Results and discussion

3.1 Ion removal mechanism

The XRD analysis of precipitates (Fig.2.3) shows diffraction predominant peaks of aragonite ($CaCO_3$) (dominant phase) and calcite (Ca. Mg)CO_3. In agreement with earlier studies, the presence of Mg^{2+} leads to the aragonite formation rather than thermodynamically favored calcite phase formation (Reddy and Wang, 1980; Karoui et al., 2013). However, the presence of crystalline brucite ($Mg(OH)_2$), fluorite (CaF_2), or sellaite (MgF_2) were not observed in the XRD spectrum. Nevertheless, some broad diffraction peaks appeared in the XRD spectrum at higher current densities of 1000-1500 C/L. These peaks may be due to the amorphous or partially crystalline nature of $Mg(OH)_2$. Saoud et al., 2014 reported in the previous study that, broad diffraction peaks represented nanoparticles of $Mg(OH)_2$ prepared by a microwave-assisted precipitation process.

Furthermore, FTIR analysis (Fig. 2.4) of the precipitate collected confirms the presence of $Mg(OH)_2$. The $Mg(OH)_2$ precipitated spectrum showed a sharp peak at 3698 cm^{-1} and is attributed to the O–H band stretches in the crystalline structure. The strong band at around 600 cm^{-1} is assigned to the Mg–O stretching vibration in $Mg(OH)_2$. These O–H and Mg–O bands can be seen from 750 to 1500 C/L levels in the collected precipitates. Moreover, O–H and Mg–O band intensities increased over the increasing charge loading and confirmed the predominance of $Mg(OH)_2$. The absorption bands at 695 and 857 cm^{-1} were attributed to the in-plane bending and out of plane bending modes of CO_3^{2-}. The presence of 857 and 695 cm^{-1} in the precipitates can be seen in the pure $CaCO_3$ precipitate as well. This result further confirms the presence of $CaCO_3$ in all precipitates. The peaks related to $MgCO_3$ are overlaid by $Mg(OH)_2$ and $CaCO_3$. Only the band at 1106 cm^{-1} recognized, or the symmetric C–O stretching vibration, can be identified in precipitates with FTIR results.

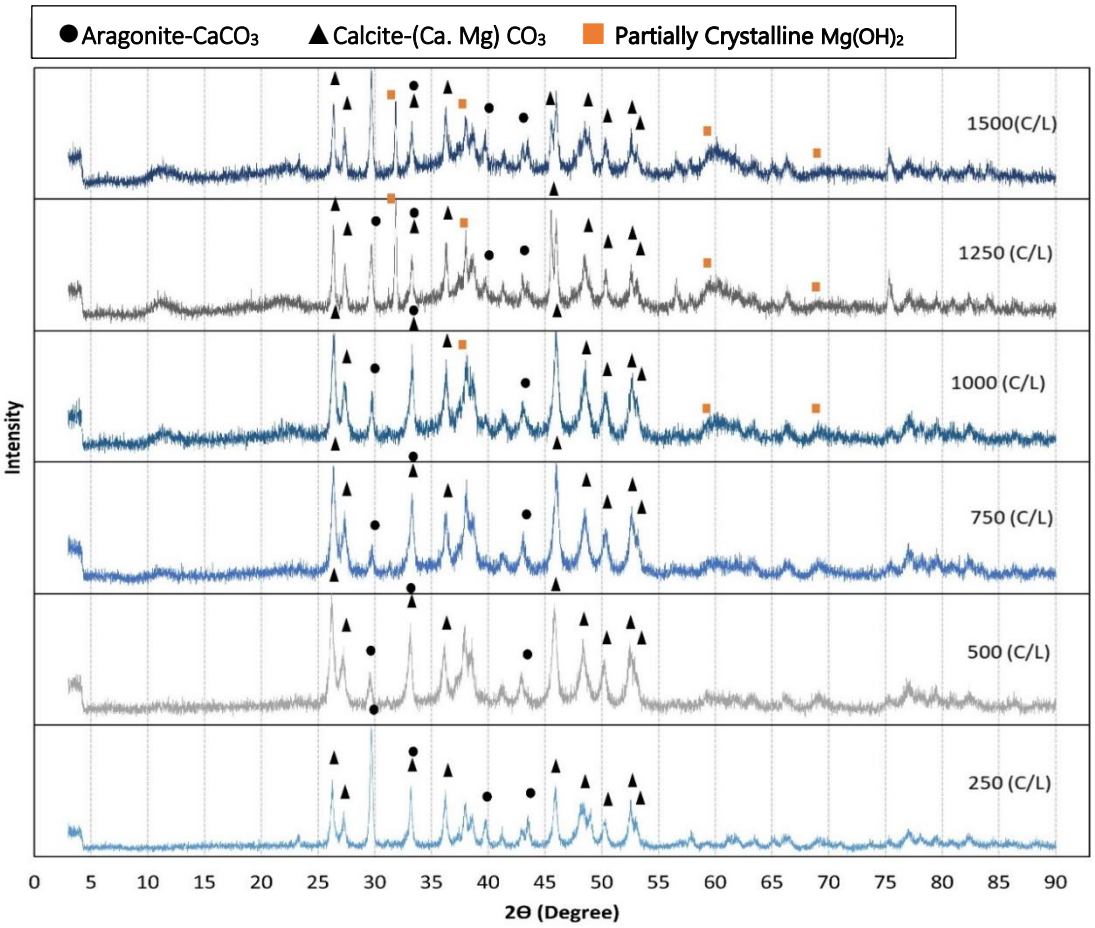

Fig. 2. 3: XRD patterns of precipitates collected from various C/Ls

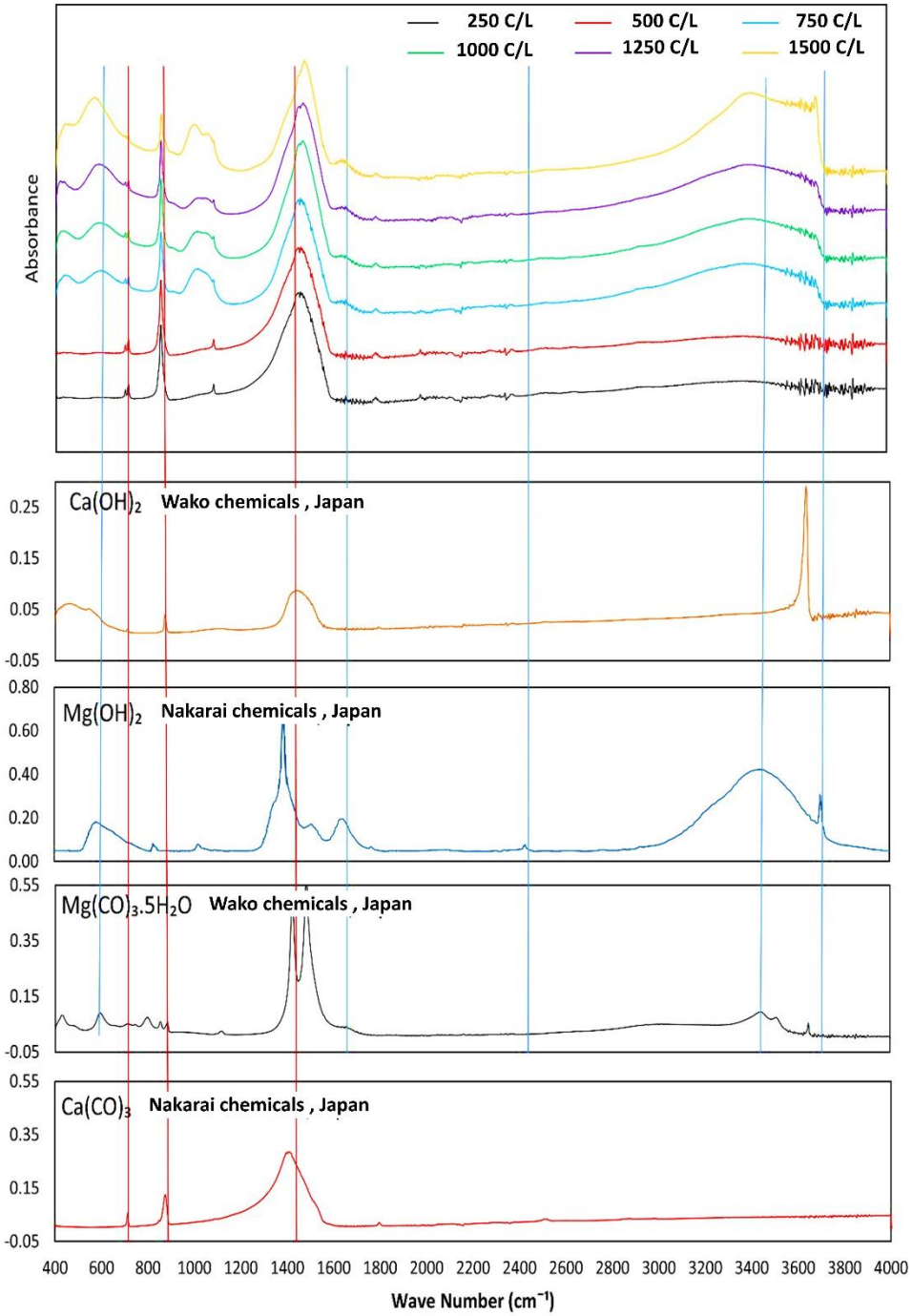

Fig. 2. 4: Precipitates FTIR spectrum and its comparison with possible forming precipitates pure form

Fluoride precipitation with Ca^{2+} ion as CaF_2 (s) is a well-known technology, but XRD results revealed that CaF_2 or MgF_2 was not formed. However, the removal of F^- by adsorption to the calcite was reported in several studies (Jain and Jayaram, 2009; Turner et al., 2005). Furthermore, adsorption isotherm experiment performed for $CaCO_3$ (discussed in Chapter1) revealed that $CaCO_3$ did not significantly contributed to the removal of F^-. According to the chemical composition of the precipitate and XRD observations, it can be concluded that F^- was removed by adsorption to the calcite phase at lower current densities.

For larger current densities, $Mg(OH)_2$ starts oversaturating and is involved in F^- co-precipitation. F^- adsorption Isotherm experiment showed that $Mg(OH)_2$ did not adsorb F^-, thus the only mechanism for F^- removal was Co-precipitation. The previous studies of de-fluoridation of water using nano-magnesium oxide also suggested that, F^- replacement with OH^- in $Mg(OH)_2$ could occur due to the iso-electric nature and the similar size of F^- and OH^- ions (Devi et al., 2012, Oladoja et al., 2016). Furthermore, co-precipitation for F^- removal by $Mg(OH)_2$was proposed by Nidheesh and Singh (2017) and Kawakami et al., 2019. Accordingly, two main fluoride removal mechanisms of adsorption to $CaCO_3$ and co-precipitation with $Mg(OH)_2$ can be concluded as F^- removal mechanisms. Accordingly, the same ion removal mechanisms discussed in Chapter 1 can be employed to discuss the ion removal mechanisms in this section and the mathematical model proposed in Chapter 1 can be employed for the estimation of ion removals.

3.2 Effect of charge loading on ion-removal efficiencies and model application

To investigate the effect of charge loading, the initial conditions mentioned in Table 2.1 were utilized. Iteratively calculated thermodynamic K_2' values were shown in Table 2.2 and were used to calculate HCO_3^-+ CO_3^{2-} concentrations in the anode and the cathode. Variations of F^-, Cl^-, Na^+, Mg^{2+}, Ca^{2+}, and HCO_3^-+ CO_3^{2-} removal percentages in the cathode, anode and the aerator for increasing charge loading, are shown in Figs. 2.5a, 2.5b and 2.5c, respectively. Related pH values are shown in Fig.

2.5d. According to Fig. 2.5a, the removal of F^- and Mg^{2+} showed a significant rise over the applied charge loading. At 250 C/L charge loading, the removal percentages of F^- and Mg^{2+} ions in the cathode bath were 20% and 16%, respectively, steadily reaching maximums of 57% and 61% at 1500 C/L. Removal of Ca^{2+} was more than 86% with a slight rise over the charge loading. With the increasing charge loading HCO_3^-+ CO_3^{2-} removals increased gradually. At 250 C/L, 55% of HCO_3^-+ CO_3^{2-} had been removed, gradually increasing to a maximum of 82 % at 1500 C/L. Total removal of HCO_3^-+ CO_3^{2-} in the anode was observed from 69 to 99% with respect to increased charge loading of 250 to 1500 C/L (Fig. 2.5a). Thereafter, the aerator HCO_3^-+ CO_3^{2-} removal was reduced to the range of 41-56% (Fig 2.5c).

According to Fig 2.5a, the removal of both F^- and Mg^{2+} increased similarly with an increase of charge loading. Therefore, suggesting an effect of F^- removal, by the plausible Mg^{2+} forming agents $Mg(OH)_2$, $MgCO_3$ and MgF_2. Due to the alkaline nature in the cathode, obviously, Mg^{2+} could form $Mg(OH)_2$ and $MgCO_3$ precipitates. A minimum of 87% and a maximum of 95% of Ca^{2+} were removed at 250 C/L and 1500 C/L, respectively. The average level of the Ca^{2+} removal was 92% for 250 C/L-1500 C/L. According to the $HCO_3^-$and CO_3^{2-} equilibrium (Chapter 1, Eq. 1.4), a significant amount of CO_3^{2-} can be formed at a higher pH. At operational pH levels of 9.07 to 9.54, CO_3^{2-} ion existed as the most dominant. Therefore, the removal of more than 92% of Ca^{2+} could take place by forming $CaCO_3$ precipitation.

Table 2.2: Iteratively calculated K_2' (mol/L) and respective ionic strength of the solution

	Charge loading (C/L)	**K_2'**	**Ionic strength of the solution**
Raw Water	0	1.35×10^{-11}	0.062
Anode	250	1.61×10^{-11}	0.044
	500	1.45×10^{-11}	0.050
	750	1.52×10^{-11}	0.047
	1000	1.57×10^{-11}	0.048
	1250	1.55×10^{-11}	0.045
	1500	1.50×10^{-11}	0.049
Cathode	250	1.54×10^{-11}	0.043
	500	1.65×10^{-11}	0.042
	750	1.70×10^{-11}	0.040
	1000	1.77×10^{-11}	0.037
	1250	1.89×10^{-11}	0.032
	1500	1.96×10^{-11}	0.029
Aerator	250	1.95×10^{-11}	0.049
	500	1.95×10^{-11}	0.049
	750	1.95×10^{-11}	0.049
	1000	1.95×10^{-11}	0.049
	1250	1.95×10^{-11}	0.051
	1500	1.95×10^{-11}	0.052

According to the observed F^- removal percentage, a set of guidelines can be introduced. As per Chapter 1 data, F^- removal percentage showed negligible variation with respect to the initial F^- concentration. Accordingly, it was assumed that removal percentage does not vary with initial F^- concentration. Accordingly, the maximum initial F^- concentration, which could be treated to meet the 1 mg/L of Sri Lankan guideline, can be calculated as 1.25-2.34 mg/L for the initial levels of 250-1500 C/Ls, respectively. Accordingly, 1.87-3.52 mg/L of initial F^- concentration can be treated from 250-1500 C/L charge loading to meet the WHO water quality guideline for the F^-(1.5 mg/L). The WHO and Sri Lankan guideline value (Table 2.1) for $HCO_3^- + CO_3^{2-}$ and Ca^{2+} can be met even in the lowest 250 C/L for initial $HCO_3^- + CO_3^{2-}$ = 10 mmol/L and Ca=100mg/L. However, to meet the WHO and Sri Lankan guidelines for Mg^{2+}, charge loading higher than 1250 C/L is required.

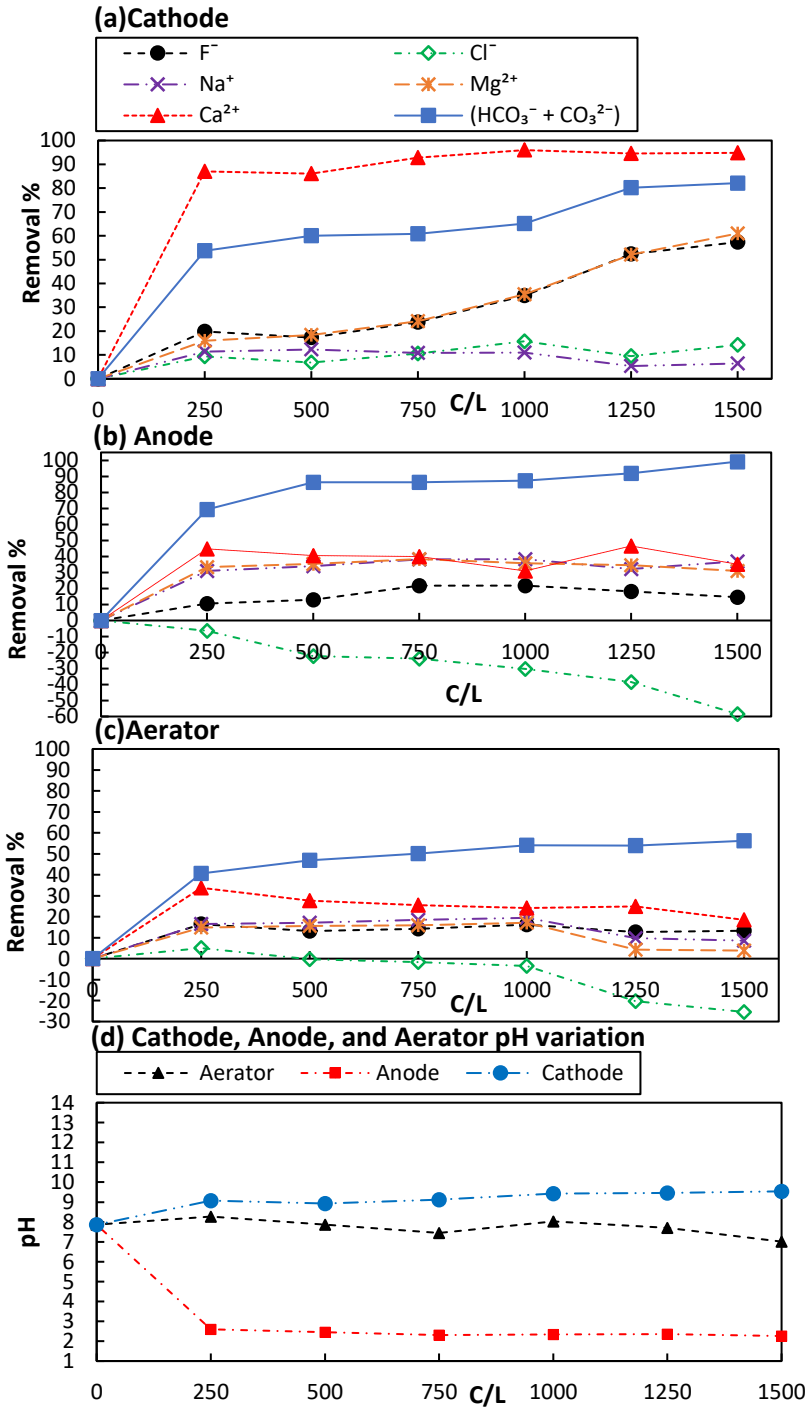

Fig. 2. 5: Influence of charge loading in electrolyte (C/L) on the ion removal percentages and pH. (a) cathode, (b) anode, (c) aerator and (d) pH variation; F^{-}_{0} = 10 mg/L, Ca^{2+}_{0} = 100 mg/L, Mg_{0}^{2+} = 100 mg/L, and $(CO_3^{2-}+HCO_3^{-})_0$=10 mmol/L

According to Fig. 2.5a, the removal of Mg^{2+} as well as $HCO_3^- + CO_3^{2-}$ were increased as the charge loading was increased. The increase of charge loading directly resulted in producing more H^+ to remove $HCO_3^- + CO_3^{2-}$ as CO_2 and OH^- ion to form $Mg(OH)_2$ causing a removal increment of both Mg^{2+} and $HCO_3^- + CO_3^{2-}$. Similarly, increases of charge loading upsurged in the formation of OH^-, thus CO_3^{2-} led to higher growth of $CaCO_3$ and $MgCO_3$ ions according to the Le Chatlier's principle (chapter 1, Eq. 1.4).

According to Fig. 2.5b, in the anode bath, the removal of Ca^{2+}, Mg^{2+}, F^-, and Na^+ did not change over the varying charge loading, while Cl^- removal showed a significant negative decrease over the increasing charge loading. The positive removal of F^-, Mg^{2+}, Ca^{2+}, and Na^+ in the anode bath resulted from ion transportation to the cathode bath by the Coulomb force and ion-concentration gradient. Ca^{2+}, Mg^{2+}, and F^- precipitated in the cathode bath, created a lower ion concentration which created an ion concentration gradient between the anode and cathode. To balance the deficiency of the ions in the cathode solution, both the ion concentration gradient and the Coulomb force transported Mg^{2+}, Ca^{2+}, and Na^+ ions through the clay diaphragm. By overcoming the Coulomb force, the ion concentration gradient alone transported F^- ion to the cathode bath, which was mainly co-precipitated with $Mg(OH)_2$.

The pH levels over the increasing charge loading (after a 24-hour operation) were shown in Fig. 2.5c. A slight increase of pH in the cathode and a slight decrease of pH in the aerator was observed for increasing charge loading. as a result of an upsurge of OH^- and H^+ ions, respectively. According to Fig. 2.5a and 2.5b, Cl^- movement from the cathode to the anode by the Coulomb force and an ion concentration gradient can be seen as positive and negative removal, respectively. The removal of Cl^- ions in the cathode bath increased slightly with increasing charge loading was due to $Cl_2(g)$ generation. The formation of $Cl_2(g)$ in the anode was an extra advantage of this system. Usually, water-dissolved $Cl_2(g)$ produced $HOCl^-$ ions contribute to water disinfection. Lower pH level in the anode was favorable for

dissociating $Cl_2(g)$, and hydrolysis into $HOCl^-$ at the aerator was almost complete at the aerator with pH >5.

Furthermore, by measuring the total chlorine concentration (Fig. 2.6) by the DPD colorimetric method (APHA, 1998), the presence of $HOCl^-$ was confirmed. However, the excessive concentration of chlorine may negatively affect the final water palatability if the water is used for drinking purposes. It was found that an increase in total chlorine over increasing charge loading showed increases up to 35 mg/L (at 1500 C/L), which is far beyond the maximum concentration of chlorine at 1.0 mg/L (SLS, 2013). Therefore, prior to the consumption of treated water, the excessive chlorine concentration should be reduced if it exceeds the acceptable limit. Water storage with aeration for a particular time and activated carbon filtration could be a reliable solution.

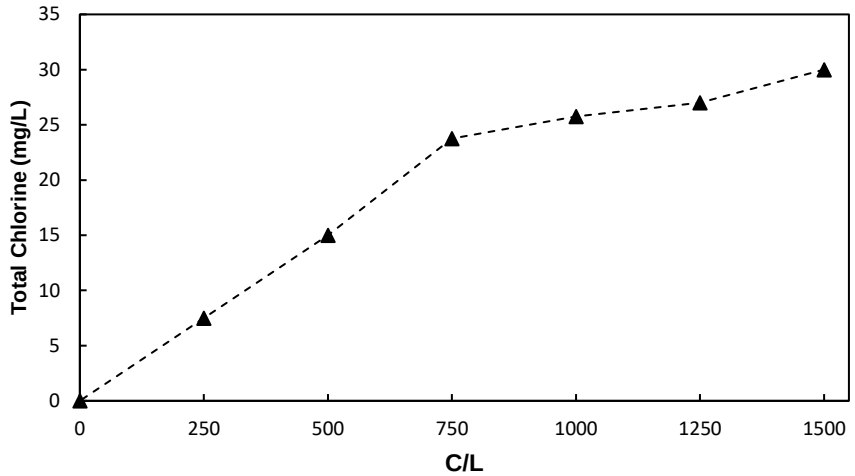

Fig. 2. 6: Total chlorine concentration in the cathode measured with DPD colorimetric method

In the presence of Natural organic matter (NOM) in the groundwater, Cl_2 reacts with NOM to form disinfection by-products (DBPs) (Rook, 1974) which are carcinogenic to human (White 1999; Gordon et al., 2008). To prevent the formation of DBPs, NOM precursor shall be removed by treating the groundwater with activated carbon (Yan et al., 2010; Golea at al.,2020). Else, anode water, where DBPs will form shall be discarded. Accordingly, prior to the system design initial level of Cl^-

concentration and NOM level should be measured and suitable pre or post treatment method such as activated carbon shall be included in the system.

In order to form a comprehensive idea about the ion removal mechanism with respect to the increasing charge loadings, H^+/OH^- introduced and actually consumed H^+/OH^- concentrations were calculated (Table 2.3). For the calculation of generated OH^- and H^+ by accounting removed Cl^-, Eq. 1.24 described in Chapter 1, section 2.4 was employed. When we consider the formation of Cl_2, H^+ generation is suppressed in the anode while the OH^- formation in the cathode takes place. HCO_3^- transferred to the anode was calculated from Eq. 2.1 and Eq 2.2 assuming $MgCO_3$ formation was negligible. CO_2 dissociation was also neglected in the calculation. For the calculation of OH^-, H^+ consumed for the reactions (Eq.2.3 and Eq. 2.4), measured ion concentrations of Mg^{2+}, Ca^{2+} and CO_3^{2-}+HCO_3- were employed, respectively. $Mg(OH)_{2\,ppt}$ was also calculated using initial and final Mg^{2+} concentrations

$$[HCO_3^-]_{aerator} - [HCO_3^-]_{transferred\ to\ anode} = [HCO_3^-]_{converted\ to\ CO_3^{2-}} + [HCO_3^-]_{final} \quad (2.1)$$

$$[HCO_3^-]_{converted\ to CO_3^{2-}} = [CO_3^{2-}]_{aerator} + CaCO_{3ppt} - [CO_3^{2-}]_{final} \quad (2.2)$$

$$[OH^-]_{consumed} = 2 \times Mg(OH)_{2\,ppt} + [HCO_3^-]_{converted\ to CO_3^{2-}} \quad (2.3)$$

$$[H^+]_{consumed} = CO_{2formed} = [HCO_3^- + CO_3^{2-}]_0 - [HCO_3^- + CO_3^{2-}]_{final} - CaCO_{3ppt} \quad (2.4)$$

According to Table 2.3 except for the charge loading 250 C/L, consumed H^+ and OH^- concentrations were lower than the generated H^+ and OH^-. Formation of the H_2O by reacting H^+ and OH^- in the electrolysis cell was the reason (hereafter neutralization). For the charge loading of 250 C/L, consumed OH^- and H^+ concentrations were found higher than that of generated H^+ and OH^-. It could be occurred due to the formation of the $MgCO_3$ in the cathode. High $MgCO_3$ peak intensities found in XRD (Fig. 2.3) further confirm the formation of $MgCO_3$ at lower charge loadings. For the charge loading >250 C/L, the difference between H^+

introduced and CO_2 formed becomes positive and could be an indication of high $Mg(OH)_2$, $CaCO_3$ and CO_2 formation rather than $MgCO_3$ formation. Accordingly, as an input concentration for the model OH^- and HCO_3^- concentrations should be corrected. The fitted curve functions were obtained as shown in Fig. 2.7 can be utilized to correct those concentrations. To correct HCO_3^-, transferred HCO_3^- from the cathode was deducted from the input water HCO_3^-. To correct the OH^- concentration, Cl^- removed and OH^- neutralized should be deducted from the OH^- generated. Moreover, to calculate the input concentration of HCO_3^- to the cathode, HCO_3^- removal in aerator and HCO_3^- transferred from the anode should be deducted from initial HCO_3^-. Fig.2.8 shows the respective fitted curve functions to calculate Cl^- and HCO_3^- removed as well as OH^- neutralized.

Measured and model calculated F^- and Mg^{2+} concentrations over the increased charge loading were shown in Fig. 2.9a and b, respectively. According to the results, Measured and model calculated Mg^{2+} concentrations were found similar except 0 C/L. Since the model was developed by assuming $Mg(OH)_2$ was saturated, the model calculated results for 0 C/L show the actual concentration of Mg^{2+} required saturation. Therefore, proposed Mg^{2+} calculation model assumptions and related removal mechanisms can be verified for the proposed aeration coupled ELC system.

Table 2.3: Comparison of ion concentrations

charge loading C/L	**H^+ Introduced (mmol/L)- Eq.1.24**	**OH^- Introduced (mmol/L)- Eq.1.24**	**Consumed OH (mmol/L)- Eq.2.3**	**HCO_3^- transferred to anode (mmol/L) –Eq. 2.1**	**H^+ consumed =CO_2 formed (mmol/L)- Eq.2.4**
250	2.78	2.50	3.97	-0.82	4.81
500	5.01	5.27	3.87	-1.60	4.25
750	7.43	7.94	4.68	-1.08	4.79
1000	9.31	10.86	5.82	-1.11	5.19
1250	11.75	13.56	7.45	0.31	6.59
1500	13.74	16.45	8.15	0.28	6.77

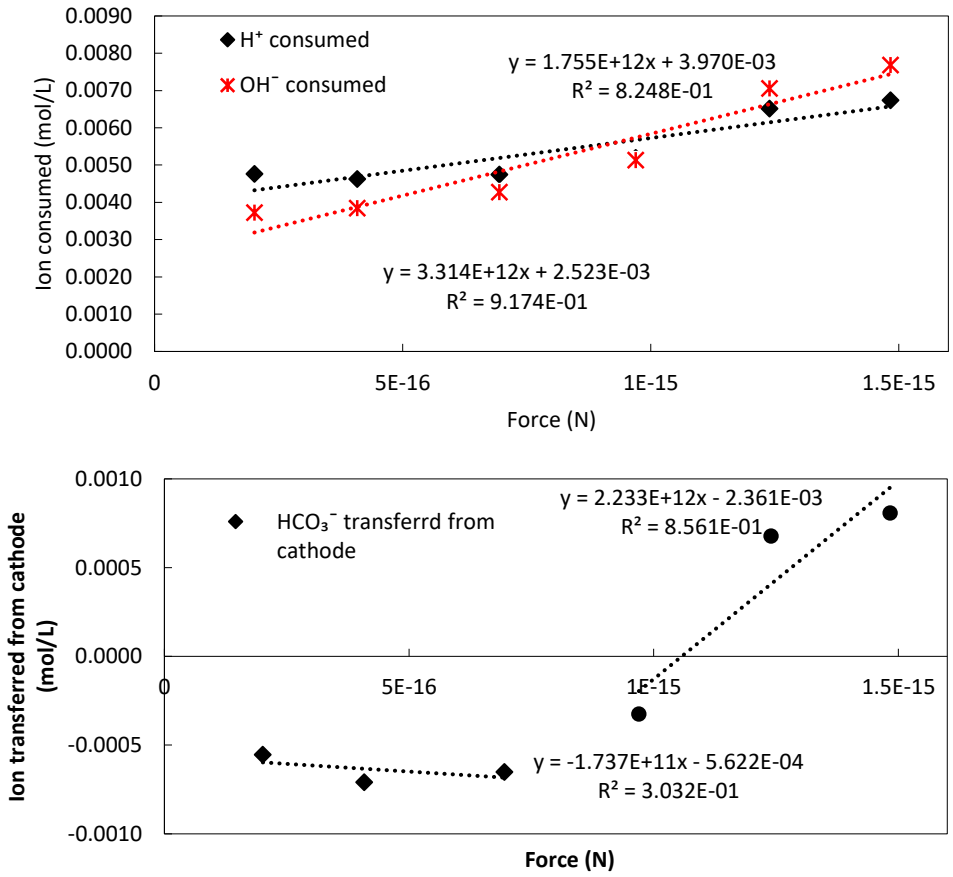

Fig. 2.7*:* Coulomb force versus ion transferred and consumed

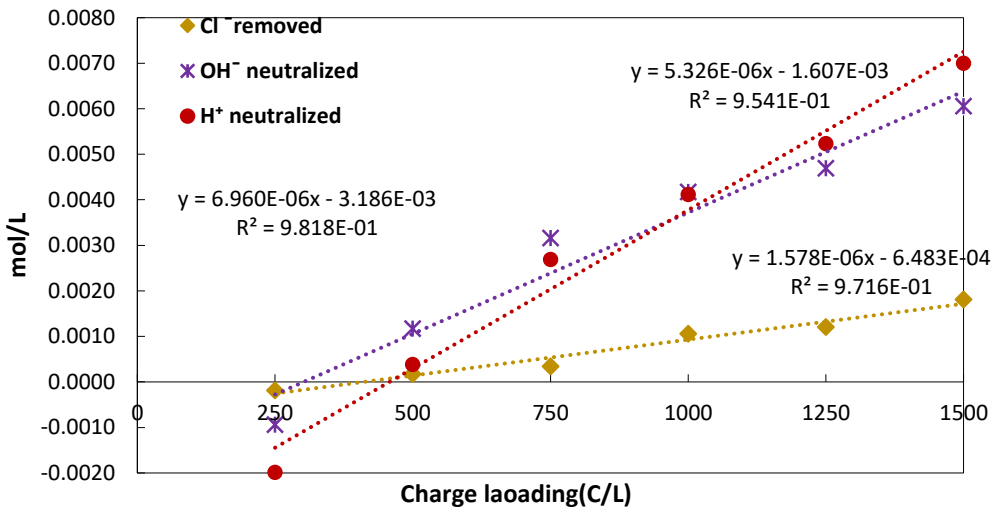

Fig. 2. 8: Charge loading vs Cl^{-} removed and OH^{-} neutralized

Furthermore, calculated model concentrations and measured concentrations of F^- were found similar for the charge loading<1000C/L where a considerable amount of CO_3^{2-}+HCO_3^- was present. Since F^- removal model was established only for the higher CO_3^{2-}+HCO_3^- concentration 10mmol/L, the F^- removal model K value was unable to regenerate the F^- concentration. A similar kind of F^- model calculation deviation can be seen in Chapter 1 Fig. 1.30. Therefore, it can be concluded that F-co-precipitation depends on the $(CO_3^{2-}+HCO_3^-)_0$

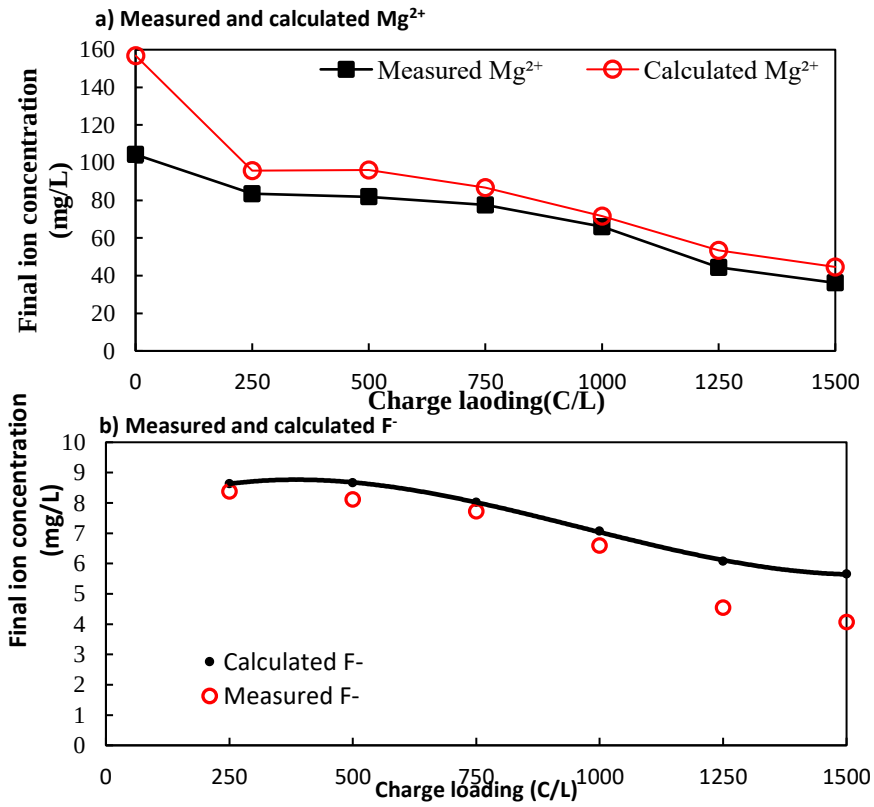

Fig. 2. 9: Model calculated and measured ion removal

3.3 Effect of the initial (HCO_3^-+ CO_3^{2-}) on ion removal efficiencies

As identified previously in section 3.1 and 3 .2 HCO_3^-+ CO_3^{2-} inhibited the formation of $Mg(OH)_2$ and F^- removal, but they increased Ca^{2+} removal. In order to have a comprehensive idea about how HCO_3^-+ CO_3^{2-} influences the system's performance, ELC experiments were performed under the conditions listed in Table 2.1. A charge loading of 750 C/L was selected to identify maximum ion removal by

minimizing the operational cost. The results obtained are summarized in Fig. 2.10. Figures 2.10a, 2.10b, 2.10c and 2.10d illustrate the removal of F^-, Cl^-, Na^+, Mg^{2+}, Ca^{2+}, and $HCO_3^- + CO_3^{2-}$ in the cathode, in the anode, in the aerator, and the pH, respectively.

According to Fig. 2.10a, in the cathode bath, the removal of F^- and Mg^{2+} steadily decreased as the $HCO_3^- + CO_3^{2-}$ increased, while Cl^- and Na^+ removal showed a slight incremental increase over the increasing $HCO_3^- + CO_3^{2-}$. For the 2.1–4.7 mmol/L of the initial $HCO_3^- + CO_3^{2-}$ concentrations, more than 96% of $HCO_3^- + CO_3^{2-}$ was removed. Most of the $HCO_3^- + CO_3^{2-}$ tended to be removed at the anode and the aerator (Fig. 2.10 b and 2.10 c) by reacting with H^+ (Chapter1, Eq. 1.2).

For the initial $HCO_3^- + CO_3^{2-}$ concentrations of 2.1–9.4 mmol/L, the total removal of 2.07–6.26 mmol/L of $HCO_3^- + CO_3^{2-}$ was detected. The removal of Ca^{2+} also showed a significant increase over the increasing $HCO_3^- + CO_3^{2-}$. At the 2.1 mmol/L $HCO_3^- + CO_3^{2-}$ concentration, Ca^{2+} removal was found to be very low due to the absence of $HCO_3^- + CO_3^{2-}$ in the cathode. Therefore, maintaining an adequate amount of $HCO_3^- + CO_3^{2-}$ was favorable for removing a significant amount of Ca^{2+} ions. However, the increment of $HCO_3^- + CO_3^{2-}$ decreases the Mg^{2+} and F^- removal. It is obvious that the lower concentration of $HCO_3^- + CO_3^{2-}$ increased Mg^{2+} and F^- removal in the cathode. As shown in Fig. 2.8d, pH variation in the cathode showed a slight decrease, while the anode pH showed a slight increase. Conversely, the aerator pH rapidly increased with increasing HCO_3^-due to insufficient H^+ for removing $HCO_3^- + CO_3^{2-}$. Therefore, for a higher concentration of the initial $HCO_3^- + CO_3^{2-}$, a higher amount of charge loading is required to maximize the removal of both F^- and Mg^{2+}.

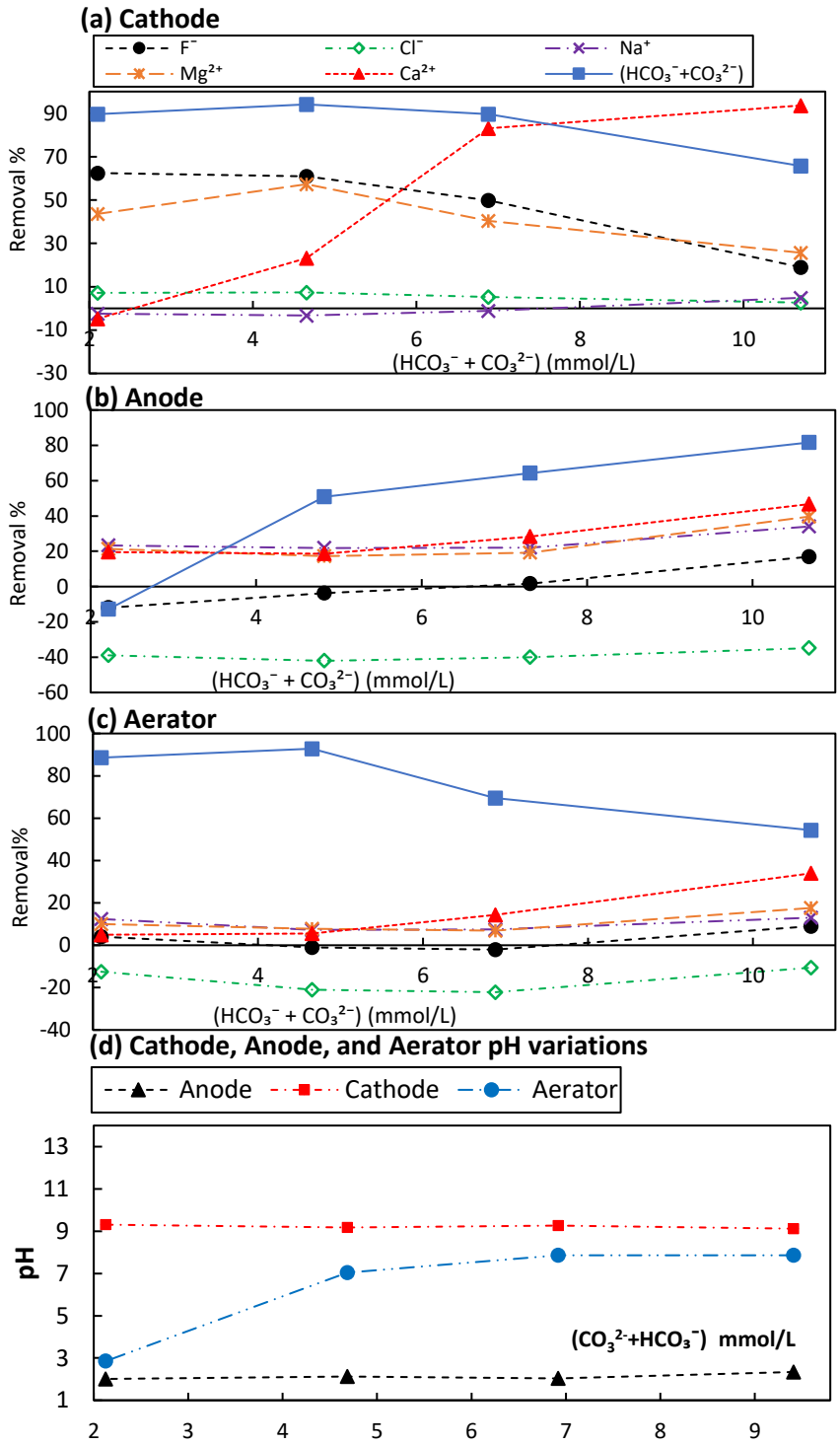

Fig. 2. 10: Influence of carbonate (HCO_3^-+CO_3^{2-}) on the ion removal percentages and pH at 750 C/L and pH. (a) cathode, (b) anode, (c) aerator and (d) pH variation; F^-_0 = 10 mg/L, Ca_0^{2+} = 100 mg/L and Mg_0^{2+} = 100 mg/L.

Following the removal percentages of F^-, maximum treatable initial F^- concentrations can be estimated as 4-3.84 mg/L to meet the WHO guideline for drinking water of 1.5 mg/L when initial HCO_3^-+ CO_3^{2-} concentration was lower than 4.68 mmol/L. To meet the Sri Lankan guideline of 1 mg/L, 2.56-2.66 mg/L is the maximum concentration of the initial F^- can be treated at 750 C/L. Ca^{2+} removal reached its WHO guideline when HCO_3^-+ CO_3^{2-} >6.92 mmol/L. The highest removal of HCO_3^-+ CO_3^{2-} observed in the system was 62%. For the initial concentration range of 2.4-10 mmol/L (HCO_3^-+ CO_3^{2-}), electrolysis system (HCO_3^-+ CO_3^{2-}) removal was high enough to meet drinking water desirable concentration (SLS, 2013).

Models developed in Chapter1, section 3.3 were used to calculate the Mg^{2+} and F^- concentration, respectively. The same procedure described in section 3.2.1 was utilized to correct the initial concentration of ions as the model input parameters. Fitted curve functions for different $(HCO_3^-+ CO_3^{2-})_0$ were shown in Fig. 2.11 and can be used to calculate initial OH^-, H^+ and HCO_3^- concentrations as input concentrations for the Mg^{2+} determination model.

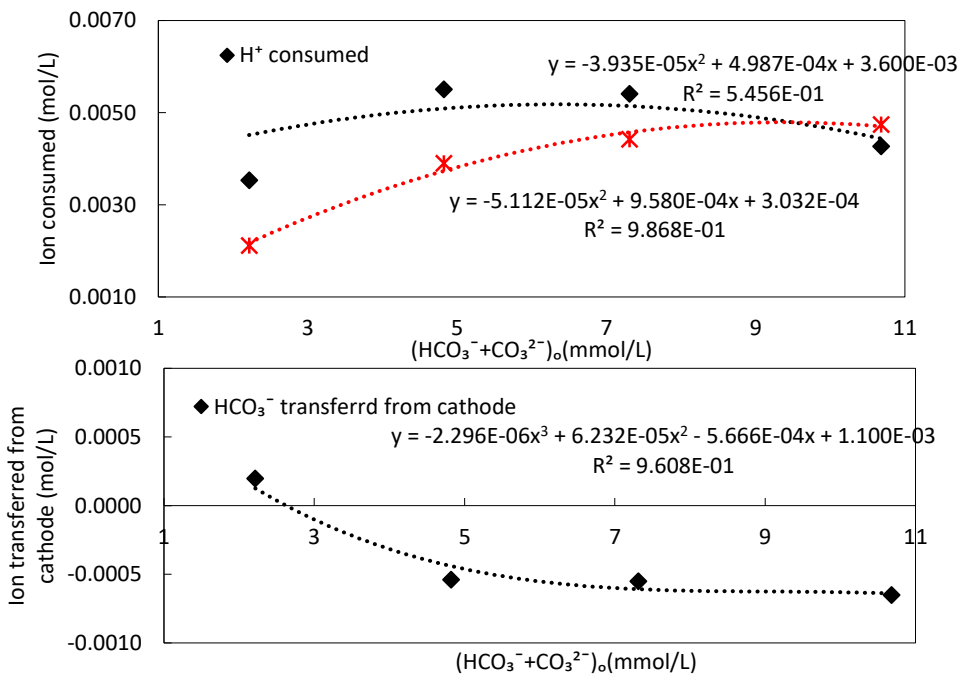

Fig. 2. 11: $(HCO_3^-+CO_3^{2-})_0$ versus ion consumed and transferred as an effect of Coulomb forces and ion concentration gradient

Measured and model calculated F^- and Mg^{2+} concentrations over the increased charge loading were shown in Fig. 2.12a and b, respectively. According to the results, measured and model calculated Mg^{2+} concentrations were found similar. However, the model calculated and measured F^- concentrations were not similar for the lower $(HCO_3^- + CO_3^{2-})_0$ concentration of 0 mmol/L. The reason was, K value used to calculate the F^- removal was 0.0083. That value was experimentally defined for $(HCO_3^- + CO_3^{2-})_0$=10 mmol/L concentration. Therefore, it seems that F^- co-precipitation is affected by the initial concentration of $(CO_3^{2-}+HCO_3^-)$. Hence, for different initial $CO_3^{2-}+HCO_3^-$ concentrations F^- removal model, K values should be re-estimated. The K value estimated for F^- determination proposed by Imai and Kawakami., 2019 has used initial $CO_3^{2-}+HCO_3^-$ concentration 0 mmol/L condition. With that K value and Calculated Mg^{2+} concentration from the prosed model F^- concentration can be estimated accurately. Without other experiments, the K value calculation formula, Eq. 2.5 was obtained by substituting, best-fit curve function to Chapter 1, Eq. 1.59 and Eq. 1.53 and rearranging. However, this formula only valid for the 1500C/L charge loading.

Similar to the Figure 1.32 in chapter 1, Eq 2.5 can be used to calculate K value for different initial $(CO_3^{2-}+HCO_3^-)$ and calculated equilibrium concentrations of Mg^{2+} for 1500C/L charge loading.

$$k = \frac{\ln\left[\frac{(0.0608\,(HCO_3^- + CO_3^{2-})_0{}^2 - 0.3089(HCO_3^- + CO_3^{2-})_0 + 4.012}{F_0^-}\right]}{(Mg^{2+}{}_{calculated} - Mg_0^{2+})} \quad (2.5)$$

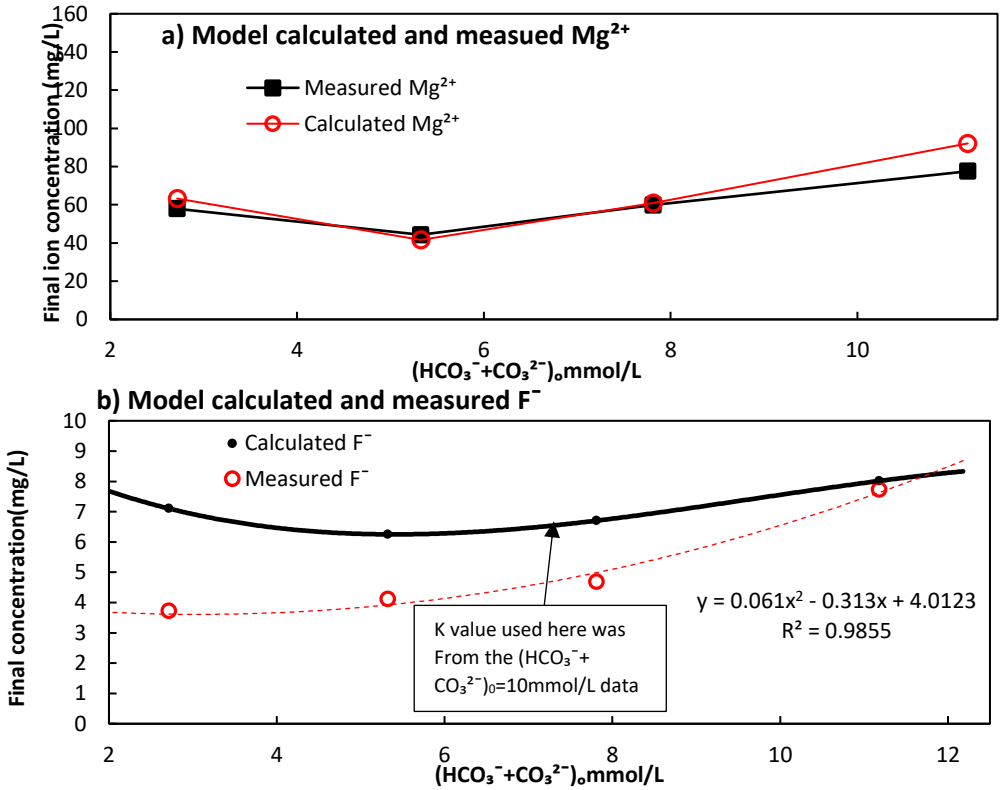

Fig. 2. 12: Measured and model-calculated final Mg^{2+} and F^- concentrations over the increasing $(HCO_3^- + CO_3^{2-})_0$

3.4 Effect of initial Mg^{2+} concentration on ion removal efficiencies

In this section, the influence of initial Mg^{2+} concentration on ion removal and model application was described at a charge loading of 750 C/L. The experimental condition described in Table 2.1 were used for the experiments. Since in the real conditions, the Mg^{2+} concentration >100 mg/L is rare, a lower Mg^{2+} concentration than 100 mg/L was used for the experiments. The flow rates of the system were maintained according to Table 2.1. The results obtained are shown in Fig. 2.13.

According to Fig. 2.13a e, F^- removal in the cathode showed a slight increase ranging from 3.8 to 24 % for the initial concentration of 0–100 mg/L $(Mg^{2+})_0$ which was significantly low. With this lower removal of F^-, maximum of 1.31 and 1.97 mg/L of initial F^- could meet Sri Lankan and WHO drinking water quality guidelines of 1 mg/L and 1.5 mg/L. However, applying higher charge loading could enhance the F^- removal by agreement with section 3.1 data. Noticeably, more than 90% removal of Ca^{2+} was observed for all concentrations of Mg^{2+}. Carbonate removal was insignificant for 0–100 mg/L Mg^{2+}. The removal of Mg^{2+} was found to be around 25 % for 23–100 mg/L at initial Mg^{2+} concentrations.

A slight decrease in Ca^{2+} removal was observed with increasing Mg^{2+}. It is known that Mg^{2+} acts to inhibit the crystal growth of $CaCO_3$. The inhibition of $CaCO_3$ growth by the presence of Mg^{2+} is caused by Mg^{2+} being incorporated into the original $CaCO_3$ seed surface and developing a new crystal surface (Lin and Singer, 2009; Zhang and Dawe, 2000). Therefore, in our system, Mg^{2+} was not actively participating in the removal of $HCO_3^- + CO_3^{2-}$ as $MgCO_3$; however, the degree of Ca^{2+} removal with increasing Mg^{2+} indicates that Mg^{2+} inhibits the formation of $CaCO_3$. Since we used $MgCl_2$ for preparing the synthetic water, with increased Mg^{2+}, Cl^- ion concentration increased. Therefore, Cl^- removal percentage decreased. According to Fig. 2.13b and c insignificant changes of ion removals in the anode and aerator were observed. Also, pH levels were found almost the same for different Mg^{2+} concentrations (Fig. 2.13d).

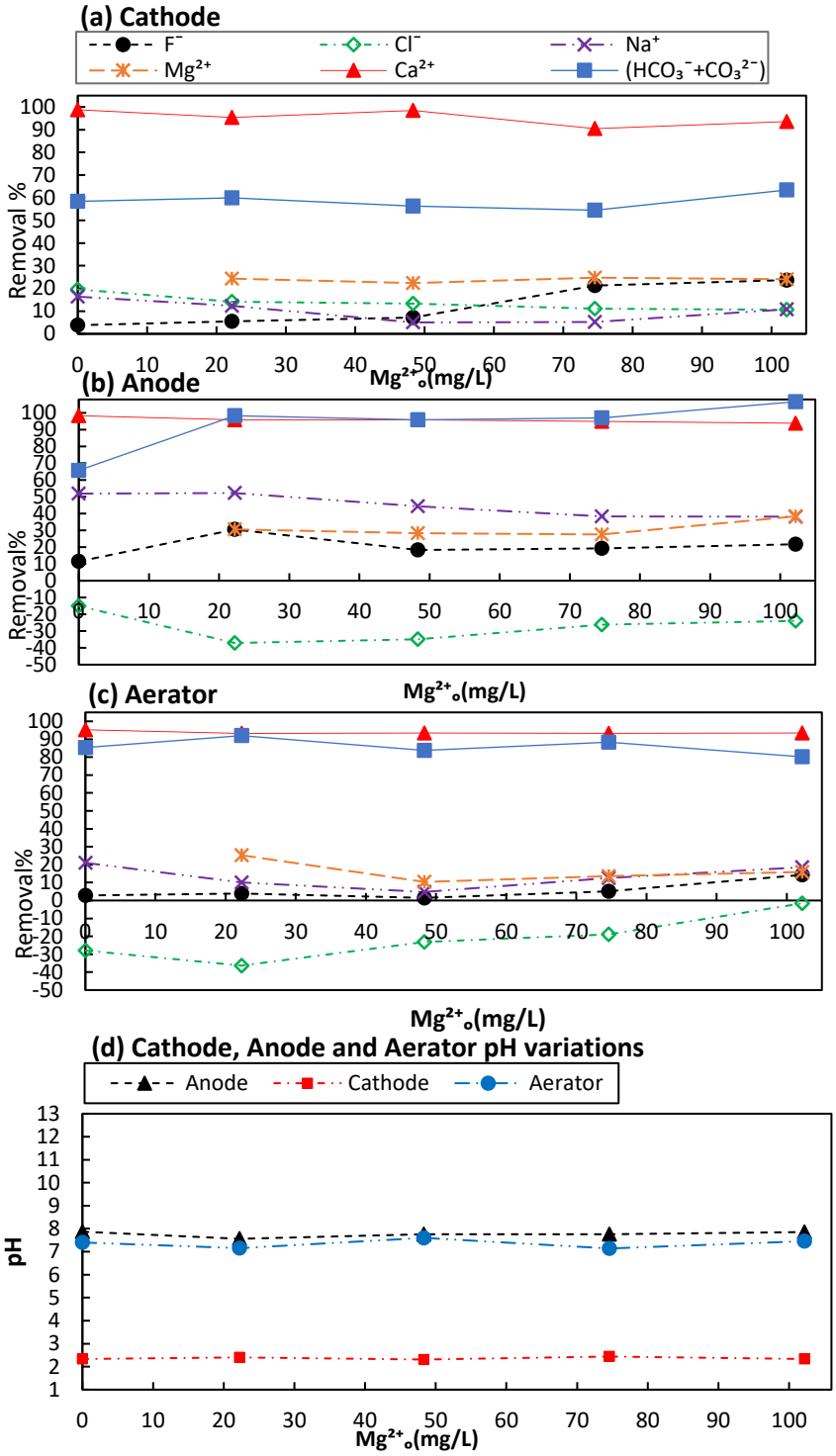

Fig. 2. 13: Influence of initial Mg^{2+} concentration on ion removal percentages and related pH at 750 C/L.(a) cathode, (b) anode, (c) aerator and (d) pH variation; F^{-}_{0} =10 mg/L, Ca^{2+}_{0} =100 mg/L and HCO_3^{-}+ CO_3^{2-} =10 mmol/L,

Final Mg^{2+} and F^- concentration calculating models developed in Chapter1, section 3.3 were used to calculate the Mg^{2+} and F^- concentration, respectively. The same procedure described in section 2.2.1 was utilized to correct the initial concentration of ions as the model input parameters. Fitted curve functions for different $(HCO_3^- + CO_3^{2-})_0$ were shown in Fig. 2.14 and can be used to correct initial OH^-, H^+ and HCO_3^- concentrations. K value of 0.00843 was used for the F-concentration calculations.

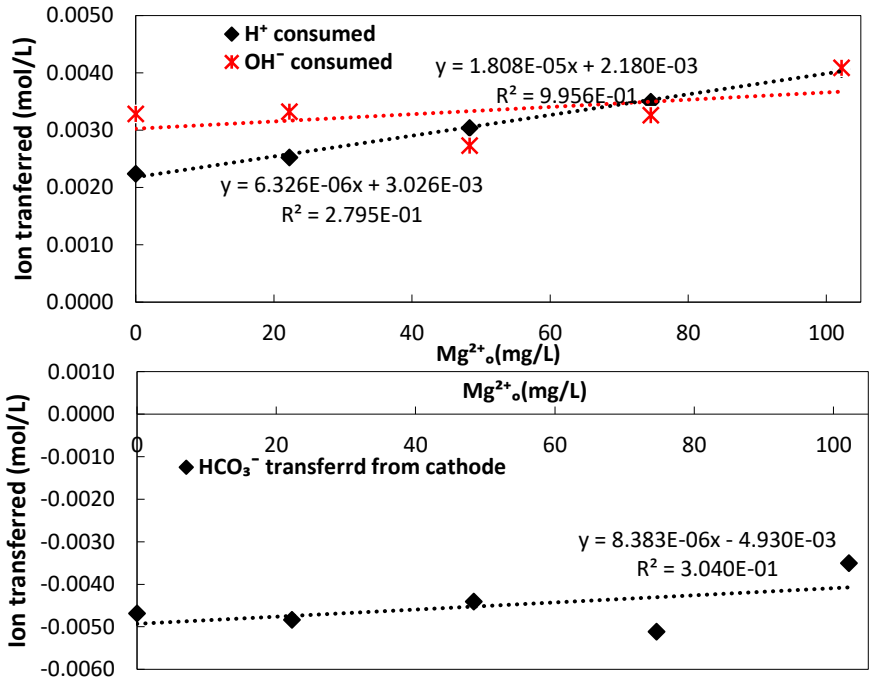

Fig. 2. 14: Mg^{2+}_o versus ion consumed and transferred

Figure 2.15 shows the model calculated and measured ion concentrations in treated water. According to Fig. 2.15a and b measured and calculated Mg^{2+} and F^- concentrations were similar. Thus, F^- and Mg^{2+} calculations and model assumptions of ion removal mechanisms can be applied for this system.

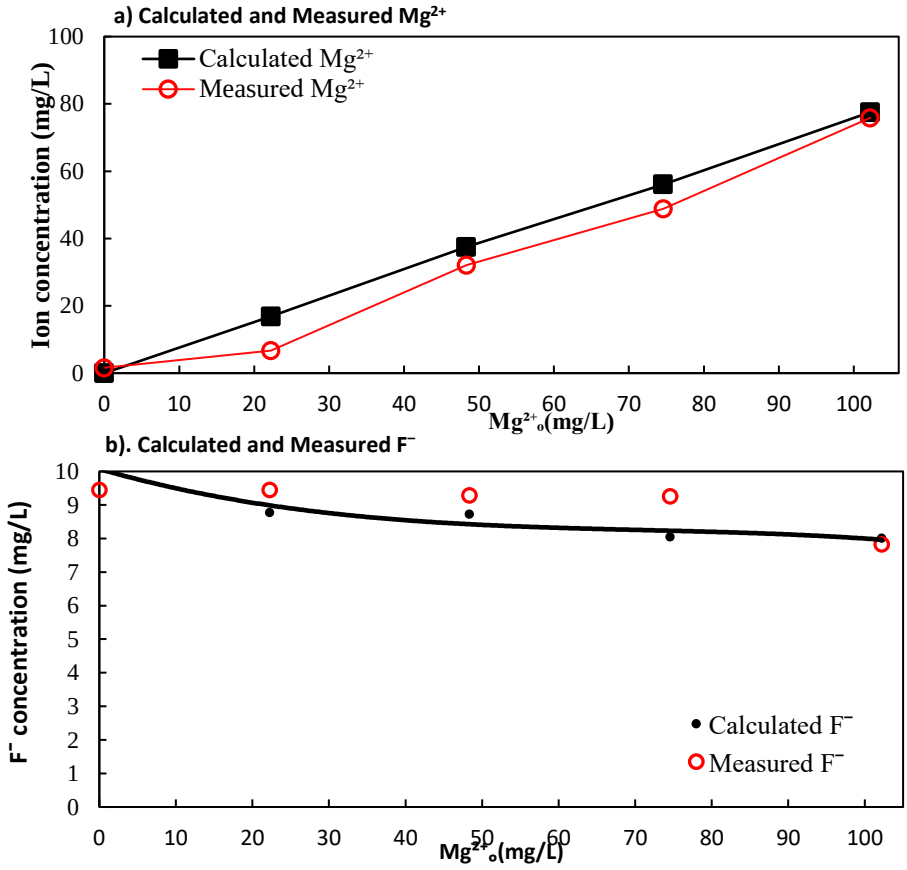

Fig. 2.15: Model calculated and measured ion removal

3.5 Development and operation of a community-scale water treatment plant to remove F^- and elements causing hardness

According to Kawakami et al (2014), groundwater in the northern part of Sri Lanka was found to be rich in natural contaminants such as F^-, Mg^{2+}, Ca^{2+}, and alkalinity. Additionally, people in the northern part of the country had dental and skeletal fluorosis due to high concentrations of F^- (Chandrajith et al., 2011; Kawakami et al., 2014; Perera et al., 2008; Weragoda et al., 2013). Accordingly, for the design and implementation of an operational-scale water treatment plant (Fig. 2.16), a location in Sri Lanka was selected where, naturally contaminated groundwater had become a threat to humans. Medawachchiya area (location: 8°32'02.8"N

80°29'57.6"E) was selected for the installation of the community-scale treatment system with a production capacity of 374 L/day.

The well water quality for a continuous operational period of 59 days is shown in Table 2.4. According to Table 2.4, a high concentration of F^- was found in the well water, exceeding the Sri Lankan limit of 1 mg/L as well as the WHO guideline of 1.5 mg/L (SLSI, 2013; WHO, 2017). Other ion concentrations were also found at extremely high levels and did not fluctuate significantly during the operating period. Figure 2.17 shows the charge loading calculated at the sampling time for 59 days of continuous operation. It was found that the charge loading and the current densities fluctuated by 1143-1408 C/L and 25.63-27.23 A/m^2, respectively. This fluctuation is attributed to the changes in well water quality.

The water quality of the raw water and the treated water for the operation were shown in Figure 2.18. After being treated with the system, F^- concentration was reduced dramatically and was stable during the operational period (Fig. 2.18a). Furthermore, F^- concentration in the treated water was found to be less than that both of Sri Lankan and WHO guidelines. Figure 2.18b shows the Mg^{2+} concentration of the well water and treated water. A high concentration of Mg^{2+} was found in the well water, exceeding the Sri Lankan limit of 30 mg/L, without significant fluctuations during the operating period. Except for three samples, treated water showed an Mg^{2+} concentration lower than 30mg/L; however, all are lower than 40 mg/L.

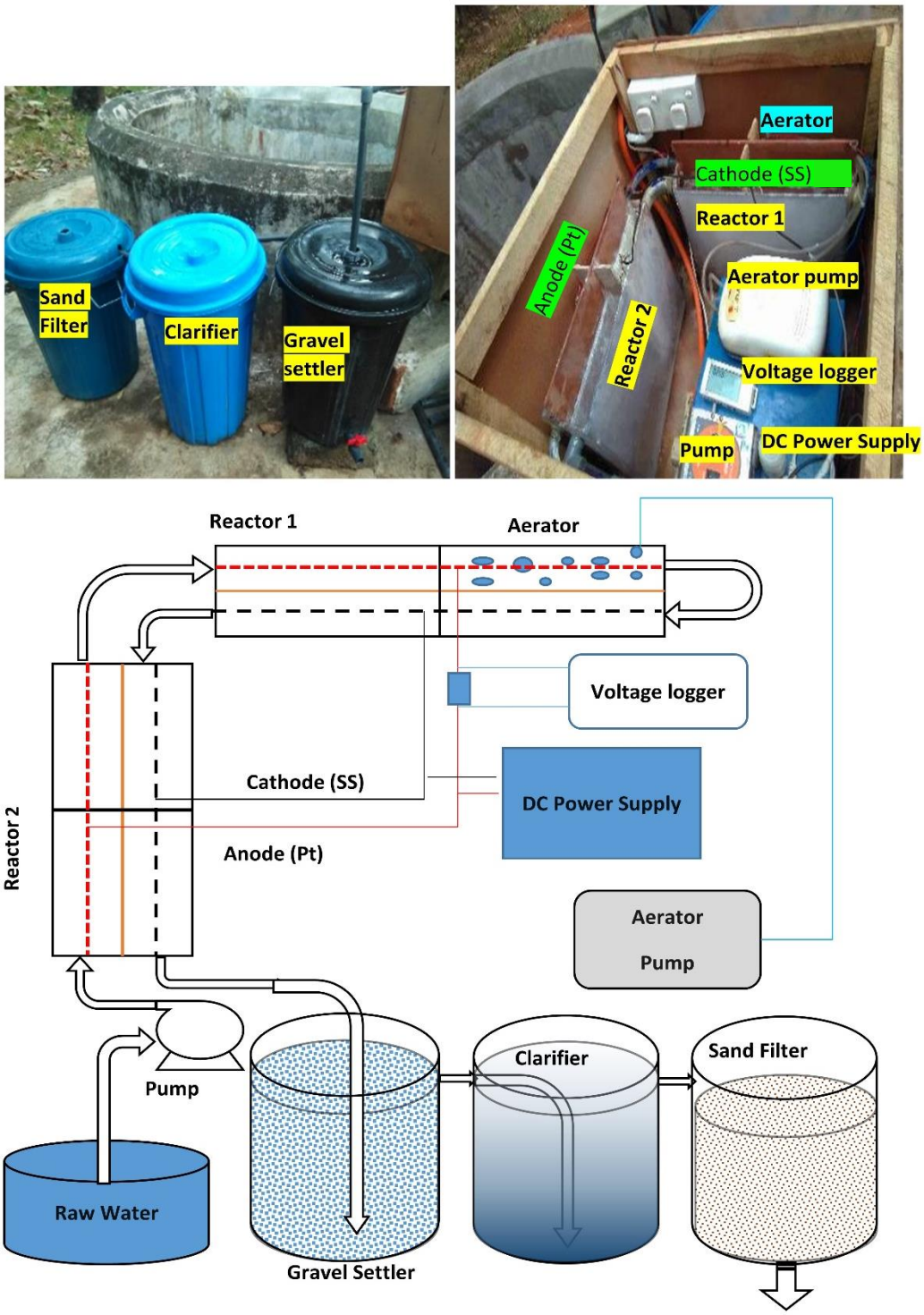

Fig. 2. 16: Community-scale Electrolysis treatment system

Table 2.4: Water quality of well water

Date	mg/L										meq/L	mmol/L	
	F^-	Cl^-	SO_4^{2-}	NO_3^-	PO_4^{3-}	Na^+	NH_4^+	K^+	Mg^{2+}	Ca^{2+}	Alkalinity	($HCO_3^- + CO_3^{2-}$)	pH
8/7/2018	2.4	156.9	21.1	0.0	0.0	144.0	0.0	0.9	105.8	47.5	12.4	12.2	8.4
9/7/2018	2.4	157.3	21.2	0.2	0.0	144.4	0.0	0.9	106.1	47.4	12.4	12.3	8.3
14/7/2018	2.4	160.9	21.7	0.0	0.0	146.1	0.0	0.8	108.4	47.7	12.5	12.5	8.1
16/7/2018	2.4	166.4	22.0	0.0	0.0	150.7	0.0	1.3	111.6	52.6	13.1	13.0	8.3
20/7/2018	2.4	169.5	22.6	0.0	0.0	153.9	1.1	1.1	102.9	71.9	13.4	13.4	8.0
23/7/2018	2.5	172.9	23.8	0.0	0.0	154.4	0.0	1.0	107.9	55.4	12.9	12.7	8.4
26/7/2018	2.5	169.1	22.5	0.0	0.0	152.6	0.0	0.1	110.0	55.1	13.1	13.0	8.2
28/7/2018	2.1	91.7	19.8	0.0	0.0	132.0	0.0	2.2	99.6	48.1	13.3	13.1	8.3
31/7/2018	2.5	170.1	21.9	0.5	0.0	153.3	0.0	1.9	108.2	57.3	13.1	13.0	7.9
5/8/2018	2.4	165.2	21.8	0.3	0.0	149.9	0.7	0.6	105.0	44.8	12.2	12.0	8.4
12/8/2018	2.6	167.1	21.3	0.2	0.0	150.5	0.8	0.8	106.8	41.9	12.2	12.0	8.4
19/8/2018	2.6	157.3	19.5	0.0	0.0	146.6	0.6	0.6	104.2	43.7	12.2	12.1	8.2
26/8/2018	2.4	151.5	18.2	0.1	0.0	137.2	0.6	0.5	101.2	46.2	11.8	11.8	8.1
2/9/2018	2.4	147.4	18.0	0.2	0.0	135.1	0.6	0.5	99.7	46.0	11.7	11.7	8.0
Averaged	**2.4**	**157.4**	**21.1**	**0.1**	**0.0**	**146.5**	**0.3**	**0.9**	**105.5**	**50.4**	**12.6**	**12.5**	**8.2**
WHO guideline	**1.5**	**250.0**	**500.0**	**50.0**	**-**	**200.0**	**-**	**-**	**50.0**	**75.0**	**6.1**	**-**	**8.5**
Sri Lankan guideline (max)	**1.0**	**1200.0**	**400.0**	**10.0**	**2.0**	**-**	**0.06**	**-**	**30.0**	**240.0**	**4.9**	**-**	**9.0**

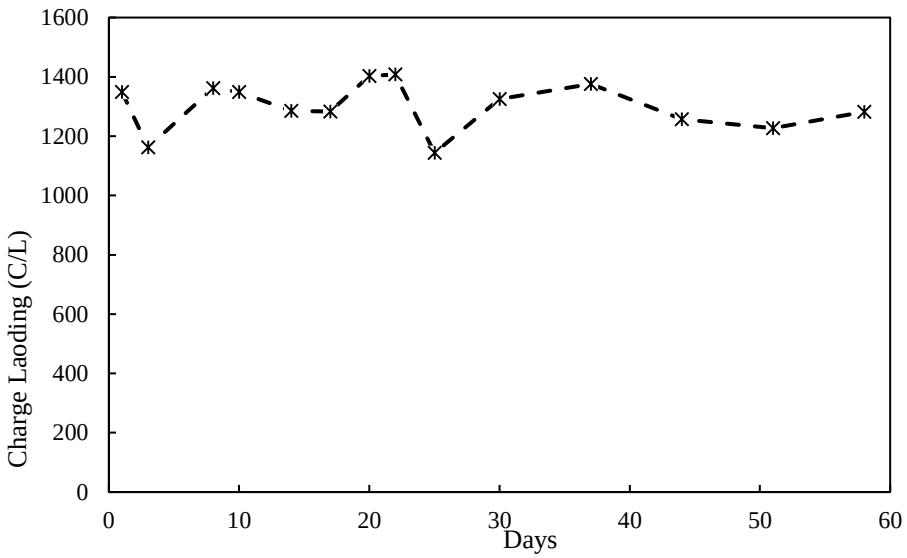

Fig. 2. 17: Changes of charge loading in the community- scale treatment system

Figure 2.18c shows the removal of Ca^{2+}, and it demonstrates that Ca^{2+} was effectively removed from the system. According to Fig. 2.18d, extremely high HCO_3^- concentrations were observed in the well water, and the partial removal of HCO_3^-+ CO_3^{2-} at the anode was observed as expected. The partial removal of HCO_3^-+ CO_3^{2-} led to the removal of high quantities of Ca^{2+}. The concentration of HCO_3^-+ CO_3^{2-} in the treated water was observed to be below 5172 µeq/L. To meet the desired concentration of HCO_3^-, Ca^{2+} ions should be introduced. Increment of charge loading cannot be performed since more HCO_3^- ions will be transferred to cathode due to increment charge loading (Force) see Fig. 2.7). With the applied current, HCO_3^-+ CO_3^{2-} and other ions were removed effectively by the system. Fig. 2.18e shows the pH profile of WW and treated water.

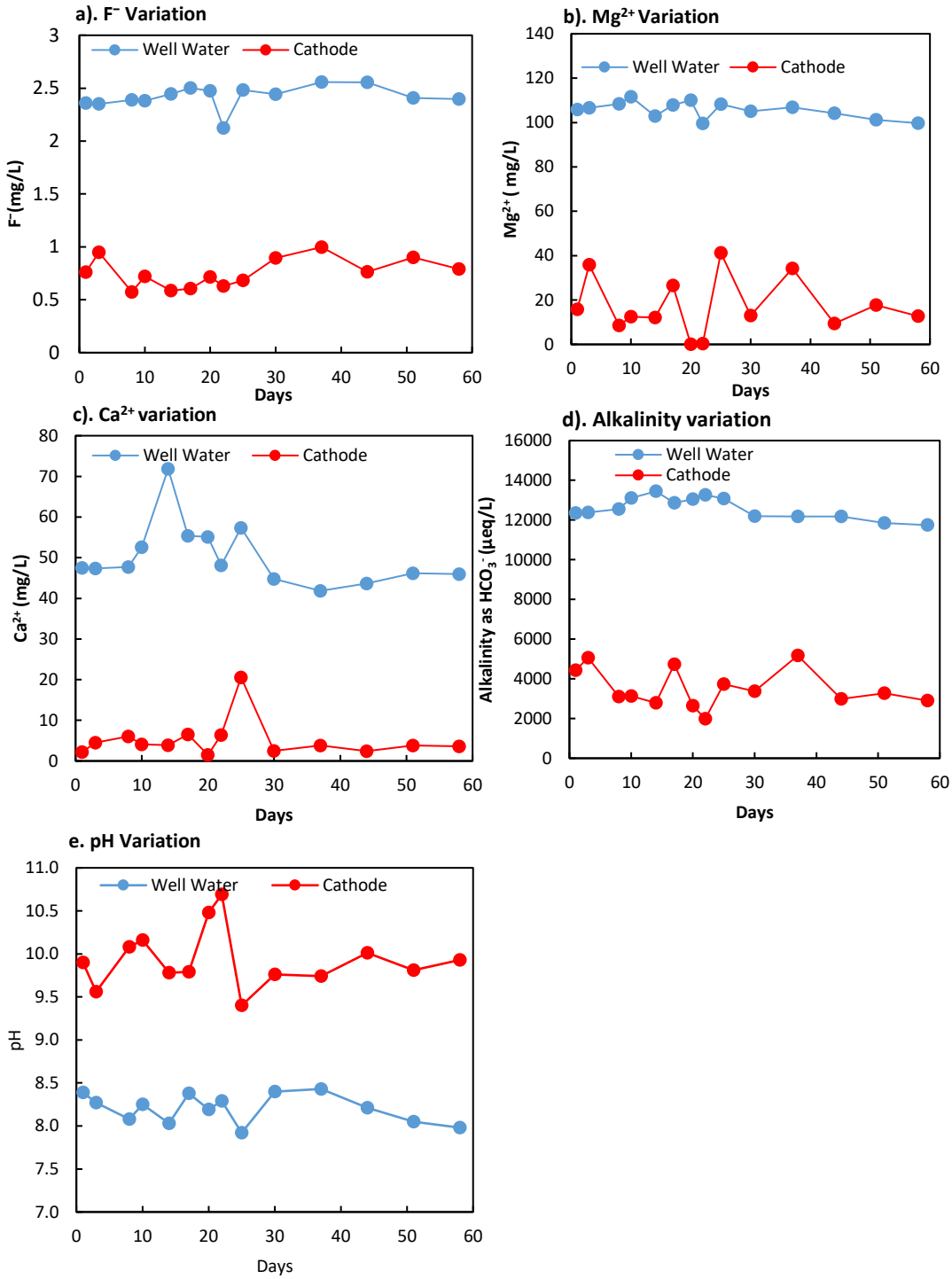

Fig. 2. 18: Time series of variation in ion concentration and pH in the community-scale treatment plant; a) F^-, b) Mg^{2+}, c) Ca^{2+}, d) Alkalinity and e) pH

The proposed system utilized a slightly different system than the experimental system, thus the calculation of neutralized OH^- and H^+ was disastrous. Therefore, to compare the applicability of the model, initial concentrations obtained from the measured results were used. Figs 2.19 a, and b showed the measured and calculated Mg^{2+} and F^- concentrations, respectively. Both models calculated and measured F^- and Mg^{2+} were found very much similar thus, the real groundwater treatment system ion removal mechanisms were similar to ion removal mechanisms proposed for the model development. Moreover, generated waste of Mg.Ca (CO_3) (dolomite) and $Mg(OH)_2$ precipitate can be used as long term fertilizer for the coconut cultivation areas where currently dolomite is widely used as fertilizer in Sri Lanka.

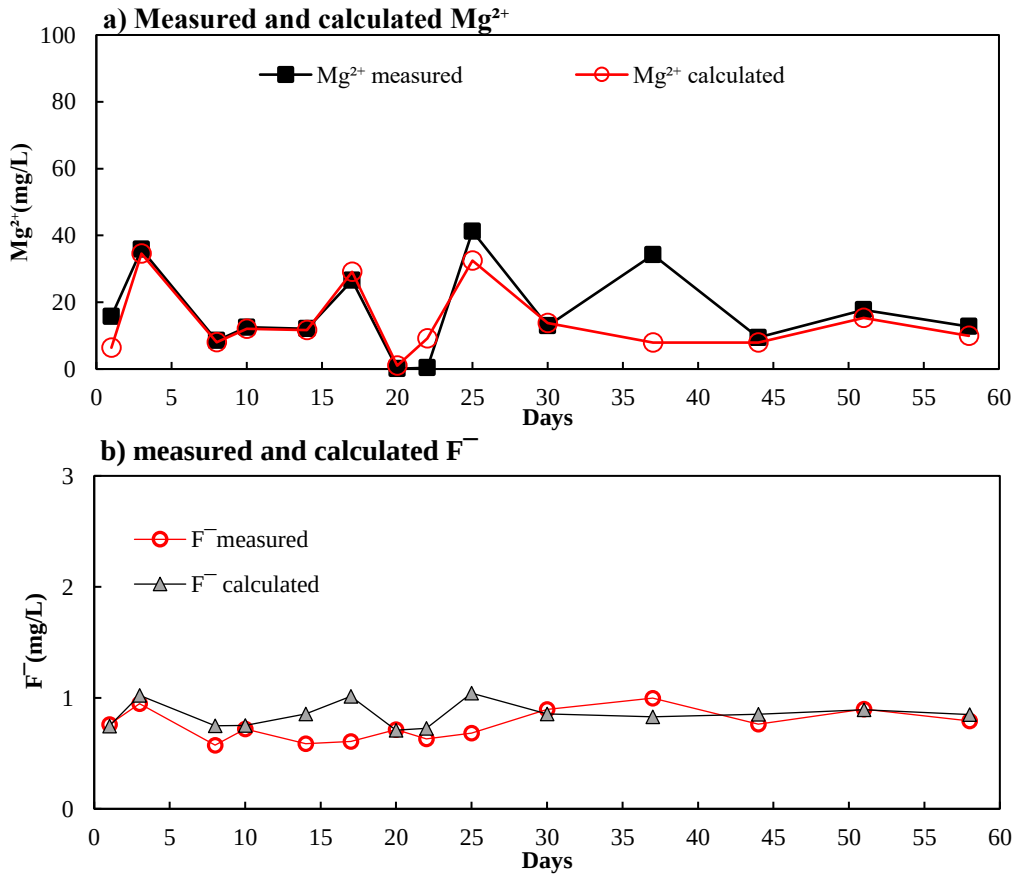

Fig. 2. 19: Measured and model calculated ion concentrations in community scale treatment system

3.6 Estimation of operational costs

The proposed system's operational cost depends largely on the cost of electricity. Accordingly, operational costs were calculated utilizing Eq.2.5. The average current used for the community level treatment plant that employed terra cotta diaphragm was found to be 5.70 A at a constant 80 V. The market price of electricity (0.061 US$/kWh) in Sri Lanka for the year 2019 (CEB, 2019) was used for the calculations. Accordingly, the operational cost was calculated to be 1.78 US$/$m^3$. Unit production cost for the treatment plant was 2672 US$.

$$Power\ Cost\left(\frac{US\$}{m^3}\right)$$

$$= \frac{Average\ Voltage(V) \times Current(A)}{Flow\ rate\ (m^3/h) \times 10^3} \times Energy\ Price\ \left(\frac{US\$}{kWh}\right) \qquad (2.5)$$

4 Conclusions

ELC system was modified to enhance the removal of CO_3^{2-} and HCO_3^- which interfered the removal of F^-, Mg^{2+}, Ca^{2+}. Furthermore, system was developed to increase water recovery as well as to operate in lower energy levels. the Ion removal mechanism was studied in order to imply the mathematical model derived in the first section. System performances to remove F^-, Mg^{2+}, Ca^{2+}, CO_3^{2-} and HCO_3^- ions versus charge loading, HCO_3^-+ CO_3^{2-} and Mg^{2+} were studied in the laboratory as well as in the field for performances and mathematical model validation.

The proposed system equipped with aerator in the anode, was found highly effective in removing HCO_3^-+ CO_3^{2-} even in lower charge loadings. Anode water circulation increased the removal of HCO_3^-+ CO_3^{2-} and improved the removal of both F^- and Mg^{2+}. Moreover, it enhanced water recovery up to 100%.

The chemical analysis and XRD data of precipitation confirmed the presence of $CaCO_3$ and amorphous $Mg(OH)_2$ particles which removed F^- mainly by co-precipitation similar to the section 1 removal mechanism. Accordingly, the mathematical model derived in section 1 was used for modeling the analytical results.

High removal efficiencies for F^-, Mg^{2+}, Ca^{2+}, and HCO_3^-+ CO_3^{2-} were observed at higher charge loadings. Increased Mg^{2+} concentration increased the removal of F^- from the system. With a lower concentration of initial HCO_3^-, Ca^{2+} and Mg^{2+} removal of both were reduced and the proposed Mg^{2+} and F^- models were able to simulate final water Mg^{2+} and F^- concentrations. Notably, the proposed system was unable to remove high initial F^- concentrations when low concentrations of Mg^{2+} were present. The formation of $MgCO_3$ was also conceivable but seems not significant at a higher charge loading.

Based on the laboratory experiments, a community-scale treatment facility with a capacity of 374 L/day was installed in Sri Lanka as a simple and cost-effective system with a 100% water recovery. The plant was operated continuously for 59 days. Plant stabilization and water output quality data were studied and compared with the simulated results from the model. It was found that the proposed system had significant F^-, hardness and alkalinity removal efficiencies and was capable of removing multiple elements F^-, Mg^{2+}, Ca^{2+}, $HCO_3^-$and CO_3^{2-} in groundwater to meet WHO and Sri Lankan drinking water quality standards. Averaged F^- removed percentage in the pilot-scale treatment plant was observed as 68.8%. Model-calculated and measured Mg^{2+} and F^- concentrations were found similar thus, the proposed ion removal mechanism was verified. Furthermore, a by-product of $Cl_2(g)$ generation was found to be an added advantage that disinfects the final water. Initial carbonate and Mg^{2+} concentrations could affect the removal of F^- and elements causing hardness.

References

APHA (1998) Standard Methods for Examination of Water and Wastewater, 20th ed., Washington, DC, Method 4500-Cl D.

Ayoob, S., Gupta, A. K. (2006) Fluoride in drinking water: A review on the status and stress effects. *Critical Reviews in Environmental Science and Technology*, 36(6), 433-487.

Bhattacharya, P., Samal, A. C. (2018) Fluoride contamination in groundwater, soil and cultivated foodstuffs of India and its associated health risks : A review. *Research Journal Recent Sciences*. 7, 36–47.

Brillas, E., Cabolt, P. L., Casado, J. (2003) Chemical degradation methods for wastes and pollutants: environmental and industrial applications (M. Tarr, ed.), Edited by: CRC press, New York.

Brillas, E., Martínez-huitle, C. A. (2015) Decontamination of wastewaters containing synthetic organic dyes by electrochemical methods. An updated review. "*Applied Catalysis B, Environmental*," 166–167, 603–643.

Browne, D., Whelton, H., Mullane, D. (2005) Fluoride metabolism and fluorosis. *Journal of Dentistry*, 33(3 SPEC. ISS.), 177–186.

Ceylon Electricity Board, (2019), Tariff Plan, CEB, last accessed 2019.11.21: *https://www.ceb.lk/commercial-tariff/en*

Chandrajith, R., Nanayakkara, S., Itai, K., Aturaliya, T. N. C., Dissanayake, C. B., Abeysekera, T., Harada, K., Watanabe, T., Koizumi, A. (2011) Chronic kidney diseases of uncertain etiology (CKDue) in Sri Lanka: geographic distribution and environmental implications. *Environmental Geochemistry and Health*, 33(3), 267–278.

Devi, R. R., Umlong, I. M., Raul, P. K., Das, B., Banerjee, S., Singh, L. (2014) Defluoridation of water using nano-magnesium oxide. *Journal of Experimental Nanoscience*, 9(5), 512-524.

De Francesco, M., Costamagna, P. (2004) "On the design of electrochemical reactors for the treatment of polluted water" in *Journal of Cleaner Production*., 12(2), 159–163.

Farooqi A., Masudaa H. and Firdousb N. (2007). Toxic fluoride and arsenic contaminated groundwater in the Lahore and Kasur districts, Punjab, Pakistan and possible contaminant sources. *Environ. Pollut*., 145(3), 839-849.

Gordon, B., Callan, P., & Vickers, C. (2008). WHO guidelines for drinking-water quality. *WHO chronicle*, 38(3), 564.

Golea D.M., Jarvis P., Jefferson B., Moore G., Sutherland S., Parsons S.A., Judd S.J., (2020). Influence of granular activated carbon media properties on natural organic matter and disinfection by-product precursor removal from drinking water,*Water Research*,174.

Hasson, D., Sidorenko, D., Semiat, R. (2010) Calcium carbonate hardness removal by a novel electrochemical seeds system, *Desalination*, 263(1–3), 285-289.

Heikens A., Sumarti S., Van Bergen M., Widianarko B., Fokkert L., Van Leeuwen K. and Seinen W. (2005). The impact of the hyperacid Ijen Crater Lake: risks of excess fluoride to human health. *Science of the Total Environment*, 346(1-3), 56-69.

Holt, P. K., Barton, G. W., Mitchell, C. A. (2005) The future for electrocoagulation as a localised water treatment technology. *Chemosphere*, 59(3), 355–367.

Iano, F. G., Ferreira, M. C., Quaggio, G. B., Fernandes, M. S., Oliveira, R. C., Ximenes, V. F., Buzalaf, M. A. R. (2014) Effects of chronic fluoride intake on the antioxidant systems of the liver and kidney in rats. *Journal of Fluorine Chemistry*, 168, 212–217.

Imai, Y., Kawakami, T., (2019) Fluoride removal from hot spring waste water by an electrolysis method and its mechanism., Global Environment Engineering Research, *J stage*, 27(5), 403-410

Jain, S., Jayaram, R. V., (2009). Removal of fluoride from contaminated drinking water using unmodified and aluminium hydroxide impregnated blue lime stone waste. *Separation Science and Technology*. 44, 1436–1451.

Kawakami, T., Motoyama, A., Nagasawa, S., Weragoda, S., Chaminda, T. (2014) Groundwater Quality Atlas of Sri Lanka, Kandy, Sanduni Offset Printers.

Kawakami, T., Nishino M., Imai Y., Miyazaki H., Amarasooriya A.A.G.D., (2018). De-fluoridation of drinking water by co-precipitation with magnesium hydroxide in electrolysis, *Cogent Eng*. 5(1), 1–13.

Karoui, H., Riffault, B., Jeannin, M., Kahoul, A., Gil, O., Ben-Amor, M., Tlili, M.M., (2013). Electrochemical scaling of stainless steel in artificial seawater: Role of experimental conditions on $CaCO_3$ and $Mg(OH)_2$ formation. *Desalination* 311, 234–240.

Lin, Y. P., Singer, P. C. (2009) Effect of Mg^{2+} on the kinetics of calcite crystal growth. *Journal of Crystal Growth*, 312(1), 136-140.

Mandinic, Z., Curcic, M., Antonijevic, B., Carevic, M., Mandic, J., Djukic-Cosic, D., Lekic, C. P. (2010) Fluoride in drinking water and dental fluorosis. *Science of the Total Environment*, 408(17), 3507–3512.

Martínez-Huitle, C. A, Ferro, S., Martı, C. A. (2006) Electrochemical oxidation of organic pollutants for the wastewater treatment: direct and indirect processes. *Chemical Society reviews*, 35(12), 1324–40.

Mollah, M. Y., Schennach, R., Parga, J. R., Cocke, D. L. (2001) Electrocoagulation (EC)--science and applications. *Journal of hazardous materials*, 84(1), 29–41.

Nidheesh, P. V., Singh, T. S. A. (2017) Arsenic removal by electrocoagulation process: Recent trends and removal mechanisam. *Chemosphere*, 181, 418–432.

Oladoja, N. A., Hu, S., Drewes, J. E., Helmreich, B. (2016) Insight into the defluoridation efficiency of nano magnesium oxide in groundwater system contaminated with hexavalent chromium and fluoride. *Separation and Purification Technology*, 162, 195–202.

Perera, A. P. G. R. L., Gonawala, J. M. L., Wijekoon, D. (2008) "Groundwater quality in Anuradhapura district with special reference to fluoride" in Groundwater in Sri Lanka. *National Academy of Science*, 48–64.

Plummer, L. N., Busenberg, E. (1982) The solubilities of calcite, aragonite and vaterite in CO_2-H_2O solutions between 0 and 90°C, and an evaluation of the aqueous model for the system CaCO3-CO_2-H_2O. *Geochimica et Cosmochimica Acta*, 46(6), 1011-1040.

Pulkka, S., Martikainen, M., Bhatnagar, A., Sillanpää, M. (2014) Electrochemical methods for the removal of anionic contaminants from water - A review. *Separation and Purification Technology*, 132, 252–271.

Reddy M., M., Karin Wang, K., (1980). Crystallization of calcium carbonate in the presence of metal ions. *Journal of Crystal Growth* 50, 470–480.

Sandoval, M. A., Fuentes, R., Nava, J. L., Rodríguez, I. (2014) Fluoride removal from drinking water by electrocoagulation in a continuous filter press reactor coupled to a flocculator and clarifier. *Separation and Purification Technology*, 134, 163–170.

Saoud, K. M., Saeed, S., Al-Soubaihi, R. M., Bertino, M. F., (2014). Microwave Assisted Preparation of Magnesium Hydroxide Nano-sheets. *American Journal of Nanomater*. 2, 21–25.

SLSI (2013) "Sri Lanka Standards for potable water-(SLS 614)" in Drinking water standards. Sri Lankan Standards Institute.

Tiwari, A. K., Singh, A. K., Mahato, M. K. (2017) GIS based evaluation of fluoride contamination and assessment of fluoride exposure dose in groundwater of a district in Uttar Pradesh, India. *Human and Ecological Risk Assessment*, 23 (1), 56–66.

Turner, B. D., Binning, P., Stipp, S. L. S.,(2005). Fluoride removal by calcite: Evidence for fluorite precipitation and surface adsorption. *Environmental Science and Technology*. 39, 9561–9568.

Weragoda, S. K., Kawakami, T., Motoyama, A., Kodithukakku, S. (2013) "Is groundwater in Dry Zone, Sri Lanka Safe to Drink?" in Sri Lanka Collaborative Research.

White, C.,(1999). Handbook of Chlorination and Alternative Disinfectants, 4th ed. *Chemical Health and Safety*, Willy publishers.

WHO (2017) Guidelines for drinking-water quality: fourth edition incorporating the first addendum, World Health Organization.

Yan M., Wang D., Ma X., Ni J., Zhang H.,(2010).THMs precursor removal by an integrated process of ozonation and biological granular activated carbon for typical Northern China water, *Separation and Purification Technology*,72(3), 263-268,

Zeppenfeld, K., (1998). Electrolysis as a method for partial decarbonisation. *GWF Wasser-Abwasser*, 139(2), 86-91.

Zeppenfeld, K. (2011) Electrochemical removal of calcium and magnesium ions from aqueous solutions. *Desalination*, 1(3), 99-105.

Zhang, Y., Dawe, R. A. (2000) Influence of Mg^{2+} on the kinetics of calcite precipitation and calcite crystal morphology. *Chemical Geology*,163(1-4),129-138.

Zuo, Q., Chen, X., Li, W., Chen, G. (2008) Combined electrocoagulation and electroflotation for removal of fluoride from drinking water. *Journal of Hazardous Materials*, 159(2–3), 4

CHAPTER 3

Electrolysis Removal of Fluoride by Magnesium Ion-assisted Sacrificial Iron Electrode and the Effect of Coexisting Components

1. Introduction

According to the results of Chapter 1 and Chapter 2, a significant level of F^- removal was observed when the initial Mg^{2+} concentration was high. Therefore, proposed electrolysis (ELC) methods cannot apply to F^- removal for drinking purposes when no or lower Mg^{2+} concentrations are co-existed. Since one of the main focuses of the study was the removal of F^- from Sri Lankan groundwater, we had to find a suitable F^- removal technique for the groundwater with no or lower Mg^{2+} concentration. Accordingly, I focused on the other electrochemical technologies to address this issue.

Among the electrocoagulation (EC) methods, Aluminum (Al) is commonly used as a sacrificial electrode for de-fluoridation due to its effectiveness of removing F^-. Adversely, high Al intake could cause neurotoxicity (Campbell, 2002; Krewski et al., 2009). Therefore, the use of Al-based coagulant in the electrochemical process of removing F^- from water could negatively influence human health and the ecosystem. Apart from the Al electrode in EC for F^- removal, an iron (Fe) electrode has been used. The Fe electrode in EC has the additional advantages of being inexpensive, abundant, and of lower toxicity compared to the Al electrode. However, few studies described its usability, and the high ratio of Fe sludge volume to F^- removed could be the main reason that Fe electrodes are not commonly used (Drouiche et al., 2012, 2008; Govindan et al., 2015).

Combining Fe with other elements could increase F^- removal in the EC process. Among the studies of F^- removal using sacrificial Fe electrodes, few described the effect of coexisting ions on F^- removal. Drouiche et al. (2012) proposed

removing F^- from photovoltaic wastewater with Fe-EC bipolar electrodes by pretreating water with $Ca(OH)_2$. Later, Govindan et al. (2015) investigated influence of coexisting ions Ca^{2+}, Mg^{2+}, and Al^{3+} on F^- removal by the Fe-EC system, and showed that Mg^{2+} had an effect on F^- removal, although this was not studied in detail. Furthermore, their findings revealed that the removed weight fraction of Fe to F^- appears to be significantly higher than that of the Al electrode EC. Concisely, neither study gave much attention to minimizing Fe sludge volume, the effects of Fe^{2+}, Mg^{2+}, Ca^{2+}, alkalinity and pH, on the removal of F^-. Even though, Fe and Mg^{2+} can assist F^- removal in EC, further scientific improvements are limited by the single-cell EC reactor.

Usually, in the single-cell EC reactor, faradaic contribution to anodic dissolution leads to a higher electrode material loss (Gu et al., 2009). Apart from the anodic dissociation, H^+ formed near the anode transferred and neutralization took place near the cathode region where a high density of OH^- ions are available. That neutralization buffered the pH to a near neutral level and leads to the incomplete removal of the dissolved metal ion by the formation of the floc (anode metal hydroxide). Incomplete removal of the dissolved metal ion minimizes the EC's pollutant removal efficiency (Nidheesh and Singh, 2017). Therefore, overcoming the total effects of the residual electrode materials and the partial removal of F^- in the final water becomes problematic when using the common single-cell EC system.

ELC is a widely used technology for the generation of H_2 and Cl_2. The essential difference between EC and ELC is a permeable diaphragm which separates the anode and cathode in the ELC reactor. The ELC cell's permeable diaphragm splits the anode solution and the cathode solution, and allows the high pH and low pH solutions to be conserved in each compartment. Furthermore, the Coulomb force in the ELC allows transferring ions through the ELC cell diaphragm. These specific functions can be utilized to minimize the electrode dissociation and to optimize the process performances of EC. Furthermore, to date, no ELC study reported F^- removal with Fe electrodes as well as the effect of co-existing Mg^{2+} and other ions.

Therefore, the main objectives of this work are to study the F^- removal by sacrificial Fe electrode, to minimize the sludge volume generated by EC by increasing the F^- removal efficiency, to study the effect of co-existing Mg^{2+} and other ions, studying the F^- removal by sacrificial Fe electrode, to study the removal of co-existing Mg^{2+}, Ca^{2+}, F^-, HCO_3^- and CO_3^{2-} in the presence of low concentration of Mg^{2+} to optimize F^- removal for different concentrations of Fe and Mg^{2+}, and to confirm the proposed ELC systems' performance and stability for groundwater treatment in Sri Lanka.

Accordingly, with a batch type reactor, F^- removal was studied with and without Mg^{2+} ion assistive Fe electrode ELC system. Furthermore, the performance optimization of F^- removal for different concentrations of Fe and Mg^{2+} was studied to minimize Fe and Mg^{2+} concentrations. Furthermore, the effects of coexisting ions Ca^{2+}, F^-, HCO_3^-, and CO_3^{2-}on F^- removal were also investigated. In addition, a continuous flow ELC system was operated to remove F^- from synthetic groundwater and results were compared with the previous ELC methods.

2. Materials and methods

2.1 Chemicals, instruments and quality control

De-fluoridation experiments were performed with artificially prepared groundwater containing different concentrations of Fe, F^-, Mg^{2+}, Ca^{2+}, HCO_3^-, and CO_3^{2-}. The chemicals, instruments for anion, cation and pH measurements, and analytical methods used in this experiment were as same as mentioned in Chapter1. Fe concentrations were measured with an atomic absorption spectrophotometer (AAS) (Hitachi A2000, Japan). To measure total Fe with the AAS, 20 mL of solution collected from the first stage was dissolved in 31 % HNO_3 acid and filtered by a 0.45 µm membrane filter before inject to the AAS. The standard blank, and the standard solutions were injected after every 10 samples for quality control.

2.2 Experimental setup and process description

Batch ELC experiments were performed with a square-shaped cell having two equal compartments made of PVC (9.5(H)×8.5(W)×10.5(L) cm^3). Two equal compartments, an anode, and a cathode were equally separated by using a mixed cellulose ester membrane filter as a diaphragm with a pore size of 0.2 µm (Advantec, Toyo Roshi Kaisha, Ltd., Japan). The membrane filter was used as a diaphragm to allow both anion and cation transfer through anode and cathode without special ion selectivity. Pt electrodes were purchased from the Nilaco Corporation, Japan, and SS and Fe electrodes were obtained from the local market in Japan. Throughout all the experiments, an inter-electrode distance of 5 cm was maintained and a constant current power supply (TSS TAKASAGO, Japan) was used to apply the current.

The batch type experiments were performed with the two-stage ELC by using different electrode configurations. Two parallelly connected iron (Fe) electrodes (effective length=5.5 cm, φ=3 mm) and single U-shaped stainless steel (SS) (effective length=15 cm, φ=1 mm) were used in the first stage ELC. Platinum (Pt) wire (effective length=15 cm, φ=0.40 mm) electrode and SS electrodes were used for the second stage ELC. The first-stage ELC (Electrode configuration: Fe anode/SS cathode) was performed for dissociation of Fe into the anode solution, and the second-stage ELC (Electrode configuration: Pt anode/SS cathode) was for forming floc of metal hydroxides which co-precipitates F^- in the cathode. In the second stage, first-stage anodes and cathodes were converse as cathodes and anodes, respectively, by replacing the electrodes as shown in Fig. 3.1. For the first stages ELC, 320 mL of water was put in the anode and the cathode. Twenty mL of water was collected from both the anode and the cathode cells after the first and second stage ELC was finished.

Figure 3.2 shows the continuous flow ELC system coupled with aeration in the anode for mixing Fe. The system was comprised of a Fe dissociation reactor (the first stage ELC) and ELC reactor (the second stage ELC). In the anode of the second stage ELC, low pH environment and the aeration removed $HCO_3^- + CO_3^{2-}$. The inflow

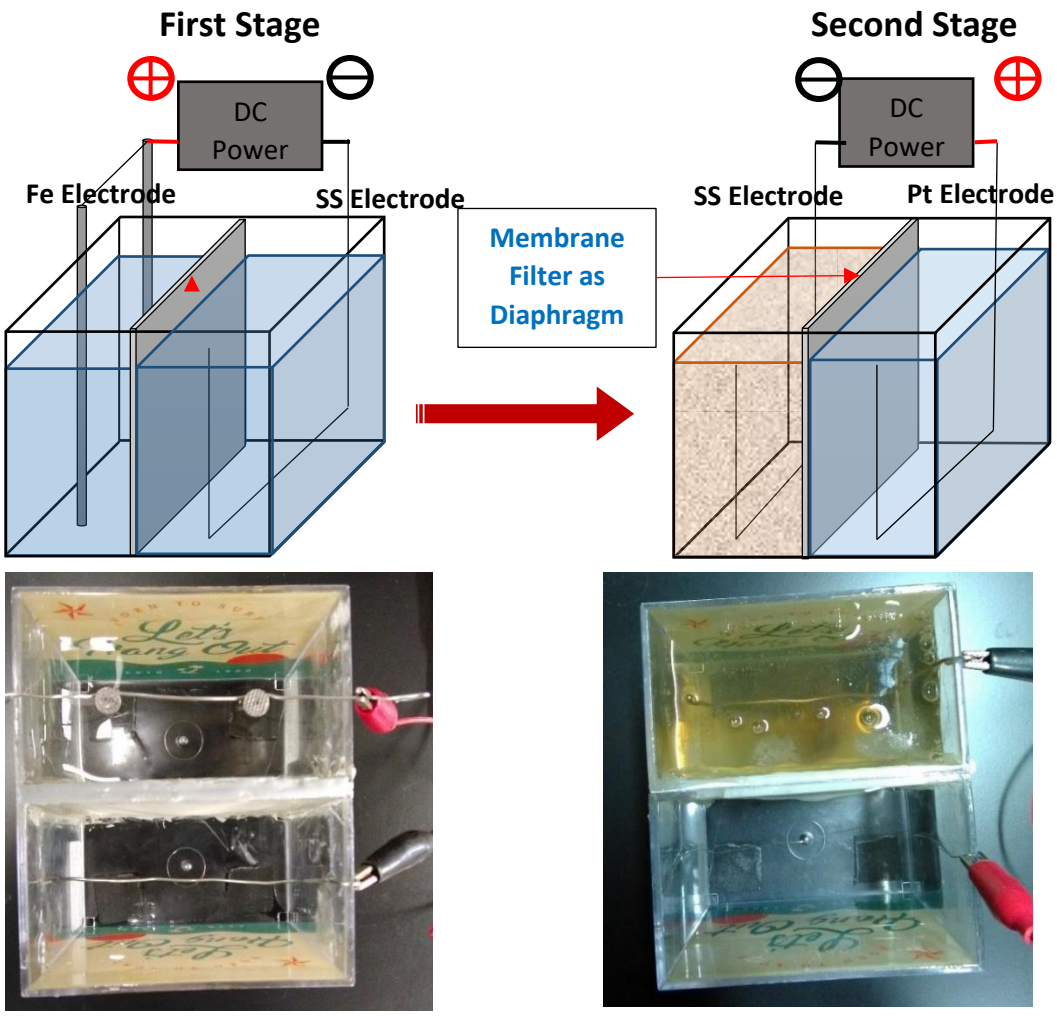

Fig. 3.1: Electrolysis electrocoagulation cell configuration in the first and second stages

rate of the raw water to the anode of the second stage ELC was kept at 15 mL/min. From the anode of the second ELC, water was sent by gravity at a rate of 10 mL/min to the anode of the first stage ELC. The remaining water (5mL) was pumped through the cathode of the first stage ELC and discarded at a rate of 5mL/min. The outflow from the anode of the first stage ELC was lead to the cathode of the second stage ELC at a flow rate of 10 mL/min (Fe dissociated water) where most of the ions precipitated.

Applied charge loading in the second stage ELC was maintained at 1500 C/L in the cathode and 1000 C/L in the anode. In the first stage ELC, the charge loading

of 120 C/L was used in the anode while 240 C/L in the cathode. The difference of charge loading in both reactors was caused by different flow rates maintained in the anode and the cathode.

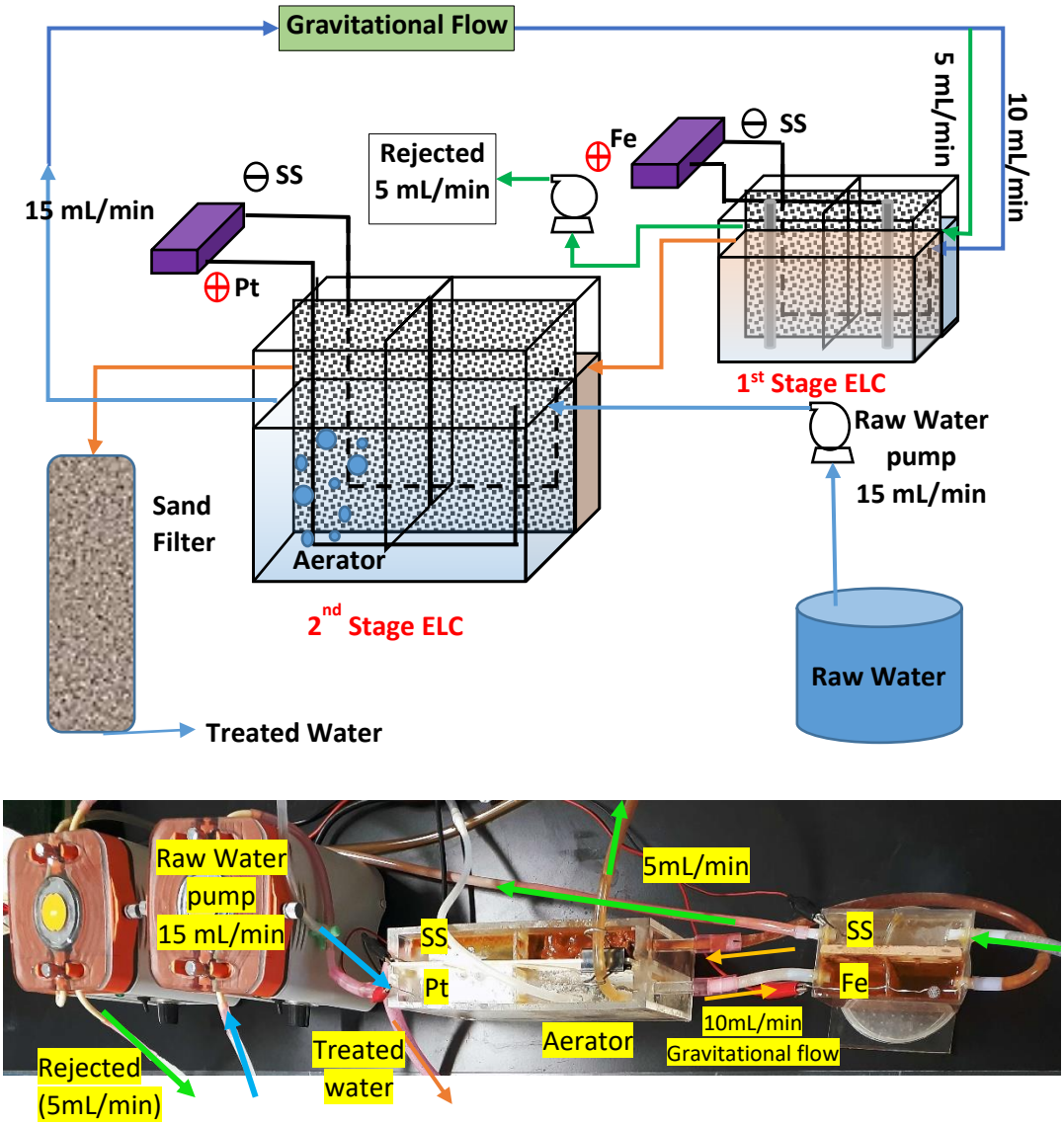

Fig. 3.2. Schematic diagram and laboratory scale image of continuous flow ELC system

2.3 Experimental conditions and calculations

Applied charge loading is very important in EC to control electrode dissociation as well as the flocculation process. According to Faraday's law (Eq. 3.1), the amount of Fe dissociated can be controlled by changing the applied current or time. Practically 100% of electrons did not contribute to the leaching of metal ions from the sacrificial electrode. Some electrons could be used to form H^+ ions in the vicinity of the anode. Therefore, calculating the amount of dissolved Fe could be problematic. To determine the Fe leached, the weight differences of the Fe electrode, before and after the first-stage current application, were used to calculate the total amount of Fe dissolved. Prior to each experiment, Fe electrode surfaces were polished with sandpaper, washed, and dried to remove the oxidized layer. Furthermore, the concentration of Fe in the anode solution was verified with AAS measurements.

$$[Metal]^{M+} dissolved\ (mol) = \frac{Current\ (A) \times Time\ (s)}{Faraday\ constant (96485)(C/mol)} / M \quad (3.1)$$

Where M is the valence of the ion

During the second-stage ELC, pH in the anode effluent decreased, while the cathode effluent increased significantly according to Eq. 1.1 and 1.3 (Chapter 1). Fe^{3+} or/and Fe^{2+} and Mg^{2+} combined with OH^- to generate metallic-hydroxides ($Mg(OH)_2$, $Fe(OH)_2$ or and $Fe(OH)_3$). The precipitation of Fe and Mg hydroxides could eliminate F^- either by adsorption or co-precipitation. Moreover, Coulomb force contributed to transport the ions through the diaphragm membrane. Total F^- removal by Coulomb force and by precipitation was calculated by Eq. 3.2 and Eq. 3.3.

Fluoride transferred to the anode by Coulomb force (mg) = $(C_a - C_i) \times V$

Percentage of F^- transferred to the anode by Coulomb force $= \frac{(C_a - C_i)}{C_i} \times 100$ (3.2)

Fluoride removed by precipitation can be described as (Total decrease in F^- in the cathode - F^- transferred to the anode by Coulomb force)

Accordingly,

Fluoride removal by precipitation (mg)= $(C_i - C_f) \times V - (C_a - C_i) \times \mathrm{V}$

Fluoride removal % by precipitation $= \frac{(C_i - C_f) - (C_a - C_i)}{C_i} \times 100 = \frac{(2C_i - C_a - C_f)}{C_i} \times 100$ (3.3)

Where:

C_i : Initial F^- concentration in the anode and cathode (before the first stage) (mg/L)

C_a : Final F^- concentration in the anode (after second stage) (mg/L)

C_f : Final F^- concentration in the cathode(after second stage) (mg/L)

V: Anode volume (L)=Cathode volume (L)

To date, no data are available in ELC for F^- removal using the Fe electrode in electrolysis system; thus, it is worth studying the effect of the dissolved Fe concentration on F^- removal with and without Mg^{2+}. The dissolved Fe concentrations were controlled at the first stage by changing the ELC time and current. In the second stage ELC, electrolysis was continued for 60 minutes by applying a constant current of 100 mA to supply 1200 C/L to obtain the adequate amount of OH^- in the cathode which could precipitate 99% of dissolved Mg^{2+} and Fe in the form of its hydroxides.

To investigate the minimum initial Mg^{2+} concentration required to meet the WHO's F^- guideline for drinking water of 1.5 mg/L, initial F^- concentrations ranging from 1–5 mg/L and Mg^{2+} concentrations ranging from 5–20 mg/L were used at a constant concentration of initial Fe (20 mg/L) in ELC. Groundwater contains several other ions that may interfere with F^- removal during ELC. The most common ion found in water is Ca^{2+}. Therefore, the effect of the presence of the Ca^{2+} ion was studied. Initial concentrations of Fe 20 mg/L, Mg^{2+} 20 mg/L, and F^- 5 mg/L were investigated with varying Ca^{2+} concentrations. Other than the Ca^{2+}, the most abundant naturally

occurring ions in the water that may affect process efficiency are carbonates ($HCO_3^-$and CO_3^{2-}). Due to the diprotic nature of carbonic acid (H_2CO_3) in the solution, both CO_3^{2-} and HCO_3^- (hereafter (HCO_3^-+ CO_3^{2-})) are existing, and their concentrations change with the pH value of the solution. The charges of (HCO_3^-+ CO_3^{2-}) were calculated by accounting ions charge balances as shown in Eq. 1.13 (Chapter 1). For calculating individual $HCO_3^-$and CO_3^{2-} concentrations as mmol/L, as described in Eq. 1.16 and Eq. 1.17(Chapter 1), the carbonates' charge balance equation (Eq. 1.14) and carbonates' equilibria (Eq. 1.15) were employed (Chapter 1).

3. Results and discussion

3.1 Effect of the initial Fe concentration on F^- removal in the absence of Mg^{2+}

By varying the first-stage time and current (for dissolving the desired concentration of Fe) with the constant second-stage charge loading (100 mA for 60 min=1200 C/L), the rate of F^- removal from the synthesized groundwater was investigated. Table 3.1 shows the Fe concentration calculated with applied charge loadings (Eq. 3.1) by AAS measurement and calculated with weight loss of the electrode. Table 3.1 shows that Fe concentration measured by weight was slightly higher than that by the AAS measurement and mostly equal to the concentration calculated by the applied charge loading when Fe^{2+} formation was considered as Eq. 3.1. Usually, the anode electrode leach Fe and produced H^+ ions around its surface which caused decreasing of pH. As described by Stefánsson,(2007), pH level<3 was favorable for the formation of Fe^{2+} (EQ. 3.4) but it can be further oxidized to the Fe^{3+}(Eq. 3.5). At the end of the second stage of electrolysis, pH in the anode (First stage anode) increased. Increasing pH was favorable for the formation of $Fe(OH)_3$ species and precipitation could occur (Eq. 3.8). Accordingly, measured Fe concentrations were considered for the experiments.

Table 3.1: Fe leachate measurements and calculations for different charge loading

Charge loading in First Stage (C/L)	Fe^{2+} concentration calculated from applied charge loading (mg/L)	Total Fe concentration measured by AAS (mg/L)	Fe concentration calculated from electrode weight loss (mg/L)
75	21.7	19.4	21.9
176	50.9	50.2	55.6
332	96.1	90.0	93.1
938	271.5	282.1	292.5
1650	477.6	486.2	495.3

Variations of F^- removals are shown in Fig. 3.3 as a function of initial Fe concentration and the first-stage charge loading. According to Fig. 3.3, when the initial Fe concentrations increased, F^- removal by precipitation increased marginally. The maximum F^- removal by precipitation (14%) was achieved with an initial Fe concentration of 486 mg/L. Accordingly, the maximum F^- removal capacity by precipitation was calculated as 1.43 mg/g for the initial F^- concentration of 5 mg/L. For initial Fe concentrations of 50–100 mg/L, around 4 % of F^- was removed by precipitation; however, higher F^- removal as 72–71% by Coulomb force was experienced. This level was 34 % higher than that without Fe in the solution.

During the second stage of electrolysis, pH level increased. The predominant aqueous species of Fe in the pH range of 8–8.4 were $Fe(OH)^+_2$. But in the pH 8.4-10 both $Fe(OH)^+_2$ and $Fe(OH)_3(aq)$ were existing at an approximately equal concentration (Stefánsson, 2007). Since second-stage pH levels of 11.75–8.76 were observed for initial Fe concentrations of 0–486 mg/L, precipitation of $Fe(OH)_3$ and $Fe(OH)_2$ took place in the cathode of the second stage. With the Ksp's from Lide, 2005 study, Ksp $Fe(OH)_2$=4.87×10^{-17} $(mol/L)^3$ and Ksp $Fe(OH)_3$ = 2.79×10^{-39} $(mol/L)^4$, formation of $Fe(OH)_3$ and $Fe(OH)_2$ was verified (Table 3.2).

Table 3.2: Calculated Ion Activity product (IAP) and Ksp of $Fe(OH)_2$ and $Fe(OH)_3$; Ksp<IAP (supersaturated), Ksp=IAP(Equilibrium), Ksp>IAP (under saturated)

pH	dissolved Fe (mol/L)	OH (mol/L)	Concentration of Fe^{2+}=Fe^{3+}at pH 8.4-10 (Stefansson, 2007)		Ksp $Fe(OH)_2$=4.87E-17	Ksp $Fe(OH)_3$=2.79 E-39
			Fe^{2+}(mol/L)	Fe^{3+}(mol/L)	IAP of $Fe(OH)_2$	IAP of $Fe(OH)_3$
11.59	0.0004	0.0039	-	0.00039	-	2.11E-11
11.49	0.0009	0.0031	-	0.00031	-	2.65E-11
10.65	0.0016	0.0004	0.0008	0.0008	1.61E-10	7.18E-14
9.87	0.0050	0.0001	0.0025	0.0025	1.39E-11	1.03E-15
8.76	0.0087	0.0000	0.0044	0.0044	1.44E-13	8.29E-19

As mentioned in the previous studies, the amorphous metallic hydroxide (Al and Fe) formed has a large surface area with a high adsorption capacity, which forms a floc and makes a bond with pollutants (Kobya et al., 2006; Nidheesh and Singh, 2017). Furthermore, as described in the previous studies, F^- removal may occur due to sweep coagulation or the enmeshment of F^- ions by insoluble Fe hydroxide precipitate (co-precipitation) in the solution (Drouiche et al., 2008; Singh et al., 1998). Accordingly, overall reactions in the first and second stages can be summarized as Eqs. 3.4–3.9.

As the initial Fe concentration increased, the total surface area of $Fe(OH)_3$ increased. Thus, the removal of F^- increased agreeing with Fig. 3.3 results. When the initial Fe concentration was increased, $Fe(OH)_3$ formation increased, causing increased F^- removal as a form of precipitate in the cathode. Clear evidence of this phenomenon can be seen in Fig. 3.3 with initial Fe concentration of 90 to 480 mg/L, as the removal of F^- as precipitates, increases over the initial Fe concentration, while F^- removal by Coulomb force plunged significantly.

At the anode (first stage)

$$Fe_{(s)} \rightarrow Fe^{2+}{}_{(aq)} + 2e^- \quad (3.4)$$

$$Fe^{2+}{}_{(aq)} \rightarrow Fe^{3+}{}_{(aq)} + e^- \quad (3.5)$$

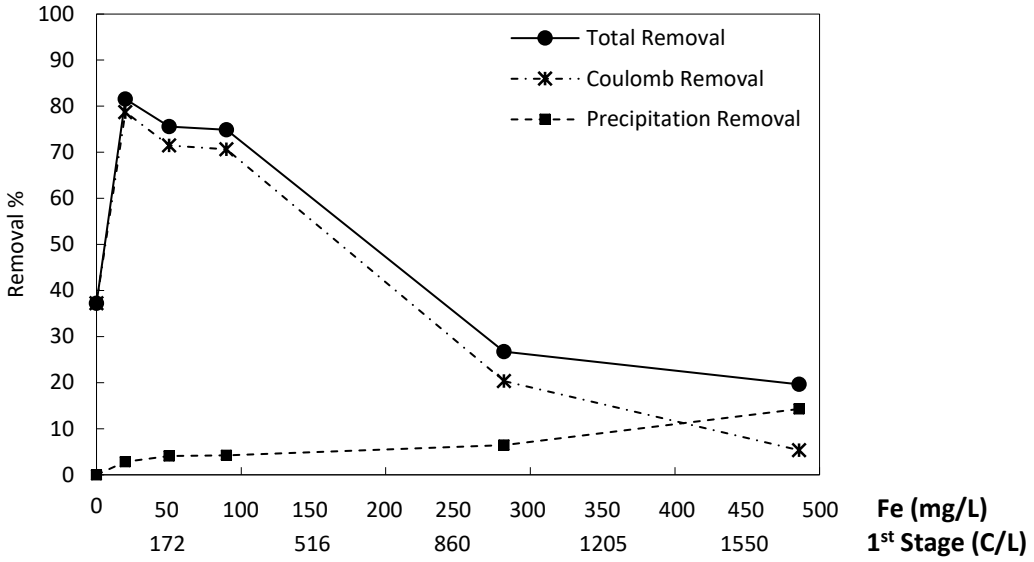

Fig. 3.3: Variation of F^- removal as a function of varying initial Fe concentrations/first-stage charge loadings in the cathode (initial F^- = 5.0 mg/L, NaCl=2 mg/L; Ca^{2+}=0; HCO_3^- +CO_3^{2-}=0 mmol/L; applied at the second-stage =1200 C/L)

At the cathode (second stage)

$$2H_2O_{(l)}+2e^- \rightarrow 2OH^-{}_{(aq)} + H_{2(g)} \tag{3.6}$$

$$Fe^{3+}{}_{(aq)} + 3OH^-{}_{(aq)} \xleftrightarrow{Ksp_{Fe(OH)_3}=2.79\times10^{-39}(mol/L)^4} Fe(OH)_{3(s)} \tag{3.7}$$

Fluoride co-precipitation

$$Fe^{3+}{}_{(aq)} + (3-\alpha)OH^-{}_{(aq)} + \alpha F^-{}_{(aq)} \rightarrow Fe(OH)_{3-\alpha}F_{\alpha_{(s)}} \downarrow \tag{3.8}$$

Fluoride Adsorption

$$Fe(OH)_3(s) + \alpha F^-(aq) \rightarrow Fe(OH)_{(3-\alpha)}F_{(\alpha)_{(s)}} \downarrow + \alpha OH^-(aq) \tag{3.9}$$

With the limited data available from studies of F^- removal by Fe electrode, the data from the current study are summarized in Table 3.3. It appears that the proposed Fe-ELC system is capable of removing F^- to some degree. However, it seems that removal was slightly less efficient than that in the previous studies. As described by Drouiche (2012), optimum F^- removal in EC was achieved at pH 6, and, as the pH increased, F^- removal tended to decrease (Drouiche et al., 2012). Similarly, the pH value was higher than 6 of this system could decrease F^- removal compared to the previous studies with neutral pH-operated EC studies.

Table 3.3: F^- removal by sacrificial Fe electrodes in EC and ELC

Initial		Removal as precipitate %	First stage C/L (Fe)	Total C/L	Fe^{2+} leachate (mg/L)	Removal of F^- by Fe (mg/g)	Reference
F^- (mg/L)	Mg^{2+}(mg/L)						
25	0	40.0	0	3600	1042	9.6	EC-(Drouiche et al., 2008)
4.5	0	8.1	0	922	267	1.4	EC-(Zhao et al., 2011)
10	0	18.0	0	1620	469	3.8	EC-(Govindan et al., 2015)
5	0	4.1	176	1376	50	4.0	ELC- (this study)
5	0	4.2	332	1532	90	2.4	
5	0	6.5	938	2138	282	1.2	
5	0	14.4	1650	2850	486	1.5	

3.2 Effect of the initial Fe concentration on F^- removal in the presence of Mg^{2+}

The role of the dissolved Fe concentrations (at the end of first stage) on ions and F^- removal in the presence of Mg^{2+} is shown in Fig. 3.4. Throughout the ELC experiments, the initial Mg^{2+} concentration was kept constant at 20 mg/L, and initial

Fe concentrations were varied from 0-53 mg/L. According to Fig. 3.4a, in the absence of Fe, Mg^{2+} alone removed F^- as a precipitate (37%). The removal of F^- in the absence of Fe and increasing of initial Mg^{2+} concentration is shown in Fig. 3.5. F^- removal by precipitation increased with increasing initial Mg^{2+} concentration (maximum 80% at 100 mg/L of Mg^{2+}). Therefore, obviously $Mg(OH)_2$ contributed to removing the F^- in the form of a precipitate due to the higher alkaline nature at the cathode (pH=11.32-9.34 for Mg^{2+} 0-100 mg/L).

In addition, F^- could also precipitate as MgF_2, however, when comparing the solubility products (Ksp) of MgF_2 (5.16×10^{-11} $(mol/L)^3$) with that of $Mg(OH)_2$ (5.61×10^{-12} $(mol/L)^3$), formation of $Mg(OH)_2$ was predominant in the operational pH level. Previous studies of de-fluoridation of water using nano-magnesium oxide suggested that exchange of F^- with $Mg(OH)_2$'s OH could occur due to the isoelectric nature and the similar radius of F^- and OH^- (Devi et al., 2012; Oladoja and Helmreich, 2016). Accordingly, it can be proposed that the F^- could be exchanged with OH^- and co-precipitated with $Mg(OH)_2$ (Eq. 3.10).

$$aMg(OH)_2(s)\downarrow + bF^-(aq) \rightarrow aMg(OH)_{\left(2-\frac{b}{a}\right)}F_{\left(\frac{b}{a}\right)(s)}\downarrow + bOH^-{}_{(aq)} \qquad (3.10)$$

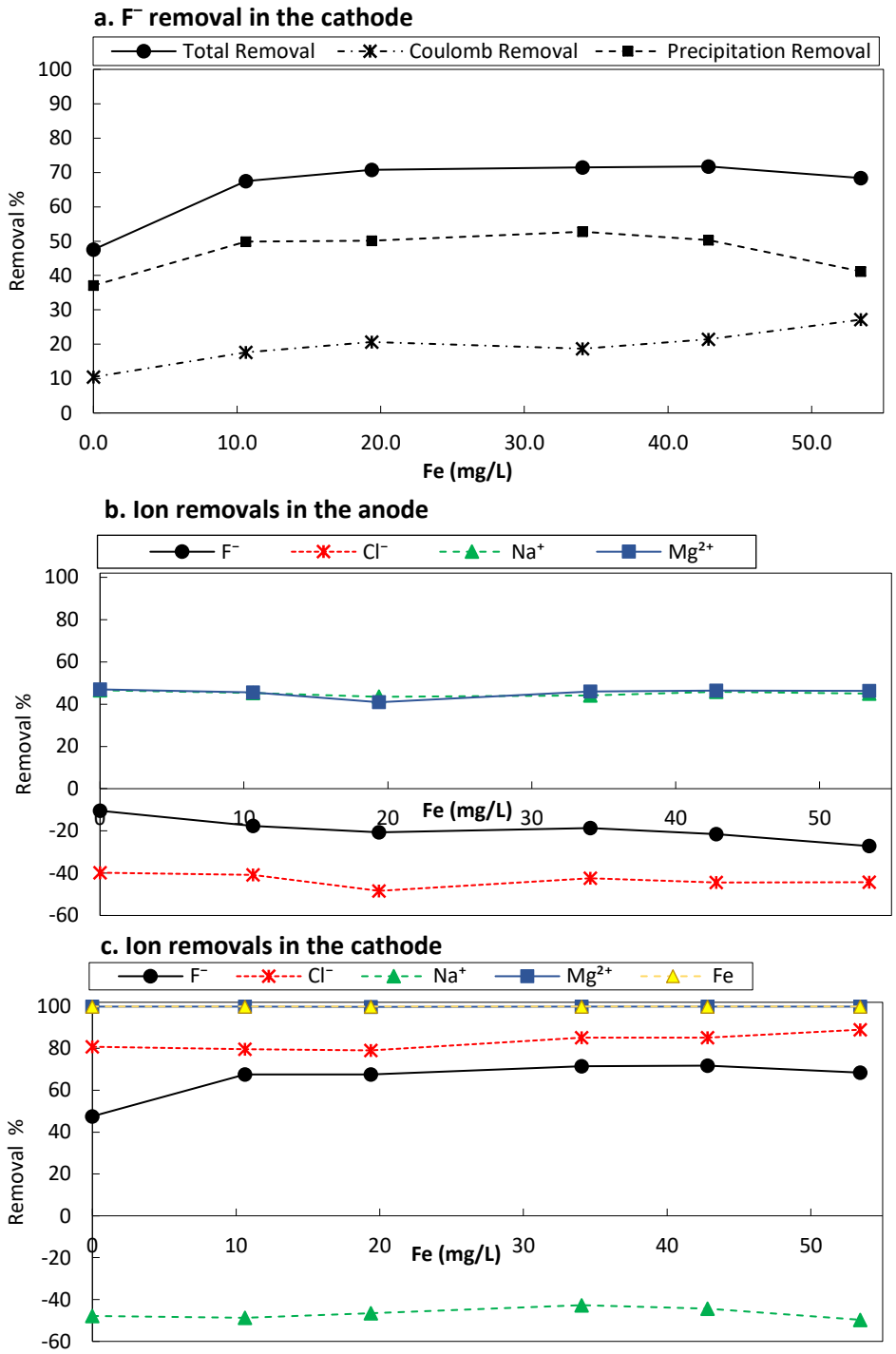

Fig. 3.4: Variation of F^- removal with initial Fe concentration, charge loading applied at first stage=19–188, Charge loading applied at second stage=1200C/L, initial Mg^{2+} concentration=20 mg/L, initial F^- concentration=5 mg/L, $HCO_3^- + CO_3^{2-}$ =0 mmol/L

As shown in Fig. 3.4a, at the initial Fe concentrations of 11-43 mg/L, the removal of F^- as precipitates was maximized and approximately remained at a constant level. Therefore, the co-existence of Mg^{2+} along with the Fe at an initial molar ratio of Mg: Fe = 1: (0.24-0.94) was the most favorable condition in removing F^-. Mg: Fe = 1: (0.24) is the best condition when taking power consumption into consideration. As described previously, both $Mg(OH)_2$ and $Fe(OH)_3$ exhibit F^- co-precipitation properties. As a result, the predominant mechanism of the F^- removal could be co-precipitation as expressed in Eq. 3.15.

$$xMg^{2+} + yFe^{3+} + (2x + 3y)OH^- + zF^- \rightarrow Fe.Mg(OH)_{2x+3y-z}(F^-)_z\,(s) \downarrow + zOH \qquad (3.15)$$

As the dissolved Fe concentration increased, F^- removal by Coulomb force increased in the cathode (Fig. 3.4a), while F^- in the anode showed a negative removal (Fig. 3.4b). As described previously, F^- in the cathode was retransferred to the anode at the second stage by Coulomb forces, resulting in an increase in F^- concentration. The data from Fig. 3.3 and Fig. 3.5 make it clear that the precipitative removal of F^- by $Fe(OH)_3$ was weaker than that by $Mg(OH)_2$. Accordingly, to Fig. 3.4, increase of the initial Fe concentration > 43 mg/L decreased the precipitative removal of the F^-. Therefore, the increase in the formation of $Fe(OH)_3$, inhibited the precipitative removal of F^-. Probably, high $Fe(OH)_3$ formation could prevent the F^- ion exchange with the OH^- due to increased competition. Hence, the increase of Fe concentration beyond 43 mg/L could negatively affect F^- removal as observed in Fig. 3.4a.

Figure 3.4c showed that Mg^{2+} in the cathode was removed more than 99% by precipitation. Figure 3.4b showed that 47% of Mg^{2+} was removed from the anode by coulomb transferred to the cathode. More than 99% of Fe removal in the cathode was observed for all concentrations of initial Fe, assuring the absence of electrode material in the treated water. The Cl^- was transferred to the anode by the Coulomb force creating negative removal in the anode bath. However, there was a 40% difference between cathode and anode ion transfer. The production of Cl_2(g) and its evaporation at the anode caused this difference.

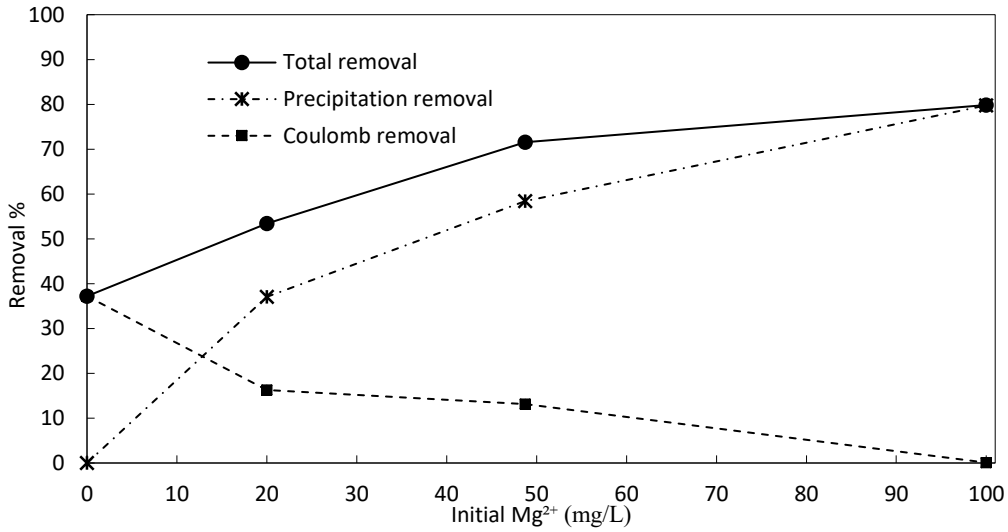

Fig. 3.5: Variation of F^- removal as a function of initial Mg^{2+}concentrations (initial F^- = 5.0 mg/L, Fe=0 mg/L, NaCl=20 mg/L; Ca^{2+}=0; HCO_3+CO_3^{2-}=0; mmol/L; applied charge loading =1200C/L)

3.3 Effect of initial Mg^{2+} concentration on F^- removal in the presence of Fe

Figures 3.6a, 3.6b, and 3.6c illustrate the effect of the initial Mg^{2+} concentration on the ion removal and F^- removal efficiencies at the constant initial Fe concentration (averaged value=20 mg/L). According to Fig. 3.6c, with increasing initial Mg^{2+}, removal of total F^- showed a slight decrement. Distinctly, the increase of Mg^{2+} brought down F^- removals by Coulomb force, while removal by precipitation increased. Even though the same charge loading was applied in the second stage,

applied voltage decrement was observed as the solution conductivity increased. Solution conductivity was increased due to dissociation of Mg^{2+} along with Cl^{-}.

According to Chapter 1, Eq. 1.56, Coulomb force which was experienced by individual ion depended on the charge of the ion and applied voltage. Therefore, the higher removal of F^{-} by Coulomb force was predominant when Mg^{2+} concentration was less than 50 mg/L. F^{-} removal percentages described in previous sections and this section were summarized in Table 3.4. According to that data, an increment of both initial concentrations of Mg^{2+} and Fe led to the highest total removal of F^{-}. Nevertheless, increased initial concentrations of Fe and Mg^{2+} of more than 20 mg/L, showed a decrease in the total F^{-} removal (4% decrease total increment); however, increasing both initial concentrations of Fe and Mg^{2+} to more than 20 mg/L, F^{-} removal by precipitation showed a significant increase (14%). Furthermore, compared to previous batch type electrocoagulation (EC) studies which utilized Fe electrodes (Table 3.3), the proposed ELC system showed much higher removal efficiency with lower electrode material dissociation and sludge generation.

Table: 3.4: Comparison of F^{-} removal

Section	**Initial Ion**		**Total F^{-} removal %**	**F^{-} removed by precipitation %**
	Mg^{2+}	**Fe**		
3.1	0	0	37	0
3.2	20	0	47	37
3.2	20	20	71	50
This section	50	20	67	64

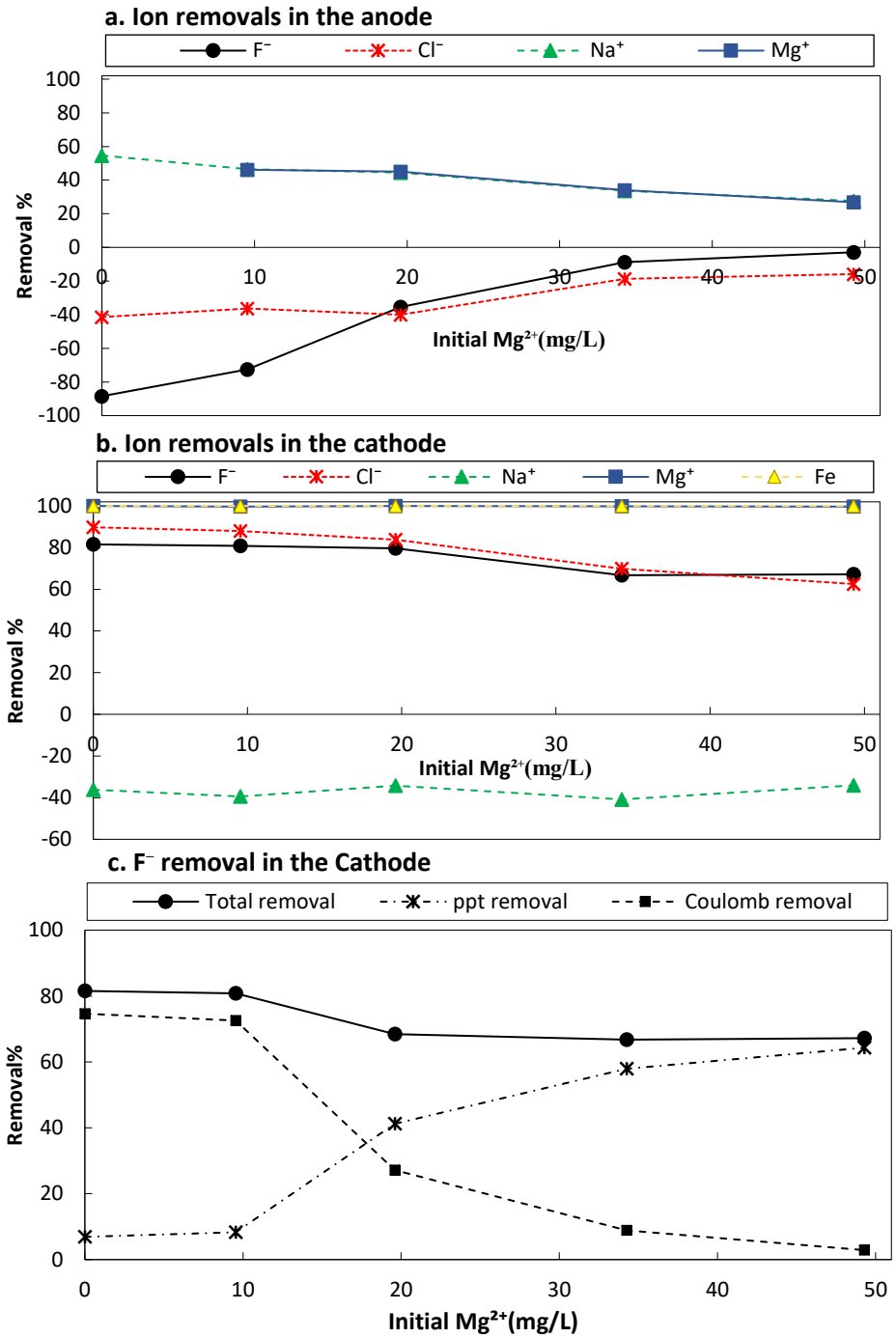

Fig. 3.6: Variation of F^- removal with initial Mg^{2+} concentration, C/L applied at first stage=75, C/L applied at second stage=1200, averaged initial Fe concentration=20 mg/L, initial F^- concentration=5 mg/L,initial CO_3^{2-}+HCO_3^- concentration =0 mmol/L

3.4 Effect of the initial F^- and Mg^{2+} concentration on F^- removal

To evaluate the initial concentrations of Mg^{2+} and F^- on F^- removal, a series of ELC experiments were performed with a different initial concentration of F^- and Mg^{2+}. Initial Fe concentration was kept constant at 20 mg/L, and 1200 C/L of charge loading was applied at the second stage. The results are shown in Fig. 3.7a, 3.7b, and 3.7c. The black color dashed line represents the percentage of F^- removal regulated to meet the WHO drinking water quality guideline of 1.5 mg/L. According to Fig. 3.7a, to meet the guideline of 1.5 mg/L at the initial F^- concentrations of 3 mg/L, a minimum of 10 mg/L initial Mg^{2+} was required. When the initial concentration of Mg^{2+} was 5 mg/L, to meet the guideline of 1.5 mg/L, F^- concentration of the raw water should be less than 2.25 mg/L. Furthermore, with a minimum of Mg^{2+} 10 mg/L and a maximum of 3 mg/L initial F^- concentrations were available, the optimum F^- removal of 75 mg/Fe(g) can be reached.

According to Fig. 3.7a, precipitation removals of F^- for the initial F^- concentration of 5 mg/L, and Mg^{2+} 5, 10, or 20 mg/L were found to be insufficient to meet the WHO guideline of 1.5 mg/L. The data in section 3.3 Fig. 3.6 showed that the presence of initial Mg^{2+} and Fe concentrations of 46 mg/L and Fe 20 mg/L meet the guideline of 1.5 mg/L F^- by achieving 72% removal. Therefore, to meet the guideline of F^- concentration in drinking water, the initial concentrations of Mg^{2+} should be increased. As shown in Fig. 3.7c, the total removal of F^- kept more than 70% for all initial F^- and Mg^{2+} concentrations, which were adequate to meet the WHO guideline of 1.5 mg/L. Furthermore, for all experiments shown in Fig. 3.7, the final removal of Fe and Mg^{2+} from the treated water was higher than 99%, ensuring the absence of dissociated electrode material.

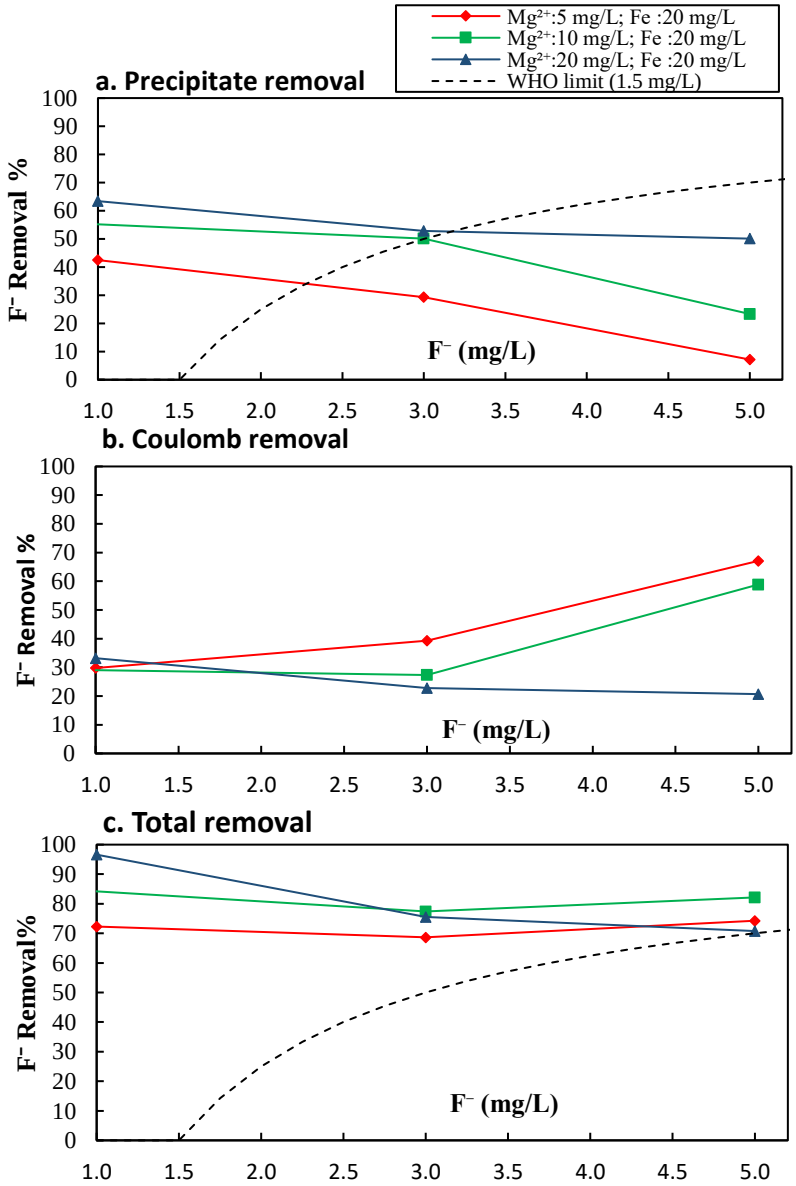

Fig. 3.7: Variation of F^- removal with various initial F^- and Mg^{2+} concentrations, charge loading applied at first stage=75C/L, charge loading applied at second stage=1200C/L, initial Fe concentration=20 mg/L, initial HCO_3^- +CO_3^{2-} concentration =0 mmol/L

3.5 Effect of the Ca^{2+} concentration on the F^- removal process

The effect of the Ca^{2+} concentration on F^- removal in the ELC process is described in this section. Figs. 3.8a and b show the ion removals in the anode and in the cathode respectively, over the increasing Ca^{2+} concentration. Fig. 3.8c shows the F^- removal by precipitation and by the coulomb forces over the increasing Ca^{2+} concentration in the cathode. According to Fig. 3.8, F^- removal by precipitation was reduced to 22% from 50% when the initial Ca^{2+}concentration changed from 0 to 150 mg/L.

By using the Ksp of $Ca(OH)_2$=5.02×10^{-6} $(mol/L)^3$ (Lide, 2005) and measured pH range of 11.69–11.43 for the initial Ca^{2+} 17–148 mg/L, the amount of $Ca(OH)_2$ precipitated was calculated to be 8.7×10^{-3}–27.8 ×10^{-3}mg/L. Therefore, $Ca(OH)_2$ cannot be formed in the system. However, the experimentally removed Ca^{2+} concentration was found far higher than the calculated concentrations range of 8.7×10^{-3}–27.8 ×10^{-3}mg/L. Due to the highly alkaline nature of the cathode bath, atmospheric CO_2 (g) could dissociate in the cathode solution. Dissolved CO_2 (g) formed $HCO_3^-$and CO_3^{2-}, which could remove Ca^{2+} as $CaCO_3$.

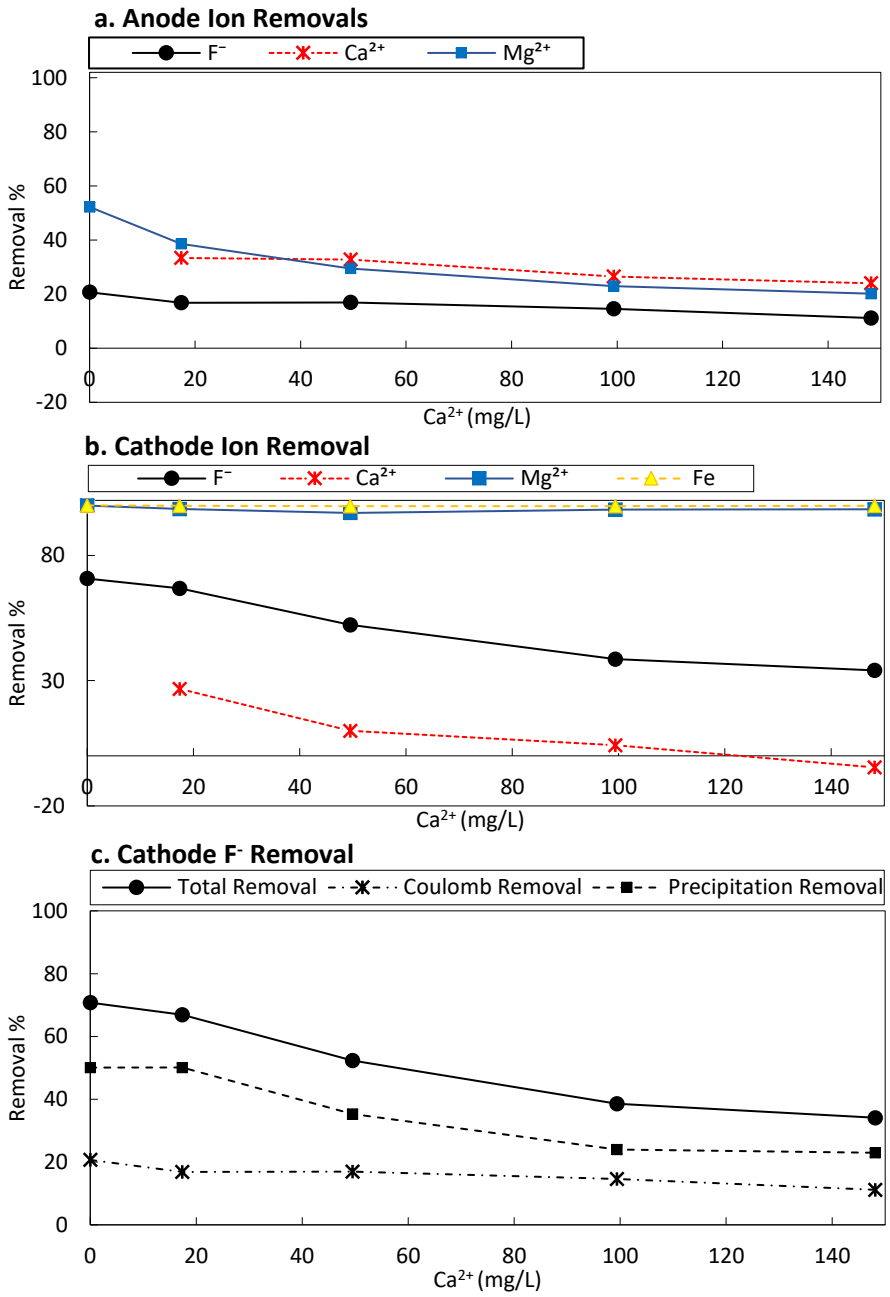

Fig. 3.8: Ions and F^- removal with varying initial Ca^{2+}, charge loading applied at first stage=75C/L, charge loading applied at second stage =1200C/L, initial F^- concentration =5 mg/L, initial Fe concentration =20 mg/L, initial Mg^{2+} concentration 20 mg/L, initial, HCO_3^- +CO_3^{2-} concentration =0 mmol/L

3.6 Effect of HCO_3^- +CO_3^{2-} ions on the F^- removal process

In this section, the effect of, HCO_3^- +CO_3^{2-} on ELC is discussed. Figs. 3.9a and b show the ion removals in the anode and the cathode respectively over the increasing HCO_3^- +CO_3^{2-} concentration. Fig. 3.9c shows the F^- removal by precipitation and by coulomb forces in the cathode. The presence of HCO_3^- +CO_3^{2-} showed a significant negative impact on F^- removal by precipitation. At the initial HCO_3^- +CO_3^{2-} concentration of 2.74 mmol/L, F^- removal by precipitation rapidly decreased to 0.4%. The presence of HCO_3^- +CO_3^{2-} reduced the formation of $Mg(OH)_2$ and $Fe(OH)_3$ by forming $MgCO_3$. The solubility product values of $Mg(OH)_2$, $Fe(OH)_3$, $MgCO_3$, and $Fe_2(CO_3)_3$ are 5.16×10^{-11}(mol/L)^3, 2.79×10^{-39}(mol/L)^4, 6.82×10^{-6} (mol/L)^2, 3.36×10^{-9} (mol/L)^5 respectively (Lide, 2015). Those values were used to confirm the formation of $Mg(OH)_2$, $Fe(OH)_3$ for all the levels of HCO_3^- +CO_3^{2-} and $MgCO_3$ concentrations at a level of 10 mmol/L, HCO_3^- +CO_3^{2-} concentrations (Table 3.5).

Table 3.5: HCO_3^- +CO_3^{2-} concentrations vs. Ion Activity Products (IAP) ; KSp<IAP (supersaturated), KSp=IAP(Equilibrium), KSp>IAP (under saturated)

OH (mol/L)	Assuming Fe2+ converted to Fe3+ in the solution(mol/L)	Mg^{2+}(mol/L)	CO_3^{2-} (mol/L)	Ksp $Mg(OH)_2$ = 5.61E-11	Ksp $Fe(OH)_3$ = 2.79E-39	Ksp $MgCO_3$= 6.82E-6	Ksp $Fe_2(CO_3)_3$ = 3.36E-9
				IAP $Mg(OH)_2$	IAP $Fe(OH)_3$	IAP $MgCO_3$	IAP $Fe_2(CO_3)_3$
0.0039	0.0004	0.0008	0.0027	1.25E-08	2.11E-11	2.20E-06	2.44E-15
0.0042	0.0004	0.0008	0.0049	1.43E-08	2.59E-11	4.06E-06	1.54E-14
0.0044	0.0004	0.0008	0.0070	1.57E-08	2.98E-11	5.72E-06	4.31E-14
0.0041	0.0004	0.0008	0.0093	1.37E-08	2.42E-11	7.66E-06	1.03E-13

Furthermore, the calculated and the measured molar concentrations of individual ion removals are shown in Table 3.6. The H^+ and OH^- concentrations (Table 3.6, column 2) were calculated by assuming all electrons contributed to form H^+ and OH^-. According to the H^+ concentrations and the total carbon removed, H^+ produced alone could remove all of the $HCO_3^- + CO_3^{2-}$ as CO_2 (columns 2 and 7). Therefore, the probability of the formation of $Fe(OH)_3$ and $Mg(OH)_2$ are higher than that of $MgCO_3$ and $Fe_2(CO_3)_3$ formation. Therefore, F^- co-precipitation could take place. However, if CO_3^{2-} and HCO_3^- was not properly removed, it can increase the formation of $MgCO_3$ and $Fe_2(CO_3)_3$ which prohibit the precipitative removal of F^-. Therefore, CO_3^{2-} and HCO_3^- ions should be removed before the second stage of the proposed system. The solution from the second-stage anode can be utilized conveniently for a lower concentration of $HCO_3^- + CO_3^{2-}$ removal since it had pH values of 2.6-2.9 (Approximate generation of H^+=2.5-1.3 mmol/L). If higher $HCO_3^- + CO_3^{2-}$ ions are present in the raw water, the charge loading can be increased appropriately. Considering those findings, the continuous flow ELC system was designed, and its ion removal efficiencies were described in section 3.7.

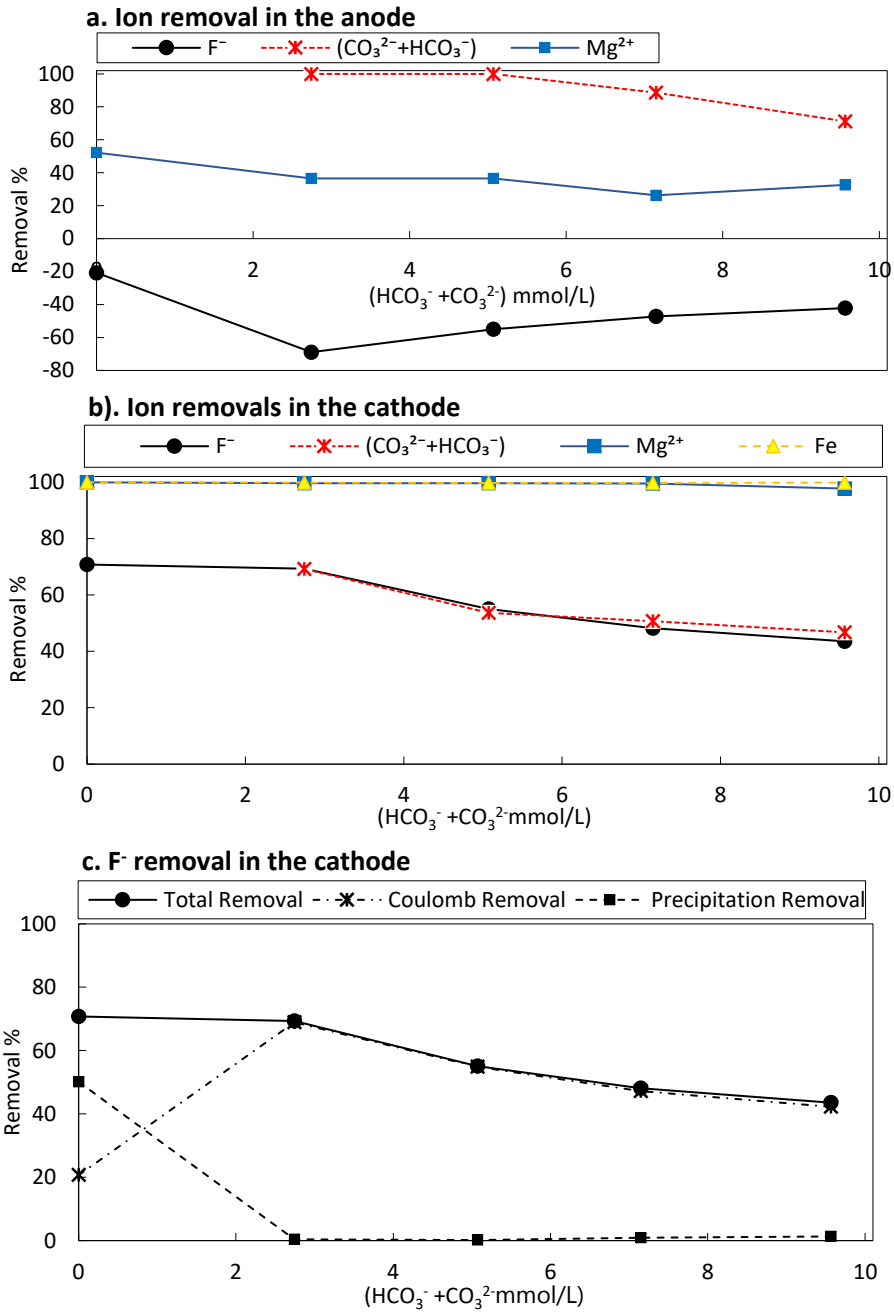

Fig. 3.9: Variation of F^- removal with different HCO_3^- +CO_3^{2-} concentration, charge loading applied at first stage=75 C/L, charge loading applied at second stage=1200C/L, initial F^-concentration=5 mg/L, initial Fe concentration =20 mg/L, initial Mg^{2+} concentration =20 mg/L

Table 3.6: Total ion removals in the (HCO_3^-+CO_3^{2-}) system

Initial (HCO_3^- +CO_3^{2-}) mmol/L	(mmol/l)					
	H^+/OH^-	Mg^{2+}	Fe^{3+}	Carbon removed at the cathode	Carbon removed at the anode	Total carbon removal
0	12.4	0.8	0.4	0.0	0.0	0.0
2.75	12.4	0.8	0.4	1.9	2.7	4.6
5.07	12.4	0.8	0.4	2.7	5.1	7.8
7.15	12.4	0.8	0.4	3.6	6.3	10.0
9.57	12.4	0.8	0.4	4.5	6.8	11.3

3.7 Continuous flow ELC system

Continuous flow ELC system (Fig.3.2) was operated with a low initial Mg^{2+} concentration of 35 mg/L for the initial F^- concentrations of 3 ,10 mg/L, Fe 20 mg/L Ca^{2+} 50, 100 mg/L and HCO_3^-+CO_3^{2-}= 10 mmol/L to simulate the Sri Lankan groundwater conditions. Charge loading 1500 C/L was selected so that anode solution pH was acidic enough to remove most of the HCO_3^-+CO_3^{2-} ions. Those concentrations (especially F^-, Ca^{2+} and HCO_3^-+CO_3^{2-}) were used to generate comparable data with Chapter 1 and Chapter 2 laboratory-scale continuous flow systems with a low level of Mg^{2+} concentration. Figure. 3.10 compared the ion removal of continuous flow ELC system (CELC), non-aeration ELC system (NELC) (data from Chapter 1) and aeration couples ELC system (AELC) (data from and Chapter 2).

Fig. 3.10 shows comparison of ion removal efficiencies of Fe and Mg^{2+} assisted continuous flow ELC system (ELC-Fe) with non-aeration ELC system (NELC) and aeration couples ELC system (AELC). According to Fig. 3.10a, the CELC system operated with the initial concentration of F^-=3 mg/L met WHO drinking water quality guideline of 1.5 mg/L with 49% removal. Therefore, initial concentrations of 35 mg/L

of Mg^{2+} and 20 mg/L of Fe can be identified as the minimum ratio of Mg^{2+} and Fe required for the treatment of 3 mg/L F^{-}. When the initial F^{-} concentration is more than 3mg/L, co-existing Mg^{2+} concentration should be higher than 35 mg/L. Compared to the NELC and AELC system's anode and cathode ion removals (Fig. 3.10a and 3.10b), the proposed CELC-Fe system was able to remove higher Ca^{2+}, Mg^{2+} as well as $HCO_3^{-}+CO_3^{2-}$. Moreover, F^{-} removal was found comparatively higher with respect to the initial Mg^{2+} concentration.

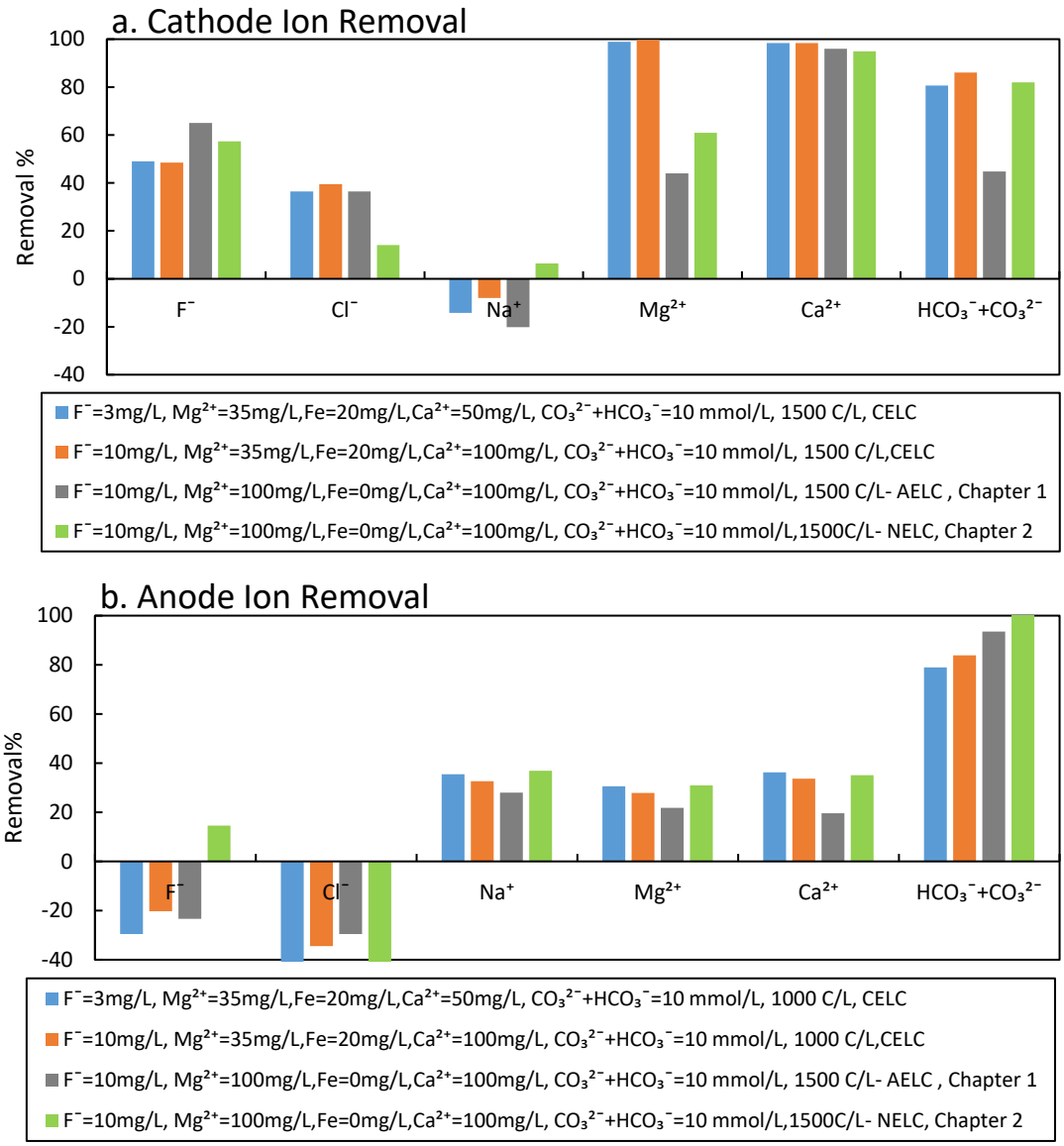

Fig. 3.10: Comparison of ion removal efficiencies of Fe and Mg^{2+} assisted continuous flow ELC system (ELC-Fe) with non-aeration ELC system (NELC) and aeration coupled ELC system (AELC)

3.8 Estimation of energy consumption and operating cost

The power consumption of the ELC system directly depends on the diaphragm resistance and the conductivity of the solution. In this study, no real attention was paid to decrease the power consumption by utilizing a commercial type diaphragm or by increasing the electrical conductivity of the solution. In this preliminary cost analysis, only the cost for power consumption, Mg and the sacrificial electrodes were taken into consideration. Market prices of electricity (0.061 US$/kWh) (CEB,2019), 99% pure Mg salt $MgCl_2.6H_2O$ (0.60 US$/kg) and the 99% pure Fe (0.60 US$/kg) in Sri Lanka for the year 2019 were used for the calculations. The average voltage values during the constant 100 mA operation (both first and second stages) were observed in between 17- 25 V for the initial Mg^{2+}, Fe and F^- concentrations of 20 mg/L, 10-53 mg/L and 5 mg/L respectively. The power consumption cost was calculated by using Eq. 3.18 and it was varied from 0.35 to 0.51 US$/m^3 respectively for the initial Mg^{2+} 20, Fe 10 mg/L and Mg^{2+} 20, Fe 53 mg/L. By using Eq. 3.19, sacrificial Fe electrode and Mg^{2+} chemical costs were calculated separately. By adding power, chemical Mg and Fe electrode costs, the total cost was calculated and it varied between 0.46 to 0.64 US$/m^3 respectively for the initial Mg^{2+}20, Fe 10 mg/L and Mg^{2+} 20, Fe 53 mg/L.

$$Power\ Cost(US\$/m^3) = \frac{Average\ Voltage(V) \times Current(A) \times Time\ (h)}{Volume\ treated\ (m^3) \times 10^3} \times Energy\ Price\ \left(\frac{US\$}{kWh}\right) \quad (3.18)$$

$$Material\ Cost(US\$/m^3) = \frac{Material\ Price\left(\frac{US\$}{mg}\right) \times Dissolved\ amount\ \left(\frac{mg}{L}\right) \times Molar\ fraction}{10^{-3}} \quad (3.19)$$

The recent study by Thakur et al., 2019, reported that the cost of removing F^- by Al sacrificial electrodes with EC was 0.36 US$/m^3 with the industrial electricity price of 0.08 US$/kWh in India(Thakur et al., 2019). By comparison with those data

calculated total cost for ELC varied from 0.56 to 0.80 US$/$m^3$ and was found to be higher than the most recent Al electrode EC process.

4 Conclusions

The Fe ELC technique was studied to study the F^- removal by sacrificial Fe electrode, minimize the sludge volume generated by EC by increasing the F^- removal efficiency, studying the effect of co-existing Mg^{2+} and other ions, studying the F^- removal by sacrificial Fe electrode, studying the removal of co-existing Mg^{2+}, Ca^{2+}, F^- HCO_3^- and CO_3^{2-} in the presence of a low concentration of Mg^{2+} and optimizing F^- removal for different concentrations of Fe and Mg^{2+} and to confirm the proposed ELC systems' performance and stability for groundwater treatment in Sri Lanka.

Findings revealed that the Fe ELC system was capable of removing F^- in a form of precipitate and by Coulomb forces, even in the absence of Mg^{2+}. In the absence of Mg^{2+}, the highest amount of Fe required to remove F^- was found as 1.1 mg/g. However, precipitation removal sharply increased in the presence of Mg^{2+} from 14% to 72% for initial 0 Mg^{2+}, 486 Fe mg/L and 50 Fe, 50 Mg^{2+} mg/L, initial concentrations respectively. In the absence of HCO_3^- +CO_3^{2-}, F^- was removed by co-precipitation with $Mg(OH)_2$ and $Fe(OH)_3$ as a result of the exchange of F^- ions with OH^- ions. Increasing the initial Fe concentration increased F^- removal to a certain level in the presence of Mg^{2+}; however, increasing the Fe concentration further caused a decrease in F^- removal. The minimal levels of the Fe and Mg^{2+} ratio required to meet WHO standards for F^- were found to be 5:20, 10:20, and 50:50 mg/L, respectively, for the initial concentrations of 2, 3, and 5 mg/L F^-. The presence of Ca^{2+} ions inhibited the removal of F^- by precipitation, to some extent. The presence of HCO_3^- +CO_3^{2-} inhibited the removal of F^- by precipitation, even at low concentrations. Therefore, HCO_3^- +CO_3^{2-} should be removed before operation.

The laboratory-driven pilot-scale treatment plant coupled with an aeration system and Fe ELC systems effectively removed HCO_3^- +CO_3^{2-} and removed its interference for F^- removal in the presence of a low concentration of Mg^{2+}. Therefore, the applicability of the proposed system on a real level was confirmed. The operating cost was calculated as 1.02 to 1.50 US$/$m^3$ in the developed country of Japan and 0.56 to 0.80 US$/$m^3$ in a developing country in Asia.

References

Bhatnagar, A., Kumar, E., Sillanpää, M., 2011. Fluoride removal from water by adsorption-A review. *Journal of Chemical Engineering*. 171, 811–840.

Campbell, A., 2002. The potential role of aluminium in Alzheimer's disease. *Nephrol. Dial. Transplant.* 36, 17–20.

Chung, Y., Shin, D., Park, S., Lim, Y., Choi, Y., Cho, S., Yang, J., Hwang, M., Park, Y., Lee, H., 1997. Risk assessment and management of drinking water pollutants in Korea, in: *Water Science and Technology*. 309–323.

Devi, R.R., Umlong, I.M., Raul, P.K., Das, B., Banerjee, S., Singh, L., 2012. Defluoridation of water using nano-magnesium oxide. *Journal of Experimental. Nanoscience*1, 512–524.

Dissanayake, C.B., 2005. Water quality in the dry zone of Sri Lanka -some interesting health aspects. *Journal of National Science Foundation* Sri Lanka 33, 161–168.

Drouiche, N., Aoudj, S., Lounici, H., Drouiche, M., Ouslimane, T., Ghaffour, N., 2012. Fluoride removal from pretreated photovoltaic wastewater by electrocoagulation: An investigation of the effect of operational parameters. *Procedia Engneering*. 33, 385–391.

Drouiche, N., Ghaffour, N., Lounici, H., Mameri, N., Maallemi, A., Mahmoudi, H., 2008. Electrochemical treatment of chemical mechanical polishing wastewater: removal of fluoride - sludge characteristics - operating cost. *Desalination* 223, 134–142.

Fu, H., Wang, M., Ho, Y., 2013. Mapping of drinking water research : A bibliometric analysis of research output during 1992 – 2011. *Science of the Total Environment*. 443, 757–765.

Govindan, K., Raja, M., Uma Maheshwari, S., Noel, M., Oren, Y., 2015. Comparison and understanding of fluoride removal mechanism in Ca^{2+}, Mg^{2+} and Al3+ ion assisted electrocoagulation process using Fe and Al electrodes. *Journal of Environmental Chemical Engineering*, 3, 1784–1793.

Gu, Z., Liao, Z., Schulz, M., Davis, J.R., Baygents, J.C., Farrell, J., 2009. Estimating Dosing Rates and Energy Consumption for Electrocoagulation Using Iron and Aluminum Electrodes Estimating Dosing Rates and Energy Consumption for Electrocoagulation Using Iron and Aluminum Electrodes. *Industrial & Engineering Chemistry Research*, 3112–3117.

Jadhav, S. V., Bringas, E., Yadav, G.D., Rathod, V.K., Ortiz, I., Marathe, K. V., 2015. Arsenic and fluoride contaminated groundwaters: A review of current technologies for contaminants removal. *Journal of Environmental Management*,162-1,306-325

Kobya, M., Hiz, H., Senturk, E., Aydiner, C., Demirbas, E., 2006. Treatment of potato chips manufacturing wastewater by electrocoagulation. *Desalinatio*n 190, 201–211.

Krewski, D., Yokel, R. a, Nieboer, E., Borchelt, D., Cohen, J., Kacew, S., Lindsay, J., Mahfouz, A.M., Rondeau, V., 2009. Human Health Risk Assessment For Aluminium, Aluminium Oxide, and Aluminium Hydroxide, *J Toxic. Env. Heal*. B. 10 (1) 2009 1-269.

Kuokkanen, V., Kuokkanen, T., Rämö, J., Lassi, U., 2013. Recent Applications of Electrocoagulation in Treatment of Water and Wastewater—A Review. Green Sustain. Chem. 03, 89–121.

Lide, D.R. (Ed.), 2005. CRC Handbook of Chemistry and Physics, Internet Version 2005, 93rd ed, CRC Handbook of Chemistry and Physics. CRC Press, Boca Raton, FL.

Mameri, N., Yeddou, A.R., Lounici, H., Belhocine, D., Grib, H., Bariou, B., 1998. Defluoridation of septentrional Sahara water of north Africa by electrocoagulation process using bipolar aluminium electrodes. *Water Research*. 32, 1604–1612.

Mohapatra, M., Anand, S., Mishra, B.K.K., Giles, D.E., Singh, P., 2009. Review of fluoride removal from drinking water. *Journal of Environment Management* 91, 67–77.

Mollah, M.Y., Schennach, R., Parga, J.R., Cocke, D.L., 2001. Electrocoagulation (EC)--Science and Applications. J. Hazard. Mater. 84, 29–41.

Nidheesh, P.V., Singh, T.S.A., 2017. Arsenic removal by electrocoagulation process:Recent trends and removal mechanisam. *Chemosphere* 181, 418–432.

Oladoja, N.A., Helmreich, B., 2016. Calcium aluminate-diatomaceous earth composite as a reactive filter material for aqua defluoridation. *J. Water Process Eng*. 9, 58–66.

Plummer, L.N., Busenberg, E., 1982. The solubilities of calcite, aragonite and vaterite in CO2-H2O solutions between 0 and 90°C, and an evaluation of the aqueous model for the system CaCO3-CO2-H2O. *Geochim. Cosmochim. Acta* 46, 1011–1040.

Pulkka, S., Martikainen, M., Bhatnagar, A., Sillanpää, M., 2014. Electrochemical methods for the removal of anionic contaminants from water - A review. *Separation and Purification Technology*, 132 (2014) 252–271

Rook, J. J., 1974. Formation of haloforms during chlorination of natural water. *Journal of Water Treatment Examination*, 23(2), 234–243.

Shen, J., Schafer, A., 2014. Removal of fluoride and uranium by nanofiltration and reverse osmosis: A review. *Chemosphere*, 117 (2014) 679–691.

Singh, M.M., Szafran, Z., Ibanez, J.G., 1998. Laboratory Experiments on the Electrochemical Remediation of Environment. Part 4: Color Removal of Simulated Wastewater by Electrocoagulation-Electroflotation. *J. Chem. Educ*. 75, 1040.

Spencer, H., Lewln, I., 1970. Fluoride Metabolism in Man. *Am. J. Med.* 49, 807–813.

Stefánsson, A., 2007. Iron(III) hydrolysis and solubility at 25°C. *Environ. Sci. Technol*. 41, 6117–6123.

Thakur, L.S., Goyal, H., Mondal, P., 2019. Simultaneous removal of arsenic and fluoride from synthetic solution through continuous electrocoagulation: Operating cost and sludge utilization. J. *Environ. Chem. Eng*. 7, 102829.

WHO, 2017. Guidelines for drinking-water quality: fourth edition incorporating the first addendum, 4th ed. World Health Organization.

Zhao, X., Zhang, B., Liu, H., Qu, J., 2011. Simultaneous removal of arsenite and fluoride via an integrated electro-oxidation and electrocoagulation process. *Chemosphere* 83, 726–729.

GENERAL CONCLUSIONS

Electrochemical techniques, electrolysis (ELC) was investigated in order to remove F^-, hardness-causing elements (Ca^{2+}, Mg^{2+}) and alkalinity from drinking or contaminated water in relation to the Sri Lankan context. The main focus was groundwater treatment for drinking purposes whereas many people in those areas are affected with dental and skeletal fluorosis, as well as F^- related chronic kidney disease. Three ELC systems were proposed and the ion removal mechanism and removal efficiencies were studied with artificial and real groundwater concentrations.

Findings revealed that the proposed system in the first Chapter was capable of removing coexisting F^-, Ca^{2+}, Mg^{2+}, CO_3^{2-}, and HCO_3^- ions without adding any chemicals. F^-, Ca^{2+}, and Mg^{2+} ions were significantly removed in the cathode, while CO_3^{2-} and HCO_3^- removal was found significant in the anode. The system was able to deliver the adequate quality of drinking water from its cathode for the highest level of initial F^- concentration 4.76 mg/L even if the initial Mg^{2+} concentration was 100 mg/L. However, the system had major drawbacks which were water rejection and underperformance in higher $(CO_3^{2-} + HCO_3^-)_0$ and lower $Mg^{2+}{}_0$ concentrations.

The system proposed in Chapter two also showed significant F^-, hardness and alkalinity removal efficiencies and is capable of removing multiple elements F^-, Mg^{2+}, Ca^{2+}, $HCO_3^-$and CO_3^{2-} in groundwater to meet WHO and Sri Lankan drinking water quality standards without any water rejection. Furthermore, a byproduct of $Cl_2(g)$ generation was found to be an added advantage that disinfects the final water. It was found that initial carbonate and Mg^{2+} concentrations could affect the removal of F^- and elements causing hardness. With a lower concentration of initial HCO_3^-, Ca^{2+} and Mg^{2+} removals were reduced. Therefore, similar to the proposed system in Chapter one, this system was unable to remove high initial F^- levels when low levels of Mg^{2+} were present.

As proposed in Chapter three, fluoride removal by magnesium ion-assisted sacrificial iron electrode showed high efficiency of F^- removal even in the lower level of initial Mg^{2+} concentration. Furthermore, findings revealed that the Mg^{2+} assisted ELC system was capable of removing F^- in a form of precipitate and by Coulomb forces, even in the absence of Mg^{2+}.

Furthermore, advantages and disadvantages comparison for each studied system was described as below table 4.1.

Table 4.1: Advantages and disadvantages of the ELC systems

ELC System	**Advantages**	**Disadvantages**
Non-aeration ELC system (NELC)-Chapter 01	• Higher removal of F^- in the presence of high concentration Mg^{2+} • Higher removal of Ca^{2+}	• 50% water recovery • Lower removal of (HCO_3^-+CO_3^{2-}) in cathode (treated water) • Low removal of Mg^{2+} in the presence of high concentration of (HCO_3^- +CO_3^{2-}) • Lower removal of F^- in the presence of low concentration Mg^{2+}
Aeration coupled ELC system (AELC)-Chapter 02	• Higher removal of Mg^{2+} • High precipitative removal of the F^- • Higher removal of HCO_3^- +CO_3^{2-} • 100% water recovery	• Lower removal of Ca^{2+} in the presence of low concentration (HCO_3^- +CO_3^{2-}) • Lower removal of F^- in the presence of low concentration Mg^{2+}
Fe and Mg $^{2+}$ assisted continuous flow ELC system (ELC-Fe)	• Higher removal of F^- in the presence of low concentration Mg^{2+}	• 66.7% water recovery • Lower removal of F^- in the presence of high concentration (HCO_3^- +CO_3^{2-})

PUBLICATIONS

First Author

1. **A.A.G.D. Amarasooriya**, Tomonori Kawakami, Electrolysis removal of fluoride by magnesium ion-assisted sacrificial iron electrode and the effect of coexisting ions, Journal of Environmental Chemical Engineering (**Cite Score: 7.5, Impact Factor: 5.909(2021)**), Volume 7, Issue 3, 2019, 103084, ISSN 2213-3437.
   Publisher: Elsevier
   DOI: 10.1016/j.jece.2019.103084
   URL: http://www.sciencedirect.com/science/article/pii/S2213343719302076

2. **A.A.G.D. Amarasooriya**, Tomonori Kawakami, Removal of fluoride, hardness and alkalinity from groundwater by electrolysis, Groundwater for Sustainable Development **(Cite Score: 5.21, Impact Factor: 4.700 (2021)**), Volume 9, October 2019, ISSN 2352-801X.
   Publisher: Elsevier
   DOI: 10.1016/j.gsd.2019.100231
   URL: http://www.sciencedirect.com/science/article/pii/S2352801X18302157

3. **A.A.G.D. Amarasooriya**, Tomonori Kawakami, Removal of co-existing fluoride, calcium, magnesium, and carbonates, by non-chemical induced electrolysis system for drinking and industrial purposes, H2Open Journal, Accepted **on 03 feb 2020,** paper ID H2Open-D-19-00022R1, Volume (3)1. 9th March 2020, Open Access article distributed under the terms of the Creative Commons Attribution Licence (CC BY-NC-ND 4.0

   Publisher: IWA

   DOI: 10.2166/h2oj.2020.022

   URL:https://iwaponline.com/h2open/article/3/1/10/72605/Removal-of-co existing-fluoride-calcium-magnesium

Related Publications; Co-Author

1. H.M. Ayala S. Herath, Tomonori Kawakami, Shiori Nagasawa, Yuka Serikawa, Ayuri Motoyama, G.G. Tushara Chaminda, S.K. Weragoda, S.K. Yatigammana & **A.A.G.D. Amarasooriya**. (2018) Arsenic, Cadmium, Lead, and Chromium in Well Water, Rice, and Human Urine in Sri Lanka relation to Chronic Kidney Disease of unknown etiology. Journal of Water and Health, 16 (2).
   Publisher: International Water Association (IWA)
   DOI: 10.2166/wh.2018.070
   URL:https://iwaponline.com/jwh/article/16/2/212/37995/Arsenic-cadmium-lead-and-chromium-in-well-water

2. Tomonori Kawakami, Miki Nishino, Yuki Imai, Hikaru Miyazaki, **A.A.G.D Amarasooriya,** De-fluoridation of drinking water by co-precipitation with magnesium hydroxide in electrolysis, Cogent engineering, Volume 5, Issue 1, 2018,
   Publisher: Taylor & Francis
   DOI: 10.1080/23311916.2018.1558498
   URL: http://doi.org/10.1080/23311916.2018.1558498

PUBLICATIONS IN ACADEMIC SYMPOSIUMS

1. Fluoride and Hardness Species Removal in Drinking Water by Novel Electrochemical Method**, A.A.G.D. Amarasooriya**, Tomonori Kawakami, 12th International Forum on Ecotechnology, Toyama International University, Toyama, Japan, 2nd-3rd December 2017.

2. Potential of Sri Lankan Apatite as a fluoride removal Agent from aqueous solution against Various Apatite Materials, **A.A.G.D. Amarasooriya**, Hikaru Miyazaki, Tomonori Kawakami, 6th international conference on Structural Engineering and Construction Management, 2015, Earl's Regency Hotel, Kandy, Sri Lanka,11th - 13th December 2015

3. Pilot Scale Experiment of Fluoride Removal from Well Water in Sri Lanka by Chicken Bone Char H.M. Ayala S. Herath, **A.A.G.D. Amarasooriya**, S.K. Weragoda, Kawakami Tomonori 23rd Symposium on Apatite, Toyama, Japan,11th December 2014

4. Fluoride Removal from Drinking Water in Sri Lanka by Chicken Bone Char, H.M. Ayala S. Herath, **A.A.G.D. Amarasooriya**, S.K. Weragoda, Kawakami Tomonori 9th International Forum on Ecotechnology, Hotel OACity Kyowa, Miyako Island,Okinawa, Japan,20th-23rd December 2014

5. A Community Scale Filter of Chicken Bone Char for Fluoride Removal from Drinking Water in Sri Lanka, H.M. Ayala S. Herath, **A.A.G.D. Amarasooriya**, S.K. Weragoda, Kawakami Tomonori, The49th Annual Conference of Japan Society on Water Environment, Ishikawa, Japan,16th March 2015

6. Community Based Fluoride Removal Filter with Chicken Bone Char in Sri Lanka, H.M. Ayala S. Herath, **A.A.G.D. Amarasooriya**, S.K. Weragoda, K. Tomonori, 6th international conference on Structural Engineering and Construction Management, 2015, Earl's Regency Hotel, Kandy, Sri Lanka,11th -13th December 2015

ACKNOWLEDGMENTS

Firstly, I would like to express my sincere gratitude to my advisor Prof. Tomonori Kawakami, Department of Environmental Engineering, Toyama Prefectural University for the continuous support of my PhD study and related research, for his motivation, his patience, dedication, and his immense knowledge. His guidance helped me in the time of my research works, writing and submitting articles and writing of this thesis. I could not imagine having a better advisor and mentor for my PhD study as well as living in Japan.

I gratefully acknowledge, all the co-authors and Professor Watanabe and Professor Takashi Kusui, Department of Environmental Engineering, Toyama prefectural university and Prof. Masamoto Tafu, Dept. Appl. Chem. & Chem. Eng., National Institute of Technology, Toyama College, Japan for providing me the specific analysis facilities and guidance during my research work. Furthermore, would like to express my sincere gratitude to Dr. Sujithra K. Weragoda, National water supply, and drainage Board Sri Lanka for coordinating and assisting the pilot-scale treatment system established in Sri Lanka. Staff members of the library, Toyama Prefectural University is also acknowledged

Financial support is given by the JSPS KAKENHI Grant Numbers 23404003, 15H05120, 17K18910 and 25257306. Furthermore, I would like to thank all Japanese citizens involved in raising the fund for my PhD scholarship “Monbukagakusho: MEXT and Ministry of Education, Culture, Sports, Science, and Technology Japan.

Finally, a special thanks to my dearest wife, and daughter who kept faith in me, along with all the sacrifices that they have made. Also, my beloved parents and my wife’s parents are kindly acknowledged for their guidance and help throughout these years.